



저작자표시-비영리-변경금지 2.0 대한민국

이용자는 아래의 조건을 따르는 경우에 한하여 자유롭게

- 이 저작물을 복제, 배포, 전송, 전시, 공연 및 방송할 수 있습니다.

다음과 같은 조건을 따라야 합니다:



저작자표시. 귀하는 원저작자를 표시하여야 합니다.



비영리. 귀하는 이 저작물을 영리 목적으로 이용할 수 없습니다.



변경금지. 귀하는 이 저작물을 개작, 변형 또는 가공할 수 없습니다.

- 귀하는, 이 저작물의 재이용이나 배포의 경우, 이 저작물에 적용된 이용허락조건을 명확하게 나타내어야 합니다.
- 저작권자로부터 별도의 허가를 받으면 이러한 조건들은 적용되지 않습니다.

저작권법에 따른 이용자의 권리는 위의 내용에 의하여 영향을 받지 않습니다.

이것은 [이용허락규약\(Legal Code\)](#)을 이해하기 쉽게 요약한 것입니다.

[Disclaimer](#)

工學博士學位論文

**Synthesis and Characterization of Polymer
Membranes Containing Carbonaceous Structures
for Water Purification**

탄소구조를 포함하는 고분자 막의 합성과 분석,
그리고 수처리로의 응용

2017年 2月

서울대학교 大學院

化學生物工學部

金 熙 仲

**Synthesis and Characterization of Polymer
Membranes Containing Carbonaceous Structures
for Water Purification**

by

Hee Joong Kim

Adviser: Professor Jong-Chan Lee, Ph. D.

**Submitted in Partial Fulfillment
of the Requirements for the Degree of
DOCTOR OF PHILOSOPHY**

February, 2017

**School of Chemical and Biological Engineering
College of Engineering
Graduate School
Seoul National University**

Abstract

Synthesis and Characterization of Polymer Membranes Containing Carbonaceous Structures for Water Purification

김 희 중 (Hee Joong, Kim)

공과대학 화학생물공학과 (Chemical and Biological Engineering)

고분자 합성 전공 (Polymer Synthesis)

The Graduate School

Seoul National University

This study presents synthesis and characterization of polymeric membranes having carbonaceous structures, and their applications to water purification including nanofiltration (NF) and reverse osmosis (RO) processes. Firstly, polyamide RO membranes with carbon nanotubes (CNTs) were prepared by interfacial polymerization using trimesoyl chloride (TMC) solutions in *n*-hexane and aqueous solutions of *m*-phenylenediamine (MPD) containing functionalized CNTs. CNTs prepared by an optimized reaction condition were found to be well-dispersed in the polyamide layer, which was confirmed from atomic force microscopy, scanning electron microscopy, and Raman

spectroscopy studies. The polyamide RO membranes containing well-dispersed CNTs exhibited larger water flux values than polyamide membrane prepared without any CNTs, although the salt rejection values of these membranes are close. Furthermore, the durability and chemical resistance against NaCl solutions of the membranes containing CNTs were found to be improved compared with those of the membrane without CNTs. The high membrane performance and the improved stability of the polyamide membranes containing CNTs were ascribed to the hydrophobic nanochannels of CNTs and well-dispersed states in the polyamide layers formed through the interactions between CNTs and polyamide in the active layers.

Second, polyamide RO membranes with deposited CNTs coated with poly(vinyl alcohol) (PVA) on the surface were prepared by interfacial polymerization followed by the deposition of oxidized CNTs and the coating of PVA on the surface. The polyamide membrane with the oxidized CNTs and PVA coating (PA–CNT–PVA membrane) showed much improved mechanical properties and durability compared with the polyamide membrane without CNTs (PA membrane). The PA–CNT–PVA membrane also exhibited much better antifouling properties than the PA membrane and the commercial RO

membrane (LFC-1). The improved durability and antibiofouling performances of the PA–CNT–PVA membrane were possible when the CNTs were well-dispersed on the top of the polyamide active layers and stabilized by the thin crosslinked PVA coatings.

Third, polyamide RO membranes containing both carbon nanotubes with acidic groups (CNTa) and graphene oxides (GOs) were prepared by the interfacial polymerization. When the mixtures of CNTa and GO were used as the filler materials for the preparation of the membranes, much larger amounts of the carbon nanomaterials could be well-dispersed in the polymer layers than when CNTa or GO was used by alone, because GO can increase the dispersion of CNTs in the aqueous solutions and the polymer matrix. Therefore, the polyamide membrane containing the mixture of CNTa and GO showed the best membrane performances.

Fourth, GOs coated by tannic acid (GOT) can be obtained easily by the self-polymerization of tannic acid in basic buffer solution on a GO surface. Polyamide RO nanocomposite membranes containing GOT in the active layer were prepared by the interfacial polymerization. The polyamide membrane containing GOT (PA-GOT) showed significantly improved performances such as water flux, chlorine

resistance, and antimicrobial properties, compared to the polyamide membrane without any additives and the polyamide membranes containing only tannic acid and/or GO. These high performances of PA-GOT membrane could be ascribed to a various of ad vantageous properties of GOT such as improved hydrophilicity, oxidative stress capability, barrier property, and compatibility with the polymer matrix.

Finally, a carbonaceous NF membranes (C-PIM-1) were prepared by the controlled carbonization of a PIM-1 membrane. Sub-1 nm-sized, interconnected, low frictional carbonaceous pores of the C-PIM-1 membrane facilitated the permeation of water molecules through the membrane, leading to a high water flux and good salt rejection rate. Moreover, the O₂ plasma treatment of the C-PIM-1 membrane resulted in water flux enhancement without decreasing the salt rejection rate, as well as high fouling resistance against proteins. These properties were attributed to the negatively charged hydrophilic membrane surface that decreases the entrance/exit resistance of the carbonaceous pores while facilitating the Donnan exclusion and reduces the interaction of proteins with the membrane surface.

Keywords: Polymeric membranes, carbonaceous structures, polyamide, polymers of intrinsic microporosity, carbon nanotubes, graphene oxides, water purification, filtration membranes

Student Number: 2011-21033

TABLE OF CONTENTS

Abstract	i
List of Tables	x
List of Figures	xii

Chapter 1

Introduction

1.1. Current Needs of Clean Water and Desalination	2
1.2. Polymeric Membranes for Desalination	3
1.3. Rapid Water Transport through Carbonaceous Structures	4
1.4. Motivation	6
1.5. References	7

Chapter 2

High Performance Reverse Osmosis CNT/Polyamide Nanocomposite Membrane by Controlled Interfacial Interactions

2.1. Introduction	10
2.2. Experimental.....	15
2.3. Results and Discussion	24

2.4. Conclusions	45
2.5. References	46

Chapter 3

The Improvement of Antibiofouling Properties of Reverse Osmosis Membrane by Oxidized CNTs

3.1. Introduction	80
3.2. Experimental.....	82
3.3. Results and Discussion	91
3.4. Conclusions	108
3.5. References	109

Chapter 4

High Performance Reverse Osmosis Nanocomposite Membranes Containing the Mixture of Carbon Nanotubes and Graphene Oxides

4.1. Introduction	132
4.2. Experimental.....	135
4.3. Results and Discussion	144
4.4. Conclusions	165
4.5. References	166

Chapter 5

Reverse Osmosis Nanocomposite Membranes Containing Graphene Oxides Coated by Tannic Acid With Chlorine-Tolerant and Antimicrobial Properties

5.1. Introduction	201
5.2. Experimental.....	203
5.3. Results and Discussion	212
5.4. Conclusions	227
5.5. References	228

Chapter 6

A Carbonaceous Membrane based on a Polymer of Intrinsic Microporosity (PIM-1) for Water Treatment

6.1. Introduction	259
6.2. Experimental.....	262
6.3. Results and Discussion	271
6.4. Conclusions	284
6.5. References	286

Abstract in Korean	313
---------------------------------	-----

List of Tables

- Table 2.1.** Membrane separation performance in current works in other CNT-polymer composite membranes and that of commercialized membrane.
- Table 2.2.** CNTs having different amounts of functional groups at different experimental conditions and their XPS elemental composition and O/C ratio.
- Table 2.3.** Results of water flux and salt rejection values of polyamide membranes from different monomer and CNT4 concentration.
- Table 2.4.** Surface compositions of polyamide-modified silicon wafer and PA membrane.
- Table 3.1.** Water flux and salt rejection of the PA, LFC-1, PA-PVA and PA-CNT-PVA membranes tested by cross-flow filtration (2000 ppm of NaCl feed solution, 15.5 bar of feed pressure and 500 ml min^{-1} of cross flow rate).
- Table 3.2.** XPS elemental composition (in at %) of the surface of PA and PA-CNT0.2-PVA0.2 membrane for before and after 3 days of pure water filtration.
- Table 3.3.** Mechanical strength of PA, PA-PVA0.2, PA-CNT0.2-PVA0.2, and LFC-1 membranes.
- Table 3.4.** The root mean square (RMS) roughness of PA, PA-PVA0.4, LFC-1, and PA-CNT0.2-PVA0.2 membranes.

Table 4.1. XPS elemental composition (at%) and O/C ratio of pristine CNT, CNTa, graphite, and GO.

Table 4.2. Maximum dispersity (g L^{-1}) of CNTa, GO, and CNTa/GO mixture in water.

Table 4.3. Water flux and salt rejection values of the membranes prepared in 2 and 3 wt% of MPD (PA-CNT, PA-GO membrane were prepared with 0.001 wt% of CNT and GO in aqueous solution, respectively and PA-CNT/GO membrane was prepared with 0.02 wt% of CNT/GO mixture in aqueous solution, the membranes were tested by cross-flow filtration, 2000 ppm NaCl solution as a feed solution, 15.5 bar of feed pressure, and 500 mL min^{-1} of flow rate).

Table 5.1. Water flux and salt rejection values of the membranes.

Table 5.2. Water flux and salt rejection values of PA membrane prepared 2 wt% MPD aqueous solution with additives; 0.5 wt% of DMSO, 2 wt% of TEA, 1 wt% of CSA, and 0.5 wt% of SDS.

Table 5.3. XPS elemental composition and O/C ratio of Graphite, GO, and GOT.

Table 6.1. Pure water flux (PWP), water flux (WF), and salt rejection (R) values of the membranes in this study. The water flux and salt rejection values were obtained by filtration of MgSO_4 solution (2,000 ppm).

Table 6.2. Bulk and surface elemental compositions (at%) of PIM-1,

C-PIM-1, and PC-PIM-1 (40% carbonization) membranes obtained by EA and XPS, respectively.

Table 6.3. Diffusion coefficient values (D_i) of salts (at 25 °C) and hydrated ionic radius (R_i) of the corresponding ions.

Table 6.4. MgSO_4 rejection (R, %) and water flux (WF, LMH bar^{-1}) values of optimized C-PIM-1 and PC-PIM-1 membranes in this study and other NF membranes in the literature.

List of Figures

- Figure 1.1.** Polyhedral oligomeric silsesquioxane (POSS).
- Figure 1.2.** (a) Star-shaped polymers with different architectures and (b) general synthetic approaches to star-shaped polymers.
- Figure 1.3.** Antifouling properties of poly(ethylene glycol) (PEG).
- Figure 1.4.** Li-ion conducting properties of poly(ethylene glycol) (PEG).
- Figure 1.5.** Schematic illustration of organic/inorganic hybrid star-shaped polymers containing PEG and POSS side groups for antifouling coating and solid polymer electrolyte applications
- Figure 2.1.** Water flux and salt rejection of membranes prepared by various types of CNT (tested by dead-end filtration, 2000 ppm of NaCl feed solution, 15.5 bar of feed pressure).
- Figure 2.2.** Functionalization procedure of AFM tip to polyamide repeating unit.
- Figure 2.3.** O/C ratios of CNTs modified in various conditions.
- Figure 2.4.** XPS spectra of CNTs in Table 2.1.

Figure 2.5. TEM images of each CNT treated using the acid mixture at different reaction condition; (a), (b) CNT1, (c) CNT2, (d) CNT3, (e) CNT4, (f) CNT5, (h) and (g) CNT6 (scale bar means 200 nm).

Figure 2.6. TEM images of each CNT treated using the acid mixture at different reaction condition; (a), (b) CNT1, (c) CNT2, (d) CNT3, (e) CNT4, (f) CNT5, (h) and (g) CNT6 (scale bar means 200 nm).

Figure 2.7. SEM images of bottom side of the (a) PA membrane (prepared by 2 wt% of MPD in aqueous solution) (x 20,000), (b) and (c) PA-CNT4 membrane (x 20,000 and x 100,000) (All the PA-CNT membranes were prepared by 2 wt% of MPD and 0.002 wt% of CNT in aqueous solution).

Figure 2.8. TEM images of cross-section of (a) PA, (b) PA-CNT1, and (c) PA-CNT4 membranes.

Figure 2.9. Raman spectroscopic mapping images of (a) PA-CNT1 and (b) PA-CNT4 membrane and (c) Raman spectra of polyamide, CNT1, CNT4 and (1), (2) and (3) region in Raman mapping area.

Figure 2.10. The mean interaction forces with standard deviations of polyamide-modified tips for the flat plates of CNT1 to CNT6.

Figure 2.11. (a) Water flux and (b) salt rejection of PA membrane (prepared by 2 wt% of MPD in aqueous solution) and PA-CNT4 membrane (prepared by 2 wt% of MPD and

0.001 wt% of CNT4 in aqueous solution) (tested by cross-flow filtration, 2000 ppm of NaCl feed solution, 15.5 bar of feed pressure, 700 ml min⁻¹ of cross flow rate).

Figure 2.12. Contact angles of PA, PA-CNT1, and PA-CNT4 membranes measured by captive bubble method.

Figure 2.13. Pure water flux of PA and PA-CNT4 membranes with time (operated under the 40 bar of feed pressure).

Figure 2.14. Water flux and salt rejection measurement with time: (a) pure water flux, (b) water flux and (c) salt rejection of 2000 ppm NaCl solution of PA membrane (prepared by 2 wt% of MPD) and PA-CNT4 membrane (prepared by 3 wt% of MPD and 0.001 wt% of CNT4) (tested by cross-flow filtration, 2000 ppm of NaCl feed solution, 15.5 bar of feed pressure, 700 ml min⁻¹ of cross flow rate).

Figure 2.15. Mechanical properties of PA and PA-CNT4 membrane tested by UTM.

Figure 2.16. Comparison of the result in this work with other results by others for NaCl separation membranes containing CNTs (Detailed information is shown in Table 2.1).

Figure 2.17. Typical force-extension curves recorded with a polyamide-modified tip against various types of CNT; (a) CNT1, (b) CNT2, (c) CNT3, (d) CNT4, (e) CNT5 and (f) CNT6.

Figure 2.18. Interaction force histograms which were used to determine the mean interaction forces; (a) CNT1, (b) CNT2, (c) CNT3, (d) CNT4, (e) CNT5 and (f) CNT6.

Scheme 2.1. Schematic illustration of the fast transport of water molecules through CNT embedded membrane.

Figure 3.1. Raman spectra of pristine and oxidized CNT.

Figure 3.2. (a) XPS spectra and (b) O/C ratios of pristine and oxidized CNT.

Figure 3.3. TEM micrographs of (a) pristine and (b) oxidized CNTs.

Figure 3.4. FT-IR spectra of PA membrane, PA-CNT0.2-PVA0.2 membrane without heat treatment, and PA-CNT0.2-PVA0.2 membrane; (a) at 4000 - 2500 cm^{-1} and (b) at 2500 - 850 cm^{-1} .

Figure 3.5. SEM images of (a) PA membrane, (b) magnified image of square lined region in (a), (c) PA-CNT0.2-PVA0.2 membrane, and (d) magnified image of square lined region in (c).

Figure 3.6. Photographs of PA membrane (left) and PA-CNT-PVA membrane prepared by 0.2 wt% of CNT-dispersed solution and 0.2 wt% of PVA solution (right).

Figure 3.7. Water flux variations of PA, PA-CNT-PVA, and LFC-1 membranes with time obtained by cross-flow filtration using the feed solutions containing *P. aeruginosa* PAO1 at 15.5 bar of feed pressure and 270 mL min^{-1} of cross flow rate.

- Figure 3.8.** SEM images of PA-CNT-PVA membrane prepared by 0.4 wt% of CNT-dispersed solution and 0.2 wt% of PVA solution (PA-CNT0.4-PVA0.2 membrane).
- Figure 3.9.** CLSM images of (a) PA, (b) LFC-1, (c) PA-PVA0.4, and (d) PA-CNT0.2-PVA0.2 membranes obtained after 24 h cross-flow test using the feed solutions containing *P. aeruginosa* PAO1.
- Figure 3.10.** Cell viability tests for PA, LFC-1, PA-PVA0.4 and PA-CNT0.2-PVA0.2 membranes, where PA membrane is used as the control standard.
- Figure 3.11.** Contact angles of PA, PA-PVA0.4, and PA-CNT0.2-PVA0.2 membranes measured by captive bubble method.
- Figure 3.12.** AFM images of (a) PA, (b) PA-PVA0.4, (c) PA-CNT0.2-PVA0.2, and (d) LFC-1 membranes.
- Figure 4.1.** XPS spectra of (a) pristine CNT and CNTa, and (b) graphite and GO.
- Figure 4.2.** Raman spectra of pristine CNT, CNTa, graphite, and GO.
- Figure 4.3.** FT-IR spectra of pristine CNT, CNTa, graphite, and GO.
- Figure 4.4.** TEM images of (a) pristine CNT, (b) CNTa, (c) graphite, and (d) GO.
- Figure 4.5.** UV/vis absorption spectra of (a) CNTa, (a) GO, and (c) CNTa/GO dispersed aqueous solution and (d) their UV/vis absorption intensity changes by the

concentration.

Figure 4.6. Zeta potential values of CNTa, GO, and CNTa/GO dispersed in water (50 mg mL^{-1}).

Figure 4.7. FT-IR spectra of PSf, PA, PA-CNTa (prepared using the MPD aqueous solution containing 0.001 wt% of CNTa), PA-GO (prepared using the MPD aqueous solution containing 0.001 wt% of GO), and PA-CNTa/GO (prepared using the MPD aqueous solution containing 0.02 wt% of CNTa/GO) membranes; wavenumber at (a) $2050\text{-}850 \text{ cm}^{-1}$, and (b) $4000\text{-}2050 \text{ cm}^{-1}$.

Figure 4.8. SEM (top and bottom part) and Raman spectroscopic mapping images of (a), (c), (e) PA, and (b), (d), (f) PA-CNTa/GO (prepared using the MPD aqueous solution containing 0.02 wt% of CNTa/GO) membranes.

Figure 4.9. Cross-sectional TEM images of PA and PA-CNTa/GO (prepared using the MPD aqueous solution containing 0.02 wt% of CNTa/GO) membranes.

Figure 4.10. SEM images at the top surfaces of (a) PA-CNTa (prepared using the MPD aqueous solution containing 0.01 wt% of CNTa), (b) PA-GO (prepared using the MPD aqueous solution containing 0.01 wt% of GO), and (c) PA-CNTa/GO (prepared using the MPD aqueous solution containing 0.03 wt% of CNTa/GO) membranes.

Figure 4.11. Water flux and salt rejection of (a) PA-CNTa, (b) PA-GO, and (c) PA-CNTa/GO membranes (water flux and salt rejection values of PA membrane were marked with

black and blue dot lines, respectively) (tested by cross-flow filtration, 2000 ppm NaCl solution as a feed solution, 15.5 bar of feed pressure, and 500 mL min⁻¹ of flow rate).

Figure 4.12. Unit water flux changes of PA, PA-CNTa (prepared using the MPD aqueous solution containing 0.001 wt% of CNTa), PA-GO (prepared using the MPD aqueous solution containing 0.001 wt% of GO), and PA-CNTa/GO (prepared using the MPD aqueous solution containing 0.02 wt% of CNTa/GO) membranes under different applied feed pressure (tested by cross flow filtration, 2000 ppm NaCl solution as a feed solution, and 500 mL min⁻¹ of flow rate).

Figure 4.13. Salt rejection measurement of the PA, PA-CNTa (prepared using the MPD aqueous solution containing 0.001 wt% of CNTa), PA-GO (prepared using the MPD aqueous solution containing 0.001 wt% of GO), and PA-CNTa/GO (prepared using the MPD aqueous solution containing 0.02 wt% of CNTa/GO) membranes at different applied pressure (tested by cross-flow filtration, 2000 ppm NaCl solution as a feed solution, and 500 mL min⁻¹ of flow rate).

Figure 4.14. (a) Pure water flux measurement and (b) water flux and salt rejection behaviors with time for PA, PA-CNTa (prepared using the MPD aqueous solution containing 0.001 wt% of CNTa), PA-GO (prepared using the MPD aqueous solution containing 0.001 wt% of GO), and PA-CNTa/GO (prepared using the MPD aqueous solution

containing 0.02 wt% of CNTa/GO) membranes (tested by cross-flow filtration, 2000 ppm NaCl solution as a feed solution, 15.5 bar of feed pressure, and 500 mL min⁻¹ of flow rate).

Figure 4.15. Normalized pure water flux measurement with time at 50 bar of feed pressure for PA, PA-CNTa (prepared using the MPD aqueous solution containing 0.001 wt% of CNTa), PA-GO (prepared using the MPD aqueous solution containing 0.001 wt% of GO), and PA-CNTa/GO (prepared using the MPD aqueous solution containing 0.02 wt% of CNTa/GO) membranes (tested by cross-flow filtration, and 350 mL min⁻¹ of flow rate).

Figure 4.16. Mechanical properties of PA, PA-CNTa (prepared using the MPD aqueous solution containing 0.001 wt% of CNTa), PA-GO (prepared using the MPD aqueous solution containing 0.001 wt% of GO), PA-CNTa/GO^a (prepared using the MPD aqueous solution containing 0.001 wt% of CNTa/GO), and PA-CNTa/GO (prepared using the MPD aqueous solution containing 0.02 wt% of CNTa/GO) membranes.

Figure 4.17. Membrane performance behaviors under the active chlorine exposures; (a) PA, (b) PA-CNTa (prepared using the MPD aqueous solution containing 0.001 wt% of CNTa), (c) PA-GO (prepared using the MPD aqueous solution containing 0.001 wt% of GO), and (d) PA-CNTa/GO (prepared using the MPD aqueous solution containing 0.02 wt% of CNTa/GO) membranes (tested by cross-flow filtration, measured after the chlorine

exposure using 500 ppm chlorine solution, 2000 ppm NaCl solution as a feed solution, 15.5 bar of feed pressure, and 500 mL min⁻¹ of flow rate).

Figure 4.18. Typical chlorination of polyamide membrane and antioxidant mechanism of CNT and GO.

Figure 4.19. Membrane performance behaviors under the active chlorine exposures of PA-CNTa/GO membrane prepared using the MPD aqueous solution containing 0.001 wt% of CNTa/GO (tested by cross-flow filtration, after the chlorine exposure using 500 ppm chlorine solution, 2000 ppm NaCl solution as a feed solution, 15.5 bar of feed pressure, and 500 mL min⁻¹ of flow rate).

Figure 4.20. TGA analysis of the membrane active layers under air; PA, PA-CNTa (prepared using the MPD aqueous solution containing 0.001 wt% of CNTa), PA-GO (prepared using the MPD aqueous solution containing 0.001 wt% of GO), and PA-CNTa/GO (prepared using the MPD aqueous solution containing 0.02 wt% of CNTa/GO) membranes.

Figure 4.21. ESR spectra obtained during the active chlorine exposure to membrane active layers; (a) PA, (b) PA-CNTa (prepared using the MPD aqueous solution containing 0.001 wt% of CNTa), (c) PA-GO (prepared using the MPD aqueous solution containing 0.001 wt% of GO), and (d) PA-CNTa/GO (prepared using the MPD aqueous solution containing 0.02 wt% of CNTa/GO) membranes.

Figure 4.22. Time-dependant relative ESR intensity changes during the active chlorine exposure to membrane active layers; PA,

PA-CNTa (prepared using the MPD aqueous solution containing 0.001 wt% of CNTa), PA-GO (prepared using the MPD aqueous solution containing 0.001 wt% of GO), and PA-CNTa/GO (prepared using the MPD aqueous solution containing 0.02 wt% of CNTa/GO) membranes.

Figure 4.23. Contact angle values of PA, PA-CNTa (prepared using the MPD aqueous solution containing 0.001 wt% of CNTa), PA-GO (prepared using the MPD aqueous solution containing 0.001 wt% of GO), PA-CNTa/GO^a (prepared using the MPD aqueous solution containing 0.001 wt% of CNTa/GO), and PA-CNTa/GO (prepared using the MPD aqueous solution containing 0.02 wt% of CNTa/GO) membranes.

Figure 5.1. Preparation of graphene oxide coated by tannic acid (GOT).

Figure 5.2. (a) FT-IR spectra, (b) Raman spectra of carbon materials, and XPS spectra of (c) GO and (d) GOT from XPS spectra.

Figure 5.3. FT-IR spectrum of TA.

Figure 5.4. TGA results of graphite, GO, and GOT (10 min °C min⁻¹, under N₂ atmosphere).

Figure 5.5. TGA results of TA and polymerized-TA (10 min °C min⁻¹, under N₂ atmosphere).

Figure 5.6. (a) FT-IR spectra and (b) Raman spectra of PA (prepared using 2 wt% MPD aqueous solution), PA-T (prepared

using 3 wt% MPD aqueous solution containing 0.005 wt% of TA), PA-GO (prepared using 3 wt% MPD aqueous solution containing 0.005 wt% of GO), and PA-GOT (prepared using 3 wt% MPD aqueous solution containing 0.005 wt% of GOT) membranes.

Figure 5.7. SEM images of top/bottom surface of active layer of the membranes; (a), (e) PA, (b), (f) PA-T (prepared using 0.005 wt% TA in aqueous solution), (c), (g) PA-GO (prepared using MPD aqueous solution containing 0.005 wt% of GO), and (d), (h) PA-GOT (prepared using MPD aqueous solution containing 0.005 wt% of GOT) membranes (size of the images is 12 μm (width) \times 9.5 μm (height)).

Figure 5.8. Magnified SEM images at the top surfaces of PA-T membrane (prepared using 3 wt% MPD aqueous solution containing 0.005 wt% of TA).

Figure 5.9. SEM images at the top surfaces of (a) PA-GO and (b) PA-GOT membranes prepared using 3 wt% MPD aqueous solution containing 0.01 wt% of GO and GOT, respectively.

Figure 5.10. Contact angle values of PA (prepared using 2 wt% MPD aqueous solution), PA-T (prepared using 3 wt% MPD aqueous solution containing 0.005 wt% of TA), PA-GO (prepared using 3 wt% MPD aqueous solution containing 0.005 wt% of GO), and PA-GOT (prepared using 3 wt% MPD aqueous solution containing 0.005 wt% of GOT) membranes.

Figure 5.11. Water flux and salt rejection of (a) PA-GO, and (b) PA-GOT membranes prepared using various GO and GOT concentrations in 3 wt% MPD aqueous solution. The water flux and salt rejection values of PA membrane prepared using 2 wt% MPD aqueous solution were marked with black and blue dot lines, respectively. The feed pressure was controlled to 15.5 bar.

Figure 5.12. Cross-sectional TEM images of (a) PA, (b) PA-GO (prepared using MPD aqueous solution containing 0.005 wt% of GO), (c) PA-GOT (prepared using MPD aqueous solution containing 0.005 wt% of GOT) membranes.

Figure 5.13. Water flux and salt rejection behaviors of the membranes under chlorine exposure; (a) PA (prepared using 2 wt% MPD aqueous solution), (b) PA-T (prepared using 3 wt% MPD aqueous solution containing 0.005 wt% of TA), (c) PA-GO (prepared using 3 wt% MPD aqueous solution containing 0.005 wt% of GO), and (d) PA-GOT (prepared using 3 wt% MPD aqueous solution containing 0.005 wt% of GOT) membranes. The feed solution containing 2000 ppm of NaCl and 500 ppm sodium hypochlorite was used and the feed pressure was controlled to 15.5 bar.

Figure 5.14. Water flux and salt rejection behaviors of the membranes under chlorine exposure; (a) commercial LFC-1 membrane for brackish water purification, and (b) PA-T-GO membrane (prepared using 3wt% MPD aqueous solution containing 0.0025 wt% of TA and 0.0025 wt% of GO).

Figure 5.15. ESR spectra obtained during the active chlorine exposure to membrane active layers; PA (prepared using 2 wt% MPD aqueous solution), PA-T (prepared using 3 wt% MPD aqueous solution containing 0.005 wt% of TA), PA-GO (prepared using 3 wt% MPD aqueous solution containing 0.005 wt% of GO), and PA-GOT (prepared using 3 wt% MPD aqueous solution containing 0.005 wt% of GOT) membranes.

Figure 5.16. Time-dependant relative ESR intensity changes during the active chlorine exposure to membrane active layers; PA (prepared using 2 wt% MPD aqueous solution), PA-T (prepared using 3 wt% MPD aqueous solution containing 0.005 wt% of TA), PA-GO (prepared using 3 wt% MPD aqueous solution containing 0.005 wt% of GO), and PA-GOT (prepared using 3 wt% MPD aqueous solution containing 0.005 wt% of GOT) membranes.

Figure 5.17. ESR spectra obtained during the active chlorine exposure to (a) GO and (b) GOT for 2 h and (c) time-dependant relative ESR intensity changes.

Figure 5.18. Cell viability of *E. coli* after contacting with the membranes for 24 h at room temperature; PA (prepared using 2 wt% MPD aqueous solution), PA-T (prepared using 3 wt% MPD aqueous solution containing 0.005 wt% of TA), PA-GO (prepared using 3 wt% MPD aqueous solution containing 0.005 wt% of GO), and PA-GOT (prepared using 3 wt% MPD aqueous solution containing 0.005 wt% of GOT) membranes.

Figure 5.19. Mechanical properties of PA (prepared using 2 wt%

MPD aqueous solution), PA-T (prepared using 3 wt% MPD aqueous solution containing 0.005 wt% of TA), PA-GO (prepared using 3 wt% MPD aqueous solution containing 0.005 wt% of GO), and PA-GOT (prepared using 3 wt% MPD aqueous solution containing 0.005 wt% of GOT) membranes.

Figure 6.1. Preparation and characteristics of PIM-1 and C-PIM-1 membranes. (a) Preparation procedure of PIM-1 and C-PIM-1 membranes. (b) Photographs of the PIM-1 and C-PIM-1 membranes. (c) XPS C 1s spectra, (d) Raman spectra, and (e) pore size distributions of the PIM-1 and C-PIM-1 (40% carbonization) membranes.

Figure 6.2. TGA curve of PIM-1.

Figure 6.3. Raman spectra of C-PIM-1 membranes. G band peak intensities in all the Raman spectra were normalized for clear comparison. a) Raman spectra of C-PIM-1 membranes with different degrees of carbonization. Deconvoluted Raman spectra of C-PIM-1 membranes with b) 40%, c) 50%, and d) 60% carbonization using Gaussian curve fitting for the D1, D3, D4, and G band peaks. e) D3 band peaks of C-PIM-1 membranes with different degrees of carbonization.

Figure 6.4. SEM images of PIM-1 and C-PIM-1 (40% carbonization) membrane surfaces.

Figure 6.5. AFM surface morphologies and root mean square (RMS) roughness values of a) PIM-1 and b) C-PIM-1 (40% carbonization) membranes (left, 10 $\mu\text{m} \times 10 \mu\text{m}$; right, 2 $\mu\text{m} \times 2 \mu\text{m}$ images).

Figure 6.6. N₂ adsorption and desorption isotherms of PIM-1 and C-PIM-1 (40% carbonization) at 77 K.

Figure 6.7. Water flux and salt rejection performance of the PIM-1 and C-PIM-1 membranes. The effect of degree of carbonization on water flux and salt rejection of the membranes with a thickness of 30 μm upon (a) pure water and (b) MgSO_4 solution (2,000 ppm) filtrations. (c) The effect of membrane thickness on water flux and salt rejection of the membranes with the degree of carbonization of 37.5% upon MgSO_4 solution (2,000 ppm) filtration. The red solid and dotted lines indicate the water flux and salt rejection of a commercial polyamide NF membrane (NF2A), respectively.

Figure 6.8. $C_{\text{W,F}}^{\text{m}}$ values of PIM-1 and C-PIM-1 membranes (carbonization = 40–60%) obtained from water uptake measurements.

Figure 6.9. a) Sessile drop water contact angle values of PIM-1, C-PIM-1, and PC-PIM-1 membranes. Wetting behaviors of water droplets on b) PIM-1, c) C-PIM-1 (40% carbonization), and d) PC-PIM-1 (40% carbonization) membranes. The relative humidity was maintained over 65% to minimize the evaporation of water droplets during the wetting experiment. Much shorter frame time (1 frame = 0.025 sec), compared to that for PIM-1 and C-PIM-1 membranes (1 frame = 0.5 sec), was used for the PC-PIM-1 membrane due to the rapid decrease of water contact angle on the membrane surface.

Figure 6.10. Preparation and performance of O_2 plasma-treated C-PIM-1 membrane (PC-PIM-1). (a) Preparation procedure of PC-PIM-1 membrane. (b) Pure water flux, water flux, and salt rejection performance of NF2A, and C-PIM-1 and PC-PIM-1 membranes with a

thickness of 20 μm and a degree of carbonization of 60%. (c) Time-dependent normalized water flux variations of the NF2A, C-PIM-1, and PC-PIM-1 (20 μm , 60% carbonization) membranes during BSA solution (1 g L^{-1}) filtration. (d) MgSO_4 rejection rate and water flux performance of optimized C-PIM-1 and PC-PIM-1 membranes in this study and other NF membranes in the literature.

Figure 6.11. Raman spectra of C-PIM-1 and PC-PIM-1 membranes with 40% carbonization. The G band peak intensities were normalized for clear comparison.

Figure 6.12. SEM images of the PC-PIM-1 (40% carbonization) membrane surface.

Figure 6.13. AFM surface morphologies and root mean square (RMS) roughness value of the PC-PIM-1 membrane (40% carbonization) (left, $10\ \mu\text{m} \times 10\ \mu\text{m}$; right, $2\ \mu\text{m} \times 2\ \mu\text{m}$ images).

Figure 6.14. Zeta potential values of PIM-1, C-PIM-1 (40% carbonization), and PC-PIM-1 (40% carbonization) membranes.

Figure 6.15. Salt rejection rates of C-PIM-1 and PC-PIM-1 membranes (40% carbonization) for various salt solutions (10 mM). Filtrations were conducted under 5 bar of feed pressure with a stirring speed of 200 rpm.

Chapter 1

Introduction

1.1. Current Needs of Clean Water and Desalination

The demand in fresh water has been dramatically increased because of increase in population and reduction in fresh water availability that originate from the pollution and climate change.[1-3] It is projected that global water demand of fresh water increases from 4,500 billion m³ on current to 6,900 billion m³ on the year 2030.[3, 4] In spite of these increases in water demand, more than 2.5 billion people do not have access to water sanitation systems, which could cause a various epidemic diseases based on the data from World Health Organization (WHO).[3, 4]

Since there are more than 97 % of water reservoir in sea among the earth, the desalination, a technology that converts sea water into fresh water, has been attracted as a solution to these water crisis problems. In general, desalination technologies could be divided to two separation processes; thermal based- and membrane-based mechanism.[4] The thermal processes include include multi-stage flash (MSF), multiple effect distillation (MED) and vapor compression distillation (VCD). The membrane-based processes include reverse osmosis (RO), nanofiltration (NF) and electrodialysis (ED). Among these technologies,

RO membrane desalination is the primary choice where it dominates up to 44% of the total world desalination capacity due to its advantages such as low operation temperature, high energy efficiency, and high productivity.[3, 4]

1.2. Polymeric Membranes for Desalination

Currently, there are two types of commercial RO membranes; cellulose acetate (CA) and aromatic polyamide (PA). The CA membrane was firstly developed from cellulose diacetate polymer in the 1950's.[2] The CA membranes exhibited good water flux and salt rejection rate, however, they has met some limitation such as neutral surface resulting organic-fouling, poor chlorine resistance, narrow operating pH range (4.5 to 7.5), and susceptibility to biological attack. To resolve these problems, PA thin film composite (TFC) membranes were developed in the 1970's. The PA TFC membraens feature a thin- and highly selective-aromatic polyamide layer on the physically stable microporous sublayer, which has a polymer different form the top layer such as polysulfone derivatives. Compared to asymmetric CA membrane, it is generally agreed that PA TFC membrane offers many

advantages such as high water molecules transport rate, excellent mechanical properties (under high pressure of seawater desalination applications) and relatively stable over wide range of pH. Therefore, the PA TFC membranes are widely used in commercial desalination plants over the worldwide. Still, polyamide membranes have some drawbacks in the desalination processes, such as chlorine and fouling susceptibility, which may affect the membrane performance. For example, shortening membrane lifetime, and reducing flux or salt rejection.

1.3. Rapid Water Transport through Carbonaceous Structures

Although advances in RO membrane have provided the large-scale fresh water production, more efficient desalination process still has been required due to current energy issues. Carbon-based membranes have been attracted as a breakthrough for the development of ultra high flux membranes because carbonaceous pores could provide fast water transport.[5-11] The fast water transport through carbonaceous pores is ascribed to the two reasons; (1) low friction between water molecules

and hydrophobic carbon surface and (2) ordered hydrogen bonds formed by the single file of water molecules.[12] Carbon nanotube (CNT)-based filtration membranes have been developed in the early of 2000's. The vertically aligned CNT membrane exhibited ultra-high flux with good rejection rate. Hinds et al. have experimentally investigated mass transport through aligned multiwalled CNT membranes and reported high water flux, over 4 orders of magnitude larger than conventional hydrodynamic flow prediction.[6, 11] Other several reports have also investigated the vertically-aligned CNTs membranes for filtration and separation applications.[13, 14] Undoubtedly, aligned CNTs membranes are a fine model for nanofluidics research, which mainly concerns the manner of liquid flowing confined in nanosized channels. In the late of 2000's, graphene oxide (GO)-based filtration membranes have been developed by simple vacuum filtration method. The drawbacks of CNT membranes including high cost, complex preparation procedure, and small membrane size could be overcome by the GO membrane.[12] The GO membrane exhibited high flux with good rejection rate, and the membrane properties could be controlled by functionalization and thickness. However, practical applications of these membranes are still limited by several issues, such as high cost

and complicated fabrication for CNT-based membranes, as well as poor stability under hydrated conditions and difficult pore size control for GO-based membranes. In addition, both membranes often suffer from relatively low salt rejection rates, attributed to the large pore size of CNT-based membranes and the deterioration of integrity of graphene-based membranes by the hydration, which in turn hampers the application of the membranes for nanofiltration (NF) or reverse osmosis (RO). Hence, a more convenient and efficient method for preparing carbonaceous membranes with a high flux and salt rejection rate is required for the water treatment applications.

1.4. Motivation

Based on the understanding of unique features of carbonaceous pores and polymeric membranes, the polymeric membranes having carbonaceous pores are designed and prepared. The main drawbacks of conventional carbon-based membranes as discussed above could be overcome by polymer nanocomposite systems by utilizing both advantages; fast water transport of carbonaceous structures and high salt rejection and mass production of polymeric membranes. The

carbonaceous structures in the polymeric membranes are CNT, GO, the mixture of CNT and GO, GO coated by natural polyphenol, and carbonized intrinsic micropores of polymer, and water molecules could be rapidly transported by them.

1.5. References

- [1] M. A. Shannon, P. W. Bohn, M. Elimelech, J. G. Georgiadis, B. J. Marinas, A. M. Mayes, *Nature* **2008**, 452, 301.
- [2] D. Li, H. T. Wang, *J. Mater. Chem.* **2010**, 20, 4551.
- [3] K. P. Lee, T. C. Arnot, D. Mattia, *J. Membr. Sci.* **2011**, 370, 1.
- [4] L. F. Greenlee, D. F. Lawler, B. D. Freeman, B. Marrot, P. Moulin, *Water Res.* **2009**, 43, 2317.
- [5] B. J. Hinds, N. Chopra, T. Rantell, R. Andrews, V. Gavalas, L. G. Bachas, *Science* **2004**, 303, 62.
- [6] J. K. Holt, H. G. Park, Y. M. Wang, M. Stadermann, A. B. Artyukhin, C. P. Grigoropoulos, A. Noy, O. Bakajin, *Science* **2006**, 312, 1034.
- [7] R. K. Joshi, P. Carbone, F. C. Wang, V. G. Kravets, Y. Su, I. V. Grigorieva, H. A. Wu, A. K. Geim, R. R. Nair, *Science* **2014**, 343, 752.

- [8] S. Karan, S. Samitsu, X. S. Peng, K. Kurashima, I. Ichinose, *Science* **2012**, 335, 444.
- [9] B. X. Mi, *Science* **2014**, 343, 740.
- [10] D. R. Paul, *Science* **2012**, 335, 413.
- [11] D. S. Sholl, J. K. Johnson, *Science* **2006**, 312, 1003.
- [12] Y. Han, Z. Xu, C. Gao, *Adv. Funct. Mater.* **2013**, 23, 3693.
- [13] B. Lee, Y. Baek, M. Lee, D. H. Jeong, H. H. Lee, J. Yoon, Y. H. Kim, *Nat. Commun.* **2015**, 6.
- [14] H. Y. Yang, Z. J. Han, S. F. Yu, K. L. Pey, K. Ostrikov, R. Karnik, *Nat. Commun.* **2013**, 4.

Chapter 2

High Performance Reverse Osmosis CNT/Polyamide Nanocomposite Membrane by Controlled Interfacial Interactions

2.1. Introduction

Purification of sea water or waste water to produce fresh water is known to be one of the most important issues in the environmental engineering and science fields, due to the current water shortage problems, mainly caused by the rapid growth of the world population and environment pollution.[1–6] A various membrane processes using different types of membranes, such as microfiltration (MF), ultrafiltration (UF), nanofiltration (NF), and reverse osmosis (RO) membranes, have been most widely used for the water purification, although other methods, such as distillation and chemical treatment, also have been used.[3,7–10] The advantages of the membrane processes are low operating temperature, low energy consumption, and high productivity.[3] In particular, the RO membrane system has been known to be most efficient to remove small-sized ions such as sodium and chloride ions in the sea water. Currently, polyamide membranes are widely used in the commercial RO systems because they offer a combination of high water flux and high rejections of the ions.[3] However, the polyamide membranes used in the RO systems has several disadvantages in the applications for desalination process, such

as low chlorine resistance and low antifouling, which shortens membrane life time and decreases the membrane performance such as water flux and salt rejection.[3,5,6,11]

There have been many attempts to improve RO membrane performances and properties such as water permeability, salt rejection, antifouling property, and chemical/mechanical stability.[11–16] Recently, nanocomposite membranes containing nanomaterials such as metal oxide, silica nanoparticle, zeolite, graphene, graphene oxide, and carbon nanotube (CNT) have been prepared to improve these membrane properties and/or performances.[17–26] For example, titanium dioxide and silver nanoparticles were incorporated into the membranes to increase antifouling and antibiofouling properties,[19,27] and zeolite was embedded into RO membranes to improve the water flux.[18,23] In particular, CNTs have been studied for water treatment process due to its unique properties. Membranes containing CNTs have been known to have high gas or liquid permeability,[25,26,28–33] antibacterial property,[34–36] and mechanical stability. Above all, polymeric membranes having aligned CNT structures showed ultra-high water flux values larger than $1000 \text{ L m}^{-2} \text{ h}^{-1} \text{ bar}^{-1}$ (LMH bar^{-1}).[25,26,28,30,41,42] This high water flux of the polymeric

membranes having aligned CNTs were ascribed to the unique hydrophobic character of the CNT surfaces and uniformly aligned nano-sized pores of CNT materials. However, there has been no report for the preparation of polymeric membranes with aligned CNTs having large enough effective membrane area and high enough NaCl rejection for practical RO membrane application, possibly due to the difficulties of incorporating uniformly aligned CNT layers into the physically stable polymer matrix materials as well as other possible technical problems.

Although the polymeric membranes with aligned CNTs for practical water treatment process have not been reported, polymeric membranes having dispersed CNTs as fillers in the polymer matrixes have been reported quite many times because the techniques to incorporate CNTs into the polymers are very well-known.[36,43,48,78-82] Therefore a various polymeric membranes containing dispersed CNTs in the selective and/or support layers were prepared and their membrane performances were measured. However when these membranes containing dispersed CNTs were used for the NaCl separation systems, most of them showed quite small salt rejection values as listed in Table 2.1. We believe that the small NaCl rejection values obtained from

these nanocomposite membranes containing CNTs should be caused by the poor dispersion of the CNTs in the polymer matrix that generates defects, which can increase the water flux while results in decreasing the NaCl rejection efficiency. Quite large NaCl rejection values up to 98.6 % were reported from the RO membranes containing zwitterion-functionalized CNTs, while their water flux values were found to be quite small about 1.33 LMH bar⁻¹, then the practical application in the RO system is not possible.[43] This small water flux value from the membrane containing the zwitterion-functionalized CNTs should be caused by the very thick polyamide layers. They probably fabricated thick polymer layers to cover the defects between CNTs and polymer matrixes, which in-turn results in the small water flux values. To the best of our knowledge, nanocomposite membrane with dispersed CNT showing high water flux in company with high salt rejection has not been reported yet.

Polymer nanocomposites have been widely used in battery researches, sensor studies, electronic devices fabrications, and other various researches as well as membrane applications.[44–48] The interactions between the polymers and the nano materials have been known to be very crucial factor to impart the desired properties to

polymer nanocomposite systems. Thus, various experimental methods to increase their interactions have been developed and various methods for the measurement of the interactive forces have been suggested.[36,40,49–51] It has been known that the functionality of nano materials and/or the amount of functional groups are the key parameters to increase the physical properties and/or performances of nanocomposite materials. In this work, we prepared a series of CNTs having different degree of functionality and length by changing the chemical treatment conditions. When a series of RO membranes were prepared through interfacial polymerizations of trimesoyl chloride (TMC) and *m*-phenylenediamine (MPD) with these functionalized CNTs, the degree of dispersion of the CNTs in the membranes and the interactions of the CNTs with the polymer matrix were found to affect the membrane performances. When the polyamide RO membranes were prepared with the optimized CNTs showing well dispersed CNTs in the polymer active layers and maximum interactions between the CNTs and polymer matrixes, their salt rejection values were comparable to those of common polyamide RO membranes without any CNTs, and their water flux and membrane stability were found to be much better than those of common polyamide RO membranes

without any CNTs.

2.2. Experimental

2.2.1. Materials

Multi-walled carbon nanotubes from Nanocyl (Belgium) were used as carbon nanotube (CNT) materials; the average diameter and average length of CNT are 10 – 20 nm and 10 – 20 μm , respectively. Polysulfone (PSf) membranes were supplied from Woong-jin chemicals (Republic of Korea) and used as a support membrane. Sulfuric acid (H_2SO_4 , 98 %), nitric acid (HNO_3 , 60 %) and isopropyl alcohol (IPA) were received from Daejung chemicals (Republic of Korea) and used as received. *m*-phenylenediamine (MPD, 99 %), trimesoyl chloride (TMC, 98 %) and sodium chloride (NaCl , 99 %) were supplied from Aldrich and used without any purification. Deionized (DI) water was obtained from water purification system (Synergy, Millipore, USA), having a resistivity of 18.3 $\text{m}\Omega\text{ cm}$. *n*-hexane (95 %) was received from Samchun Chemicals (Republic of Korea).

2.2.2. Modification of CNTs

The CNTs from Nanocyl were treated using an acid mixture (sulfuric acid and nitric acid of 3:1 volume ratio) to impart possible functional groups such as carboxylic acid by varying amount of acid mixture, reaction temperature, and reaction time. The modified CNTs were named as CNT1 to CNT6 and the number increases with the increase of the acid content in the reaction mixture and the increase of the reaction time and temperature. The experimental conditions for the preparation of the modified CNTs and their composition observed by XPS are shown in Table 2.2. The following procedure was used for the preparation of CNT4 and it was applied to prepare the composite RO membranes showing best membrane performance. 0.2 g of pristine CNTs and 60 mL of acid mixture solution were placed into 100 mL or 250 mL round-bottom flask equipped with a magnetic stirring bar and the mixture was sonicated for 30 min. Then the flask was placed into an oil bath thermo stated at 65 °C with stirring. After 4 h of reaction, the solution was cooled to room temperature and diluted with 1.5 L of water. The diluted solution was filtered by anodic aluminum oxide (AAO) filter whose pore size is 0.2 μm . Water was poured onto the

filtering system until a neutral pH is attained. The resulting CNTs on filter were dried in the 35 °C vacuum oven.

2.2.3. Preparation of the Polyamide Membranes with CNT and without CNT (PA-CNT and PA Membrane)

Polysulfone support membrane was treated with IPA for 10 min to enlarge pores and washed several times with water. The pretreated membrane was placed in the water bath for 3 h to stabilize the pores. A series of aqueous solution were prepared with 2 wt% of MPD and 0.002 wt% of various types of CNTs prepared using different reaction conditions. Another series of aqueous solution were prepared with different amount of CNT4 and MPD. 0.15 g of TMC was added into 250 mL of round-bottom flask equipped with a magnetic stirring bar in glove box filled with argon gas. 149.85 g of *n*-hexane was added into the flask using syringe and the solution was stirred at room temperature. Polysulfone membrane was placed into the bath with 500 g of aqueous solution. After 3 h, membrane was taken out and air bubbles and droplet of aqueous solution formed on the membrane surface were removed by rolling a rubber roller. The membrane was fixed on the

acryl flat board with rubber mold. The TMC solution was poured on the membrane saturated with the aqueous solution. After 60 s, the excess of organic solution on the membrane was removed and the membrane was placed in the 100 °C oven for 5 min to induce crosslinking as well as further polymerization. Then the resulting membrane was washed with water several times. The prepared composite membranes with and without CNTs were named as PA-CNT membrane and PA membrane, respectively.

2.2.4. Membrane Filtration Test

Water flux and salt rejection values were obtained by two test method such as dead-end filtration cells (CF042, Sterlitech Corp., Kent, WA) and lab-scale cross-flow RO membrane test unit. The effective membrane areas were $2.16 \times 2.16 \times \pi \text{ cm}^2$ and $3.3 \times 6.8 \text{ cm}^2$ with the 0.3 cm of channel height, respectively. The pressure was maintained at about 15.5 bar (225 psi) and the feed solution was $2,000 \text{ mg L}^{-1}$ of NaCl solution whose conductivity was about 3.86 mS cm^{-1} . These membrane operating conditions have been generally used in the BWRO membrane researches by others.[5,23,73,78] Cross flow velocity at the

membrane surface was 700 mL min^{-1} in cross-flow system. Water flux was measured by weighing the permeate solution after the membranes were compressed for 1 h at 15.5 bar. Membrane flux, J , was calculated using equation (1):

$$J = \Delta V / (A \times \Delta t) \quad (1)$$

where ΔV is the volume of permeate collected between two weight measurements, A is the membrane surface area, and Δt is the time between two weight measurements.

Salt rejection was calculated using the following equation (2):

$$R = (1 - C_p / C_f) \times 100 \% \quad (2)$$

where R is salt rejection parameter, C_p is the salt concentration in permeate, and C_f is the salt concentration in feed. The salt concentrations were measured using conductivity meter (InoLab Cond 730P, WTW 82362, weilheim). All membrane performance results shown in the Figure 2.1 and Table 2.3 are the average values obtained by more than three measurements from the three membrane samples

prepared at different times.

2.2.5. Interaction Force Measurement

The interactive forces between the CNT and polyamides were measured by an atomic force microscope (AFM, Seiko Instrument, SPA-400, Japan).[52] AFM tip could not be coated with the polymers by the coating method because cross-linked polymers are obtained from the polymerization of MPD and TMC and the resulting polymer, polyamide, is insoluble in any common solvents such as tetrahydrofuran (THF), dimethylformamide (DMF), dimethyl sulfoxide (DMSO) and dimethylacetamide (DMAc). Therefore the polyamide unit could be tethered on the AFM tip from the following procedure (Figure 2.2). A silicon cantilever (Nanosensors, CONTR) was washed with IPA, ethanol and water subsequently dried with N₂ gas. Then the tip was treated with oxygen plasma (150 W, 30 s) and it was chemically modified with 3-aminopropyltriethoxysilane toluene solution (10 mM) for 2 h at room temperature. This amine terminated AFM tip was further treated with TMC (0.1 wt% in *n*-hexane) for 30 min, which was followed by reaction with MPD in water (2 wt%) for 30 min. Then, the

tip was washed with ethanol and dried in the natural air. The silicon wafer was modified from the same procedure used for the modification of the AFM tip to confirm the modification of the tip because the size of the tip is too small to be analyzed. Surface composition analysis of modified silicon wafer and PA membrane is shown in Table 2.4. CNT films were prepared by filtering procedure as reported by others.[53] 5 mg of CNT (pristine and functionalized) was dispersed in 200 mL of water using sonication bath and the CNT dispersed solution was filtered by AAO filter. Then the flat CNT film on the filter was obtained and dried in the air.

As pristine or functionalized CNT film approached the polyamide (PA)-modified AFM tip, an interaction was generated between the surface of CNT film and the tip, inducing a cantilever deflection. The interaction force could be calculated by multiplying the spring constant of the cantilever by the deflection distance. The force could be detected in the same manner as the CNT film was retracted. Then, force-extension curve could be constructed from these measurements. We used a spring constant of 0.2 N m^{-1} , supplied by the manufacturer. A speed of $0.2 \text{ } \mu\text{m s}^{-1}$ was applied to obtain the force extension curves during approach and retraction of the surface of CNT film from the PA-

modified tip. All experiments were carried out in the air at room temperature. Approximately 100 approach/retract cycles were carried out for each CNT sample.

2.2.6. Raman Spectroscopic Mapping

Raman spectroscope (LabRam ARAMIS, Horiba Jobin-Yvon, France) was used for the Raman spectroscopic mapping of PA membrane, PA-CNT membranes, polyamide, and CNT. Thin active layers of PA and PA-CNT membranes were transferred on the silicon wafer because fluorescences from polysulfone could disturb detecting the Raman scattering from polyamide and CNT. Non-woven felt layer was taken off with sharp tweezers from thin film composite membrane. Then, polyamide layer on polysulfone membrane was placed on the silicon wafer. Purified THF was dropped slowly on the membrane until all of polysulfone layer was dissolved, and then the remaining polyamide layer was removed from the silicon wafer. Very thin polyamide layer was obtained after drying in vacuum oven at 30 °C for 24 h. The excitation source was a diode laser with an excitation wavelength of 785 nm and a power of 5 mW. The laser excitation was focused using a

100× objective and the Stokes-shifted Raman scattering was recorded using a 1400/600 groove min^{-1} grating. Raman mapping images were collected within a $15 \times 15 \mu\text{m}^2$ area of the active layer of the membrane on a silicon substrate in order to visualize the distribution and interaction of the CNT in the polyamide matrix. The Raman mapping images of the membranes were obtained by integrating the area of maximum peak intensity ($\pm 10 \text{ cm}^{-1}$).

2.2.7. Characterizations

Morphology of CNTs prepared with different reaction conditions was observed by transmission electron microscopy (TEM, LIBRA 120, Carl Zeiss, Germany). 1 mg of CNT was dispersed in 50 mL of water using sonication bath and then the dispersed solution was dropped on the carbon grid. The grid was dried in the $35 \text{ }^\circ\text{C}$ vacuum oven over 8 h. For the observation of membrane cross-sectional images by TEM, small pieces of the membrane samples were embedded in Spur resin. Approximately 60-70 nm thick sections were cut by an ultramicrotome (MTX, RMC) and placed on TEM grids. The sections were observed at an accelerating voltage of 120 kV. The surface compositions of the

CNTs, membranes, and silicon wafer modified by the polyamide unit were analyzed by X-ray photoelectron microscopy (XPS, PHI-1600) using Mg K α (1254.0 eV) as radiation source. Survey spectra were collected over a range of 0–1100 eV, followed by high resolution scan of the C 1s, O 1s and N 1s regions. Surface morphologies of the membranes were inspected by scanning electron microscopy (SEM, JSM-6701F, JEOL) using a field emission scanning electron microscope (FESEM).

2.3. Results and Discussion

2.3.1. Modification of CNTs

The pristine CNTs were treated using the strong acid mixture of sulfuric acid and nitric acid in 3 to 1 volume ratios by varying the amount of acid mixture, reaction temperature, and reaction time (Table 2.2) to prepare CNTs having acid functional groups.

Although there are only 5 different acid-treated CNTs in Table 2.2 used in this study, we prepared more than 35 different CNTs having different degree of functionality as shown in Figure 2.3. Since our main

objective in this study is to observe the effect of the functionality of CNT on the interaction with polyamide and to prepare the membrane with high salt rejection value by controlling the interfacial interactions between CNT and polyamide matrix, 5 different CNTs having various O/C ratio values were chosen to observe the interfacial effects on membrane performances.

We could conclude that the acid groups such as carboxylic acid are attached on the CNT surface during the modification process from our XPS, TEM, Raman spectroscopy results. Others also reported the incorporation of carboxylic acid groups on the CNT from the acid treatment.[35,54] The detailed discussions about the XPS, TEM, and Raman spectroscopy results are listed in the later part of this chapter. We intentionally imparted the acid groups on the surface of CNTs to disperse the CNTs in the aqueous solution well, then it is possible to prepare polyamide active layer containing well-dispersed CNTs from the interfacial polymerizations. Also it was expected that the acid functionalized CNTs could have interactions with the polyamide through the H-bonding and/or dipole-dipole interactions. The interaction was confirmed by AFM studies shown in the later part of this chapter.

Surface compositions of the CNTs such as CNT1 to CNT6 prepared from the different conditions were characterized by XPS analysis (Table 2.2 and Figure 2.4). The content of oxygen increases as the increase of the amount of the acid mixture, reaction temperature, and time. The atomic ratios of oxygen to carbon (O/C) indicate the contents of acid groups on the CNT surface by the acid treatment. The acid group formed on CNT can increase the dispersion of CNTs in the aqueous solution and in the polyamide matrix by the H-bonding and/or dipole-dipole interactions.

2.3.2. Membrane Filtration Test

Since the dead-end membrane filtration test is simpler than the cross-flow filtration, the screening test to evaluate the membrane performance of PA and PA-CNT membranes were carried out using the dead-end filtration method. While the detailed studies for the membrane tests were done using the cross-flow filtration method shown in the later part of this chapter. Water flux and salt rejection values of PA and the PA-CNT membranes containing CNT1 to CNT6 are shown in Figure 2.1. These membranes were prepared using

aqueous solutions with 0.002 wt% of CNT and 2 wt% of MPD and 0.01 wt% of the organic solution with TMC, respectively. All the membranes containing CNTs showed larger water flux values than PA membrane without CNT (36.4 LMH), while the salt rejection values of PA-CNT1, PA-CNT2, PACNT3 and PA-CNT6 membranes are smaller than that of the PA membrane. Interestingly water flux value of PA-CNT4 membrane was found to be larger than that of PA membrane and the salt rejection value of PA-CNT4 membrane is close to PA membrane. This remarkable membrane performance behavior was further studied by exploring the interaction behavior of the CNTs and the polyamide and also the dispersion of the CNTs in the polar matrix such as the polyamide and water.

2.3.3. Effects of Interaction and Dispersion of CNTs on Salt Rejection

TEM, SEM, AFM, and Raman mapping analysis were performed to elucidate the changes of the salt rejection and water flux values of PA and PA-CNT membranes. Since the polyamide, the active layer, is prepared by interfacial polymerization using aqueous solution

containing CNTs with organic solution, the dispersion of CNTs in the water is very important to obtain the polymers having well-dispersed CNTs. 0.002 wt% of CNT aqueous solution (0.02 mg mL^{-1}), the same concentration of CNTs in the aqueous solutions used for the interfacial polymerization, was used to obtain the TEM images (Figure 2.5). If CNTs are well dispersed in this solution, then it is very possible that CNTs in the polymerization solution should be well-dispersed. TEM image of CNT1, the pristine CNT without any acid treatment, shows the bundle morphology without any dispersed structures. Similar bundle or entangled structures were observed from CNT2 and CNT3 (Figure 2.5b to d) although they are less entangled than CNT1. For the CNT4 and CNT5, prepared from harsher conditions, such entanglements disappear and well dispersed CNT structures were observed, while it is also clear that CNTs were cut down to shorter tubes.[54,55] For CNT6, prepared by the harshest condition, does not have much tube structures, while mostly small spots possibly composed of debris of carbon materials were observed (Figure 2.5g and h). Since CNT1 to CNT3 are not fully dispersible in water, those aggregated structures can be transferred into polyamide forming aggregated domains working as defects in PA-CNT membranes, which can

decrease the salt rejection values for the PA-CNT membranes prepared from these CNTs. We strongly believe that the large salt rejection values of PA-CNT membranes prepared using CNT4 and CNT5 should be related to this well dispersed CNT morphology in water. The well-dispersed CNTs in those PA-CNT membranes can minimize the defects in the membrane, so their salt rejection values are close to or even larger than that of PA membrane. PA-CNT6 membrane shows smaller salt rejection value and slight larger water flux value. The aggregated particles, produced by the oxidation reactions of very harsh condition, possibly generate some defect structures in the polyamide layers that in turn can increase the water flux. Still the water flux value of PA-CNT6 membrane is smaller than that of PA-CNT2 and PA-CNT3 membranes because CNT6 is more functionalized than CNT2 and CNT3, then CNT6 can be more interactive with the polymers than CNT2 and CNT3. As a result, although there are defects in PA-CNT6, they are less than in those in PA-CNT2 and PA-CNT3 membranes.

Surface morphology of PA and PA-CNT membranes was observed from SEM images (Figure 2.6). Similar noodle structures from polyamide were observed on the surfaces of the PA and PA-CNT membranes, similarly as previously reported.[56-59] Large clusters

from aggregated CNTs were observed on the PA-CNT membranes prepared using CNT1 and CNT2 (Figure 2.6c to e), while small clusters were observed on the PA-CNT6 membrane. These large and small clusters were formed from aggregations of CNTs in aqueous solution. On the contrary, two bundles of CNTs were observed from the PA-CNT4 membrane, as shown in Figure 2.6f and such one or two bundles of CNTs were observed all over the surfaces of the PA-CNT4 membrane, indicating that CNTs are well dispersed. We tried to observe the bottom side of active layer of PA and PA-CNT4 membrane (Figure 2.7). In contrast to the clean and uniform images of the PA membrane, the bottom part images of the PA-CNT4 membrane shows several in and out line from single bundle of CNTs. Since the density of CNT ($1.3\text{--}1.4\text{ g cm}^{-3}$) is larger than that of the aqueous solution, CNTs sink into the bottom part during the membrane preparation procedures. Therefore the bottom side image of PA-CNT membrane shows a larger amount of CNTs than the top side images. The longer or shorter line images might indicate that the CNTs are located more or less parallel or tilted to the polyamide layer. The brightness changes of the longer lines might indicate the location of CNT stems at different heights. The diameter of the CNT shown in Figure 2.7c, about 17 nm, is within the

range of the diameter of the CNT, 10–20 nm. We also tried to observe the membrane cross-sectional images by TEM (Figure 2.8). PA, PA-CNT1, and PA-CNT4 membranes exhibited nano-scale surface roughness ranging from 100 to 400 nm thickness. Since the content of CNTs in the membranes are very small (0.002 wt% of CNT and 2 wt% of MPD, respectively in the polymerization solution), it was quite difficult to observe the CNTs in the cross-section. However it was very clear that PA membrane does not show any CNT images in the polyamide layer, while a few of the cross-sections from the PA-CNT1 and PA-CNT4 membranes clearly show the CNTs in the polyamide layers. CNTs are mostly entangled on the membrane surface in the PA-CNT1 membrane while, a few bundles of CNTs with dispersed structures were observed mostly at the bottom side of the PA-CNT4 membrane.

Raman spectroscopic mapping was carried out to further confirm the spatial distribution of CNTs in the polyamide membranes. Raman spectroscopic mapping has been utilized to visualize spatially the distribution of CNTs or other nanomaterials in other matrix materials including polymers.[51,60-64] Figure 2.9c shows the Raman spectra of polyamide, CNT1, and CNT4; distinct characteristic peaks of

polyamide and D and G bands of CNT were observed at 998 cm^{-1} , 1308 cm^{-1} , and 1600 cm^{-1} , respectively. The D/G ratio, the peak intensity ratios of D band and G band, of CNT4 (1.81) is larger than that of CNT1 (0.32), indicating that the acid treatment for the functionalization increases the defects on CNT surfaces. Similar results increasing the D band intensity by the functionalization were reported by others before.[54,65] Raman mapping images were collected within a $15 \times 15\ \mu\text{m}^2$ area of the PA-CNT membrane surfaces in order to visualize the dispersion of CNTs in the polyamide and the interactions of CNTs with the polyamide (Figure 2.9a and b). The Raman mapping of the PA-CNT membrane was obtained by integrating the area of the three peaks at 998 cm^{-1} for polyamide and at 1308 cm^{-1} and 1600 cm^{-1} for CNTs, where the green and red regions represent polyamide and CNT, respectively. Figure 2.9a illustrates the Raman mapping of the PA-CNT1 membrane, in which green and red area were separated, indicating that CNT1 is aggregated in the polyamide. On the contrary well-dispersed image of red and green colors is observed from the Raman mapping of PA-CNT4 membrane, indicating that CNTs are well-dispersed in the polyamide layers. Raman spectra of (1), (2), and (3) regions in Figure 2.9a and b are shown in Figure 2.9c. Region (1)

Raman spectrum shows mostly polyamide peak and region (2) Raman spectrum shows mostly CNT peaks, on the contrary and region (3) Raman spectrum shows both CNT and polyamide peaks. Therefore, in the most area of PA-CNT4, both CNT and polyamide are well mixed due to the interactions between the two materials. The D and G bands in region (3) Raman spectrum of PA-CNT4 membrane shifted from those in CNT, while any shift was not observed for the peak from polyamide. L. Bokobza *et al.* reported that these CNT peaks from Raman spectra shift to higher wavenumbers due to the decrease of the intertube interactions when CNTs are debundled or well-dispersed.[66] In addition, larger shift of D band than G band is also reported when there are interactions between CNTs and matrix materials.[66-68]

For the detailed and systematical investigation of the interactive forces between polyamide and CNT1 to CNT6, AFM analysis was carried out. The interaction between CNT and polyamide should be the important parameter that determines compatibility between CNTs with polyamide and the membrane performances of the PA-CNT membranes. Since the AFM tip was modified to have the amide groups in the polyamide units and the amine groups in the MPD monomer (Figure 2.2), the interactive forces between the modified AFM tip and the CNTs

recorded by AFM analysis can represent interactions between the CNTs with the amide groups and/or with amine groups. Therefore the chemical composition of AFM tip surface is similar to the compositions of the membranes and also to those in the interfacial polymerization systems. It is well-known that carboxylic acid groups (which are attached on the CNTs) can have dipole-dipole interactions and/or hydrogen bondings with amide and amine groups.[86] Similar AFM analysis has been widely used to measure the interactive forces between CNT and polymers in the composites.[52,69] Figure 2.10 shows the mean interaction forces of polyamide-modified tips for the flat films of CNT1 to CNT6. Typical force-extension curves and interaction force histograms are also shown in Figure 2.17. Since uneven CNT powders can affect the interaction forces between CNT and polyamide-modified tip, thin and even CNT films deposited on the AAO membrane were intentionally used. Small mean interaction forces were recorded for both CNT1 (0.68 ± 0.40 nN) and CNT2 (1.03 ± 0.50 nN) films. While, larger pull-off force about 3.74 ± 1.20 nN, indicating the larger negative values was observed for CNT4 and this value is about 5.5 times larger than that for CNT1. The interaction force behavior of the CNT films for CNT1, CNT2, CNT3, and CNT4 was

found to be same as the salt rejection behavior for PA-CNT1, CNT2, CNT3, and CNT4 membranes; the interaction force and salt rejection both increase from CNT1, CNT2, CNT3, to CNT4. Although interactive forces for CNT4, CNT5, and CNT6 with polyamide were quite close, the salt rejection value of PA-CNT6 membrane is quite smaller than those of PA-CNT4 and PA-CNT5 membrane. Since CNT6 was prepared from harshest oxidation condition, it has a large amounts of acid groups to have quite large interactive forces with polyamide, while the aggregated structure of CNT6 in the aqueous solutions used in the interfacial polymerization could be transferred into the polyamide layers and the defect structures generated from the aggregation decrease the salt rejection (Figure 2.6g and h). Therefore, since CNT4 and CNT5 have larger interactive forces with polyamide and aggregation-free structures, PA-CNT membranes prepared from these CNTs show larger salt rejection values than those prepared from less-functionalized CNTs (CNT1, CNT2, and CNT3) and over-functionalized CNT6.

2.3.4. Membrane Performance of PA-CNT4 Membrane

Both PA-CNT4 and PA-CNT5 membranes show very good membrane performance behavior (high water flux and salt rejection) and CNT4 and CNT5 show the larger interactive forces with polyamide than other CNTs. Still the salt rejection value of PA-CNT4 membrane is larger than that of PA-CNT5 membrane and the interactive force of CNT4 is also slightly larger than that of CNT5, while PA-CNT5 membrane shows larger water flux value than PA-CNT4 membrane, although their differences are not much. For our convenience to derive the conclusion of this study, the detailed data on the membrane performance of the PA-CNT membranes are focused on PA-CNT4 membrane.

We could prepare a series of PA-CNT4 membranes by changing the MPD and CNT4 concentrations in the interfacial polymerization, while we could not change the TMC concentrations because the solubility of TMC is too low (only 0.1 wt% TMC solution was used) to change. Figure 2.11 and Table 2.3 shows the water flux and salt rejection values of the membrane prepared by various MPD and CNT concentrations. It is well known that salt rejection values measured by cross-flow filtration are usually larger than those measured by dead end filtration. For the comparison of the membrane performance of PA and PA-CNT

membranes, the dead end filtration method was used due to the convenience of the method, while for the detailed study of the membrane performance of PA-CNT4 membranes, the cross-flow filtration method was used because it is close to the practical RO membrane filtration system. When PA-CNT4 membrane was prepared using the aqueous solution containing less than 0.0002 wt% of CNT, water flux and salt rejection values were found to be close to those of PA membrane. For example, water flux and salt rejection values of PA-CNT4 membrane prepared using aqueous solution containing 0.00004 wt% of CNT were 34.81 LMH and 97.50 %, respectively. It is clear that the very small amount of CNT does not affect the membrane performances. In contrast, when PA-CNT4 membrane was prepared using the aqueous solution containing larger than 0.005 wt% of CNT, a large increase of water flux and a large decrease of salt rejection were observed. For example, very large water flux of 52.64 LMH and very small salt rejection of 18.86% were observed from PA-CNT4 membrane prepared using aqueous solution containing 0.025 wt% of CNT. This result indicates that a larger amount of CNT (larger than 0.025 wt%) decreases the membrane performance, possibly due to the formation of aggregated CNT bundles in the polyamide (Figure 2.6).

Therefore, from 0.0005 to 0.005 wt% of CNT concentrations in the aqueous solution were used for the preparation of PA-CNT4 membranes.

Most of the PA-CNT4 membranes show larger water flux value than PA membrane when the same amount of MPD (the same concentration of MPD in aqueous solution) was used. It was also found that PA-membrane prepared by 2 wt% of MPD shows the largest water flux with a large enough salt rejection value (Table 2.3). It is very possible that there is an optimized monomer concentration ratio for the interfacial polymerization to produce polyamide active layers having optimized crosslinking density, polarity, and polymer structure to give maximum water flux and salt rejection values. For example, if the crosslinking density of polyamide is very high (it could be obtained using large amount of trifunctional TMC in the polymerization), water flux through the polymer layer could be interrupted because densely packed polymers normally have smaller free volumes.[16] We could obtain maximum water flux value from PA-CNT4 membranes when 3 wt% of MPD in aqueous solution was used, while the maximum water flux value from the PA membrane was obtained when 2 wt% of MPD was used. Therefore slightly larger amount of MPD is needed to obtain

the maximum water flux for the PA-CNT4 membranes than for the PA membrane. The functionalized CNTs having carboxylic acid groups on CNTs can form salt structure with the amine groups of MPD in aqueous solution and the hydrogen bonding between the acid groups on CNT and amine groups is also possible. Then some of the amine groups in MPD complexed with the acid groups on the CNTs cannot go through the polymerization, and a slightly larger amount of MPD (1 wt% for our case) is needed to get the polyamide structure showing maximum water flux. The maximum water flux of the PA-CNT4 membrane is larger than that of PA membrane by 7.65 LMH (17.2 % increase), while slightly smaller salt rejection value by 2.24 % was observed. Schematic illustration demonstrating the fast water transport of water molecules through the PA-CNT membrane is presented in Scheme 1. CNTs are well-dispersed in the polyamide membrane and this membrane structure can offer the fast transport way to pass water molecules. Water molecules can go into the inside of CNT by capillary force because of the nano-sized capillary structure of CNT and they can pass through the hydrophobic inner side of CNT.[28,30,41,42] Therefore, the possible pathway of water molecules through polyamide matrix could be shorten resulting in the increase of the water flux. Hydrated ions of sodium and

chlorine can also pass through the CNT channel quickly, because diameter of CNTs in the membrane is large enough to pass ions with water. According to the previous studies,[46,84,85] CNTs with diameters in the range of 0.6 - 1.1 nm can exclude the ions from water. Therefore the high salt rejection values of our membranes indicates that polyamide covering well dispersed CNTs can reject the ions. Water molecules can go through the way between polyamide matrix and the wall surface of CNT which has relatively hydrophobic nature. Although the CNT surface was functionalized by acid groups, still it is very possible that many part of the CNT surfaces are intact, then water can slide quickly on the surface. Similarly others reported that nanofillers like zeolite in the polymer membrane can increase the water flux because the space produced between fillers and polymer matrix can give the fast path for the water molecules.[18,23] In our case, PA-CNT4 membranes containing well-dispersed functionalized CNTs in the polymer matrix show larger water flux values with the relatively small decrease of the salt rejection values, while PA-CNT1 to -CNT3 membranes having coagulated CNTs show very large water flux and very small salt rejection values. Therefore, CNTs can increase the water flux due to its hydrophobic nature and high salt rejection can be

observed only when CNTs and polyamide have high interactive forces to form well-dispersed CNT structures producing defect-free membrane layers.

In addition, the CNTs having acid groups can increase the hydrophilicity of the membrane which also can increase the water flux. Contact angles of the membranes were measured by the captive bubble method because it is more accurate than the sessile drop method for the RO membrane surfaces as reported in our previous work.[83] As shown in Figure 2.12, the air contact angle value of PA-CNT1 membrane is slightly larger than that of PA membrane possibly because the small amount of hydrophobic pristine CNTs can increase the hydrophobicity on the surfaces. While, the air contact angle of PA-CNT4 membrane was found to be smaller than those of PA and PA-CNT1 membranes because hydrophilic CNT4 is incorporated into the membrane. Although the contents of CNTs in the membrane is very small, the water droplet having diameter in range in the range 2 to 4 mm can be contacted with some of the CNTs which can affect the changes of the contact angle.

2.3.5. Durability of PA-CNT4 Membrane

Water flux and salt rejection values of PA and PA-CNT4 membranes were measured with time using pure water and NaCl feed solution (Figure 2.14). The water flux of PA membrane decreased by 32.80 % after 48 h, while that of the PA-CNT membrane decreases by only 18.40 %. The decrease of the water flux in pressure driven system has been known to be caused by the compression of the membranes.[36,55] This behavior could be further proved by the operation at high pressure, such as 40 bar of feed pressure. In addition, we also performed the membrane performance test using the commercialized membrane (LFC-1 membrane) for BWRO membrane received from Hydranautics. Flux decrease of PA-CNT4, LFC-1, and PA membranes under the 40 bar of feed pressure were 18.11 %, 22.10 %, 42.15 %, respectively (Figure 2.13). Possibly, one of the most important advantages of CNTs using as filler in the nanocomposite materials is the increase of physical properties including the mechanical stability. Nanofillers including CNTs in the polymer matrix can disturb the polymer chain mobility to form the compressed polymer packing structures.[56] Therefore the polyamide layer in PA-CNT4 membrane can be less compressed than that in PA membrane and which in turn results in the less decrease of

water flux in the PA-CNT4 membrane than that in the PA membrane. There are a number of reports that even a small amount of CNT (less than 0.5 wt%) can increase the mechanical property of the nanocomposites.[40,57] In addition, the larger tensile strength and Young's modulus of PA-CNT4 than those of PA could be strongly related to the durability of PA-CNT 4 membrane at high pressure (Figure 2.15).

Similarly less decrease of water flux on PA-CNT4 membrane were observed when 2000 ppm NaCl solution was used for feed solution from 0 h to 10 h of cross-flow filtration experiment. After 10 h, the water flux of PA-CNT4 membrane decreases continuously, while that of PA membrane starts to increase as shown in Figure 2.14b. The increase of the water flux of PA membrane could be correlated with the large decrease of the salt rejection after 10 h. It is well known that the polyamide layers without any filler can be damaged by chlorine.[12,14,58,59] Therefore the large decrease of the salt rejection and the large increase of the water flux after 10 h of operation should be caused by the damaged structure of polyamide layers as reported by others (Figure 2.14c). It was reported that CNTs in the polyamide can increase the chemical stability to the chlorine.[60] We believe that the

interaction between the carboxylic acid group of the functionalized CNTs and the amide groups in the polymer matrix makes the membranes increase the chemical resistance to the chlorine.

We could have compared the membrane performances of PA-CNT4 membranes with those of commercial polyamide RO membranes. While it is well known that the active polyamide layers of the commercial polyamide RO membranes contain a various of additives to improve the membrane properties.[61,62] We also found that when the active top layers of PA-CNT4 membranes were coated with dilute aqueous solution of poly(vinyl alcohol), salt rejection value increased up to 99 % without much decrease of the water flux, if any. Therefore other additives included into the polyamide active layer of PA-CNT4 membranes possibly can increase the membrane performances, then they can be compared with those of the commercial RO membrane containing additives. However the main object of this chapter is to investigate the effect of CNTs in the active polyamide layer on the membrane performance. Therefore we intentionally prepared the PA membranes without CNTs and PA-CNT membranes containing CNTs from the exactly same method and their membrane performance behavior was compared. Currently we are preparing other types of PA-

CNT membranes with various additives and also using CNTs modified with various methods. Membrane performance of such PA-CNT membranes will be reported in near future, then we can compare the membrane performance of our membranes with other commercial RO membranes.

2.4. Conclusions

We have demonstrated a strategy to prepare RO membranes having high water flux and high salt rejection behavior from the interfacial polymerization of trimesoyl chloride (TMC) solutions and *m*-phenylenediamine (MPD) using functionalized CNTs. When the functionalized CNTs were prepared by the reactions of pristine CNTs with a sulfuric acid and nitric acid mixture for 4 h at 65 °C, maximum flux and salt rejection values were observed. When shorter reaction time and lower reaction temperature were used, the CNTs were not well-dispersed in the polyamide active layers, and when longer reaction time and higher reaction temperature were used, CNTs were cut down into very small pieces to form aggregated structures. The good dispersion of the functionalized CNTs in the polyamide layer was

ascribed to the high interactive force between the polyamide matrix with CNT which could be confirmed from various characterization techniques including Raman spectroscopic mapping and interaction force measurements. The membranes containing the properly modified CNTs (PA-CNT4) demonstrates outstanding membrane performances, surpassing the recent upper bounds of polyamide membranes containing CNTs for NaCl separation system (Figure 2.17). The RO membrane containing the CNTs also showed improved durability and chemical resistance against NaCl solution compared with the RO membrane without any CNTs. Our results clearly show that properly functionalized CNTs can improve the membrane performance including membrane stability, possibly because of the unique properties of CNT such as hydrophobic surface property and high compression resistance.

2.5. References

- [1] Potts, D. E; Ahlert, R. C.; Wang, S. S. *Desalination* **1981**, *36*, 235–264.
- [2] Kang, G. D; Cao, Y. M. *Water Res.* **2012**, *46*, 584–600.
- [3] Li, D; Wang, H. T. *J. Mater. Chem.* **2010**, *20*, 4551–4556.

- [4] Greenlee, L. F.; Lawler, D. F.; Freeman, B. D.; Marrot, B.; Moulin, P. *Water Res.* **2009**, *43*, 2317–2348.
- [5] Lee, K. P.; Arnot, T. C.; Mattia, D. *J. Membr. Sci.* **2011**, *370*, 1–22.
- [6] Pendergast, M. M.; Hoek, E. M. V. *Energy Environ. Sci.* **2011**, *4*, 1946–1971.
- [7] Cha, B. J.; Yang, J. M. *Macromol. Res.* **2006**, *14*, 596–602.
- [8] Alkhudhiri, A.; Darwish, N.; Hilal, N. *Desalination* **2012**, *287*, 2–18.
- [9] Wu, C. R.; Jia, Y.; Chen, H. Y.; Wang, X.; Gao, Q. J.; Lu, X. L. *Desalin. Water Treat.* **2011**, *34*, 2–5.
- [10] Nghiem, L. D.; Hildinger, F.; Hai, F. I.; Cath, T. *Desalin. Water Treat.* **2011**, *32*, 234–241.
- [11] Kosutic, K.; Kunst, B. *Desalination* **2002**, *150*, 113–120.
- [12] Colquhoun, H. M.; Chappell, D.; Lewis, A. L.; Lewis, D. F.; Finlan, G. T.; Williams, P. J. *J. Mater. Chem.* **2010**, *20*, 4629–4634.
- [13] Park, S. Y.; Kim, S. T.; Chun, J. H.; Chun, B. H.; Kim, S. H. *Desalin. Water Treat.* **2012**, *43*, 221–229.
- [14] Park, H. B.; Freeman, B. D.; Zhang, Z. B.; Sankir, M.; McGrath, J. *E. Angew. Chem., Int. Ed.* **2008**, *47*, 6019–6024.
- [15] Li, Q. L.; Elimelech, M. *Environ. Sci. Technol.* **2004**, *38*, 4683–4693.

- [16] Qiu, S.; Wu, L. G.; Zhang, L.; Chen, H. L.; Gao, C. J. *J. Appl. Polym. Sci.* **2009**, *112*, 2066–2072.
- [17] Paul, D. R. *Science* **2012**, *335*, 413–414.
- [18] Fathizadeh, M.; Aroujalian, A.; Raisi, A. *J. Membr. Sci.* **2011**, *375*, 88–95.
- [19] Li, J. F.; Xu, Z. L.; Yang, H.; Yu, L. Y.; Liu, M. *Appl. Surf. Sci.* **2009**, *255*, 4725–4732.
- [20] Hu, M.; Mi, B. X. *Environ. Sci. Technol.* **2013**, *47*, 3715–3723.
- [21] Li, J. B.; Zhu, Z. W.; Zheng, M. S. *J. Appl. Polym. Sci.* **2007**, *103*, 3623–3629.
- [22] Lu, L. Y.; Sun, H. L.; Peng, F. B.; Jiang, Z. Y. *J. Membr. Sci.* **2006**, *281*, 245–252.
- [23] Huang, H.; Qu, X. Y.; Dong, H.; Zhang, L.; Chen, H. L.; *RSC Adv.* **2013**, *3*, 8203–8207.
- [24] Uragami, T.; Okazaki, K.; Matsugi, H.; Miyata, T. *Macromolecules* **2002**, *35*, 9156–9163.
- [25] Shi, Z.; Zhang, W. B.; Zhang, F.; Liu, X.; Wang, D.; Jin, J.; Jiang, L. *Adv. Mater.* **2013**, *25*, 2422–2427.
- [26] Karan, S.; Samitsu, S.; Peng, X. S.; Kurashima, K.; Ichinose, I. *Science* **2012**, *335*, 444–447.

- [27] Dror-Ehre, A.; Adin, A.; Mamane, H. *Desalin. Water Treat.* **2012**, *48*, 130–137.
- [28] Hinds, B. J.; Chopra, N.; Rantell, T.; Andrews, R.; Gavalas, V.; Bachas, L. G.; *Science* **2004**, *303*, 62–65.
- [29] Choi, J. H.; Jegal, J.; Kim, W. N. *J. Membr. Sci.* **2006**, *284*, 406–415.
- [30] Holt, J. K.; Park, H. G.; Wang, Y. M.; Stadermann, M.; Artyukhin, A. B.; Grigoropoulos, C. P.; Noy, A.; Bakajin, O. *Science* **2006**, *312*, 1034–1037.
- [31] Thomas, J. A.; McGaughey, A. J. H. *Nano Lett.* **2008**, *8*, 2788–2793.
- [32] Hummer, G.; Rasaiah, J. C.; Noworyta, J. P. *Nature* **2001**, *414*, 188–190.
- [33] Gethard, K.; Sae-Khow, O.; Mitra, S. *ACS Appl. Mater. Interfaces* **2011**, *3*, 110–114.
- [34] Kang, S.; Herzberg, M.; Rodrigues, D. F.; Elimelech, M. *Langmuir* **2008**, *24*, 6409–6413.
- [35] Tiraferri, A.; Vecitis, C. D.; Elimelech, M. *ACS Appl. Mater. Interfaces* **2011**, *3*, 2869–2877.
- [36] Vatanpour, V.; Madaeni, S. S.; Moradian, R.; Zinadini, S.;

- Astinchap, B. *J. Membr. Sci.* **2011**, *375*, 284–294.
- [37] Chakraborty, A. K.; Plyhm, T.; Barbezat, M.; Necola, A.; Terrasi, G. P. *J. Nanopart Res.* **2011**, *13*, 6493–6506.
- [38] Sahoo, N. G.; Cheng, H. K. F.; Bao, H. Q.; Li, L.; Chan, S. H.; Zhao, J. H. *Macromol. Res.* **2011**, *19*, 660–667.
- [39] Peng, F. B.; Hu, C. L.; Jiang, Z. Y. *J. Membr. Sci.* **2007**, *297*, 236–242.
- [40] Shawky, H. A.; Chae, S. R.; Lin, S. H.; Wiesner, M. R. *Desalination* **2011**, *272*, 46–50.
- [41] Yu, M.; Funke, H. H.; Falconer, J. L.; Noble, R. D. *Nano Lett.* **2009**, *9*, 225–229.
- [42] Du, F.; Qu, L. T.; Xia, Z. H.; Feng, L. F.; Dai, L. M.; *Langmuir* **2011**, *27*, 8437–8443.
- [43] Chan, W. F.; Chen, H. Y.; Surapathi, A.; Taylor, M. G.; Hao, X. H.; Marand, E.; Johnson, J. K. *ACS Nano* **2013**, *7*, 5308–5319.
- [44] Li, J. S.; Zhang, Y. L.; To, S.; You, L. D.; Sun, Y. *ACS Nano* **2011**, *5*, 6661–6668.
- [45] Zhi, L. J.; Fang, Y.; Kang, F. Y. *New Carbon Mater.* **2011**, *26*, 5–8.
- [46] Zhai, D. Y.; Liu, B. R.; Shi, Y.; Pan, L. J.; Wang, Y. Q.; Li, W. B.; Zhang, R.; Yu, G. H. *ACS Nano* **2013**, *7*, 3540–3546.

- [47] Wilson, J. T.; Keller, S.; Manganiello, M. J.; Cheng, C.; Lee, C. C.; Opara, C.; Convertine, A.; Stayton, P. S. *ACS Nano* **2013**, *7*, 3912–3925.
- [48] Qiu, S.; Wu, L. G.; Pan, X. J.; Zhang, L.; Chen, H. L.; Gao, C. J. *J. Membr. Sci.* **2009**, *342*, 165–172.
- [49] Rahmat, M.; Das, K.; Hubert, P. *ACS Appl. Mater. Interfaces* **2011**, *3*, 3425–3431.
- [50] Chang, T. E.; Jensen, L. R.; Kisliuk, A.; Pipes, R. B.; Pyrz, R.; Sokolov, A. P. *Polymer* **2005**, *46*, 439–444.
- [51] Bassil, A.; Puech, P.; Landa, G.; Bacsa, W.; Barrau, S.; Demont, P.; Lacabanne, C.; Perez, E.; Bacsa, R.; Flahaut, E.; Peigney, A.; Laurent, C. *J. Appl. Phys.* **2005**, *97*, 34303–34304.
- [52] Poggi, M. A.; Lillehei, P. T.; Bottomley, L. A. *Chem. Mater.* **2005**, *17*, 4289–4295.
- [53] Klare, J. E.; Murray, I. P.; Goldberger, J.; Stupp, S. I. *Chem. Commun.* **2009**, 3705–3707.
- [54] Bahr, J. L.; Tour, J. M. *J. Mater. Chem.* **2002**, *12*, 1952–1958.
- [55] Flavin, K.; Kopf, I.; Del Canto, E.; Navio, C.; Bittencourt, C.; Giordani, S. *J. Mater. Chem.* **2011**, *21*, 17881–17887.
- [56] Kong, C. L.; Kanezashi, M.; Yamomoto, T.; Shintani, T.; Tsuru, T.

J. Membr. Sci. **2010**, *362*, 76–80.

[57] Ghosh, A. K.; Jeong, B. H.; Huang, X. F.; Hoek, E. M. V. *J. Membr. Sci.* **2008**, *311*, 34–45.

[58] Jeong, B. H.; Hoek, E. M. V.; Yan, Y. S.; Subramani, A.; Huang, X. F.; Hurwitz, G.; Ghosh, A. K.; Jawor, A. *J. Membr. Sci.* **2007**, *294*, 1–7.

[59] Zou, H.; Jin, Y.; Yang, J.; Dai, H. J.; Yu, X. L.; Xu, J. *Sep. Purif. Technol.* **2010**, *72*, 256–262.

[60] Anantachaisilp, S.; Smith, S. M.; Treetong, A.; Pratontep, S.; Puttipipatkachorn, S.; Ruktanonchai, U. R. *Nanotechnology* **2010**, *21*, 125102–125113.

[61] del Corro, E.; Izquierdo, J. G.; Gonzalez, J.; Taravillo, M.; Baonza, V. G. *J. Raman Spectrosc.* **2013**, *44*, 758–762.

[62] Kozielski, M.; Buchwald, T.; Szybowicz, M.; Blaszcak, Z.; Piotrowski, A.; Ciesielczyk, B. *J. Mater. Sci.: Mater. M.* **2011**, *22*, 1653–1661.

[63] Mendoza, A. J.; Hickner, M. A.; Morgan, J.; Rutter, K.; Legzdins, C. *Fuel Cells* **2011**, *11*, 248–254.

[64] Ingle, T.; Dervishi, E.; Biris, A. R.; Mustafa, T.; Buchanan, R. A.; Biris, A. S. *J. Appl. Toxicol.* **2013**, *33*, 1044–1052.

- [65] Banerjee, S.; Hemraj-Benny, T.; Wong, S. S.; *Adv. Mater.* **2005**, *17*, 17–29.
- [66] Bokobza, L.; Zhang, J. *Express Polym. Lett.* **2012**, *6*, 601–608.
- [67] Gao, Y.; Li, L. Y.; Tan, P. H.; Liu, L. Q.; Zhang, Z. *Chinese Sci. Bull.* **2010**, *55*, 3978–3988.
- [68] do Nascimento, G. M.; Barros, W. P.; Kim, Y. A.; Muramatsu, H.; Hayashi, T.; Endo, M.; Pradie, N. A.; Fantini, C.; Pimenta, M. A.; Dresselhaus, M. S.; Stumpf, H. O. *J. Raman Spectrosc.* **2012**, *43*, 1951–1956.
- [69] Barber, A. H.; Cohen, S. R.; Wagner, H. D. *Appl. Phys. Lett.* **2003**, *82*, 4140–4142.
- [70] Kim, D. G.; Kang, H.; Han, S.; Lee J. C. *J. Mater. Chem.* **2012**, *22*, 8654–8661.
- [71] Hu, Z.; Li, J.; Tang, P. Y.; Li, D. L.; Song, Y. J.; Li, Y. W.; Zhao, L.; Li, C. Y.; Huang, Y. D. *J. Mater. Chem.* **2012**, *22*, 19863–19871.
- [72] Celik, E.; Park, H.; Choi, H.; Choi, H. *Water Res.* **2011**, *45*, 274–282.
- [73] Liu, M. H.; Wu, D. H.; Yu, S. C.; Gao, C. J. *J. Membr. Sci.* **2009**, *326*, 205–214.
- [74] Glater, J.; Hong, S. K.; Elimelech, M. *Desalination* **1994**, *95*,

325–345.

[75] Junwoo, P.; Wansuk, C.; Kim, S. H.; Chun, B. H.; Joona, B.; Lee, K. B. *Desalin. Water Treat.* **2010**, *15*, 198–204.

[76] Zhao, L.; Chang, P. C. Y.; Ho, W. S. W. *Desalination* **2013**, *308*, 225–232.

[77] Lau, W. J.; Ismail, A. F.; Misdan, N.; Kassim, M. A. *Desalination* **2012**, *287*, 190–199.

[78] Zhao, H.; Qiu, S.; Wu, L.; Zhang, L.; Chen, H.; Gao, C. J. *J. Membr. Sci.* **2014**, *450*, 249–256.

[79] Roy, S.; Ntim, S. A.; Mitra, S.; Sirkar, K. K. *J. Membr. Sci.* **2011**, *375*, 81–87.

[80] Shen, J. N.; Yu, C. C.; Ruan, H. M.; Gao, C. J. *J. Membr. Sci.* **2013**, *442*, 18–26.

[81] Wu, H.; Tang, B.; We, P. *J. Membr. Sci.* **2013**, *428*, 425–433.

[82] Wu, H.; Tang, B.; We, P. *J. Membr. Sci.* **2010**, *362*, 374–383.

[83] Baek, Y.; Kang, J.; Theato, P.; Yoon, J. *Desalination* **2012**, *303*, 23–28.

[84] Corry, B. *J. Phys. Chem. B* **2008**, *112*, 1427–1434.

[85] Song, C.; Corry, B. *J. Phys. Chem. B* **2009**, *113*, 7642–7649.

[86] Amini, M.; Jahanshahi, M.; Rahimpour, A. *J. Membr. Sci.* **2013**,

435, 233–241.

Table 2.1. Membrane separation performance in current works in other CNT-polymer composite membranes and that of commercialized membrane.

Polymer matrix	CNT [wt%] ^a	Water flux [L ⁻¹ m ⁻¹ h ⁻¹ , LMH]	Rejection [%]	Feed solution	Unit water flux [LMH bar ⁻¹]	Ref.
LFC-1 (commercialized)	-	39.5	97	NaCl 2000 ppm	2.54	Tested in this work
Polysulfone	MWNT	9.3	75	Na ₂ SO ₄	2.33	36
	0.04 wt%	9.3	17	NaCl	2.33	
Polyamide	MWNT	28	76	NaCl	0.71	40
	0.015 wt%			4000 ppm		
Polyamide (PEI/IPD)	MWNT	14.04	96.0	Brilliant blue	4.07	79
	0.5 wt%			0.01 wt%		
Polyester (TMC/TEOA)	MWNT	4.7	70	Na ₂ SO ₄	0.78	81
	0.05 wt%			5 mM		
Polyamide (PIP/TMC)	MWNT	25.2	44.1	NaCl	2.52	80
	0.05 wt%			2000 ppm		
Polyamide (MPD/TMC)	Zwitt-SWNT	48.45	98.6	NaCl	1.33	43
	20 wt%			2000 ppm		
Polyamide (MPD/TMC)	MWNT	28.05	90	NaCl	1.75	78
	0.1 wt%			2000 ppm		
Polyamide (MPD/TMC)	MWNT-	44.34	95.72	NaCl	2.86	This work
	COOH			2000 ppm		
	0.17 wt%					

^awt% in polymer matrix

Table 2.2. CNTs having different amounts of functional groups at different experimental conditions and their XPS elemental composition and O/C ratio.

CNT type	CNT	Temperature	Time	Acid solution	C	O	O/C ratio
	[g]	[°C]	[hour]	[mL]	[at%]	[at%]	
CNT1 ^a	-	-	-	-	90.00	10.00	0.11
CNT2	0.2	25	3.0	20	83.42	16.58	0.20
CNT3	0.2	45	3.5	40	81.82	18.18	0.22
CNT4	0.2	65	4.0	60	78.87	21.13	0.27
CNT5	0.2	85	4.5	80	76.52	23.48	0.31
CNT6	0.2	105	5.0	100	70.68	29.32	0.41

^aCNT1 is pristine and used as received.

Table 2.3. Results of water flux and salt rejection values of polyamide membranes from different monomer and CNT4 concentration.

CNT\MPD [wt%] ^a	Water flux [L ⁻¹ m ⁻¹ h ⁻¹ , LMH] (Salt rejection [%])				
	1	2	3	4	5
0	26.86 ± 3.07 (97.11 ± 0.55)	36.60 ± 0.31 (97.57 ± 0.7)	34.34 ± 1.07 (97.49 ± 0.89)	32.60 ± 1.27 (96.80 ± 0.36)	28.31 ± 0.73 (95.50 ± 1.03)
0.0002	28.78 ± 2.2 (97.19 ± 0.30)	35.24 ± 1.58 (97.01 ± 1.01)	36.77 ± 1.2 (96.42 ± 0.64)	33.11 ± 1.98 (96.75 ± 0.57)	30.35 ± 0.67 (94.79 ± 0.64)
0.001	31.14 ± 1.34 (96.23 ± 0.56)	38.23 ± 1.49 (96.63 ± 0.52)	44.34 ± 2.37 (95.72 ± 0.38)	40.08 ± 0.15 (95.19 ± 0.34)	36.26 ± 0.81 (95.62 ± 0.67)
0.005	30.92 ± 1.2 (95.49 ± 0.75)	37.79 ± 2.52 (95.99 ± 1.13)	38.74 ± 0.83 (95.91 ± 0.38)	37.36 ± 1.39 (95.77 ± 0.32)	34.47 ± 2.32 (95.25 ± 0.81)

^awt% in aqueous solution using interfacial polymerization

Table 2.4. Surface compositions of polyamide-modified silicon wafer and PA membrane.

Atom	PA membrane [%]	Si wafer [%]
C	71.48	69.97
O	17.51	19.22
N	11.01	10.81

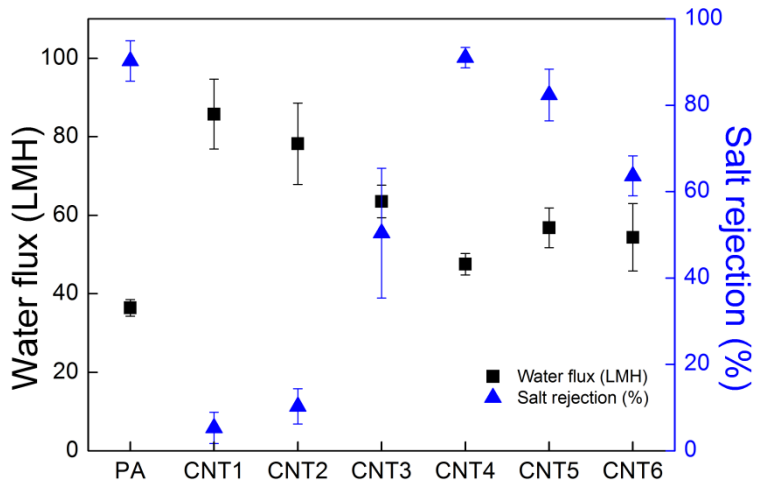


Figure 2.1. Water flux and salt rejection of membranes prepared by various types of CNT (tested by dead-end filtration, 2000 ppm of NaCl feed solution, 15.5 bar of feed pressure).

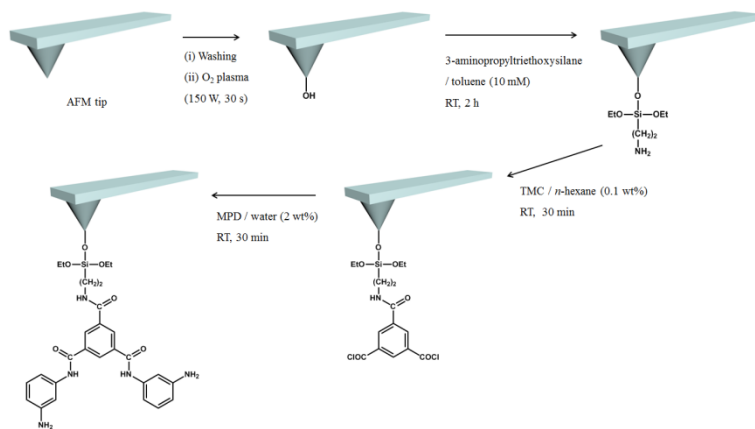


Figure 2.2. Functionalization procedure of AFM tip to polyamide repeating unit.

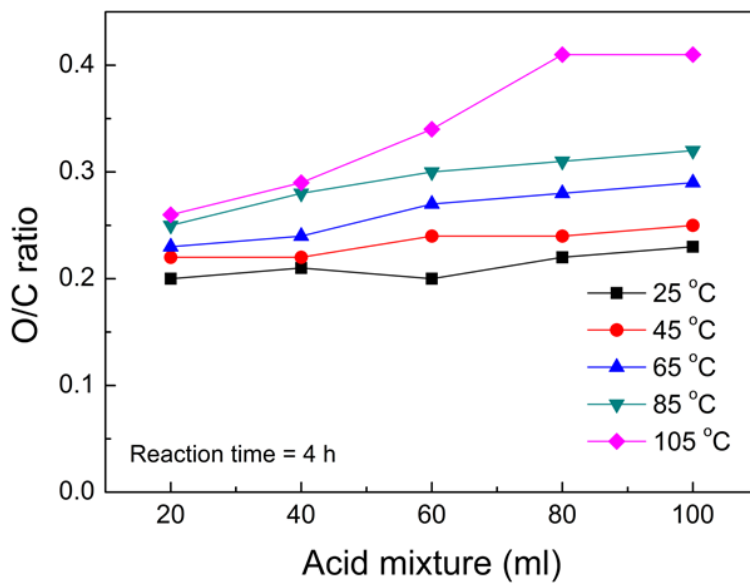


Figure 2.3. O/C ratios of CNTs modified in various conditions.

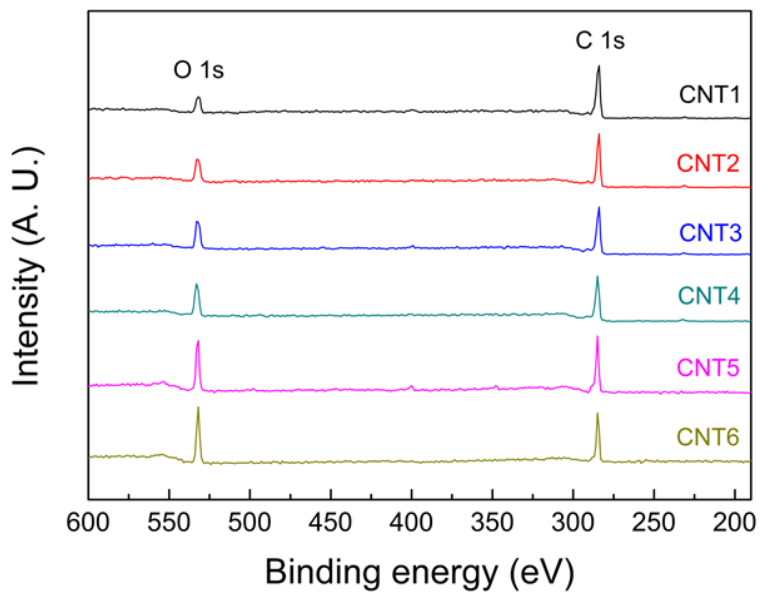


Figure 2.4. XPS spectra of CNTs in Table 2.1.

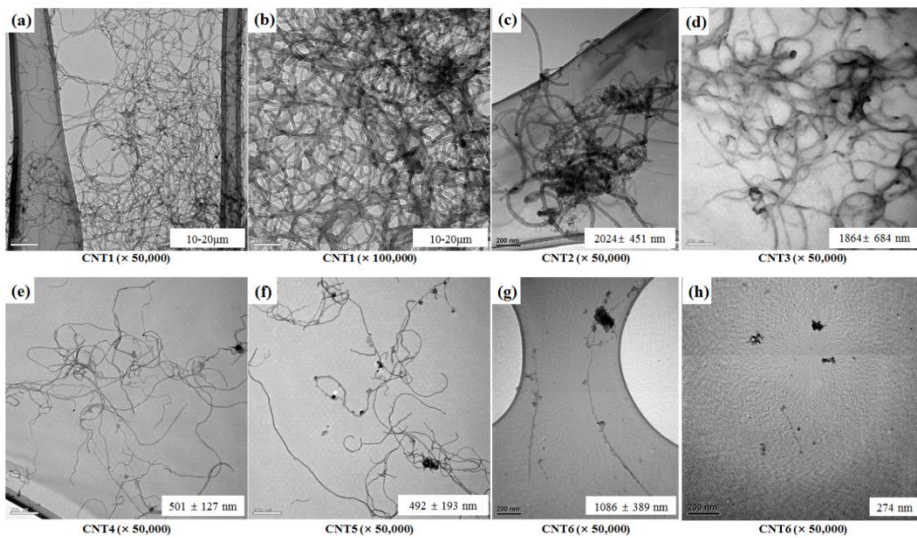


Figure 2.5. TEM images of each CNT treated using the acid mixture at different reaction condition; (a), (b) CNT1, (c) CNT2, (d) CNT3, (e) CNT4, (f) CNT5, (h) and (g) CNT6 (scale bar means 200 nm).

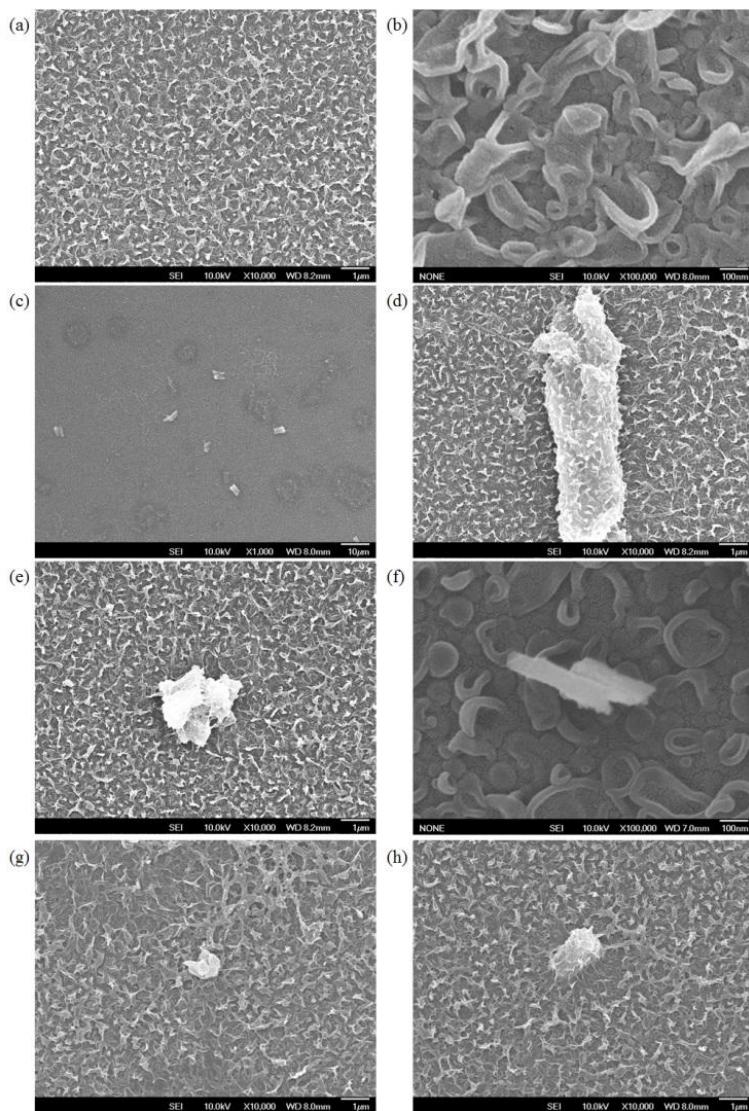


Figure 2.6. TEM images of each CNT treated using the acid mixture at different reaction condition; (a), (b) CNT1, (c) CNT2, (d) CNT3, (e) CNT4, (f) CNT5, (h) and (g) CNT6 (scale bar means 200 nm).

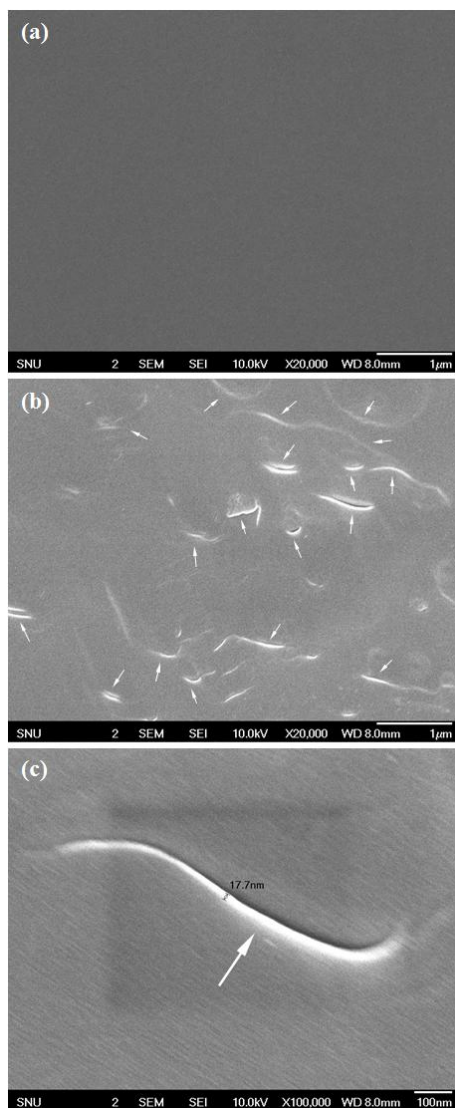


Figure 2.7. SEM images of bottom side of the (a) PA membrane (prepared by 2 wt% of MPD in aqueous solution) (x 20,000), (b) and (c) PA-CNT4 membrane (x 20,000 and x 100,000) (All the PA-CNT membranes were prepared by 2 wt% of MPD and 0.002 wt% of CNT in aqueous solution).

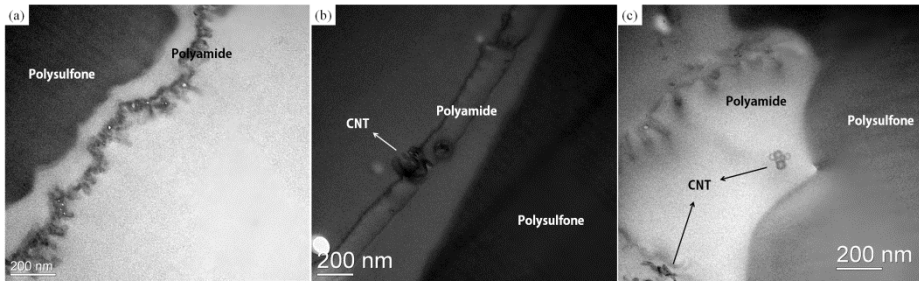


Figure 2.8. TEM images of cross-section of (a) PA, (b) PA-CNT1, and (c) PA-CNT4 membranes.

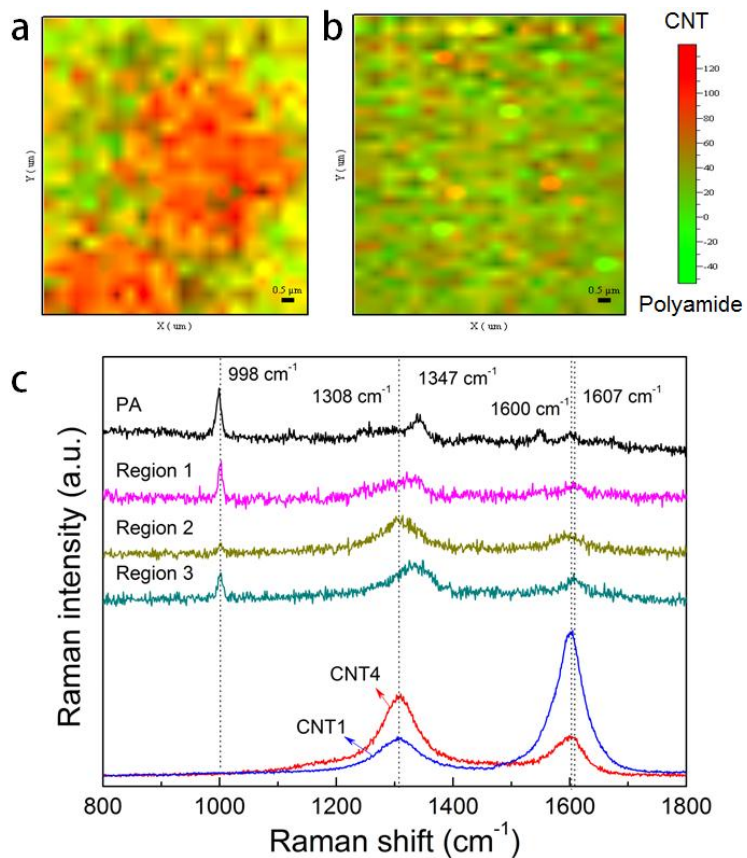


Figure 2.9. Raman spectroscopic mapping images of (a) PA-CNT1 and (b) PA-CNT4 membrane and (c) Raman spectra of polyamide, CNT1, CNT4 and (1), (2) and (3) region in Raman mapping area.

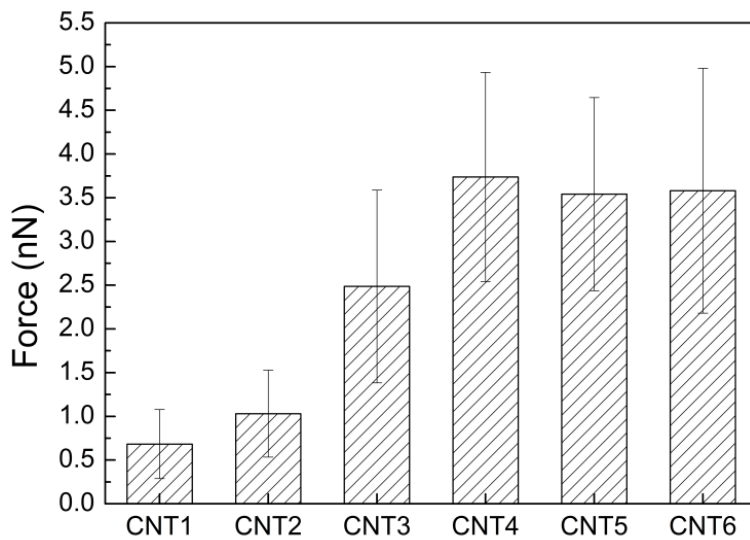


Figure 2.10. The mean interaction forces with standard deviations of polyamide-modified tips for the flat plates of CNT1 to CNT6.

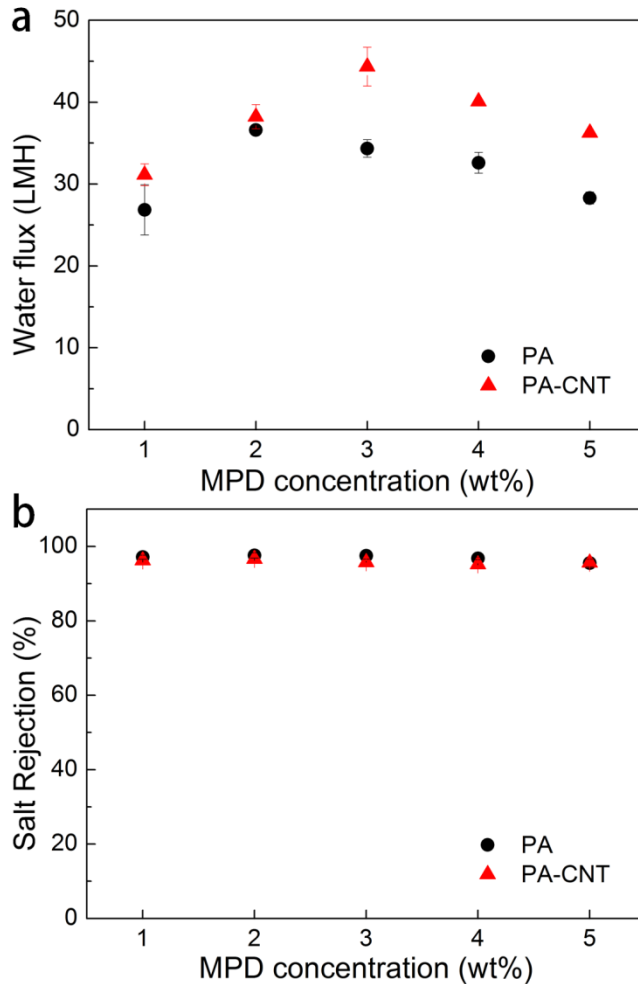


Figure 2.11. (a) Water flux and (b) salt rejection of PA membrane (prepared by 2 wt% of MPD in aqueous solution) and PA-CNT4 membrane (prepared by 2 wt% of MPD and 0.001 wt% of CNT4 in aqueous solution) (tested by cross-flow filtration, 2000 ppm of NaCl feed solution, 15.5 bar of feed pressure, 700 ml min^{-1} of cross flow rate).

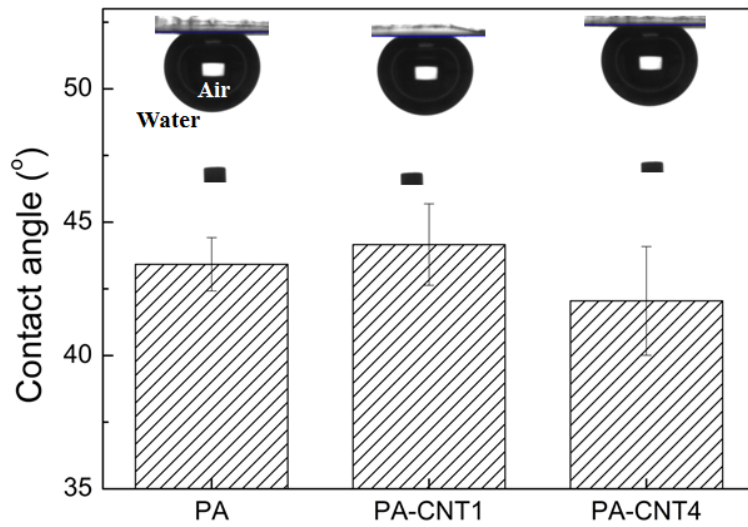


Figure 2.12. Contact angles of PA, PA-CNT1, and PA-CNT4 membranes measured by captive bubble method.

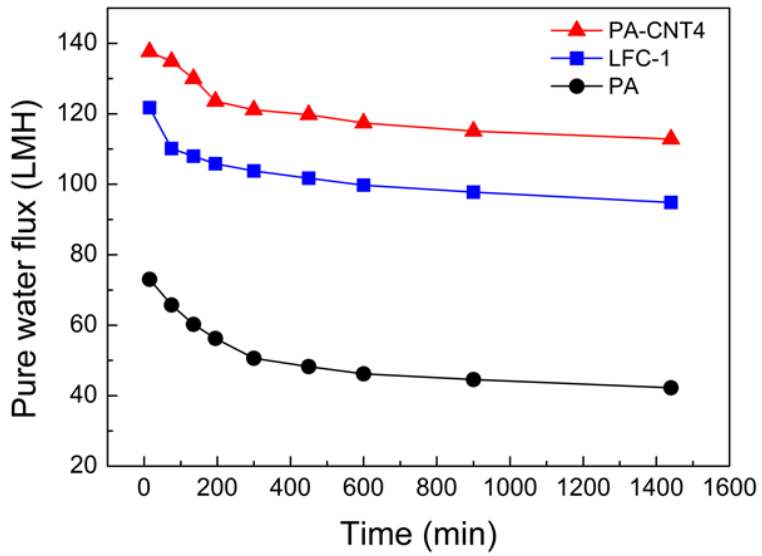


Figure 2.13. Pure water flux of PA and PA-CNT4 membranes with time (operated under the 40 bar of feed pressure).

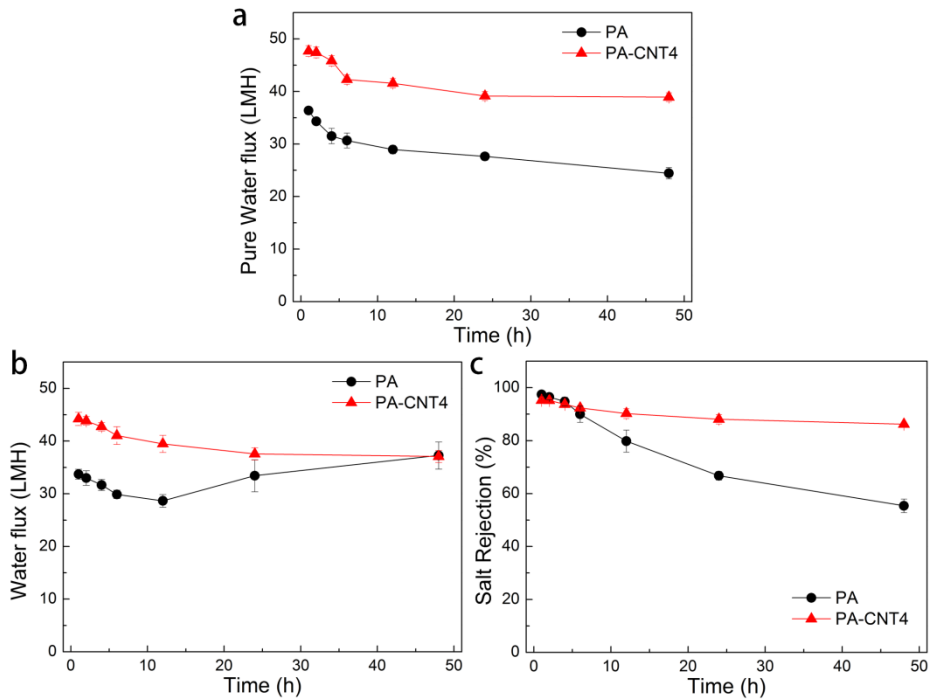


Figure 2.14. Water flux and salt rejection measurement with time: (a) pure water flux, (b) water flux and (c) salt rejection of 2000 ppm NaCl solution of PA membrane (prepared by 2 wt% of MPD) and PA-CNT4 membrane (prepared by 3 wt% of MPD and 0.001 wt% of CNT4) (tested by cross-flow filtration, 2000 ppm of NaCl feed solution, 15.5 bar of feed pressure, 700 ml min^{-1} of cross flow rate).

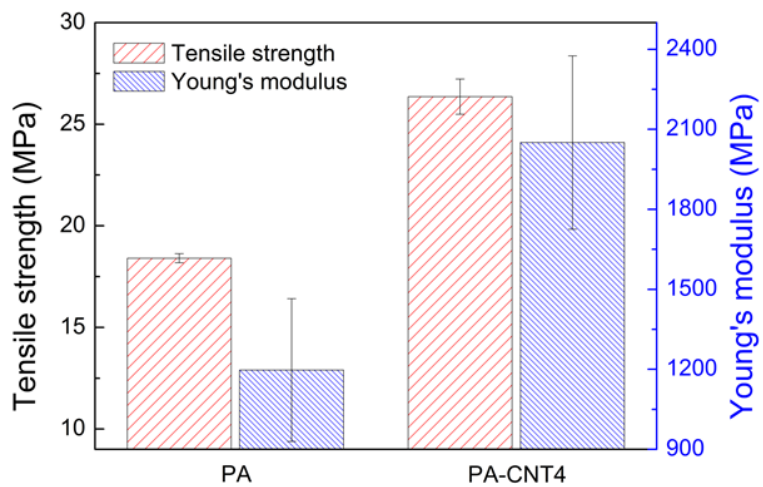


Figure 2.15. Mechanical properties of PA and PA-CNT4 membrane tested by UTM.

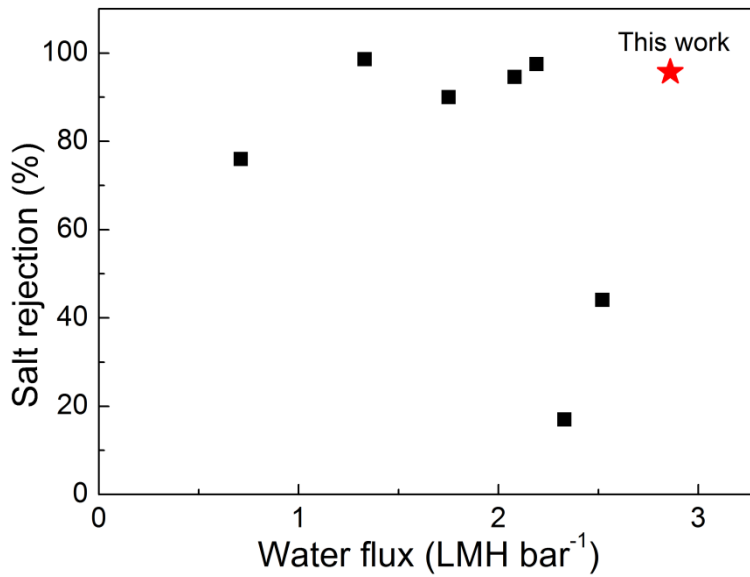


Figure 2.16. Comparison of the result in this work with other results by others for NaCl separation membranes containing CNTs (Detailed information is shown in Table 2.1).

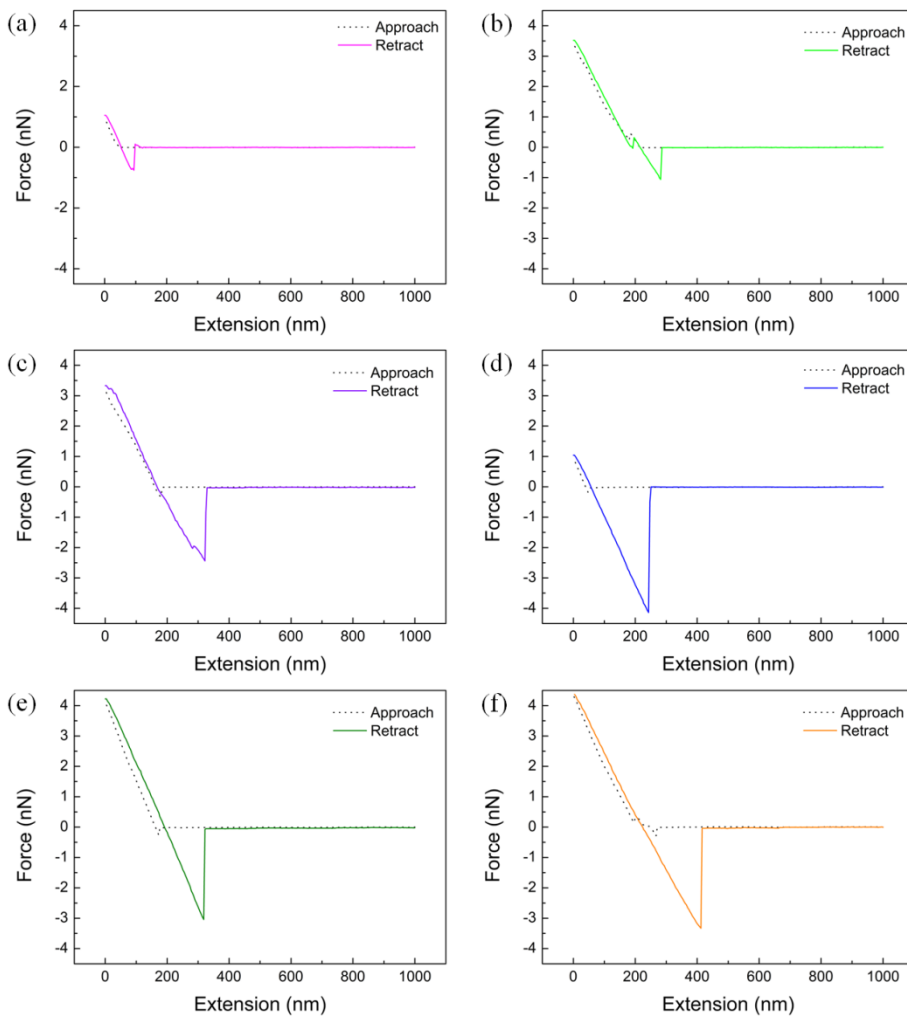


Figure 2.17. Typical force-extension curves recorded with a polyamide-modified tip against various types of CNT; (a) CNT1, (b) CNT2, (c) CNT3, (d) CNT4, (e) CNT5 and (f) CNT6.

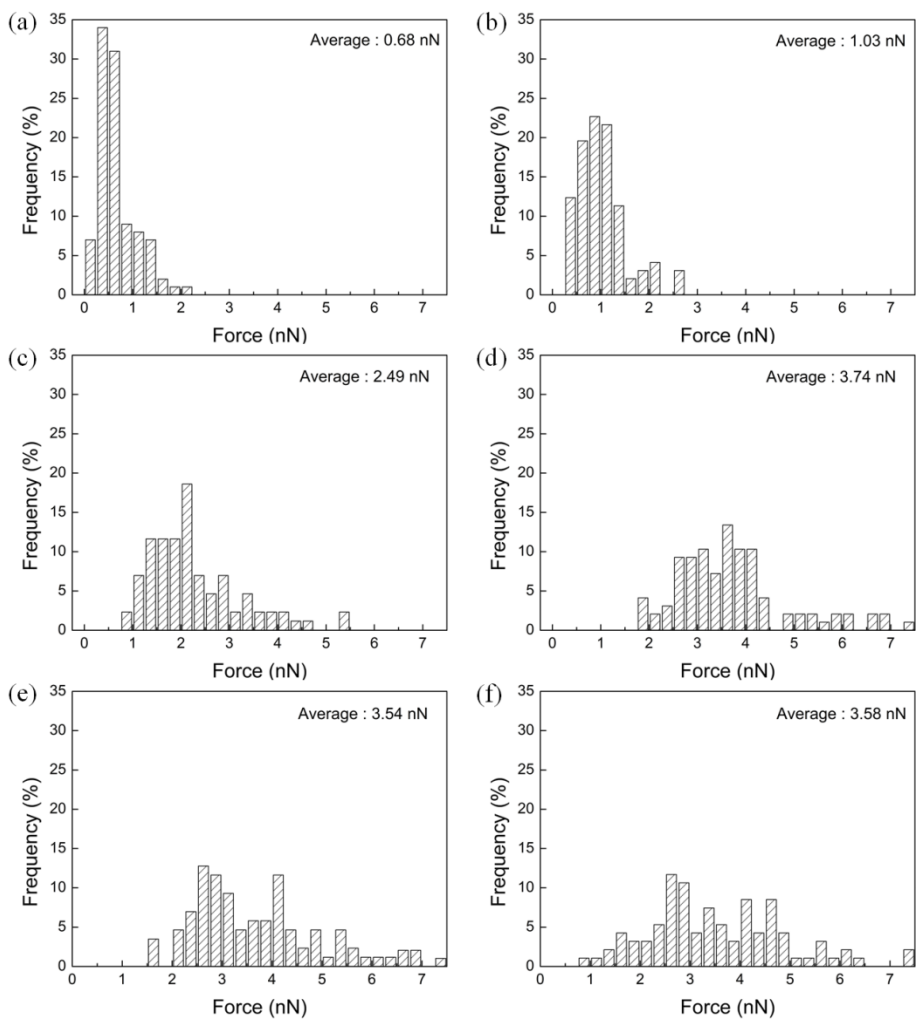
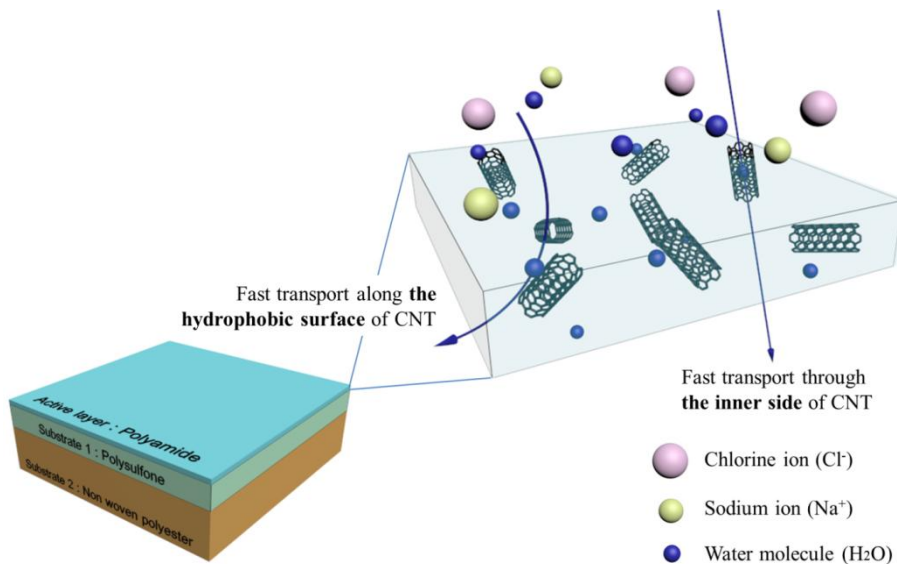


Figure 2.18. Interaction force histograms which were used to determine the mean interaction forces; (a) CNT1, (b) CNT2, (c) CNT3, (d) CNT4, (e) CNT5 and (f) CNT6.



Scheme 2.1. Schematic illustration of the fast transport of water molecules through CNT embedded membrane.

Chapter 3

The Improvement of Antibiofouling Properties of Reverse Osmosis Membrane by Oxidized CNTs

3.1. Introduction

Purification of seawater or waste water by membrane filtration has been widely used to produce fresh water for environmental, chemical and biochemical applications.[1-4] These membrane processes have some advantages such as low operating temperature and high productivity, compared with other purification systems such as thermal distillation and electro dialysis processes.[2] However, membrane fouling is an unavoidable problem in the membrane filtration process resulting in decreased water flux and reduced membrane life time, followed by the increases in operation and maintenance costs.[5] To impart the antifouling properties to the membranes, the membranes have been modified using various of techniques such as blending, surface grafting, and coating methods.[6-14] For example, hydrophilic polymers were coated on hydrophobic membranes because the repulsive forces between hydrophilic polymers and foulants created by favorable water-polymers interactions can impart the antifouling properties into the membranes.[15-18] When the ultrafiltration membranes were coated with the star-shaped polymer having hydrophilic poly(ethylene oxide)

(PEO) moieties, they showed the high antifouling ability against protein and/or oil.[19-22]

Recently, nanocomposites composed of polymeric matrix and nanomaterials have been studied in various areas due to their unique properties of the nanomaterials such as large surface area and a large numbers of functional groups. They are thereby multipotential in the mechanical properties and other functional properties such as antifouling properties of the polymer matrix. For example, nanocomposite membranes containing nanomaterials, such as silver nanoparticle, graphene oxide, and carbon nanotubes (CNTs), have been known to show the antibiofouling properties.[23-29] The antifouling properties of the membranes containing CNTs have been ascribed to the biocidal properties of the CNTs because they can damage the membranes of microorganisms and disrupt the metabolic pathways accompanied by the oxidative stress, then inactivation and/or death of microorganisms can occur.[26,27,30] In addition to the biocidal properties, CNTs have been known to increase the water flux, durability, and antifouling property of the membranes due to their hydrophobic nature and superior mechanical properties.[31-36]

In this study, we prepared polyamide membranes having deposited CNTs coated with poly(vinylalcol) (PVA) on the surfaces, because CNTs can give the antibiofouling properties to the membranes and PVA can increase the stability of CNTs on the surfaces. The biofouling behavior of the polyamide membrane with CNTs and PVA (PA-CNT-PVA membrane) was investigated with *Pseudomonas aeruginosa* PAO1 as a representative biomolecular foulant. The polyamide membrane without any CNTs (PA membrane) and the commercial low-fouling RO membrane (LFC-1 membrane) were included in this comparative study. To the best of our knowledge, it is the first report of biofouling tests of the CNT-membrane using the feed solution containing microorganisms for application in real RO operation systems.

3.2. Experimental

3.2.1. Materials

Multi-walled carbon nanotubes used as carbon nanotube (CNT) materials were received from Nanocyl (Belgium). The supplied

information of CNTs by the company is as follows; the average diameter and average length of CNT are 10–20 nm and 10–20 μm , respectively. Polysulfone (PSf) membranes were received from Woong-jin Chemicals (Republic of Korea) and used for a supporting part of the composite membrane. Sulfuric acid (H_2SO_4 , 98 %), nitric acid (HNO_3 , 60 %), and isopropyl alcohol (IPA) were supplied from Daejung Chemicals (Republic of Korea) and used without any treatment and purification. *m*-Phenylenediamine (MPD, 99 %), trimesoyl chloride (TMC, 98 %), poly(vinylalcol) ($13,000 \text{ g mol}^{-1}$, PVA), and sodium chloride (NaCl, 99 %) were supplied from Aldrich and used without any purification. Deionized (DI) water was obtained from water purification system (Synergy, Millipore, USA), having a resistivity of $18.3 \text{ m}\Omega \text{ cm}$. *n*-Hexane (95 %) was received from Samchun Chemicals (Republic of Korea).

3.2.2. Preparation of oxidized CNTs

The CNTs from Nanocyl were modified using the acid mixture of sulfuric acid and nitric acid (3:1 volume ratio) to impart the functional groups such as carboxylic acid.[33] 0.2 g of pristine CNTs and 90 mL

of the acid mixture solution were placed into 100 mL round-bottom flask equipped with a magnetic stirring bar and the mixture was sonicated for 30 min. Then the flask was placed into an oil bath thermostated at 75 °C with stirring. After 4.5 h of reaction, the solution was cooled to room temperature and diluted with 2.0 L of water. The diluted solution was filtered using anodic aluminium oxide (AAO) filter. The filtered solid was neutralized by pouring water until a neutral pH is attained. The resulting oxidized CNTs on filter were dried in the 35 °C vacuum oven.

3.2.3. Preparation of the PA, PA-CNT-PVA, and PA-PVA membranes

Polysulfone (PSf) membrane was treated using IPA for 10 min to enlarge pores and washed several times with water. The alcohol pretreated PSf membrane was put into the water bath for 3 h to stabilize the pores. 2.0 wt% of MPD aqueous solution and 0.1 wt% of TMC solution in *n*-hexane were prepared for the interfacial polymerization. The pretreated PSf membrane was placed into the bath with 500 g of the MPD aqueous solution. After 3 h, membrane

was taken out and air bubbles and droplets on the PSf membrane surface were removed by rolling a rubber roller. The membrane was fixed on the acryl flat board with rubber mold and aluminium tape. The TMC solution was poured on the PSf membrane saturated with the aqueous solution for the formation of the polyamide active layer by the interfacial polymerization. After 60 s, the excess of TMC solution on the membrane was removed and the membrane was placed in the 100 °C oven for 5 min to induce the further polymerization and crosslinking reactions. Then the resulting membrane, polyamide membrane, was washed with water several times. This membrane was named as PA membrane.

The 0.1, 0.2, or 0.4 g of oxidized CNTs were dispersed in 100 mL of water to prepare the 0.1, 0.2, or 0.4 wt% CNT-dispersed solutions, respectively. The PA membrane was placed between sintered glass filter and glass holder. Afterward, the CNT-dispersed solution was poured on the surface of the polyamide membrane. Then vacuum filtration was performed using high power vacuum pump to form uniformly deposited of CNTs on the polyamide membrane. The CNT-deposited PA membrane was fixed on the acryl flat board and placed into the bath with the aqueous solution containing 0.2, 0.5, or 1.0 wt%

of PVA for 3 h, then membrane was taken out and placed in the 100 °C oven for 10 min to remove residual water in the membrane. The PA membranes with only PVA without any CNTs were also prepared to study the effect of oxidized CNTs and/or PVA on the membrane properties. The PA membrane was coated with 0.2, 0.5, or 1.0 wt% of PVA solution. Then membrane was taken out and placed in the 100 °C oven for 10 min to remove residual water in the membrane. The polyamide membranes with only PVA and with both CNT and PVA were abbreviated as PA-PVA membrane and PA-CNT-PVA membrane, respectively. The PA-PVA and PA-CNT-PVA membranes were further specified as PA-PVA## and PA-CNT#-PVA##, where # and ## indicate the concentrations (wt%) of CNT-dispersed solutions and those of PVA coating solutions, respectively.

3.2.4. Membrane filtration test

Filtration experiments were carried out by lab-scale cross-flow membrane test unit with an effective filtration area of $3.3 \times 6.8 \text{ cm}^2$ with the 0.3 cm of channel height. The pressure was maintained at about 15.5 bar (225 psi) and the feed solution was $2,000 \text{ mg L}^{-1}$ of

NaCl solution (the conductivity values of feed solution was about 3.86 mS cm⁻¹ in this study). These membrane filtration conditions have been generally used in BWRO membrane systems by others.[57,58] Cross flow velocity at the membrane surface was 500 mL min⁻¹ in the filtration system. Water flux was measured by weighing the permeate solution after the membranes were compressed for 1 h at 15.5 bar and permeated water was collected for 2 h. Membrane flux, J , was calculated using equation (1):

$$J = \Delta V / (A \times \Delta t) \quad (1)$$

where ΔV is the volume of permeate collected between two weight measurements, A is the membrane surface area, and Δt is the time between two weight measurements.

Salt rejection was calculated using the following equation (2):

$$R = (1 - C_p / C_f) \times 100 \% \quad (2)$$

where R is the salt rejection parameter, C_p is the salt concentration in permeate, and C_f is the salt concentration in feed. The salt

concentrations were measured using conductivity meter (InoLab Cond 730P, WTW 82362, Weilheim). All membrane performance results shown in Table 3.1 are the average values obtained by more than three measurements from the three membrane samples prepared at different times.

3.2.5. Biofouling experiments

The antibiofouling property of the membranes was evaluated by a lab-scale cross-flow membrane system using the feed solution containing *Pseudomonas aeruginosa* (*P. aeruginosa*) PAO1 tagged with GFP ($150 \mu\text{g mL}^{-1}$) as a model bacterial strain. Nutrients in the feed solution were composed of 0.1 wt% of tryptic soy broth (TSB; Bacto, Franklin Lakes, NJ), 10 mM of sodium chloride, and 10 mM of sodium citrate in 6 L of water. The initial flux, cross-flow velocity, and temperature values used in the lab-scale cross-flow RO experiment were $40 \text{ L m}^{-2} \text{ h}^{-1}$ (LMH), 270 mL min^{-1} , and $25 \text{ }^\circ\text{C}$, respectively. The membrane was compacted by filtering distilled water for 18 h, conditioned by filtering the feed solution for 6 h for the biofilm formation through the bacterial adhesion, and then the flux

changes were monitored to estimate the biofouling progress by filtering the feed solution for 24 h. It is well-known that the biofilms can be easily formed after 6 h contact with the bacterial solutions and the major flux reduction was known to be resulted from the biofilm formation through the bacterial adhesion.[37] Microscopic images were taken by confocal laser scanning microscopy (CLSM, Eclipse 90i, Nikon, Japan) to observe biofouling morphology on the membrane surface after staining with a BacLight Live/Dead bacterial viability kit (Molecular Probes, USA). More details of biofouling test for the adhesion of bacteria on the membranes are described in the previous report.[37]

3.2.6. Characterizations

Raman spectroscope (LabRam ARAMIS, Horiba Jobin-Yvon, France) was used for the analysis of the modification of CNTs. Pristine and oxidized CNTs were dispersed in isopropyl alcohol in sonication bath. The dispersed solution was dropped on the glass plate and then dried in the 35 °C vacuum oven. The excitation source was a diode laser with an excitation wavelength of 785 nm and a power of 5 mW. The

laser excitation was focused using a $\times 100$ objective. The surface compositions of the CNTs and membranes were analysed by X-ray photoelectron microscopy (XPS, PHI-1600) using Mg K α (1254.0 eV) as radiation source. Survey spectra were collected over a range of 0-1100 eV, followed by high resolution scan of the C 1s, O 1s and N 1s regions. Morphology of CNTs was observed by transmission electron microscopy (TEM, LIBRA 120, Carl Zeiss, Germany). 1.0 mg of CNT was dispersed in 1.0 mL of water using sonication bath and then the dispersed solution was dropped on the carbon grid. The grid was dried in the 35 °C vacuum oven over 8 h. For confirmation of the crosslinking reaction, FT-IR spectra of dried membranes were recorded in the attenuated total reflectance (ATR) mode in the frequency range of 4000 - 650 cm^{-1} on a Nicolet 6700 instrument (Thermo Scientific, USA). The spectrum was recorded as the average of 32 scans with the resolution of 8 cm^{-1} . Each sample was put in equal physical contact with the sampling plate of the spectrometer accessory to avoid differences caused by pressure and penetration depth. Surface morphologies of the membranes were inspected by scanning electron microscopy (SEM, JSM-6701F, JEOL) using a field emission scanning electron microscope (FESEM). The mechanical

properties of PA and PA-CNT-PVA membranes were measured by universal testing machine (UTM, LS1SC-150V) with a strain of 10 mm min⁻¹ in air at 23 °C under a 45 % relative humidity. The dumbbell specimens were prepared using the ASTM standard D638 (Type V specimens dog-bone shaped samples). The mechanical properties were measured more than 4 times for each membrane. Surface roughness and morphology of the membrane were measured by atomic force microscope (AFM, Asylum Research, Santa Barbara, CA, USA). A silicon cantilever with a spring constant of 2 N m⁻¹ was used for scanning. The root mean square (RMS) roughness was determined by the scan size of 5 μm by 5 μm of the sample and 600 nm depths.

3.3. Results and Discussion

3.3.1. Preparation of oxidized CNTs

The pristine CNTs were chemically modified by the strong acid mixture of sulfuric acid and nitric acid solutions (3 : 1 volume ratios) to prepare CNTs with acid functional groups. We could conclude that

the acid groups such as carboxylic acid were incorporated on the surface of the CNT through this modification step from the Raman spectroscopy, XPS, and TEM results (Figure 3.1 and 2). In fact, it has been reported previously that such acid treatment can functionalize CNT surface to carboxylic acid groups.[26,38] Since the CNTs were deposited on the surface of the polyamide membrane by the vacuum filtration process using the CNT-dispersed aqueous solution, the dispersion of CNTs in the aqueous solution is very important to obtain the uniform CNT layers on the polyamide membrane. Figure 3.3 shows the TEM images of the 0.1 wt% of CNT dispersed solution, the lowest concentration of CNTs in the aqueous solution used for the formation of CNT layer on the polyamide membrane. If CNTs are well dispersed in this aqueous solution, then it is very possible that CNTs on the polyamide layer can be also well-dispersed. If the CNTs are well-dispersed on the membrane, they can have the large surface area to give the maximum antibiofouling properties to the membrane. TEM image of pristine CNTs shows the bundle morphology with long tube length about 15 μm , while shortened single strands without any entanglements were observed from the oxidized CNTs. Since the oxidized CNTs are very well dispersed in water, we could have

prepared the uniform CNT layer on the polyamide membrane. Although the CNTs were functionalized by the carboxylic acid to produce the aqueous solution having well dispersed CNTs, the PA-CNT-PVA membrane prepared by the deposition of CNTs in the aqueous solution was found to have some CNT bundles on the membrane surfaces. Still the PA-CNT-PVA membrane with the small CNT bundles on the surfaces showed improved membrane stability and biocidal properties as discussed in the next part of this paper.

3.3.2. Preparation of PA-CNT-PVA membranes

Since CNTs are deposited on the membrane surface using filtration method, only the physical interactions are possible between the CNTs with the polyamide layers, then they could be easily detached and flowed out of the membrane during the filtration, then this would result in the decrease of the antibiofouling ability and also the environmental problems in practical applications. To immobilize the CNTs on the membrane, PVA was coated on the CNT-deposited polyamide membrane and heated at 100 °C for the crosslinking reactions of the hydroxy groups of the PVA with the carboxylic acid

groups on CNTs and some of the unreacted carboxylic groups of TMC. It is also possible that the unreacted amine groups in MPD could react with the carboxylic groups to form further crosslinked structures. Figure 3.4 shows the FT-IR spectra of the PA membrane and the PA-CNT-PVA membranes with/without heating at 100 °C. The crosslinking reaction could be confirmed by the disappearance and/or the intensity decrease of the peaks from carboxylic acid (C=O stretch at 1670 cm^{-1} , O-H stretch at 3350 cm^{-1}), hydroxy group (O-H stretch at 3350 cm^{-1}), and amine group (N-H bend at 1538 cm^{-1}). The peaks of amine group and carboxylic acid in the spectrum of the PA membrane indicate the presence of the monomeric structures (MPD and TMC) in the membrane. The peak intensities for carboxylic acid and hydroxy group in the PA-CNT-PVA membrane without heating were found to be larger than those for the PA membrane because the oxidized CNTs and PVA have the carboxylic acid and hydroxy groups, respectively. Additionally, the increase of the intensity for alkane peaks ($\text{sp}^3\text{ C-H}$ stretch at 2976 and 2850 cm^{-1}) was observed after the PVA coating, originating from the ethylene backbone structures of PVA. After the heating process for the crosslinking reaction, the decrease in intensity (and/or disappearance) of carboxylic acid,

hydroxy, and amine group peaks was observed, while the peaks from polysulfone (doublet asymmetric O=S=O stretch at 1298 and 1325 cm^{-1} , and symmetric O=S=O stretch at 1024 cm^{-1}) were observed in all the membranes with very similar intensities. To confirm the crosslinking mediated immobilization of CNTs on the membrane, the cross-flow membrane test for the PA-CNT-PVA membrane was performed using only pure water, to observe any possible detachment of CNTs. After 3 days of filtration, 30 mL of the feed and permeate water were taken in a 50 mL vial and dropped on the TEM grid to observe any CNT detachment. Any CNTs were not observed in either the feed or permeate water, indicating that CNTs were chemically bonded stably with the polymers in the PA-CNT-PVA membrane. However, when the same pure water filtration test was performed using the PA-CNT-PVA membrane without the crosslinking, a few bundles of CNTs were observed in the feed water. The stability of PA-CNT-PVA membrane after the 3 days of filtration test was further confirmed by the XPS analysis of the membranes. The surface composition of the PA-CNT-PVA membrane after 3 days test was found to be almost identical with those of the membrane before the test as shown in Table 3.2. Our TEM and XPS results might not have

sensitivity in detection of very small amounts of CNTs detached from the top surface of the membrane due to their resolution limitations. The CNT detachment from the membrane is a very important issue for the practical application of PA-CNT-PVA membranes and should be addressed in depth. Such study was beyond the scope of this research but is required in future by various instrumental and experimental approaches. Still we strongly believe that the CNT detachment should be minimal because CNTs are covalently bonded with PVA and polyamide on the top layer of the membrane, and more importantly CNTs cannot go through the membrane because the pore size of the RO membranes are much smaller than the sizes of the CNTs used in this study, then the permeated water or the purified water should not contain any CNTs. When we tried to prepare the PA-CNT-PVA membrane using the pristine CNTs without the oxidation, CNTs were not deposited uniformly on the polyamide layer because the pristine CNTs were not dispersed in water. In addition, since pristine CNTs do not have any functional groups such as hydroxy and carboxylic acid, they could not react with hydroxy groups of PVA and/or unreacted amine groups of MPD, then such CNTs could be easily detached from the membrane during the filtration test.

SEM images in Figure 3.5 shows the surface morphology of the PA and PA-CNT-PVA membranes. Typical noodle or ridge-and-valley structures originated from polyamide layers (Figure 3.5a and b) were observed on the surfaces of the PA membrane, as previously reported by others.[39,40] Although the similar noodle structures were observed on $\times 10,000$ SEM image of PA-CNT-PVA membrane (F3c), on higher magnification (the $\times 30,000$) images of the PA and PA-CNT-PVA membranes were found to be quite different. Obviously the CNT deposition by the vacuum process and the PVA coating followed by the heat treatment changed the noodle structure of the PA membrane to a somewhat coagulated noodle structure of the PA-CNT-PVA membrane. In addition to the coagulated noodle structure, bundle structures were also observed in the PA-CNT-PVA membranes. We believe that the bundle structures originated from the oxidized CNT bundles covered by PVA. Similar coagulated images of planer structures were observed from the polyamide membrane deposited by the graphene oxide, as reported by others.[28] The existence of the CNT bundles on the PA-CNT-PVA membrane could also be observed from the optical images (Figure 3.6). Transparent polyamide layers were observed from the PA membrane, while somewhat hazy images

originating from CNT bundles were observed from the PA-CNT-PVA membrane.

Since RO systems are operated under the high pressure (from 15 to 55 bar), the compaction of membranes, causing the decrease of the water flux is commonly observed from most of the RO membranes, as reported by others.[33,41] Therefore, it is very desirable to have RO membranes with high enough mechanical stability to endure the high operating pressure. CNT has been widely used as a filler to improve the mechanical property of the nanocomposites.[41] We also found that the PA-CNT-PVA membrane has improved mechanical properties compared with PA and PA-PVA membranes. For example, the Young's modulus, tensile strength, and stress at break values of PA and PA-PVA membranes were found to be close, while those of PA-CNT0.2-PVA0.2 membrane, where 0.2's indicate the weight percent of CNT and PVA respectively in the aqueous solution used for the membrane preparations, were found to be 85.48, 48.01, and 21.39 % larger than those of the PA membrane (Table 3.3). Therefore the increase of the mechanical strength of the PA-CNT-PVA membrane could be ascribed to the incorporation of CNTs in the membranes. We also measured the mechanical property values of the commercial RO membrane (LFC-1,

received from Hydranautics) for comparison. The mechanical properties of the LFC-1 membrane were found to be even smaller than those of PA membrane possibly because non-woven polyester and polysulfone support used for LFC-1 are different from those used in this study.

3.3.3. Water flux and salt rejection of the PA-CNT-PVA membrane

The water flux and salt rejection values of PA, PA-PVA and PA-CNT-PVA membranes were obtained using the cross-flow filtration system. LFC-1 membrane, the commercialized RO membrane for the filtration of brackish water, was also tested for the comparison. Table 3.1 shows the water flux and salt rejection values of all the membranes. We also tried to observe the effect of the concentrations of the CNT and PVA in aqueous solutions, on the membrane performances. It was found that the water flux values of PA-PVA and PA-PVA-CNT membranes are always smaller than that of PA-membrane, while the salt rejection values of PA-PVA and PA-PVA-CNT membranes are always larger than that of PA-membrane. Therefore PVA coating layers decrease the

water flux, while they increase the salt rejection because the PVA coating can obviously fill some of the possible water channels in the PA layer. When the concentration of the PVA solution was larger than 1.0 wt%, the water flux value was found to be too small to be used as a RO membrane because thick and dense active layers can be formed on the top of the membrane from the quite concentrated PVA solutions. Therefore, the water flux values of PA-PVA1 and PA-CNT0.2-PVA1 membranes are only 5.44 ± 2.65 LMH and 4.15 ± 0.99 LMH, respectively, after 5 h of the operation. We could not obtain the flux value after 2 h because the amount of permeate water was too small to be measured using our equipment. When the concentration of the PVA solution was smaller than 0.05 wt%, we observed the detachment of the CNT from the membrane surfaces, which was confirmed from SEM images of the membrane surfaces and also from the TEM studies of the feed and permeate water after the pure water filtration test. Therefore, 0.05 wt% of PVA solution was not enough to make chemically and physically stable crosslinked structures, while 1.0 wt% of PVA solution makes too thick PVA coated layers to decrease the water flux although quite large salt rejection value could be obtained. When PA-PVA and PA-CNT-PVA membranes were prepared with 0.2

or 0.5 wt% of PVA solution, reasonably large enough water flux and salt rejection values were observed. Thus, 0.2 to 0.5 wt% concentrations of PVA solution were found to be optimum for the preparation of the membranes to use RO membrane application. When the concentrations of CNT were changed from 0.1 to 0.4 wt%, any obvious trends in the water flux and salt rejection values were not observed because CNTs were just deposited on the polyamide layer and do not affect transport of water molecules and ions. When 1.0 wt% of CNT-dispersed solution was used, CNTs were found to be aggregated on the membrane surface forming a chunky structure and the effective PVA coating was not possible because the surface of the membrane became too rough. Furthermore, when the membrane was used for the pure water filtration, CNT detachment was observed. CNTs in the polymeric membrane have been reported to increase the water flux because CNT could provide the hydrophobic water flow channel and/or due to the oxygen functional groups. However, in our study, all the PA-CNT-PVA membranes showed slightly smaller water flux values than the PA membrane, because CNTs were not incorporated within, but just coated on the surface of the polyamide layers. Furthermore, CNTs are crosslinked with the PVA and

polyamide on the surface for the stabilization which even can decrease the water flux. Still, PVA is an imperatively necessary component for the preparation of the PA-CNT-PVA membranes because it can prevent the detachment of the CNTs.

It was also noted that the water flux and salt rejection values of the PA membrane were smaller than those of LFC-1, the commercial RO membrane. Since the LFC-1 membrane was known to be prepared using several ingredients to increase the water flux and salt rejection, direct comparison of the PA membrane and LFC-1 might not be fair. The water flux values of most of the PA-CNT-PVA membrane are also smaller than that of the LFC-1 membrane, while the salt rejection values of the PA-CNT-PVA membrane were quite similar to that of LFC-1. Although the water filtration performances of the PA-CNT-PVA membranes are not better than that of the LFC-1 membrane, antibiofouling properties and long term stability for the feed solutions containing microorganisms were found to be much superior to those of the LFC-1 membrane, as shown in the next part of this chapter.

3.3.4. Antibiofouling properties of the PA-CNT-PVA membrane

The biofouling resistance of the membranes was evaluated from cross-flow membrane filtration using the feed solution containing *P. aeruginosa* PAO1, an oceanic microorganism, as a model of biofoulant. The initial water flux values of all the membranes were controlled with 40 LMH by adjusting the feed pressure because one of the major driving forces inducing the biofouling is the water flow velocity passing on/through the membranes.[42,43] Normalized water permeation flux variations of the PA, PA-PVA, PA-CNT-PVA, and LFC-1 membranes are shown in Figure 3.7. The PA, PA-PVA membranes showed a quite large significant flux-decline after 15 h from the initial filtration, and a further flux-decline was observed after the 24 h of the filtration test. Similar flux-decline behaviour was observed for the LFC-1 membrane. The large flux decline of PA, PA-PVA, and LFC-1 membranes could originate from the interactions between the membrane surface and microorganisms as well as active biofilm formation by the *P. aeruginosa* PAO1 fouled on the membrane surfaces. In contrast, such large flux-decline was not observed from all the PA-CNT-PVA membranes prepared using different CNT and PVA solutions. Therefore the incorporation of CNTs on the surface of

polyamide active layer can impart superior antibiofouling properties to the PA membrane.

It was also found that 0.2 wt% of CNT-dispersed solution was found to be the optimum concentration for the smallest flux-decline, as shown in the Figure 3.7a. 0.1 wt% of CNT-dispersed solution might not be enough amount of CNT on the polyamide layers to impart the effective antibiofouling properties. The CNT-dispersed solution concentration larger than 0.2 wt% was also not as effective as 0.2 wt%. For example when the 0.4 wt% solution was used, the flux-decline was larger than when the 0.2 wt% solution was used. This could be ascribed to the formation of aggregated CNT clusters (Figure 3.8). Since CNTs are aggregated in a size larger than 1 μm , the effective antibiofouling properties of each CNT are not possible. The effect of CNT-dispersed solution concentration on the antibiofouling properties was observed from the PA-CNT-PVA membranes prepared using 0.2 wt% of PVA solutions because the effective antibiofouling property was observed when the PVA solution concentration is smaller than 0.5 wt%, as shown in Figure 3.7b. When the PVA concentration is larger than 0.5 wt% such as 1.0 wt%, larger flux-decline was observed because thicker and denser PVA coating layer could be formed on the

top of the CNT-deposited polyamide layers (Table 3.1). Then the effective antibiofouling properties by the CNTs are not possible because they are mostly covered by PVA materials. The PA-PVA1 and PA-CNT-PVA membranes prepared using 1.0 wt% of PVA solution also showed a very small water flux value although the salt rejection value was largest, due to the formation of thick PVA coating layers. As mentioned previously, if the PVA solution concentration is smaller than 0.2 wt% such as 0.05 wt%, the amount of PVA is not enough to stabilize the CNTs on the polyamide layers by the crosslinking reaction. Therefore the maximum antibiofouling property of the PA-CNT-PVA membranes could be obtained when sufficient amount of CNTs were more or less uniformly dispersed on the polyamide layer and when they were crosslinked using a proper amount PVA (0.2 to 0.5 wt% of PVA solution). In addition, it was found that the PVA concentration does not affect much, if any, the antibiofouling properties of the PA-PVA membranes.

Antibiofouling morphology of the PA, PA-PVA, PA-CNT-PVA, LFC-1 membranes could be confirmed by CLSM after the biofouling experiment, as shown in Figure 3.9. In the CLSM images, green and red spots represent live and dead cells attached on the membrane

surfaces, respectively. The PA, PA-PVA and LFC-1 membranes show dense and thick biofouled layers with large numbers of live *P. aeruginosa* PAO1 and with very small red spots from the dead microorganism formed during the filtration, while the PA-CNT-PVA membrane shows a very thin biofouling layer with small numbers of the live microorganism. The dead cells (red spots) are not easily observed possibly because dead cells do not have enough active forces and/or vitality to be attached on the membrane surfaces, then they could be easily detached by the water flow of feed solute ion with the high pressure applied during the water filtration test. The CNTs exposed on the membrane surfaces should kill microorganisms, and then they are detached by the water flow during the filtration test. The antimicrobial properties of the PA-CNT-PVA membrane were further studied by the cell viability test (Figure 3.10). The cell viability of the PA-CNT-PVA membrane was found to be less than 1 %, while those of PA, PA-PVA and LFC-1 membranes were larger than 80 %. CNTs have been known to have the antimicrobial properties by damaging the membrane of microorganisms, disrupting the metabolic pathway, applying oxidative stresses, and/or changing surface roughness.[26,27,30] In addition to these possible biocidal or

antibiofouling mechanisms by the CNTs, the increase of the hydrophilicity might increase the antibiofouling property of the PA-CNT-PVA membrane compared with PA and PA-PVA membranes. The contact angle value measured by the captive bubble method of the PA-CNT-PVA membrane was found to be smaller than that of PA membrane. The smaller contact angle indicates the increased hydrophilicity in the captive bubble method (Figure 3.11).[44] Although the contact angle value of PA-CNT-PVA membrane is smaller than that of PA membrane, it is close to or even slightly larger than that of PA-PVA membrane. Since PA and PA-PVA membranes do not have any antibiofouling property, the increase of hydrophilicity on PA-CNT-PVA membrane should not affect to the antibiofouling properties in this experiments, as previously reported.⁴² Since there have been reports that surface roughness could change the antifouling properties of the membranes,[32,55] the surface roughness of the membranes were measured by AFM and the results are shown in Table 3.4 and Figure 3.12. All the membranes showed a nano-scale surface roughness, a well-known surface morphology of conventional polyamide membranes from the interfacial polymerization,[32,56] and their root mean square (RMS) roughness values are in the range from

43 to 80 nm. Although the coating process increases the surface roughness, it is not enough to affect the antifouling properties as reported by others.[59,60] Although we do not have a very clear explanation for the excellent biocidal properties of the PA-CNT-PVA membranes, it is very clear that the effective biocidal properties of CNTs can improve the membrane performance during the water treatment test using the microorganism solutions.

3.4. Conclusions

Polyamide membranes with CNTs and PVA coating (PA-CNT-PVA membrane) exhibited the excellent antibiofouling properties in a real filtration system. It was also found that there are optimum amounts of CNTs and PVA that give the reasonably high water flux and salt rejection values with accompanying high antibiofouling properties and durability. When large amounts of CNT were used, the antibiofouling property of the PA-CNT-PVA membrane decreased because of the formation of aggregated CNT clusters. When a large amount of PVA was used, the antibiofouling property was diminished due to a very dense and thick PVA layer, while CNT detachment was

readily observed when very small amounts of PVA were used. The high antibiofouling properties of PA-CNT-PVA membrane were ascribed to the antimicrobial properties of the CNTs, confirmed by the CLSM images of biofouling membrane and cell viability test. Our results clearly show that properly prepared PA-CNT-PVA membranes can manifest the antibiofouling properties for real filtration system with microorganisms without scarifying the water flux and salt rejection properties much if at all. This work will undoubtedly contribute to the latest efforts to develop the RO membranes with the antibiofouling properties and also shows the new antibiofouling test method for the water treatment membranes.

3.5. References

- [1] G. D. Kang and Y. M. Cao, *Water Research* **2012**, 46, 584-600.
- [2] D. Li and H. T. Wang, *J. Mater. Chem.* **2010**, 20, 4551-4566.
- [3] L. F. Greenlee, D. F. Lawler, B. D. Freeman, B. Marrot and P. Moulin, *Water Research* **2009**, 43, 2317-2348.
- [4] M. Elimelech and W. A. Phillip, *Science* **2011**, 333, 712-717.
- [5] J. Mansouri, S. Harrisson and V. Chen, *J. Mater. Chem*, **2010**, 20,

4567-4586.

[6] R. Yang, J. J. Xu, G. Ozaydin-Ince, S. Y. Wong and K. K. Gleason, *Chem. Mater.* **2011**, 23, 1263-1272.

[7] N. Singh, S. M. Husson, B. Zdyrko and I. Luzinov, *J. Membr. Sci.*, **2005**, 262, 81-90.

[8] D. S. Wavhal and E. R. Fisher, *Langmuir* **2003**, 19, 79-85.

[9] Y. H. Zhao, B. K. Zhu, L. Kong and Y. Y. Xu, *Langmuir* **2007**, 23, 5779-5786.

[10] D. E. Suk, T. Matsuura, H. B. Park and Y. M. Lee, *J. Membr. Sci.* **2006**, 277, 177-185.

[11] W. Zhao, Y. L. Su, C. Li, Q. Shi, X. Ning and Z. Y. Jiang, *J. Membr. Sci.* **2008**, 318, 405-412.

[12] B. D. McCloskey, H. B. Park, H. Ju, B. W. Rowe, D. J. Miller, B. J. Chun, K. Kin and B. D. Freeman, *Polymer* **2010**, 51, 3472-3485.

[13] R. Revanur, B. McCloskey, K. Breitenkamp, B. D. Freeman and T. Emrick, *Macromolecules* **2007**, 40, 3624-3630.

[14] J. Hyun, H. Jang, K. Kim, K. Na and T. Tak, *J. Membr. Sci.*, **2006**, 282, 52-59.

[15] P. Harder, M. Grunze, R. Dahint, G. M. Whitesides and P. E. Laibinis, *J. Phys. Chem. B* **1998**, 102, 426-436.

- [16] S. I. Jeon and J. D. Andrade, *J. Colloid Interf. Sci.* **1991**, 142, 159-166.
- [17] S. I. Jeon, J. H. Lee, J. D. Andrade and P. G. Degennes, *J. Colloid Interf. Sci.* **1991**, 142, 149-158.
- [18] A. J. Pertsin and M. Grunze, *Langmuir* **2000**, 16, 8829-8841.
- [19] D.-G. Kim, H. Kang, S. Han, H. J. Kim and J.-C. Lee, *RSC Adv.* **2013**, 3, 18071-18081.
- [20] D.-G. Kim, H. Kang, Y. S. Choi, S. Han and J.-C. Lee, *Polym. Chem-Uk* **2013**, 4, 5065-5073.
- [21] D.-G. Kim, H. Kang, S. Han and J.-C. Lee, *ACS Appl. Mater. Interface* **2012**, 4, 5898-5906.
- [22] D.-G. Kim, H. Kang, S. Han and J.-C. Lee, *J. Mater. Chem.* **2012**, 22, 8654-8661.
- [23] J. Yin, Y. Yang, Z. Q. Hu and B. L. Deng, *J. Membr. Sci.* **2013**, 441, 73-82.
- [24] K. Zodrow, L. Brunet, S. Mahendra, D. Li, A. Zhang, Q. L. Li and P. J. J. Alvarez, *Water Research* **2009**, 43, 715-723.
- [25] M. Ben-Sasson, K. R. Zodrow, G. G. Qi, Y. Kang, E. P. Giannelis and M. Elimelech, *Environ. Sci. Technol.* **2014**, 48, 384-393.
- [26] A. Tiraferri, C. D. Vecitis and M. Elimelech, *ACS Appl. Mater.*

Interface **2011**, 3, 2869-2877.

[27] A. S. Brady-Estevez, S. Kang and M. Elimelech, *Small* **2008**, 4, 481-484.

[28] F. Perreault, M. E. Tousley and M. Elimelech, *Environ. Sci. Technol. Lett.* **2014**, 1, 71-76.

[29] M. S. Rahaman, H. e. i. Th'erien-Aubin, M. Ben-Sasson, C. K. Ober, M. Nielsen and M. Elimelech, *J. Mater. Chem. B* **2014**, 2, 1724-1732.

[30] S. Kang, M. Herzberg, D. F. Rodrigues and M. Elimelech, *Langmuir* **2008**, 24, 6409-6413.

[31] V. Vatanpour, S. S. Madaeni, R. Moradian, S. Zinadini and B. Astinchap, *J. Membr. Sci.* **2011**, 375, 284-294.

[32] E. Celik, H. Park, H. Choi and H. Choi, *Water Research* **2011**, 45, 274-282.

[33] H. J. Kim, K. Choi, Y. Baek, D.-G. Kim, J. Shim, J. Yoon and J.-C. Lee, *ACS Appl. Mater. Interface* **2014**, 6, 2819-2829.

[34] B. J. Hinds, N. Chopra, T. Rantell, R. Andrews, V. Gavalas and L. G. Bachas, *Science* **2004**, 303, 62-65.

[35] J. K. Holt, H. G. Park, Y. M. Wang, M. Stadermann, A. B. Artyukhin, C. P. Grigoropoulos, A. Noy and O. Bakajin, *Science* **2006**,

312, 1034-1037.

[36] G. Hummer, J. C. Rasaiah and J. P. Noworyta, *Nature* **2001**, 414, 188-190.

[37] W. Lee, C. H. Ahn, S. Hong, S. Kim, S. Lee, Y. Baek and J. Yoon, *J. Membr. Sci.* **2010**, 351, 112-122.

[38] J. L. Bahr and J. M. Tour, *J. Mater. Chem.* **2002**, 12, 1952-1958.

[39] A. K. Ghosh, B. H. Jeong, X. F. Huang and E. M. V. Hoek, *J. Membr. Sci.* **2008**, 311, 34-45.

[40] C. L. Kong, M. Kanezashi, T. Yamomoto, T. Shintani and T. Tsuru, *J. Membr. Sci.* **2010**, 362, 76-80.

[41] H. A. Shawky, S. R. Chae, S. H. Lin and M. R. Wiesner, *Desalination* **2011**, 272, 46-50.

[42] Y. Baek, J. Yu, S. H. Kim, S. Lee and J. Yoon, *J. Membr. Sci.* **2011**, 382, 91-99.

[43] T. H. Chong, F. S. Wong and A. G. Fane, *J. Membr. Sci.* **2008**, 325, 840-850.

[44] Y. Baek, J. Kang, P. Theato and J. Yoon, *Desalination*, **2012**, 303, 23-28.

[55] Q. Li, and M. Elimelech, *Environ. Sci. Technol.* **2004**, 38, 4683-4693.

- [56] E. S. Kim, G. Hwang, M. G. El-Din, and Y. Liu, *J. Membr. Sci.* **2012**, 294, 37-48.
- [57] K. P. Lee, T. C. Arnot, T. C., and D. Mattia, *J. Membr. Sci.* **2011**, 370, 1-22.
- [58] H. Huang, X. Y. Qu, H. Dong, L. Zhang, and H. L. Chen, *RSC Adv.* **2013**, 3, 8203-8207
- [59] Q. Li, Z. Xu, and I. Pinnau, *J. Membr. Sci.* **2007**, 290, 173-181.
- [60] K. Boussu, B. Van der Bruggen, A. Volodin, J. Snauwaert, C. Van Haesendonck, and C. Vandecasteele, *J. Colloid Interface Sci.* **2005**, 286, 632-638

Table 3.1. Water flux and salt rejection of the PA, LFC-1, PA-PVA and PA-CNT-PVA membranes tested by cross-flow filtration (2000 ppm of NaCl feed solution, 15.5 bar of feed pressure and 500 ml min⁻¹ of cross flow rate).

	CNT ^a	PVA ^a	Water flux [LMH]	Salt rejection [%]
PA	-	-	35.41±2.37	94.55±1.51
LFC-1	-	-	37.75±1.56	97.05± 0.88
PA-PVA0.2	-	0.2	34.38±3.82	95.84±2.17
PA-PVA0.5	-	0.5	28.91± 3.67	96.87±1.67
PA-PVA1	-	1.0	(5.44±2.65) ^b	(98.62±1.37) ^b
PA-CNT0.1-PVA0.2	0.1	0.2	33.84±2.07	96.54±1.91
PA-CNT0.2-PVA0.2	0.2	0.2	32.40±2.14	96.11±1.11
PA-CNT0.4-PVA0.2	0.4	0.2	34.12±2.52	95.56±1.23
PA-CNT0.2-PVA0.2	0.2	0.2	32.40±2.14	96.11±1.11
PA-CNT0.2-PVA0.5	0.2	0.5	29.81±1.95	96.77±1.27
PA-CNT0.4-PVA1	0.2	1.0	(4.15±0.99) ^b	(98.42±0.51) ^b

^aConcentrations of solution for preparation of membranes. ^bObtained after 5h of the filtration test.

Table 3.2. XPS elemental composition (in at %) of the surface of PA and PA-CNT0.2-PVA0.2 membrane for before and after 3 days of pure water filtration.

	C 1s	O 1s	N 1s	O/C ratio
PA (before filtration)	71.60 ± 0.46	17.40 ± 0.14	11.00 ± 0.55	0.24 ± 0.00
PA (after filtration)	72.54 ± 0.42	17.50 ± 0.23	9.95 ± 0.31	0.24 ± 0.04
PA-CNT-PVA (before filtration)	68.47 ± 1.05	29.28 ± 1.36	2.25 ± 0.84	0.43 ± 0.03
PA-CNT-PVA (after filtration)	68.69 ± 0.37	28.84 ± 1.52	2.46 ± 1.56	0.42 ± 0.02

Table 3.3. Mechanical strength of PA, PA-PVA0.2, PA-CNT0.2-PVA0.2, and LFC-1 membranes.

	Young's Modulus [MPa]	Tensile Strength [MPa]	Stress at Break [MPa]
PA	1197 ± 268	18.4 ± 0.2	14.4 ± 0.4
PA-PVA	1217 ± 218	18.8 ± 0.7	15.1 ± 0.8
PA-CNT-PVA	2221 ± 118	27.3 ± 0.9	17.4 ± 1.9
LFC-1	937 ± 73	17.8 ± 0.6	13.3 ± 2.2

Table 3.4. The root mean square (RMS) roughness of PA, PA-PVA0.4, LFC-1, and PA-CNT0.2-PVA0.2 membranes.

	RMS (nm)
PA	43.7 ± 2.2
PA-PVA0.4	57.9 ± 2.9
PA-CNT0.2-PVA0.2	64.65 ± 1.5
LFC-1	80.4 ± 0.70

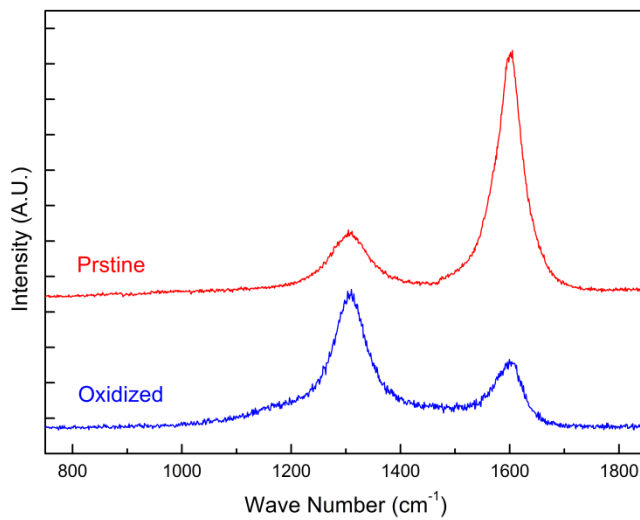


Figure 3.1. Raman spectra of pristine and oxidized CNT.

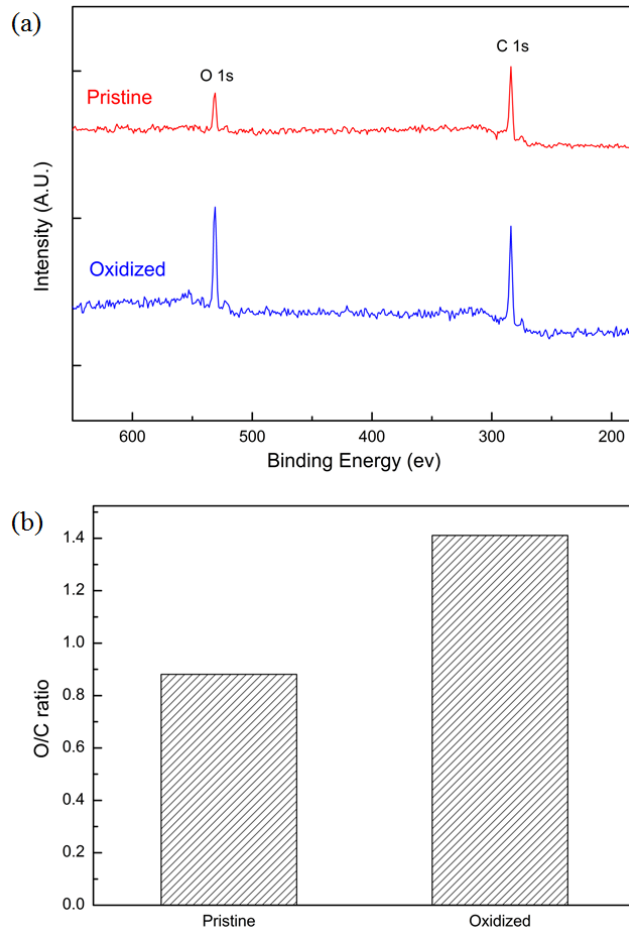


Figure 3.2. (a) XPS spectra and (b) O/C ratios of pristine and oxidized CNT.

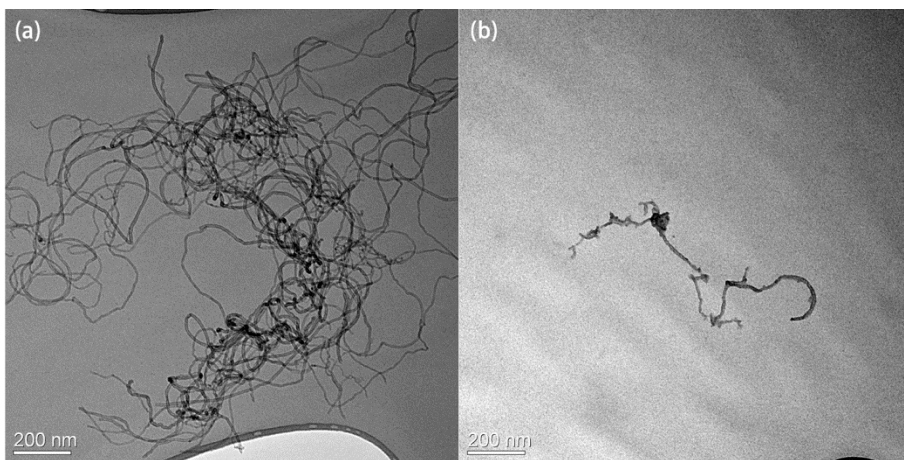


Figure 3.3. TEM micrographs of (a) pristine and (b) oxidized CNTs.

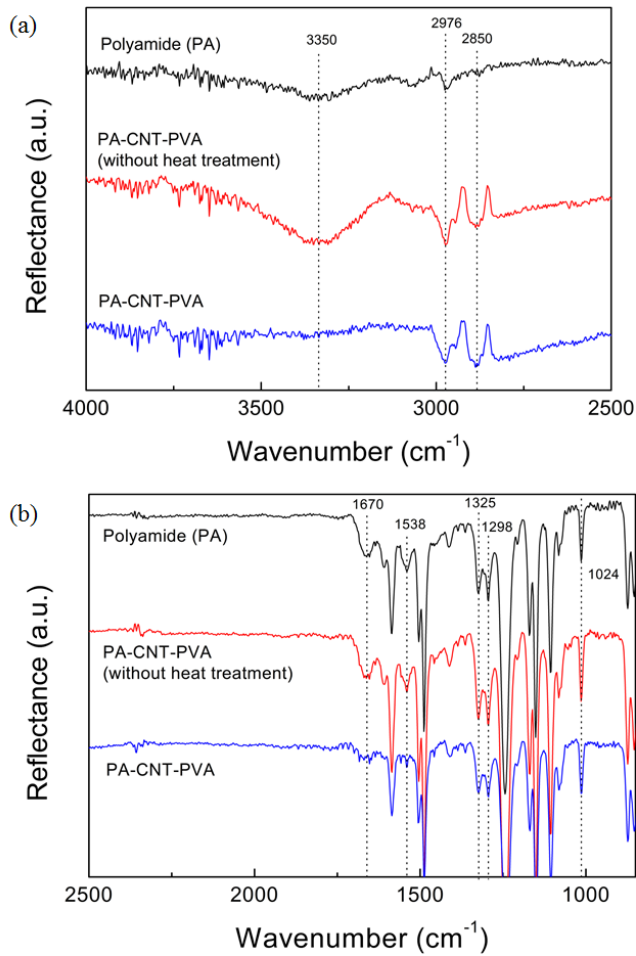


Figure 3.4. FT-IR spectra of PA membrane, PA-CNT0.2-PVA0.2 membrane without heat treatment, and PA-CNT0.2-PVA0.2 membrane; (a) at 4000 - 2500 cm^{-1} and (b) at 2500 - 850 cm^{-1} .

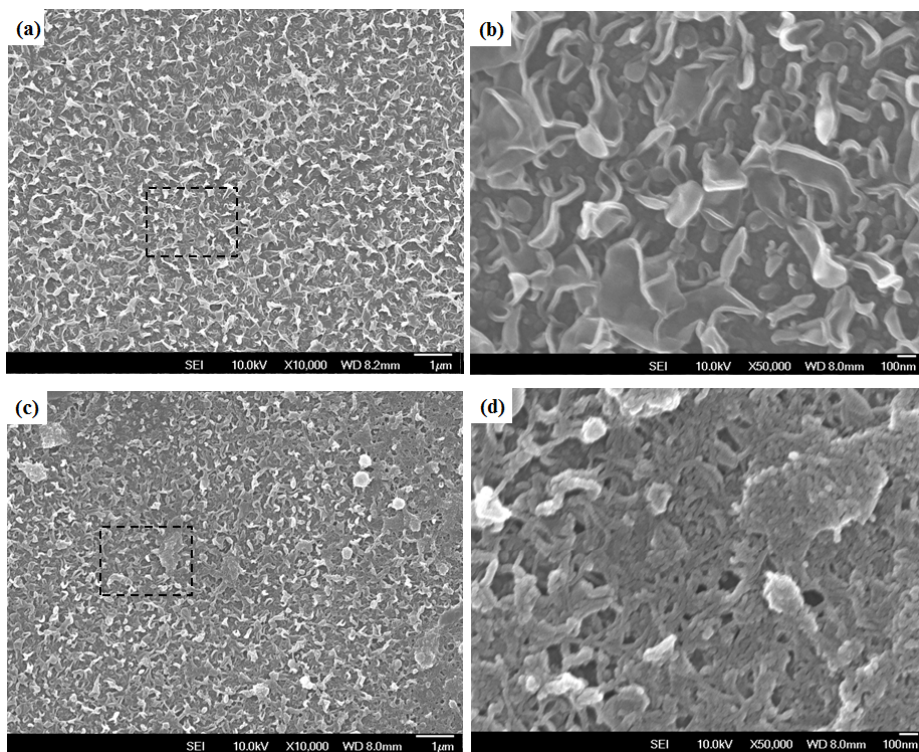


Figure 3.5. SEM images of (a) PA membrane, (b) magnified image of square lined region in (a), (c) PA-CNT0.2-PVA0.2 membrane, and (d) magnified image of square lined region in (c).

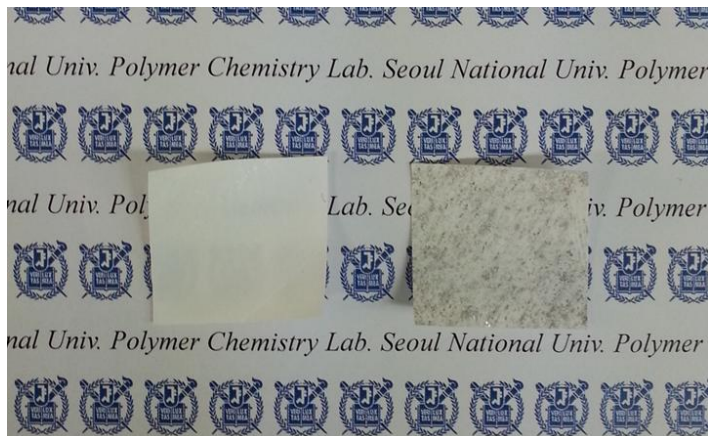


Figure 3.6. Photographs of PA membrane (left) and PA-CNT-PVA membrane prepared by 0.2 wt% of CNT-dispersed solution and 0.2 wt% of PVA solution (right).

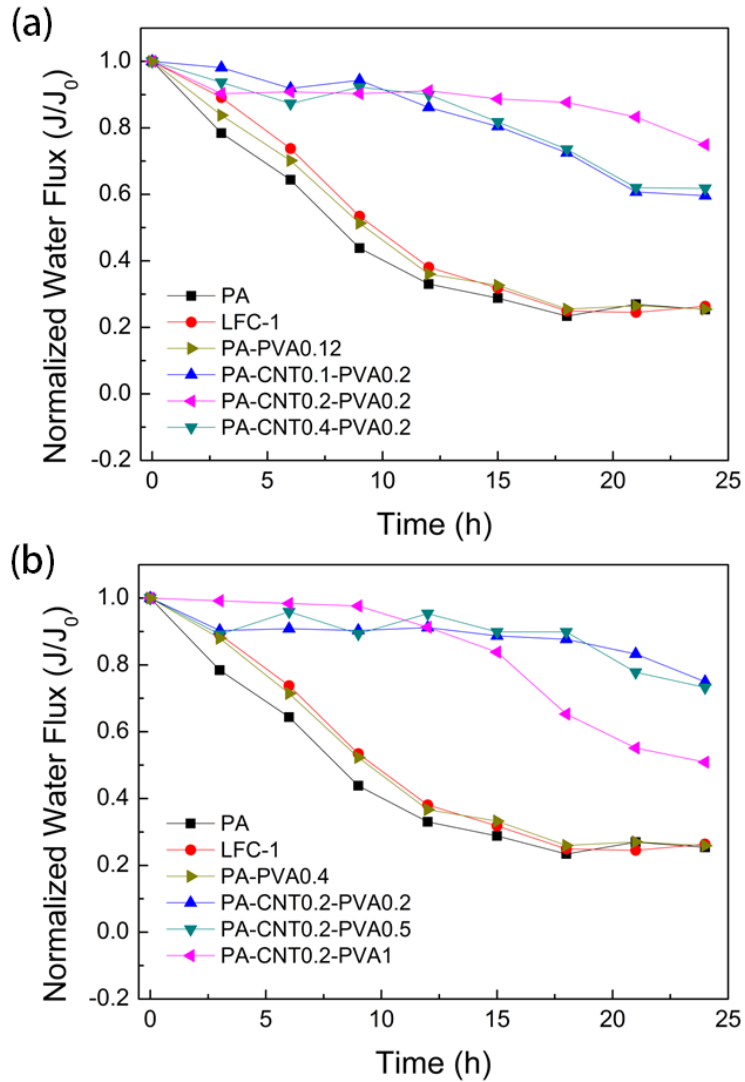


Figure 3.7. Water flux variations of PA, PA-CNT-PVA, and LFC-1 membranes with time obtained by cross-flow filtration using the feed solutions containing *P. aeruginosa* PAO1 at 15.5 bar of feed pressure and 270 mL min⁻¹ of cross flow rate.

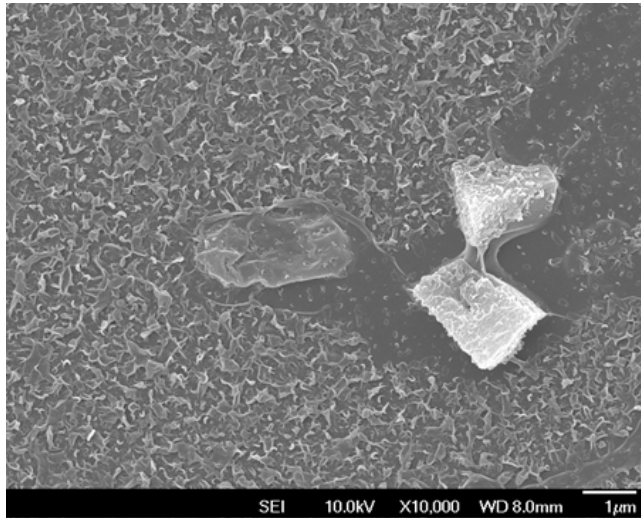


Figure 3.8. SEM images of PA-CNT-PVA membrane prepared by 0.4 wt% of CNT-dispersed solution and 0.2 wt% of PVA solution (PA-CNT0.4-PVA0.2 membrane).

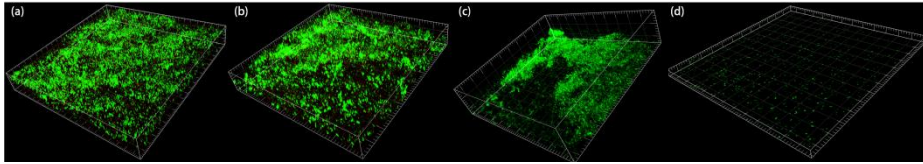


Figure 3.9. CLSM images of (a) PA, (b) LFC-1, (c) PA-PVA0.4, and (d) PA-CNT0.2-PVA0.2 membranes obtained after 24 h cross-flow test using the feed solutions containing *P. aeruginosa* PAO1.

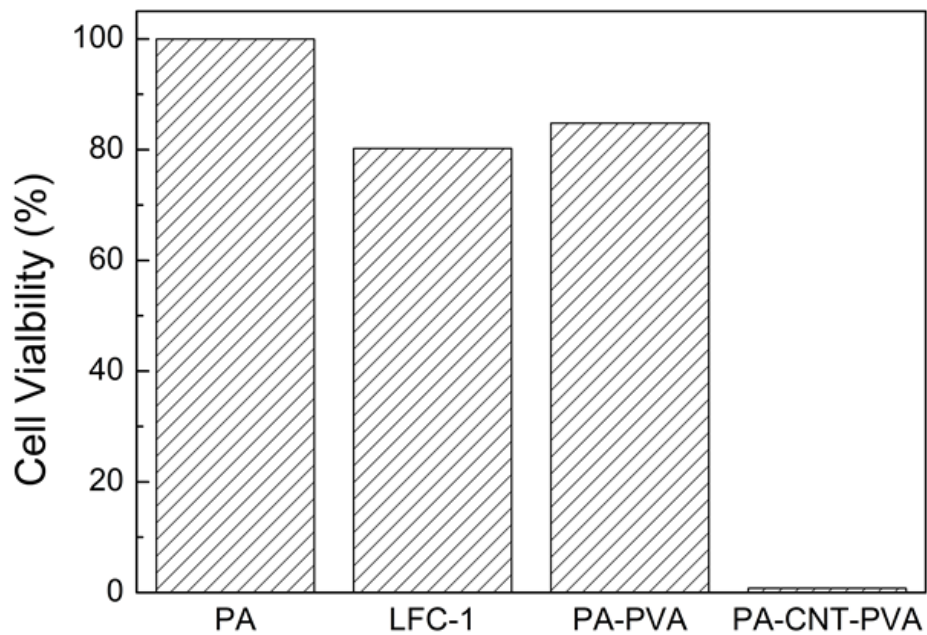


Figure 3.10. Cell viability tests for PA, LFC-1, PA-PVA0.4 and PA-CNT0.2-PVA0.2 membranes, where PA membrane is used as the control standard.

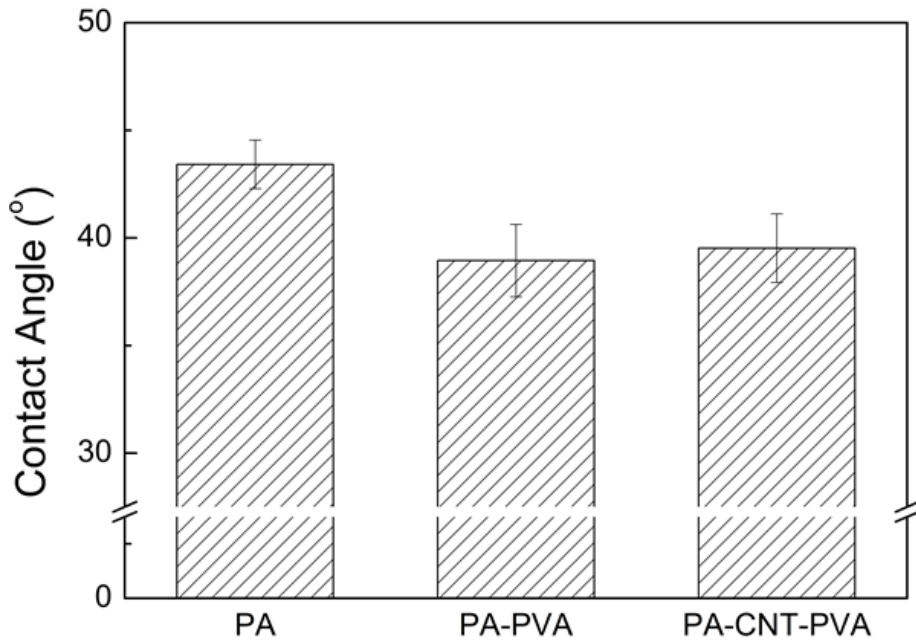


Figure 3.11. Contact angles of PA, PA-PVA0.4, and PA-CNT0.2-PVA0.2 membranes measured by captive bubble method.

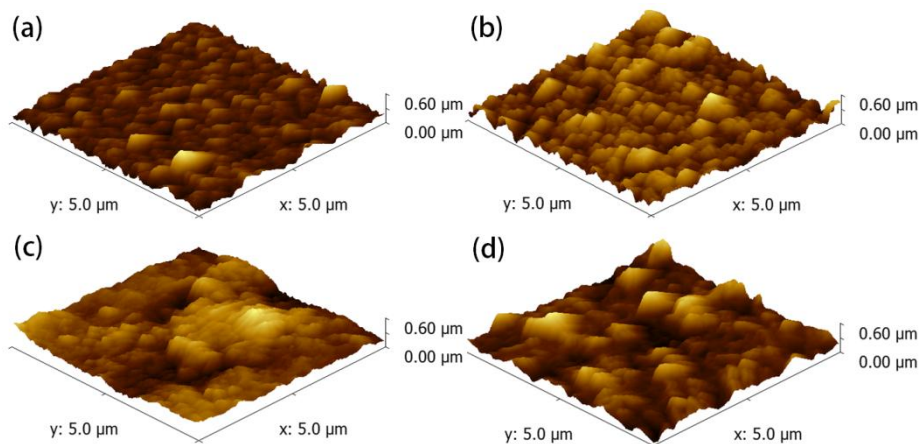


Figure 3.12. AFM images of (a) PA, (b) PA-PVA0.4, (c) PA-CNT0.2-PVA0.2, and (d) LFC-1 membranes.

Chapter 4

High Performance Reverse Osmosis Nanocomposite Membranes Containing the Mixture of Carbon Nanotubes and Graphene Oxides

4.1. Introduction

Desalination, the production of fresh water from sea water or brackish water, has been known to be one of the most important and challenging issues in the environmental engineering and science fields because of the current water shortage problems.[1-8] The number of desalination plants using reverse osmosis (RO) membrane processes have increased over the past several years due to the advantages of membrane processes, such as low operating temperature, low energy consumption, and high production efficiency.[5] Polyamide membranes synthesized from interfacial polymerization have been the most widely used as RO membranes because of their high salt rejection combined with reasonably high water flux.[8] However, they have several disadvantages for desalination processes, such as low chlorine resistance and low antifouling properties, resulting in reduction of the membrane life and decrease of membrane performances such as water flux and salt rejection capabilities.[8,9] Therefore, there is a high requirement for the development of high-flux RO membrane systems with long term stability.[10-12]

Carbon nanotube (CNT) has been widely used as a filler material for

the polymer nanocomposites to impart biocidal properties, thermal stability, and mechanical strength.[13-18] Furthermore, it was recently demonstrated by experimental and simulation results that polymer membranes containing CNTs can have very high water permeability because of the unique hydrophobic surface properties of the carbon nanomaterials.[19-21] Therefore, the polymeric films containing vertically aligned CNTs and polymer nanocomposite membranes having well-dispersed CNTs have been investigated for possible application in water purification systems. Since it is difficult or even impossible to prepare the polymeric membranes with aligned CNTs having large enough effective membrane area, polymer nanocomposite membranes having well-dispersed CNTs has been investigated more widely for possible practical applications.[11,22-26] For example, polyamide RO membranes containing well-dispersed CNTs modified by strong acids or poly(dopamine) showed higher water flux than those without CNTs.[11,23] Modification of the CNTs was a prerequisite for the preparation of polyamide active layers containing well-dispersed CNTs without any aggregated clusters by the CNTs. When the CNTs are well-dispersed in the active layer, the increase of CNT contents causes an increase in the water flux without a decrease of the salt

rejection if any. However, when the CNTs form aggregated clusters in the active layers, the polyamide membranes lose their salt rejection properties because of the large voids formed by the CNT clusters. Therefore, the best RO membrane performance showing very high water flux without losing the salt rejection property could be achieved when the largest amounts of CNTs are well-dispersed in the polyamide active layers.

Graphene oxide (GO) also has been widely studied as one of the important carbon nanofiller materials for polymer nanocomposites due to its extraordinary reinforcing efficiency of the electronic, thermal, and mechanical properties.[15, 27-30] In addition, graphene oxide (GO) can work as a surfactant to increase the dispersion of CNTs in the polymer matrix, as the oxygen functional groups and the hydrophobic carbon structures in GO can increase compatibility with the polar polymers and the CNTs, respectively.[30-34] Therefore, various polymer nanocomposites containing both CNT and GO have been developed and studied regarding applications in batteries, sensors, and electronic device fabrication, as well as membranes.[30-33, 35] Recently, we also found that polyamide RO membranes containing both CNT and GO showed much better membrane performance than those containing only

one of the two. In this chapter, the preparation, physical properties, and membrane performances of polyamide membranes containing both of CNT and GO are described and compared with those of containing only CNT or GO, and those without the inclusion of any carbon nanomaterials.

4.2. Experimental

4.2.1. Materials

Multi-walled carbon nanotubes (CNTs) were purchased from Nanocyl (Belgium). The average diameter and average length of CNT are 10 – 20 nm and 10 – 20 μm , respectively. Graphites were received from BASF (Germany) for used as graphene oxide (GO) precursor. Polysulfone (PSf) membranes were supplied from Woong-jin chemicals (Republic of Korea) and used for a support membrane of the thin film composite membranes. The PSf membrane was composed of two layers, polysulfone and non-woven polyester layer. The commercial membrane for brackish water filtration was received from Hydronautics and its model name is LFC-1 (Low Fouling

Composite). Sulfuric acid (H_2SO_4 , 98 %), nitric acid (HNO_3 , 60 %) and isopropyl alcohol (IPA) were received from Daejung chemicals (Republic of Korea) and used as received. *m*-phenylenediamine (MPD, 99 %), trimesoyl chloride (TMC, 98 %), sodium hypochlorite (NaOCl , 10 – 13 %), 5,5-dimethyl-1-pyrroline-N-oxide (DMPO, for ESR analysis), and sodium chloride (NaCl , 99 %) were supplied from Aldrich and used without any purification. Deionized (DI) water was obtained from water purification system (Synergy, Millipore, USA), having a resistivity of 18.3 $\text{m}\Omega$ cm. *n*-hexane (95 %) was received from Samchun Chemicals (Republic of Korea).

4.2.2. Preparation of CNT containing acid functional groups (CNTa)

The CNTs were modified using the acid mixture of sulfuric acid and nitric acid (3 : 1 volume ratio) to impart functional groups such as carboxylic acid. 0.2 g of raw CNTs was placed in the 250 mL of round-bottom flask with a magnetic stirring bar. The 90 mL of acid mixture solution was added into the flask. Then the flask was placed into the oil bath thermostated at 65 °C with stirring. After 4.5 h of

reaction, the solution cooled to room temperature and diluted with 2.0 L of water. The diluted solution was filtered using anodic aluminium oxide (AAO) filter having 0.2 μm of pore size. The filtered solid was washed by water until a neutral pH is attained. The resulting CNT (CNTa) was dried in the 35 $^{\circ}\text{C}$ vacuum oven.

4.2.3. Preparation of GOs

The graphene oxides (GOs) were prepared through the modified Hummers method.[27, 36] 1.5 g of graphite powders and 0.75 g of phosphorus pentoxide were placed into the 50 mL of round-bottom flask. 9.0 mL of sulfuric acid was added to the flask and the flask was placed into the oil bath thermostated at 85 $^{\circ}\text{C}$. After 5 h of reaction, the reaction solution was diluted with 300 mL of water and filtered using AAO filter. The filtrated solid was dried in the 35 $^{\circ}\text{C}$ vacuum oven over 12 h. 1.0 g of the dried solid (pre-oxidized graphite), 0.5 g of sodium nitrate, and 23 mL of sulfuric acid were placed into the 100 mL round-bottom flask with a magnetic stirring bar. The temperature was controlled at 0 $^{\circ}\text{C}$ by placing into the ice bath for 40 min without stirring. Then 3.0 g of potassium permanganate was carefully added

into the flask and the mixture was heated to 35 °C with stirring. After 2 h, the solution was diluted with 140 mL of water and 10 mL of 30 % hydrogen peroxide. Then the mixture was centrifuged at 10000 rpm for 30 min. The settled solid was washed with ethanol and water, and then filtrated with AAO filter. The resulting solid, GO, was dried in the 35 °C vacuum oven.

4.2.4. Dispersity evaluation

The maximum dispersity of CNTa and/or GO in water was evaluated using previous method reported by Park et al.³⁷ 500 mg of CNTa and/or GO were dispersed in 10 mL of water using bath sonicator for 1 h at room temperature. After dispersion, solution was left for 2 weeks and centrifuged for 30 min at 1000 rpm. The supernatant was filtered using weight-measured AAO filter. Then fully dried AAO filters with CNTa and/or GO were weighed, then the maximum dispersity value could be obtained by comparing the weights of the pristine AAO filter with that of the AAO filter with CNTa and/or GO.

4.2.5. Preparation of the polyamide membranes

with/without carbon nanomaterials

The following procedure was used for the preparation of polyamide membrane without any carbon nanomaterials (PA membrane). Polysulfone (PSf) support membrane was treated with IPA for 10 min to activate pores and washed several times with water. The IPA-treated membrane was placed in the water bath for 3 h to stabilize the pores. The membrane was placed into the bath with 2 wt% aqueous solution of MPD. 0.1 wt% of TMC solution was prepared in *n*-hexane. After 3 h, the membrane was taken out and air bubble and droplet of aqueous solution on the membrane surfaces were removed carefully by air knife. The membrane was fixed on the acryl flat board with a rubber mold. The TMC solution was poured on the membrane saturated with aqueous solution. After 60 s of reaction, the excess of TMC solution was removed and the membrane was placed in the 100 °C oven for 5 min for crosslinking as well as further polymerization. The resulting membrane was washed with water several times. The polyamide membranes containing CNTa (PA-CNTa membranes), GO (PA-GO membranes), and the mixture of CNTa and GO (PA-CNTa/GO membranes) were prepared using the same procedure for PA

membrane except the composition of aqueous solution containing 3 wt% of MPD and 0.0002 to 0.3 wt% of CNTa, GO, and CNTa/GO mixture in aqueous solution. All the membranes were prepared in the fume-hood at room temperature.

4.2.6. Membrane filtration test

Water flux and salt rejection values were measured by the lab-scale cross-flow RO membrane test unit. The effective membrane area was $3.3 \times 6.8 \text{ cm}^2$ with the 0.3 cm of channel height. The pressure was maintained at about 15.5 bar (225 psi) and the $2,000 \text{ mg L}^{-1}$ of NaCl solution was used as a feed solution (the conductivity of feed solution was about 3.84 mS cm^{-1}). Cross flow velocity at the membrane surface and the temperature were controlled to 500 mL min^{-1} and $25 \text{ }^\circ\text{C}$, respectively in the cross-flow system. This test condition has been generally used for measuring the performance of the BWRO membranes by others.[10, 38-40] Water flux was measured by weighing the permeate solution after the membranes were compressed for 1 h at 15.5 bar. Water flux, J , was calculated using equation (1):

$$J = \Delta V / (A \times \Delta t) \quad (1)$$

where ΔV is the volume of permeate collected between two weight measurements, A is the membrane surface area, and Δt is the time between two weight measurements.

Salt rejection was calculated using the following equation (2):

$$R = (1 - C_p / C_f) \times 100 \% \quad (2)$$

where R is salt rejection parameter, C_p is the salt concentration in permeate, and C_f is the salt concentration in feed. The salt concentrations were measured using conductivity meter (InoLab Cond 730P, WTW 82362, weilheim). All membrane performance results in this chapter are the average values obtained by more than three measurements from the three membrane samples prepared at different times to confirm the reproducibility.

4.2.7. Characterizations

Morphologies of CNT and GO were observed by transmission electron microscopy (TEM, LIBRA 120, Carl Zeiss, Germany). 1 mg of CNT or GO was dispersed in 50 mL of water using sonication bath and then the dispersed solution was dropped on the TEM grid. The grid was dried in the 35 °C vacuum oven over 12 h. Raman

spectroscope (LabRam ARAMIS, Horiba Jobin-Yvon, France) was used to observe the damaged crystalline structure of CNT and GO surfaces. Raman spectroscopic mapping was carried out to observe the spatial distribution of CNT and GO in the polymeric membrane using the same device. Since fluorescences from PSf layer disturbs the detection of Raman scattering, thin active layer of membranes was transferred to silicon wafer. The excitation source was a diode laser with an excitation wavelength of 785 nm and a power of 5 mW. The laser excitation was focused using a 100× objective and the Stokes-shifted Raman scattering was recorded using a 1400/600 groove min^{-1} grating. Raman mapping image was collected within a $10 \times 10 \mu\text{m}^2$ area of active layer of the membrane on silicon wafer. The Raman mapping image was obtained by integrating the area of characteristic peaks from polyamide, CNT, and GO. The surface compositions of the CNT and GO were analyzed by X-ray photoelectron microscopy (XPS, PHI-1600) using Mg $K\alpha$ (1254.0 eV) as radiation source. Survey spectra were collected over a range of 0–1100 eV, followed by high resolution scan of the C 1s and O 1s regions. The UV-Vis spectrum was measured by Agilent 8453 UV-Visible Spectrometer at room temperature. Zeta potential values of CNTa, GO, and the mixture of

CNTa and GO dispersed solution were measured by electrophoretic light scattering spectrophotometer (ELS-8000) to investigate of colloidal stabilities. Highly concentrated solution, 50 mg mL⁻¹ of carbon nanomaterials dispersed in water, was used because the device has a limitation on detecting intensity. Fourier-transform infrared (FT-IR) spectra of CNT and GO were measured in transmission mode in the frequency range of 4000–650 min⁻¹ on a Nicolet 6700 instrument (Thermo Scientific, USA). FT-IR spectra of dried membranes were recorded in attenuated total reflectance (ATR) mode in the frequency range of 4000–650 min⁻¹ on a Nicolet 6700 instrument (Thermo Scientific, USA). The spectrum was collected as the average of 32 scans with the resolution of 8 cm⁻¹. Each membrane sample was put in equal physical contact with sampling plate of the spectrometer accessory to avoid difference caused by pressure and/or penetration depth. Surface morphologies of the membranes were inspected by scanning electron microscopy (SEM, JSM-6701F, JEOL) using a field emission scanning electron microscope (FESEM). The mechanical properties of the membranes were measured by universal tensile testing machine (UTM). The dumbbell specimens were prepared using the ASTM standard D638 (Type V specimens dog-bone shaped

membrane samples). Thermal gravimetric analysis (TGA) was performed in a Q-5000 IR from TA Instruments, using a heating rate of 10 °C /min under the air atmosphere. The investigation of radical scavenging effect of the CNT and GO was performed using electron spin resonance (ESR) spectrometer (JEOL, JES-TE200). The production of free radicals from sodium hypochlorite was monitored in the presence of the spin trap agent DMPO. The membrane active layer was soaked in the solution containing sodium hypochlorite (500 ppm) and DMPO (2 ppm), and then the ESR spectrum was obtained in every 10 min.

4.3. Results and Discussion

4.3.1. Preparation of CNT having acid functional groups (CNTa) and GO

Since the polyamide nanocomposite membranes are prepared by the interfacial polymerization reaction using the aqueous solution of MPD and the organic solution of TMC, CNT should be well-dispersed either in the aqueous solution or the *n*-hexane solution to be incorporated.[41]

To disperse CNT in *n*-hexane, aliphatic hydrocarbon chains should be attached on CNT, while it needs several reaction steps with several purification procedures.[42-44] In contrast, if CNT is treated with strong acids by a one-step reaction, it could be well-dispersed in the aqueous solution.[43] Therefore, in present study, pristine CNT was modified using the strong acid mixture of sulfuric acid and nitric acid (volume ratio of 3 to 1) to prepare CNT with acidic functional groups (CNTa), following the procedure reported before.[11, 43] We previously found that when 1 g of CNT was reacted with 300 mL of the acid mixture at 65 °C for 4.5 h, it could be well-dispersed in the aqueous solution of MPD. Consequently, when RO membrane was prepared using the aqueous solution containing 0.001 wt% of CNT, maximum membrane performance was obtained.[11] The successful incorporation of oxygen functional groups, such as carboxylic acid and hydroxyl groups into CNT through the modification process could be confirmed by XPS analysis, Raman spectroscopy, and FT-IR (Table 4.1, Figure 4.1, 4.2, and 4.3). CNT was also observed to become shorter, and the entanglements of the CNTs disappeared by the acid treatment process (Figure 4.4a and b). GO was prepared to have oxygen functional groups, such as epoxy, carbonyl, hydroxyl, and

carboxylic acid groups, by the modified Hummer's method.[27, 36] The successful synthesis of GO was confirmed by XPS analysis, Raman spectroscopy, and FT-IR analysis (Table 4.1, Figure 4.1, 4.2, and 4.3). The TEM images in Figure 4.4c and d show the thin layer structure of GO formed by the exfoliation of graphite. The dark-stacked structures are observed from graphite, while the light grey-planer image is observed from GOs demonstrating single or a few layers. The CNTa and GO having the oxygen functional groups are expected to be well-dispersed in the aqueous solutions as well as in the polyamide active layer due to the hydrogen-bonding and/or dipole-dipole interactions as reported before.[11, 45]

4.3.2. Dispersion evaluation

Table 4.2 shows the maximum dispersity of the carbon nanomaterials in water. The maximum dispersity value of the CNTa/GO mixture was found to be larger than those of CNTa and GO in all cases. It is well known that the dispersion of CNT in the aqueous solution can be improved by adding GO because GO can work as a surfactant through the interactions with CNT by hydrogen bonding, π - π interactions, and

van der waals forces.[30, 33, 34] In addition, when CNTa and GO co-existed in the aqueous solution, the individual formation of the tubular bundled structure of CNTs and the sheet-stacked structure of GOs could be disturbed by forming multi-dimensional nanostructures.[32] Since the CNTa/GO mixture in 7 to 3 (CNTa to GO) ratio showed the largest maximum dispersity value, it was used for further dispersity analysis and the preparation of PA-CNTa/GO membranes. Previous studies also reported that the mixture showed the highest dispersity behavior when the CNT to GO ratio of 2 to 1 was used, because thermodynamically stable structures could be formed at that ratio.[33]

For quantitative analysis of the dispersion behavior, UV-Vis absorbance spectroscopy of CNTa, GO, and CNTa/GO dispersed solution was observed, as shown in Figure 4.5a to c. The absorptions observed at 230 and 300 nm could be ascribed to the $\pi - \pi^*$ transition and n- π^* transition, respectively. The absorption intensity at 230 nm was found to be larger than that at 300 nm because the electron transition from π to π^* is much more predominant than that from n to π^* in most compounds.[37] Therefore, the 230 nm peak showing the maximum intensity can be assigned as λ_{\max} . The intensity of λ_{\max} at 230 nm of the CNTa/GO mixture was found to be larger than those of

CNTa and GO individually, indicating that the CNTa/GO mixture is more well-dispersed in the aqueous solution than the solutions containing CNTa or GO only. The changes in absorption intensity at different concentrations are shown in Figure 4.5d, for which the slope could be assigned to the absorptivity (ϵ) in the Beer-Lambert law ($A = \epsilon l c$), where A is the measured absorbance, ϵ is the absorptivity, l is the path length of UV-Vis light, and c is the solution concentration. As expected, CNTa/GO showed the largest absorptivity (ϵ) value, and the very large absorptivity value has been known to indicate the excellent dispersion of the carbon nanomaterial.[37]

Figure 4.6 shows the zeta potential behavior of the carbon nanomaterials (500 mg in 10 mL) used in this study. Zeta potential values have been correlated with the colloidal stability of the particles in water; potentials of ± 10 to ± 30 , ± 30 to ± 40 , ± 40 to ± 60 , and $> \pm 60$ mV have been assigned to indicate incipient, moderate, good, and excellent stable colloidal states, respectively.[46,60] Therefore, the zeta potential values of CNTa, GO, and the CNTa/GO mixture of about -36 ± 6.2 mV, -58 ± 7.5 mV, and -60 ± 9.5 mV, respectively, can be assigned to the moderate, good, and excellent stable states, respectively. Negative zeta potentials were observed due to the oxygen

functional groups of carbon nanomaterials in this study. In addition to the maximum dispersity and UV-vis spectroscopy studies, the zeta potential behavior also indicated that CNTa/GO shows much better dispersion in water than CNTa or GO only. Since the CNTa/GO mixture is more well-dispersed in the aqueous solution than CNTa and GO alone in the solutions, it is expected that there are less amount of aggregated particles in the CNTa/GO solution than CNTa and GO solutions. Then CNTa/GO should have the larger surface area and smaller particle size than CNTa and GO, resulting in large zeta potential value of CNTa/GO solution. In this regard, it is also very possible that CNTa/GO would be more well-dispersed in the polyamide active layer in the membrane because the polyamide layer is prepared from interfacial polymerization using the MPD aqueous solution containing the carbon nanomaterials. The state of CNTa/GO in the polyamide matrix could be confirmed to be well-dispersed or aggregated by the SEM, TEM and Raman studies, shown in the next part of this chapter.

4.3.3. Preparation of polyamide membranes with/without the carbon nanomaterials

PA, PA-CNTa, PA-GO, and PA-CNTa/GO membranes were prepared by the typical interfacial polymerization method used for the preparation of other RO membranes except that CNTa, GO, or CNTa/GO was included in the MPD aqueous solution. The PA membrane was prepared using 2 wt% MPD aqueous solution without any carbon nanomaterials. The PA-CNTa, PA-GO, and PA-CNTa/GO membranes were prepared using 3 wt% MPD aqueous solution as this concentration showed maximum water flux and salt rejection values, while the PA membrane showed optimal performances at 2 wt% MPD aqueous solution (Table 4.3). Previously, 2 and 3 wt% of MPD were also found to be the optimized concentrations to obtain high-water flux PA and PA-CNTa membranes, respectively.[11] It is generally accepted that the monomer ratio for interfacial polymerization could determine the cross-linking density, polarity, and polymer structure, which affect the membrane performances.[40, 47] It is also possible that the oxygen functional groups on CNTa and GO could form salt structures and/or hydrogen bonding with amine groups of MPD during the interfacial polymerization. Then, a slightly larger amount of MPD would be needed to prepare the polyamide membranes with carbon

nanomaterials to allow maximum water flux and salt rejection properties due to complexing of some of the amine groups of MPD with the functional groups of CNTa and GO.

The formation of the polyamide active layer was confirmed by FT-IR analysis (Figure 4.7). Characteristic peaks from the polyamide structures were observed at 1540 cm^{-1} (N-H bend), 1608 cm^{-1} (NH-CO vibration), and 3397 cm^{-1} (O-H and N-H stretch) for the PA, PA-CNT, PA-GO, and PA-CNT/GO membranes. The characteristic peaks from the carbon nanomaterials could not be clearly detected because their content in the polyamide layers are too small; In the 3 wt% MPD aqueous solutions only 0.0002 to 0.03 wt% of carbon nanomaterials were used, making the content of carbon nanomaterials in the polyamide layer smaller than 1.0 wt%.

The morphologies of the PA and PA-CNTa/GO membranes and the dispersion of CNTa/GO in the polyamide active layer were observed by SEM and TEM. Figure 4.8a shows the SEM images of the top surface of the PA membrane. The typical ridge-and-valley structures were observed, indicating the successful formation of polyamide active layer. Since the densities of CNT and GO are larger than water, most of the mixtures of CNTa and GO sank into the bottom/inner part

of the active layer during the membrane preparation procedure. Therefore, only a small amount of CNTa/GO was observed on the top surface of the PA-CNT/GO membrane (Figure 4.8b). The embedment of CNTa and GO at the inner/bottom part of the active layer was confirmed by SEM images taken of the bottom part and cross-sectional TEM images. Fig 4c and d show SEM images of the bottom part of the active layers of PA and PA-CNTa/GO membranes. Clear and flat images were observed for the PA membrane, while protruding domains with linear and planer shapes were observed in the PA-CNTa/GO membrane. The linear and planer images should originate from the tubular structures of CNT and the planer sheet structures of GO, respectively. The embedment of CNTa/GO in the polymer matrix could be also observed from the cross-sectional TEM images, as shown in the Figure 4.9. It was very clear that PA membrane did not have any dark images from the carbon nanomaterials within the polyamide layer, which was about 200 nm thick, while dark images originating from CNTa and GO were observed in the PA-CNTa/GO membrane. When the PA-CNTa and PA-GO membranes were prepared using 0.005 wt% or smaller concentrations of CNTa and GO in the aqueous solution, respectively, CNTa and GO were found to be

well-dispersed in the polyamide layers. However, large clusters over 5 μm in size were observed in the SEM images when concentration larger than 0.005 wt% was used (Figure 4.10). Therefore, 0.005 wt% should be the maximum concentration for the preparation of the PA-CNTa and PA-GO membranes with good dispersion of the carbon nanomaterials. This could be also confirmed from the membrane performance results. In addition, any coagulated clusters by the CNTa and GO were not observed from the PA-CNTa/GO membranes when the CNTa/GO concentration in the aqueous solution was 0.02 wt% or smaller, while some clusters larger than 5 μm were observed when 0.03 wt% of CNTa/GO was used (Figure 4.10). Therefore, 0.02 wt% might be the maximum concentration for the preparation of the membrane having the CNTa/GO with well-dispersed state, which could be further confirmed from the membrane performance behavior shown in the later part of this chapter. The differences in the maximum concentration demonstrating the good dispersion of the carbon nanomaterials in the membranes could be correlated with the dispersity behavior of CNTa, GO, and CNTa/GO in the aqueous solution. The CNTa/GO with better dispersion in water can be dispersed in the polyamide active layer better than the less dispersed

CNTa or GO.

Since the amount of CNTa/GO in the polyamide was too small, it was not possible to observe the overall distribution of CNTa/GO in the nanocomposite membranes through SEM or TEM. Therefore, Raman spectroscopic mapping was carried out for further confirmation of the spatial distribution of CNT/GO in the polyamide membranes. Raman spectroscopic mapping has been used as a tool to visualize the spatial distribution of nanomaterials in other matrix materials including polymers.[11, 48-50] Raman spectroscopic mapping images of the PA and PA-CNT/GO membranes are shown in Figure 4.8e and f, respectively. The characteristic peaks of polyamide, the D band, and G band of CNTa and GO were observed at 998 cm^{-1} , 1308 cm^{-1} and 1600 cm^{-1} , respectively, and mapping images were obtained by integrating the region of those characteristic peaks. The green and red colors represent the polyamide and CNTa/GO structures, respectively. Only green color was observed in Figure 4.8e, while well-dispersed images of green and red colors and even yellow color were observed from the Raman mapping image of the PA-CNT/GO membrane, indicating that CNT and GO were well -incorporated and -dispersed in the polyamide layers.

4.3.4. Water flux and salt rejection

The water flux and salt rejection of the membranes were measured by lab-scale cross-flow equipment for possible practical application in RO systems. The water flux and salt rejection values of PA membrane measured in this study were 34.00 ± 0.67 LMH and 96.63 ± 1.34 %, respectively. These values were close to those of RO membranes having polyamide active layer, previously reported by others.[10,47,51] In addition, the LFC-1 membrane, a commercial membrane for brackish water filtration, was tested at the same operating condition for comparison. The water flux and salt rejection values of the LFC-1 membrane were 37.75 ± 1.5 LMH and 97.01 ± 0.8 %, respectively, which are smaller than those in the technical specification supplied by the company. Such discrepancy has been reported by others due to the effect of the membrane filtration conditions.[61] It is also well known that various additives and post treatment are used to prepare the polyamide active layers of commercial membranes, which can increase the membrane performances. For this reason, the water flux and salt rejection values

of our PA membrane were smaller than those of the LFC-1 membrane. However, the differences were not large, and the main objective of this chapter is to investigate the effect of CNTa/GO in the active layer. Therefore, any additives and post treatments were intentionally not used for membrane preparation, and their membrane performance behaviors were compared.

Figure 4.11 shows the water flux and salt rejection values of the membranes. When the PA-CNTa and PA-GO membranes were prepared with very small amounts of CNTa and GO, respectively (0.0002 wt% in aqueous solution), the water flux and salt rejection values were almost the same as those of the PA membrane because the amounts in the polyamide matrix were too small to affect the membrane performances. The PA-CNTa and PA-GO membranes prepared using 0.001 to 0.005 wt% of CNTa and GO in aqueous solution, respectively, showed increased water flux values without much decrease of the salt rejection. When PA-CNTa and PA-GO membrane were prepared using larger than 0.005 wt% of CNTa and GO, respectively, the water flux increased while the salt rejection decreased dramatically, possibly due to the formation of large voids caused by the aggregation of the carbon nanomaterials. The

aggregated structures were observed by SEM (Figure 4.10), working as defects in the membranes, and they could provide the large passage ways for the water and ion molecules. The maximum water flux values of the PA-CNTa and PA-GO membranes maintaining high enough salt rejection were larger than that of PA membrane by 9.45 LMH (27.2 % increase) and 6.21 LMH (17.8 % increase), respectively, while the differences of salt rejection values were smaller than 0.1 %. The increase of water flux could be explained by the water transportation mechanisms of CNT and GO, as described in previous researches.[11,20,21,23,52,53] Water molecules can enter the CNT nano-channel by capillary force and go through quickly due to the hydrophobic inner side of CNT. Thus, the possible passage of water molecules through the polyamide matrix could be shortened, resulting in the increase of water permeability. The graphitic sheet structures have been known to increase the water permeability because the hydrated ions can go through the CNT nano-channel and on the surface of CNT and GO easily by surface transporting or nano-channel mechanism. The increase of the water flux did not decrease the salt rejection because the carbon nano-materials are well-dispersed in the continuous polyamide matrix without any defects larger than the

size of the sodium or chloride ions in the hydrate state.

The water flux values of the PA-CNTa/GO membranes were found to increase with increase of the CNTa/GO concentration up to 0.02 wt% maintaining reasonably high salt rejection value; the changes of the salt rejection values were less than 0.8 %. However, when the concentration became larger than 0.03 wt%, water flux increased while there was a dramatic decrease of the salt rejection for the same reason as the PA-CNTa and PA-GO membranes. Still, the 0.02 wt% maintaining a reasonably high salt rejection value for PA-CNTa/GO membrane was much larger than 0.005 wt% for the PA-CNTa and PA-GO membranes. The maximum water flux of the PA-CNTa/GO membrane maintaining a reasonably high salt rejection value was larger than that of the PA membrane by 73.41 %. Therefore, the best membrane performance in terms of the water flux and salt rejection was observed from the PA-CNTa (44.23 LMH and 96.75 %), PA-GO (39.19 LMH and 96.97 %), and PA-CNTa/GO (58.96 LMH and 96.21 %) membranes prepared using 0.001, 0.001, and 0.02 wt% the carbon nanomaterials in MPD aqueous solution, respectively. Accordingly, these were used for further the stability and durability studies shown in the following part.

Figure 4.12 shows the water permeability (unit water flux, the water flux per applied pressure) behavior of the membranes with different applied pressure. The water permeability has been known to decrease with the increase of applied pressure because the polymer layers are compressed by the pressure, causing water transport channels to become smaller. Therefore, the PA membrane composed of only polymer without any filler showed the decrease of the water permeability with increasing applied pressure. However, the PA membranes containing carbon nanomaterials showed the increase of the water permeability value with increase of the pressure, indicating that larger amounts of water molecules passes through the surface of CNTa and/or GO or even inside of CNTa by overcoming the approach and entry resistance due to kinetic energy from the increased pressure.[23] Especially, the larger increase of the flux was observed for the PA-CNTa and PA-CNTa/GO membranes than for the PA-GO membrane indicating that the channel structures of CNTa increase the flux more than the flat GO structure. Possibly, flat GO structure might prevent the water molecule to go into the inside channel of the CNTs by wrapping the tube structures. However, such morphology could not be observed from the TEM or SEM images due to the limited

resolution of the equipment. The effect of the applied pressure on salt rejection was also measured to estimate membrane stability (Figure 4.13). Salt rejection value was found to increase slightly with the increase of applied pressure for all the membranes because to the formation of the compressed active layer by the pressure.[59] We believe that the detailed information of nanostructures of the CNTa/GO mixture should be very important to understand these membrane performance behavior of the PA-CNTa/GO membrane, while the observation and explanation of CNTa/GO nanostructure should need a serious of efforts and are beyond the scope of this study.

4.3.5. Durability of the PA-CNTa/GO membrane

Figure 4.14a shows the pure water flux of the membranes measured with time. The water flux of the PA membrane decreased by 35.5 % after 72 h, whereas those of the PA-CNTa, PA-GO, and PA-CNTa/GO membranes decreased by only 24.8, 23.1, and 15.0 %, respectively, when the filtration test was performed at 15.5 bar of applied pressure. Similar flux decline behavior was observed when the feed pressure was increased to 50.0 bar; 37.5, 27.2, 23.8, and 16.2 % of water flux

decreases were observed from PA, PA-CNTa, PA-GO, and PA-CNTa/GO membranes, respectively (Figure 4.15). The decrease of water flux with time has been ascribed to membrane compression by the pressure.[11, 23, 24] The smaller flux decrease of the PA membranes with the carbon nanomaterials should be originated from the increase of mechanical strength. It is well known that one of the most important advantages of using CNT and GO as filler materials in the polymer matrix is the increase of physical properties including mechanical strength, because the fillers can disturb the polymer chain mobility to form stiffer polymer structures.[28, 31, 33, 54] Therefore, the polyamide active layers of the PA membranes with the carbon nanomaterials can be compressed less than that of the PA membrane, which in turns the smaller decrease of water flux. In addition, since the amount of CNTa/GO in the PA-CNTa/GO membrane is larger than those in the PA-CNTa and PA-GO membranes, the decrease of flux was found to be smaller for the PA-CNTa/GO membrane than the PA-CNTa and PA-GO membranes. The same behaviour was observed from the membrane durability test using the NaCl solution as shown in Figure 4.14b. The increase of mechanical strength producing the increase of durability upon long time operation could be confirmed by

Young's modulus and tensile strength values of the membranes (Figure 4.16). The Young's modulus and the tensile strength values of the PA membranes with the carbon nanomaterials were larger than those of the PA membrane without the carbon nanomaterials, and the PA-CNTa/GO membranes showed the largest values because it contained the largest amount of the carbon nanomaterials. Comparing the PA membranes prepared with the same concentration of the carbon nanomaterials (0.001 wt% of CNTa, GO, and CNTa/GO in the aqueous solutions, respectively), the mechanical property values were in the orders of PA-CNTa < PA-GO < PA-CNTa/GO, although the differences are not large. The mechanical strength behavior followed the maximum dispersity behavior shown in Table 4.2. Obviously, the carbon nanomaterials with better dispersity in the polymer matrix can increase the mechanical strength more.[30-32]

Disinfection has been widely used in RO process to prevent biofilm formation because biofilms formed on the membrane surfaces decreases the membrane performance dramatically which in turn increases the operation costs. Chlorine is commonly applied as an oxidizing biocide for the disinfection process because of its low-cost and high-efficiency.[9, 55, 56] However, polyamide membranes have

been known to have poor resistance to oxidizing agents including chlorine.[9, 56, 57] Figure 4.17 shows the membrane performance behaviors under the active chlorine exposures. NaCl rejection of the PA membrane decreased by 8.55 % after only 7,500 ppm h (15 h) of chlorine exposure, falling off rapidly thereafter. After 40 h of chlorine exposure (20,000 ppm h), rejection ability of the PA membrane was not observed. In contrast, a smaller decrease of the salt rejection was observed from PA membranes with the carbon nanomaterials. Amide groups in polyamide layers can be attacked by oxidation reagents, such as the chlorine radical, hydroxyl radical, and hypochlorite (Figure 4.18). For example, since the hydroxyl radical is even smaller than the water molecule it can diffuse into the polyamide active layer easily and degrade the polymer structures. CNTa and GO in the polymer matrix can trap the radicals because they have the phenolic moieties having the radical scavenging ability.[14, 28, 58] Therefore, the inclusion of CNTa and GO in the polyamide active layer can increase the chlorine resistance of the membranes. The chlorine resistance ability of the PA-GO membrane was found to be slightly larger than that of the PA-CNTa membrane, indicating that GO is more effective to impart the chlorine resistance properties into

membranes than CNT. In addition, the PA-CNTa/GO membrane showed the lower decreases in rejection than the PA-CNTa and PA-GO membranes due to the larger amounts of CNTa and GO in the polyamide active layer. The other PA-CNTa/GO membrane intentionally prepared with the same amount of CNTa/GO (0.001 wt% in aqueous solution) showed the similar chlorine resistance behavior to the PA-CNTa and PA-GO membranes (Figure 4.19). Therefore, the chlorine resistance properties of the membranes with carbon nanomaterials should be mainly determined by the amount of carbon nanomaterials having the radical scavenging ability in the membranes, not much by the dispersity. The antioxidant effects (radical scavenging ability) of the carbon nanomaterials were further studied by TGA analysis under air, as reported by others (Figure 4.20).[14, 58] For the TGA study, the active layers were pulled off from the membranes and fully dried to remove the water for the accurate analysis. The antioxidant effect of the CNTa/GO was clearly demonstrated by the higher degradation temperature (such as onset temperature) of the active layer the onset temperature (T_d , 5% weight loss occurs) behavior agreed well with the chlorine resistance properties. The T_d values of the active layers of PA, PA-CNTa, PA-GO, and PA-

CNTa/GO membranes were found to be 65.8, 73.3, 76.6, and 86.2 °C, respectively. The PA-CNTa/GO membrane showed the highest T_d because it contained the largest amount of carbon nanomaterials. The radical scavenging abilities of the carbon nanomaterials were further studied by ESR spectroscopy recorded during the active chlorine exposure to membrane active layers (Figure 4.21 and 4.22) and the PA-CNTa/GO membrane was observed to have the best radical scavenging ability, which also agreed well with the TGA results.

4.4. Conclusions

The polyamide membranes containing acid functionalized CNT (CNTa) and/or graphene oxide (GO) showed much improved performances such as the water flux, mechanical strength, durability, chlorine resistance, and the radical scavenging ability compared with the polyamide membrane without any carbon nanomaterials due the unique characteristics of the carbon nanomaterials. Especially, when the mixtures of CNTa and GO were used as the filler materials for the preparation of the membranes, much larger amounts of the carbon nanomaterials could be well-dispersed in the polymer layers than

when CNTa or GO was used by alone, because GO can increase the dispersion of CNT in the aqueous solutions and the polymer matrix. Therefore, the polyamide membrane containing the mixture of CNTa and GO showed the best membrane performances. This result will undoubtedly contribute to the latest efforts to develop the polymer nanocomposites as well as the RO membranes without any trade off behaviors.

4.5. References

- [1] D. G. Kim, H. Kang, S. Han, H. J. Kim and J. C. Lee, *RSC Adv.* **2013**, 3, 18071-18081.
- [2] D. G. Kim, H. Kang, Y. S. Choi, S. Han and J. C. Lee, *Polym. Chem.-UK* **2013**, 4, 5065-5073.
- [3] D. G. Kim, H. Kang, S. Han and J. C. Lee, *ACS Appl. Mater. Interfaces* **2012**, 4, 5898-5906.
- [4] D. G. Kim, H. Kang, S. Han and J. C. Lee, *J. Mater. Chem.* **2012**, 22, 8654-8661.
- [5] L. F. Greenlee, D. F. Lawler, B. D. Freeman, B. Marrot and P. Moulin, *Water Res.* **2009**, 43, 2317-2348.

- [6] M. Elimelech and W. A. Phillip, *Science* **2011**, 333, 712-717.
- [7] G. D. Kang and Y. M. Cao, *Water Res.* **2012**, 46, 584-600.
- [8] D. Li and H. T. Wang, *J. Mater. Chem.* **2010**, 20, 4551-4566.
- [9] H. B. Park, B. D. Freeman, Z. B. Zhang, M. Sankir and J. E. McGrath, *Angew. Chem. Int. Edit.* **2008**, 47, 6019-6024.
- [10] H. Y. Zhao, S. Qiu, L. G. Wu, L. Zhang, H. L. Chen and C. J. Gao, *J. Membr. Sci.* **2014**, 450, 249-256.
- [11] H. J. Kim, K. Choi, Y. Baek, D.-G. Kim, J. Shim, J. Yoon and J.-C. Lee, *ACS Appl. Mater. Interfaces* **2014**, 6, 2819-2829.
- [12] M. Fathizadeh, A. Aroujalian and A. Raisi, *J. Membr. Sci.* **2011**, 375, 88-95.
- [13] H. J. Kim, Y. Baek, K. Choi, D. G. Kim, H. Kang, Y. S. Choi, J. Yoon and J. C. Lee, *RSC Adv.* **2014**, 4, 32802-32810.
- [14] P. C. P. Watts, P. K. Fearon, W. K. Hsu, N. C. Billingham, H. W. Kroto and D. R. M. Walton, *J. Mater. Chem.* **2003**, 13, 491-495.
- [15] H. Im and J. Kim, *Carbon* **2012**, 50, 5429-5440.
- [16] Q. F. Cheng, J. W. Bao, J. Park, Z. Y. Liang, C. Zhang and B. Wang, *Adv. Funct. Mater.* **2009**, 19, 3219-3225.
- [17] W. H. Guo, C. Liu, X. M. Sun, Z. B. Yang, H. G. Kia and H. S. Peng, *J. Mater. Chem.* **2012**, 22, 903-908.

- [18] S. Kang, M. Herzberg, D. F. Rodrigues and M. Elimelech, *Langmuir* **2008**, 24, 6409-6413.
- [19] D. R. Paul, *Science* **2012**, 335, 413-414.
- [20] J. K. Holt, H. G. Park, Y. M. Wang, M. Stadermann, A. B. Artyukhin, C. P. Grigoropoulos, A. Noy and O. Bakajin, *Science* **2006**, 312, 1034-1037.
- [21] G. Hummer, J. C. Rasaiah and J. P. Noworyta, *Nature* **2001**, 414, 188-190.
- [22] J. N. Shen, C. C. Yu, H. M. Ruan, C. J. Gao and B. Van der Bruggen, *J. Membr. Sci.*, 2013, **442**, 18-26.
- [23] H. D. Lee, H. Y. Kim, Y. H. Cho and P. H. B., *Small* **2014**, 10, 2653-2660.
- [24] V. Vatanpour, S. S. Madaeni, R. Moradian, S. Zinadini and B. Astinchap, *J. Membr. Sci.* **2011**, 375, 284-294.
- [25] E. Celik, H. Park, H. Choi and H. Choi, *Water Res.* **2011**, 45, 274-282.
- [26] H. A. Shawky, S. R. Chae, S. H. Lin and M. R. Wiesner, *Desalination* **2011**, 272, 46-50.
- [27] M. Y. Lim, H. J. Kim, S. J. Baek, K. Y. Kim, S. S. Lee and J. C. Lee, *Carbon* **2014**, 77, 366-378.

- [28] B. H. Yuan, C. L. Bao, L. Song, N. N. Hong, K. M. Liew and Y. Hu, *Chem. Eng. J.* **2014**, 237, 411-420.
- [29] J. Q. Liu, C. F. Chen, C. C. He, L. Zhao, X. J. Yang and H. L. Wang, *ACS Nano* **2012**, 6, 8194-8202.
- [30] Y. W. Cheng, S. T. Lu, H. B. Zhang, C. V. Varanasi and J. Liu, *Nano Lett.* **2012**, 12, 4206-4211.
- [31] X. L. Yang, Y. Q. Zhan, J. Yang, J. C. Zhong, R. Zhao and X. B. Liu, *J. Polym. Res.* **2012**, 19.
- [32] S. Y. Yang, W. N. Lin, Y. L. Huang, H. W. Tien, J. Y. Wang, C. C. M. Ma, S. M. Li and Y. S. Wang, *Carbon* **2011**, 49, 793-803.
- [33] Y. Q. Li, T. Y. Yang, T. Yu, L. X. Zheng and K. Liao, *J. Mater. Chem.* **2011**, 21, 10844-10851.
- [34] L. Qiu, X. W. Yang, X. L. Gou, W. R. Yang, Z. F. Ma, G. G. Wallace and D. Li, *Chem.-Eur. J.* **2010**, 16, 10653-10658.
- [35] V. C. Tung, L. M. Chen, M. J. Allen, J. K. Wassei, K. Nelson, R. B. Kaner and Y. Yang, *Nano Lett.* **2009**, 9, 1949-1955.
- [36] W. S. Hummers and R. E. Offeman, *J. Am. Chem. Soc.* **1958**, 80, 1339-1339.
- [37] M. J. Yoo, H. W. Kim, B. M. Yoo and H. B. Park, *Carbon* **2014**, 75, 149-160.

- [38] B. H. Jeong, E. M. V. Hoek, Y. S. Yan, A. Subramani, X. F. Huang, G. Hurwitz, A. K. Ghosh and A. Jawor, *J. Membr. Sci.* **2007**, 294, 1-7.
- [39] K. P. Lee, T. C. Arnot and D. Mattia, *J. Membr. Sci.* **2011**, 370, 1-22.
- [40] M. H. Liu, D. H. Wu, S. C. Yu and C. J. Gao, *J. Membr. Sci.* **2009**, 326, 205-214.
- [41] S. Mallakpour and A. Zadehnazari, *Carbon* **2013**, 56, 27-37.
- [42] B. Gebhardt, Z. Syrgiannis, C. Backes, R. Graupner, F. Hauke and A. Hirsch, *J. Am. Chem. Soc.* **2011**, 133, 7985-7995.
- [43] S. Banerjee, T. Hemraj-Benny and S. S. Wong, *Adv. Mater.* **2005**, 17, 17-29.
- [44] D. Silambarasan, K. Iyakutti and V. Vasu, *Chem. Phys. Lett.* **2014**, 604, 83-88.
- [45] M. Hu and B. X. Mi, *Environ. Sci. Technol.* **2013**, 47, 3715-3723.
- [46] D. Hanaor, M. Michelazzi, C. Leonelli and C. C. Sorrell, *J. Eur. Ceram. Soc.* **2012**, 32, 235-244.
- [47] S. Qiu, L. G. Wu, L. Zhang, H. L. Chen and C. J. Gao, *J. Appl. Polym. Sci.* **2009**, 112, 2066-2072.

- [48] A. Bassil, P. Puech, G. Landa, W. Bacsa, S. Barrau, P. Demont, C. Lacabanne, E. Perez, R. Bacsa, E. Flahaut, A. Peigney and C. Laurent, *J. Appl. Phys.* **2005**, 97, 3.
- [49] S. Anantachaisilp, S. M. Smith, A. Treetong, S. Pratontep, S. Puttipipatkachorn and U. R. Ruktanonchai, *Nanotechnology* **2010**, 21, 12-19.
- [50] C. Guiderdoni, E. Pavlenko, V. Turq, A. Weibel, P. Puech, C. Estournes, A. Peigney, W. Bacsa and C. Laurent, *Carbon* **2013**, 58, 185-197.
- [51] K. Ghosh, B. H. Jeong, X. F. Huang and E. M. V. Hoek, *J. Membr. Sci.* **2008**, 311, 34-45.
- [52] S. Karan, S. Samitsu, X. S. Peng, K. Kurashima and I. Ichinose, *Science* **2012**, 335, 444-447.
- [53] B. J. Hinds, N. Chopra, T. Rantell, R. Andrews, V. Gavalas and L. G. Bachas, *Science* **2004**, 303, 62-65.
- [54] L. Q. Liu, A. H. Barber, S. Nuriel and H. D. Wagner, *Adv. Func. Mater.* **2005**, 15, 975-980.
- [55] J. Glater, S. K. Hong and M. Elimelech, *Desalination* **1994**, 95, 325-345.

- [56] P. Junwoo, C. Wansuk, S. H. Kim, B. H. Chun, B. Joona and K. B. Lee, *Desalin. Water Treat.* **2010**, 15, 198-204.
- [57] H. M. Colquhoun, D. Chappell, A. L. Lewis, D. F. Lewis, G. T. Finlan and P. J. Williams, *J.Mater. Chem.* **2010**, 20, 4629-4634.
- [58] X. M. Shi, B. B. Jiang, J. D. Wang and Y. R. Yang, *Carbon* **2012**, 50, 1005-1013.
- [59] W. Zhou and L. Song, *Environ. Sci. Technol.* **2005**, 39, 3382-3387.
- [60] American Society for Testing and Materials. Zeta potential of Colloids in Water and Waste Water. ASTM Standard D4187-82, **1985**.
- [61] E. M. V. Wagner, A. C. Sagle, M. M. Shar, and B. D. Freeman, *J. Membr. Sci.*, **2009**, 345, 97-109.

Table 4.1. XPS elemental composition (at%) and O/C ratio of pristine CNT, CNTa, graphite, and GO.

	C contents	O contents	O/C ratio
Pristine CNT	93.02	6.98	0.075
CNTa	75.87	24.13	0.318
Graphite	89.12	10.88	0.122
GO	68.14	31.86	0.468

Table 4.2. Maximum dispersity (g L^{-1}) of CNTa, GO, and CNTa/GO mixture in water.

CNTa	GO	CNTa : GO mixture	
		1:9	30.7 ± 3.8
		3:7	33.1 ± 2.2
16.2 ± 2.0	19.7 ± 2.5	5:5	22.0 ± 6.2
		7:3	35.5 ± 3.9
		9:1	28.5 ± 4.3

Table 4.3. Water flux and salt rejection values of the membranes prepared in 2 and 3 wt% of MPD (PA-CNT, PA –GO membrane were prepared with 0.001 wt% of CNT and GO in aqueous solution, respectively and PA-CNT/GO membrane was prepared with 0.02 wt% of CNT/GO mixture in aqueous solution, the membranes were tested by cross-flow filtration, 2000 ppm NaCl solution as a feed solution, 15.5 bar of feed pressure, and 500 mL min⁻¹ of flow rate).

	MPD wt%	Water flux [LMH]	Salt Rejection [%]
PA	2	34.00 ± 0.67	96.63 ± 1.34
	3	32.63 ± 1.68	96.48 ± 0.44
PA-CNT	2	40.84 ± 1.84	96.22 ± 0.67
	3	44.23 ± 2.35	96.75 ± 0.49
PA-GO	2	36.68 ± 0.98	96.28 ± 0.83
	3	38.19 ± 1.44	96.96 ± 0.58
PA-CNT/GO	2	53.25 ± 1.88	95.84 ± 0.52
	3	58.96 ± 1.31	96.63 ± 0.65

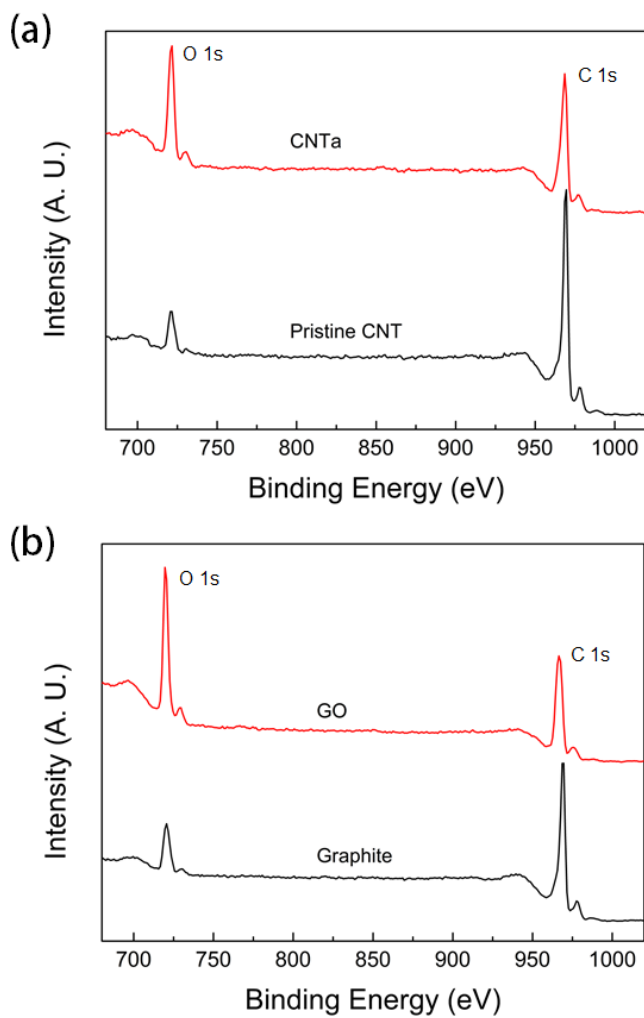


Figure 4.1. XPS spectra of (a) pristine CNT and CNTa, and (b) graphite and GO.

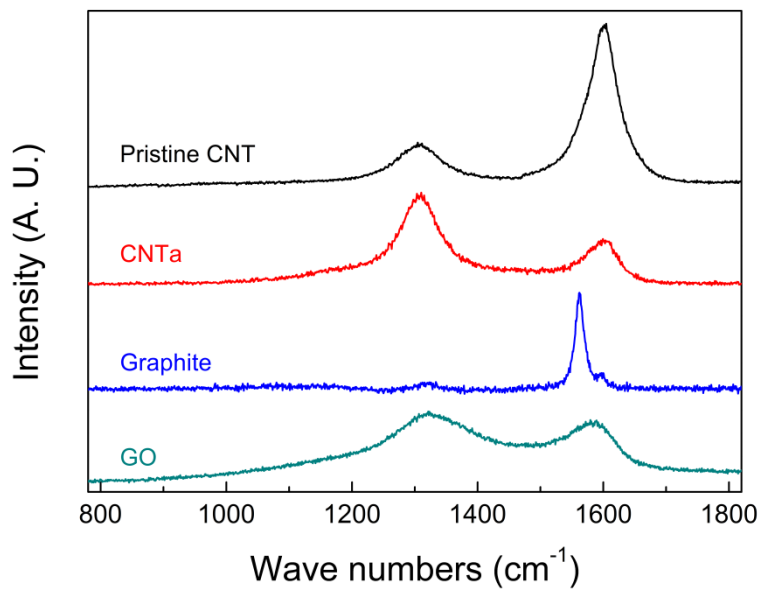


Figure 4.2. Raman spectra of pristine CNT, CNTa, graphite, and GO.

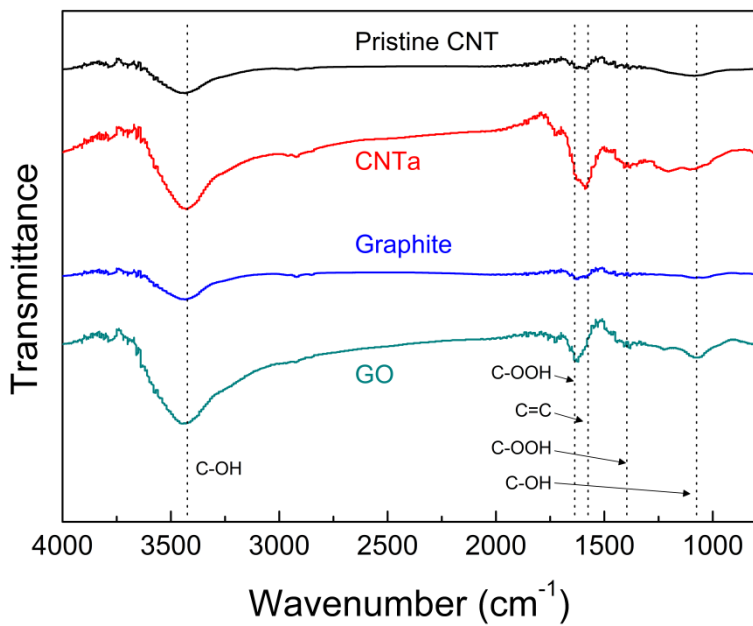


Figure 4.3. FT-IR spectra of pristine CNT, CNTa, graphite, and GO.

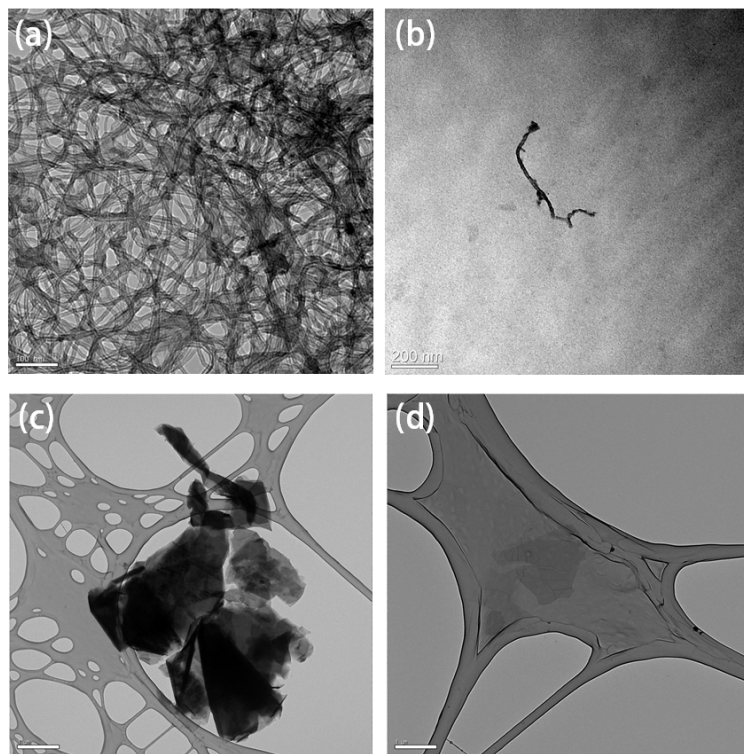


Figure 4.4. TEM images of (a) pristine CNT, (b) CNTa, (c) graphite, and (d) GO.

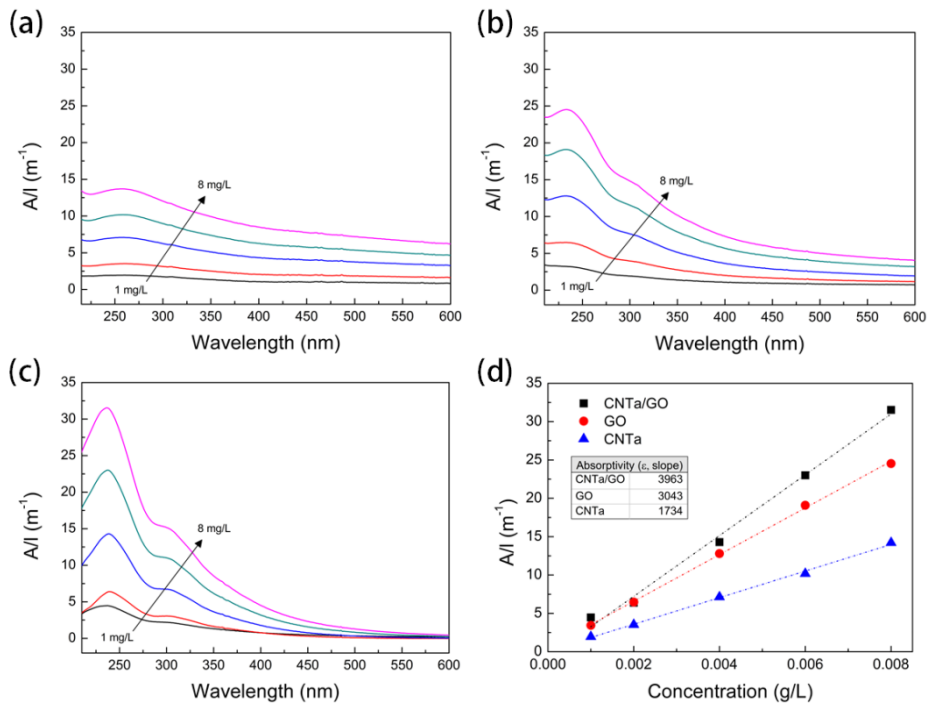


Figure 4.5. UV/vis absorption spectra of (a) CNTa, (a) GO, and (c) CNTa/GO dispersed aqueous solution and (d) their UV/vis absorption intensity changes by the concentration.

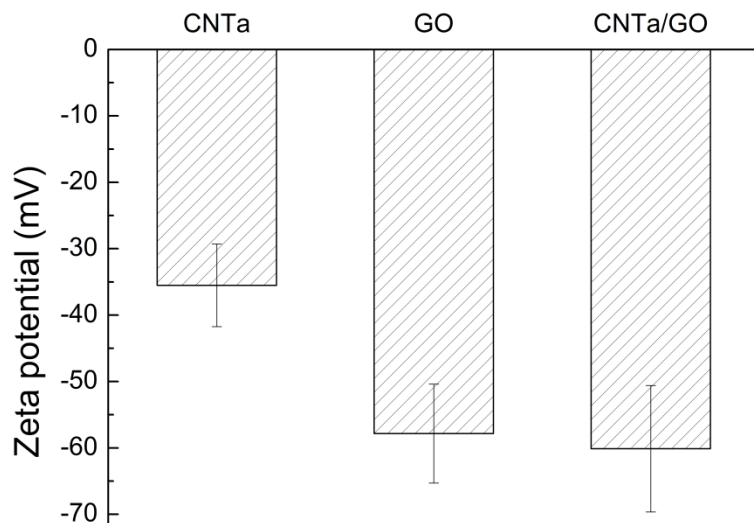


Figure 4.6. Zeta potential values of CNTa, GO, and CNTa/GO dispersed in water (50 mg mL^{-1}).

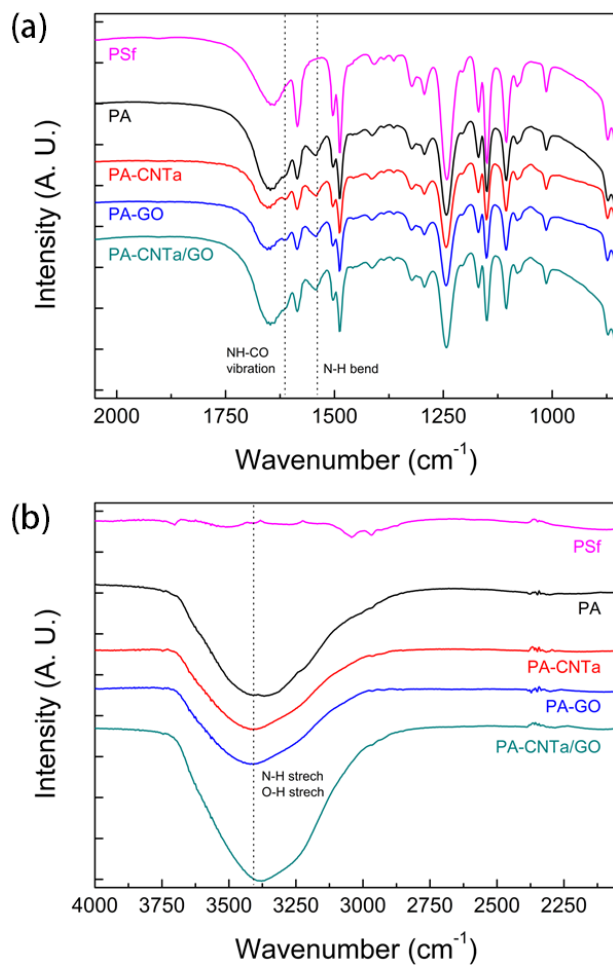


Figure 4.7. FT-IR spectra of PSf, PA, PA-CNTa (prepared using the MPD aqueous solution containing 0.001 wt% of CNTa), PA-GO (prepared using the MPD aqueous solution containing 0.001 wt% of GO), and PA-CNTa/GO (prepared using the MPD aqueous solution containing 0.02 wt% of CNTa/GO) membranes; wavenumber at (a) 2050-850 cm^{-1} , and (b) 4000-2050 cm^{-1} .

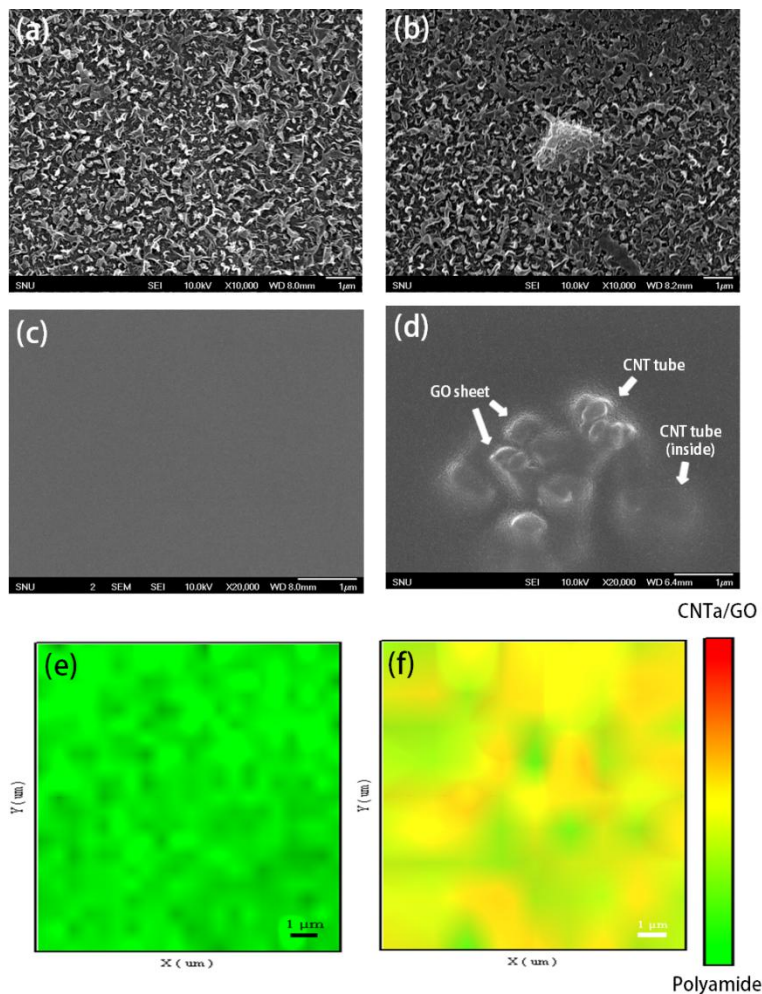


Figure 4.8. SEM (top and bottom part) and Raman spectroscopic mapping images of (a), (c), (e) PA, and (b), (d), (f) PA-CNTa/GO (prepared using the MPD aqueous solution containing 0.02 wt% of CNTa/GO) membranes.

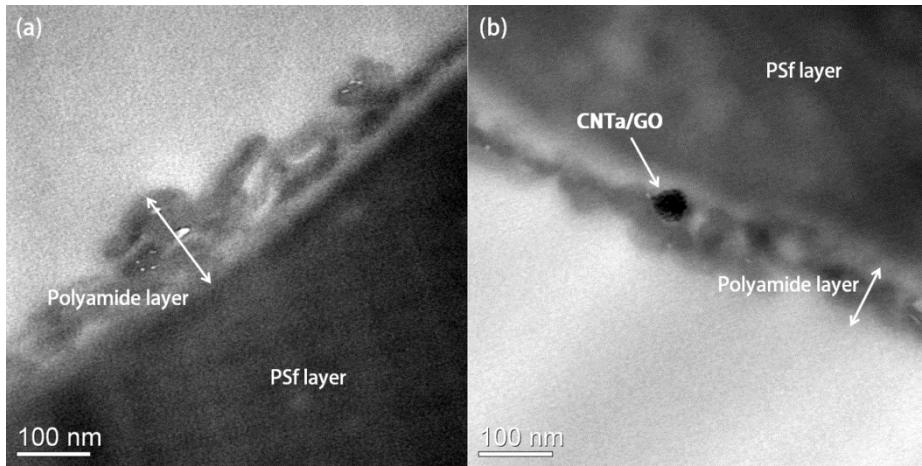


Figure 4.9. Cross-sectional TEM images of PA and PA-CNTa/GO (prepared using the MPD aqueous solution containing 0.02 wt% of CNTa/GO) membranes.

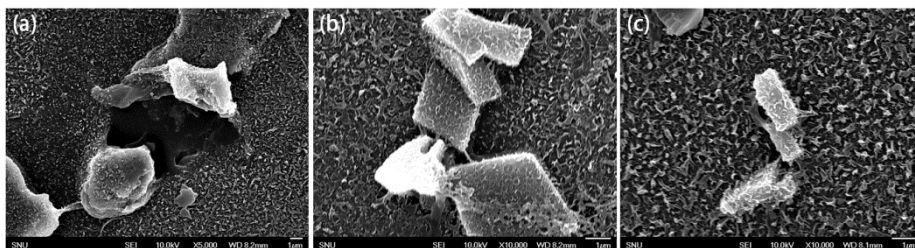


Figure 4.10. SEM images at the top surfaces of (a) PA-CNTa (prepared using the MPD aqueous solution containing 0.01 wt% of CNTa), (b) PA-GO (prepared using the MPD aqueous solution containing 0.01 wt% of GO), and (c) PA-CNTa/GO (prepared using the MPD aqueous solution containing 0.03 wt% of CNTa/GO) membranes.

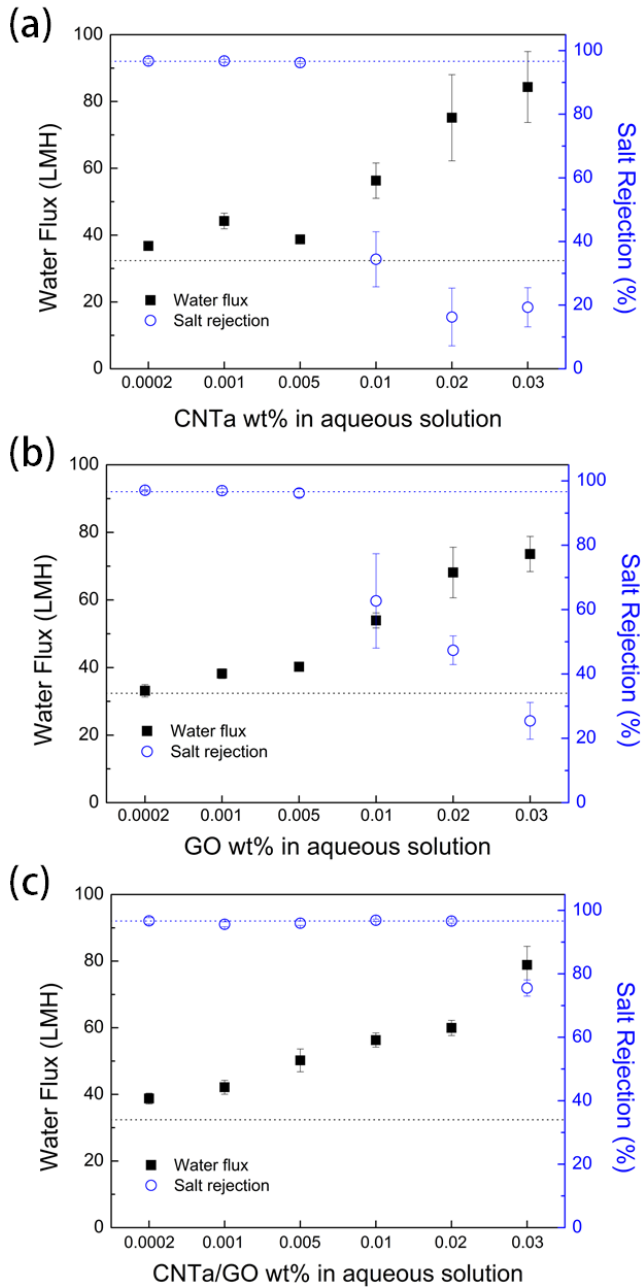


Figure 4.11. Water flux and salt rejection of (a) PA-CNTa, (b) PA-

GO, and (c) PA-CNTa/GO membranes (water flux and salt rejection values of PA membrane were marked with black and blue dot lines, respectively) (tested by cross-flow filtration, 2000 ppm NaCl solution as a feed solution, 15.5 bar of feed pressure, and 500 mL min⁻¹ of flow rate).

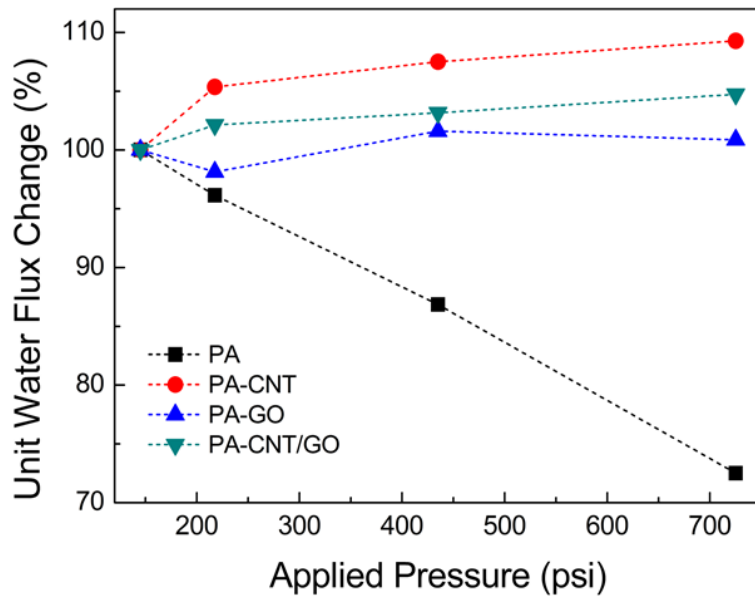


Figure 4.12. Unit water flux changes of PA, PA-CNTa (prepared using the MPD aqueous solution containing 0.001 wt% of CNTa), PA-GO (prepared using the MPD aqueous solution containing 0.001 wt% of GO), and PA-CNTa/GO (prepared using the MPD aqueous solution containing 0.02 wt% of CNTa/GO) membranes under different applied feed pressure (tested by cross flow filtration, 2000 ppm NaCl solution as a feed solution, and 500 mL min⁻¹ of flow rate).

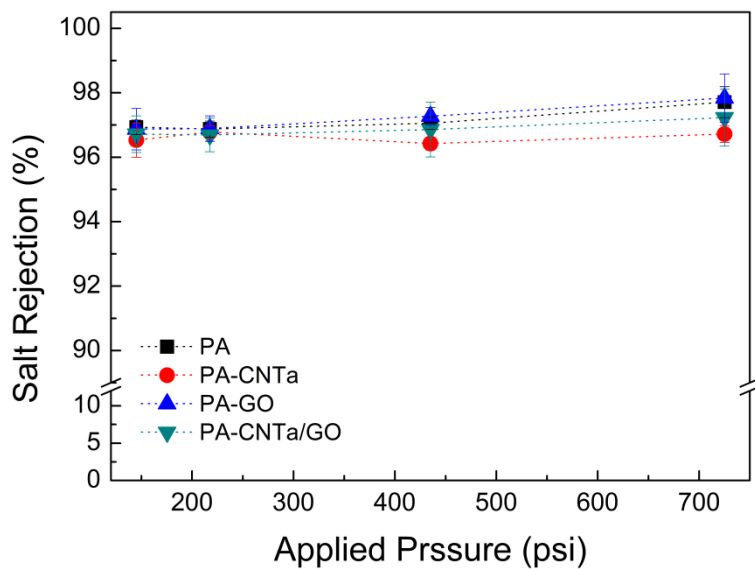


Figure 4.13. Salt rejection measurement of the PA, PA-CNTa (prepared using the MPD aqueous solution containing 0.001 wt% of CNTa), PA-GO (prepared using the MPD aqueous solution containing 0.001 wt% of GO), and PA-CNTa/GO (prepared using the MPD aqueous solution containing 0.02 wt% of CNTa/GO) membranes at different applied pressure (tested by cross-flow filtration, 2000 ppm NaCl solution as a feed solution, and 500 mL min⁻¹ of flow rate).

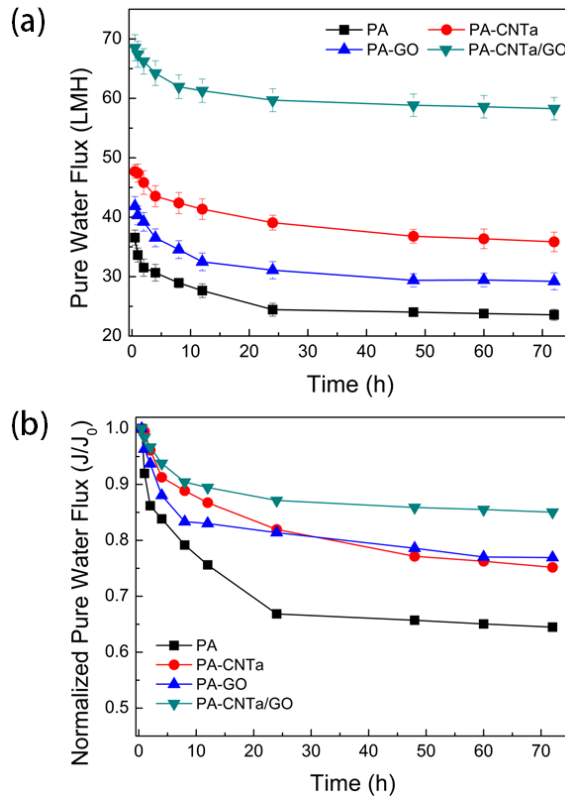


Figure 4.14. (a) Pure water flux measurement and (b) water flux and salt rejection behaviors with time for PA, PA-CNTa (prepared using the MPD aqueous solution containing 0.001 wt% of CNTa), PA-GO (prepared using the MPD aqueous solution containing 0.001 wt% of GO), and PA-CNTa/GO (prepared using the MPD aqueous solution containing 0.02 wt% of CNTa/GO) membranes (tested by cross-flow filtration, 2000 ppm NaCl solution as a feed solution, 15.5 bar of feed pressure, and 500 mL min^{-1} of flow rate).

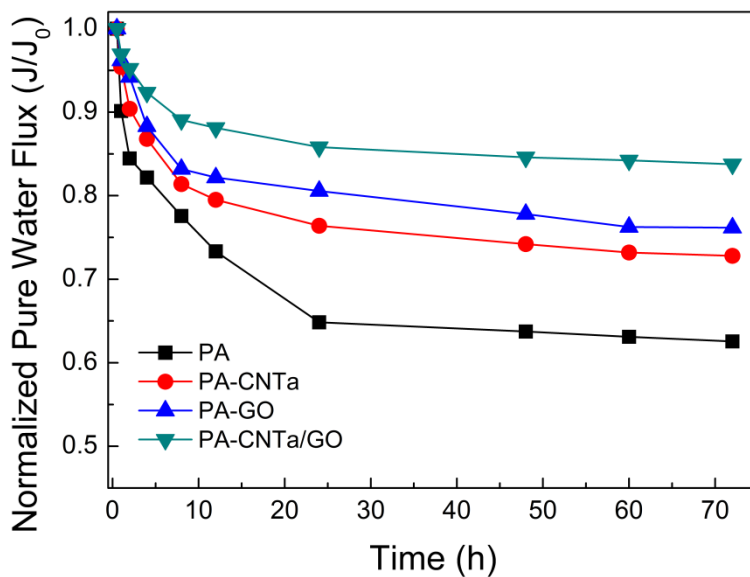


Figure 4.15. Normalized pure water flux measurement with time at 50 bar of feed pressure for PA, PA-CNTa (prepared using the MPD aqueous solution containing 0.001 wt% of CNTa), PA-GO (prepared using the MPD aqueous solution containing 0.001 wt% of GO), and PA-CNTa/GO (prepared using the MPD aqueous solution containing 0.02 wt% of CNTa/GO) membranes (tested by cross-flow filtration, and 350 mL min⁻¹ of flow rate).

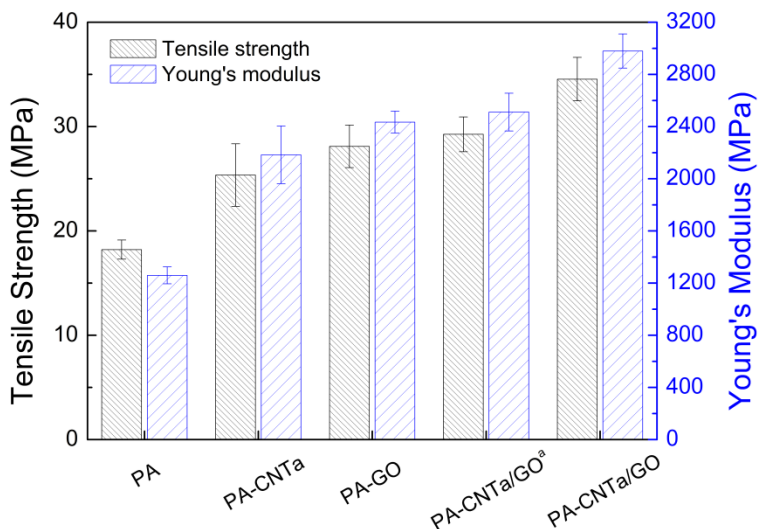


Figure 4.16. Mechanical properties of PA, PA-CNTa (prepared using the MPD aqueous solution containing 0.001 wt% of CNTa), PA-GO (prepared using the MPD aqueous solution containing 0.001 wt% of GO), PA-CNTa/GO^a (prepared using the MPD aqueous solution containing 0.001 wt% of CNTa/GO), and PA-CNTa/GO (prepared using the MPD aqueous solution containing 0.02 wt% of CNTa/GO) membranes.

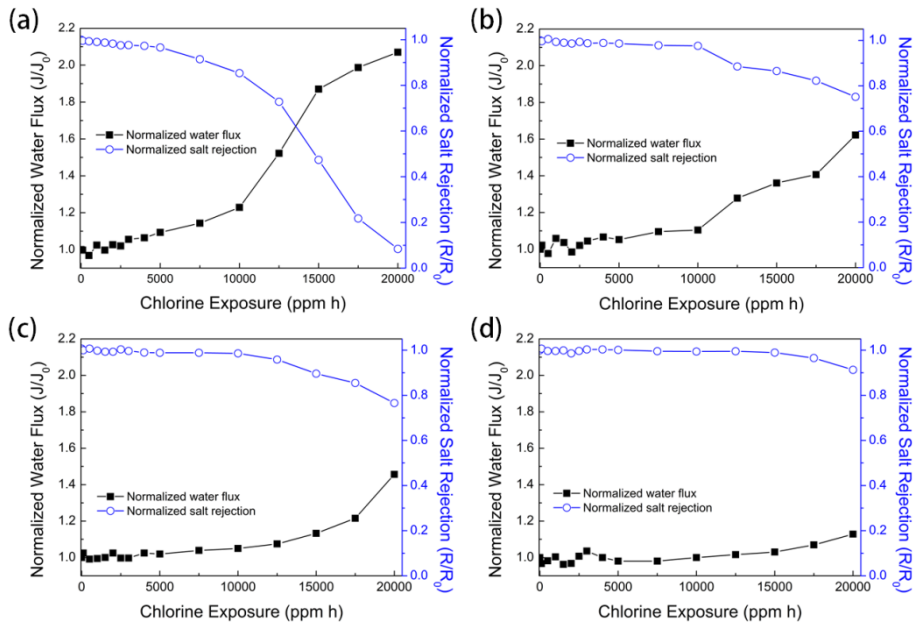


Figure 4.17. Membrane performance behaviors under the active chlorine exposures; (a) PA, (b) PA-CNTa (prepared using the MPD aqueous solution containing 0.001 wt% of CNTa), (c) PA-GO (prepared using the MPD aqueous solution containing 0.001 wt% of GO), and (d) PA-CNTa/GO (prepared using the MPD aqueous solution containing 0.02 wt% of CNTa/GO) membranes (tested by cross-flow filtration, measured after the chlorine exposure using 500 ppm chlorine solution, 2000 ppm NaCl solution as a feed solution, 15.5 bar of feed pressure, and 500 mL min⁻¹ of flow rate).

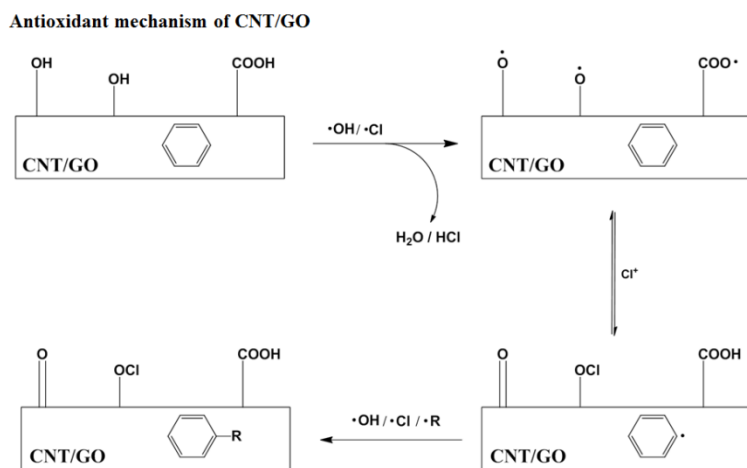
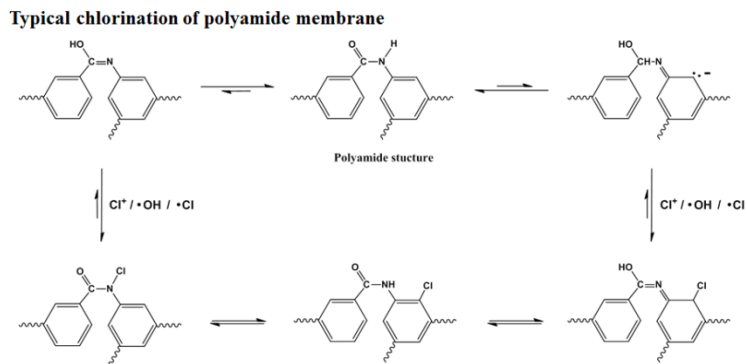


Figure 4.18. Typical chlorination of polyamide membrane and antioxidant mechanism of CNT and GO.

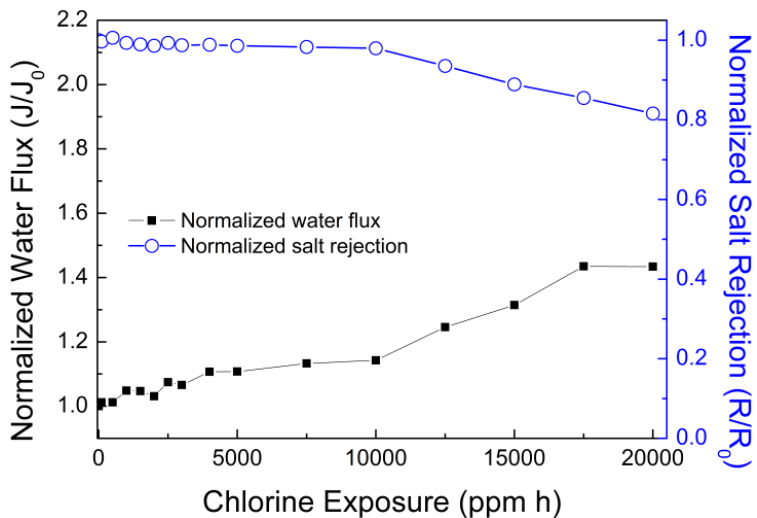


Figure 4.19. Membrane performance behaviors under the active chlorine exposures of PA-CNTa/GO membrane prepared using the MPD aqueous solution containing 0.001 wt% of CNTa/GO (tested by cross-flow filtration, after the chlorine exposure using 500 ppm chlorine solution, 2000 ppm NaCl solution as a feed solution, 15.5 bar of feed pressure, and 500 mL min⁻¹ of flow rate).

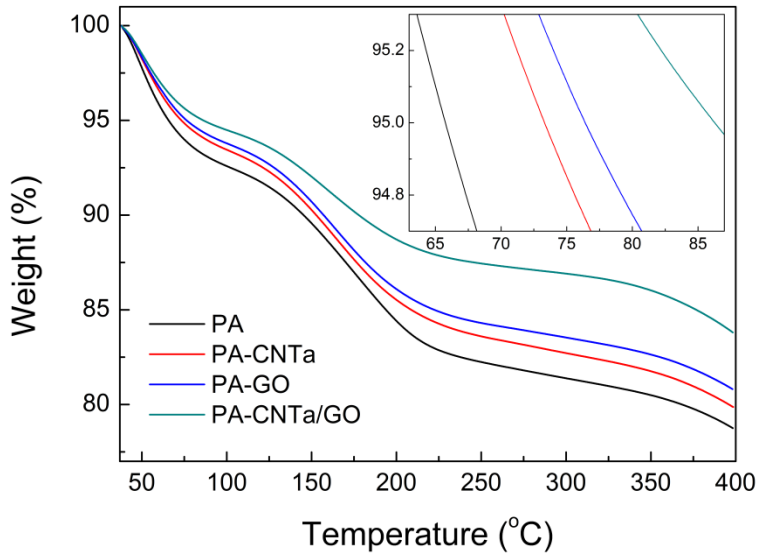


Figure 4.20. TGA analysis of the membrane active layers under air; PA, PA-CNTa (prepared using the MPD aqueous solution containing 0.001 wt% of CNTa), PA-GO (prepared using the MPD aqueous solution containing 0.001 wt% of GO), and PA-CNTa/GO (prepared using the MPD aqueous solution containing 0.02 wt% of CNTa/GO) membranes.

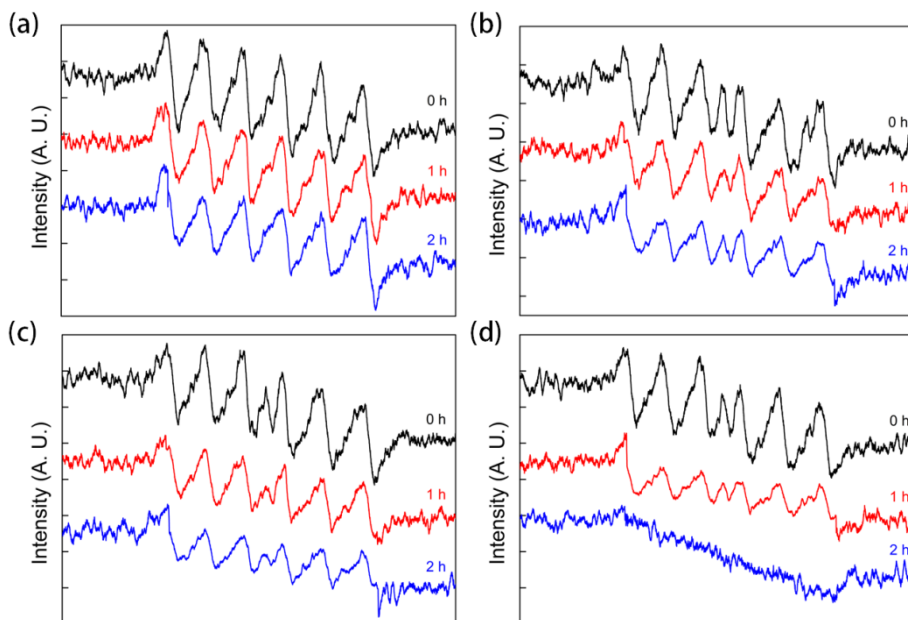


Figure 4.21. ESR spectra obtained during the active chlorine exposure to membrane active layers; (a) PA, (b) PA-CNTa (prepared using the MPD aqueous solution containing 0.001 wt% of CNTa), (c) PA-GO (prepared using the MPD aqueous solution containing 0.001 wt% of GO), and (d) PA-CNTa/GO (prepared using the MPD aqueous solution containing 0.02 wt% of CNTa/GO) membranes.

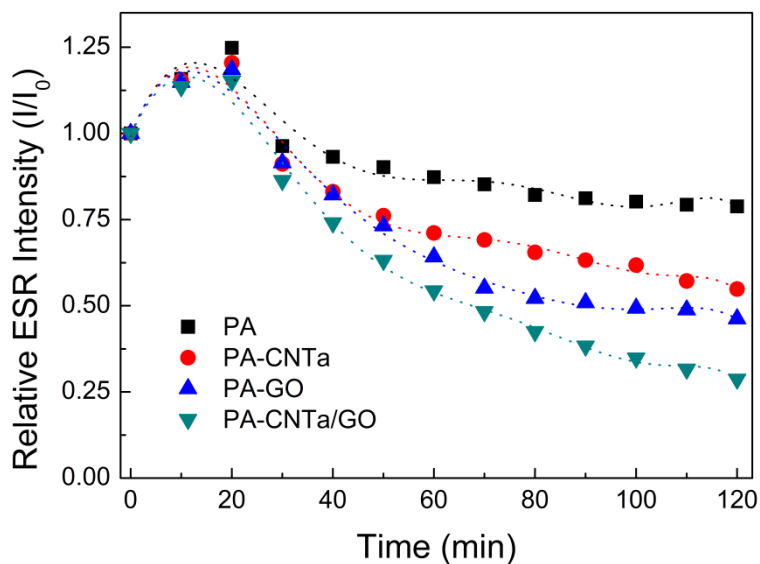


Figure 4.22. Time-dependant relative ESR intensity changes during the active chlorine exposure to membrane active layers; PA, PA-CNTa (prepared using the MPD aqueous solution containing 0.001 wt% of CNTa), PA-GO (prepared using the MPD aqueous solution containing 0.001 wt% of GO), and PA-CNTa/GO (prepared using the MPD aqueous solution containing 0.02 wt% of CNTa/GO) membranes.

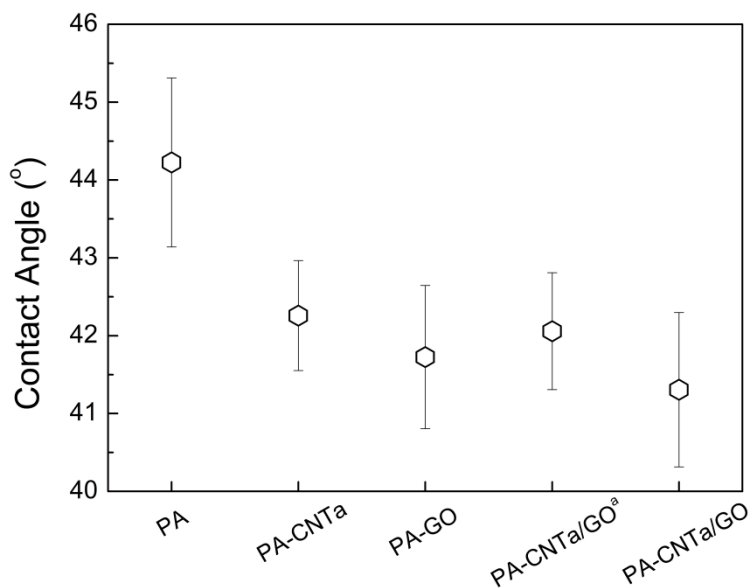


Figure 4.23. Contact angle values of PA, PA-CNTa (prepared using the MPD aqueous solution containing 0.001 wt% of CNTa), PA-GO (prepared using the MPD aqueous solution containing 0.001 wt% of GO), PA-CNTa/GO^a (prepared using the MPD aqueous solution containing 0.001 wt% of CNTa/GO), and PA-CNTa/GO (prepared using the MPD aqueous solution containing 0.02 wt% of CNTa/GO) membranes.

Chapter 5

Reverse Osmosis Nanocomposite Membranes Containing Graphene Oxides Coated by Tannic Acid With Chlorine-Tolerant and Antimicrobial Properties

5.1. Introduction

Water purification technologies have received increased attention due to the urgent increase in fresh water demand.[1, 2] Membrane-based desalination technologies such as nanofiltration (NF) and reverse osmosis (RO) process have been rapidly developed and widely used due to their many advantages. Low cost, low operating temperature and high production efficiency are a few of the advantages.[1-3] Although cellulose acetate (CA) membranes are firstly developed and used for the commercial RO process, the use of CA membranes in the RO process has been limited due to the degradation by microbiological attack, narrow available pH use range, and severe compaction at high pressure.[4-6] On the other hand, polyamide (PA) thin film composite (TFC) membranes have exhibited better separation performances, wider pH range, and better physical properties than CA membranes.[6] Therefore, PA-TFC membranes are the most widely used in the RO process.[5, 6] In spite of the advantageous properties of PA-TFC membranes, the desalination processes using PA-TFC membranes still suffers from poor chlorine resistance and biofouling problems.[5, 7-15] There have been many

studies to surmount these disadvantages of PA-TFC membranes.[5, 8, 11, 13, 16, 17] For example, PA-TFC membranes having silver nanoparticles on the membrane surface showed a significant reduction in number of live bacteria and suppressed biofilm formation.[8] PA-TFC membranes containing carbon nanomaterials also showed improved chlorine resistant properties.[11, 13-15] However, to the best of our knowledge, no RO membranes having both antimicrobial and chlorine-tolerant properties have been reported yet.

Graphene and graphene oxide (GO) have been widely used as filler materials for polymer nanocomposites to impart thermal stability, oxidation stability, biocidal properties, and mechanical strength.[11, 17-20] Furthermore, it was recently demonstrated that polymer nanocomposite membranes having graphene and its derivatives can have very high water permeability, high durability, and chlorine resistant properties due to the unique properties of carbon nano structures.[11, 14, 21-26] Especially, such high membrane performance was observed from the polymer membranes prepared using the well-modified graphene derivatives having useful functional groups that can improve miscibility with the polymer matrix and also can impart various functions.[18, 26] Plant-induced natural

polyphenols including tannic acid that can be easily obtained from common plants such as oak, green tea, and fruits, and they are also commercially available with low cost. Natural polyphenols have been widely studied and used as surface modification materials due to their unique properties such as good adhesion, coordination with metal ions, antimicrobial properties, broad chemical versatility, and radical scavenging ability.[7, 27-32] In addition, wide surface engineering applications of the polyphenols are possible because they can easily adhere to various substrates by forming covalent and/or non-covalent bonding structures and be polymerized in basic conditions by self-oxidative polymerization, then uniform coating can be formed.[7, 28, 29, 32]

Herein, GO surface was modified by tannic acid (TA), one of the polyphenol derivatives, for utilizing the advantageous properties of both GO and polyphenols. The surface modified GO by TA was incorporated into the PA membrane, and the resulting membrane exhibited a significant increase in water flux, chlorine resistance, and antimicrobial properties.

5.2. Experimental

5.2.1. Materials

Graphite kindly supplied from BASF (Germany) was used as a precursor for the preparation of graphene oxide (GO). Polysulfone (PSf) membrane was received from Woong-jin Chemicals (Republic of Korea) and used for a support membrane of the thin film composite (TFC) membranes. Sulfuric acid (H_2SO_4 , 98 %) and isopropyl alcohol (IPA) were received from Daejung chemicals (Republic of Korea) and used as received. *m*-Phenylenediamine (MPD, 99 %), trimesoyl chloride (TMC, 98 %), tannic acid (TA), Tris-buffer agents (Trizma[®] HCl and Trizma[®] base), sodium hypochlorite (NaOCl, 10 – 13 %), 5,5-dimethyl-1-pyrroline-N-oxide (DMPO, for ESR analysis), and sodium chloride (NaCl, 99 %) were purchased from Aldrich and used without any purification. Deionized (DI) water was obtained from water purification system (Synergy, Millipore, USA), having a resistivity of 18.3 m Ω cm. *n*-Hexane (95 %) was received from Samchun Chemicals (Republic of Korea).

5.2.2. Preparation of GO and GO coated by TA (GOT)

GO was prepared through the modified Hummers method, as reported elsewhere.[11, 18-20] The surface of GO was coated by TA via self-polymerization of TA. 100 mg of GO was dispersed in 200 mL of Tris-buffer solution (100 mM, pH 8.5). 200 mg of TA was dissolved in the GO-dispersed buffer solution and stirred for 24 h at room temperature. The reaction solution was diluted with 500 mL of water and filtered using anodic aluminium oxide (AAO) filter. The filtered solid (GOT) was dried in a 35 °C vacuum oven over 24 h and the product, GOT, was obtained in 82 % yield.

5.2.3. Preparation of the polyamide membrane (PA membrane) and the polyamide membranes containing TA, GO, GOT, and the mixture of TA and GO (PA-T, PA-GO, PA-GOT, and PA-T-GO membranes)

The reverse osmosis membranes were prepared by the typical interfacial polymerization between MPD aqueous solution and TMC organic solution.[3, 9, 11] The following procedure was used for the preparation of polyamide membrane (PA membrane) without any

ingredients such as TA, GO, and GOT. PSf support membrane was immersed in IPA for 10 min to activate pores and washed with water. The IPA-pretreated PSf membrane was placed in the water bath for 3 h to stabilize the pores. The membrane was placed into the bath with 1-3 wt% aqueous solutions of MPD for 3 h. The membrane was taken out and air bubbles and droplets of aqueous solution on the membrane surfaces were removed carefully by rolling a rubber roller. The membrane was fixed on a flat board with a silicon-rubber mold. The 0.1 wt% TMC solution (in *n*-hexane) was poured on the membrane saturated with aqueous solution. The excess TMC solution was removed after 1 min of reaction, and the membrane was placed in the 100 °C oven for 5 min for crosslinking as well as further polymerization. The resulting membrane was washed with water several times. Other membranes were prepared using the same procedure used for the PA membrane except the aqueous solution. The detailed compositions of the MPD aqueous solutions for the preparation of the other membranes used for comparative study are listed in Table 5.1. Another polyamide membrane was prepared using the aqueous solution containing 2 wt% of MPD, 0.5 wt% of DMSO, 2 wt% of TEA, 1 wt% of CSA, and 0.5 wt% of SDS (Table 5.2).

Although the increase in membrane performances was observed from the membranes containing additives, we intentionally did not include any additives into the membranes in this study because our aim is to systematically observe the effects of the carbon nanomaterials such as GO and GOT in active layers on membrane performances.

5.2.4. Membrane filtration test.

The water flux and salt rejection values of the membranes were obtained by the filtration experiments using lab-scale cross-flow RO membrane test unit.[3, 9, 11] The effective membrane area was $3.3 \times 6.8 \text{ cm}^2$ with 0.3 cm of channel height. The 15.5 bar (225 psi) of feed pressure, the 2,000 mg L⁻¹ of NaCl feed solution (the conductivity of feed solution was about 3.84 mS cm⁻¹), and 0.5 L min⁻¹ of cross flow velocity at the membrane surface was used. This test condition has been generally used for measuring the performance of the brackish water reverse osmosis (BWRO) membranes by others.[15, 33, 34] By weighing the permeate solution, water flux values were obtained. Membrane flux, J , was calculated using equation (1):

$$J = \Delta V / (A \times \Delta t) \quad (1)$$

where ΔV is the volume of permeate collected between weight measurements, A is the membrane surface area, and Δt is the time between two weight measurements.

Salt rejection was calculated using the following equation (2):

$$R = (1 - C_p / C_f) \times 100 \% \quad (2)$$

where R is salt rejection value, C_p is the salt concentration in permeate, and C_f is the salt concentration in feed. The salt concentrations were obtained using conductivity meter (InoLab Cond 730P, WTW 82362, weilheim). The water flux and salt rejection values were also evaluated to measure the chlorine resistant properties using the feed solution containing 2000 ppm of NaCl and 500 ppm of sodium hypochlorite. All membrane performance results in this chapter are the average values obtained by more than two measurements from the three membranes prepared at different times to confirm the reproducibility.

5.2.5. Evaluation of antimicrobial properties

Antimicrobial property of the membranes was evaluated through a shake flask method.[16, 17, 35] This method was specially designed

for specimens with non-releasing antimicrobial agents under dynamic contact conditions, as previously reported, and *Escherichia coli* (*E. coli*) was used as model of microorganism for the test. *E. coli* was grown in Nutrient broth (NB) growth solutions for 18 h at 37 °C to prepare the bacteria suspension solution. A representative colony was lifted off with a platinum loop, placed in 30 mL of NB, and incubated with shaking for 18 h at 37 °C. After washed with PBS, they were re-suspended in PBS to yield $1.0 \times 10^5 - 1.5 \times 10^5$ colony forming unit (CFU) mL⁻¹. Bacterial cell concentration was estimated by measuring the absorbance of cell suspension at 600 nm.[36] To evaluate the antimicrobial properties of the membranes, 1 cm × 1 cm of the membranes were dipped into a falcon tube containing 5.0 mL of 1.0 mM PBS culture solution with a cell concentration of $1.0 \times 10^5 - 1.5 \times 10^5$ CFU mL⁻¹. The falcon tubes were shaken at 200 rpm on a shaking incubator at 25 °C for 24 h. After shaking vigorously for detachment of the adhered cells from the membrane surfaces, the solution was diluted, and 0.1 mL of each diluent was spread onto the nutrient agar plates. After incubating the plates for 18 h at 37 °C, viable microbial colonies were counted. Bacteria inhibition rate and the normalized number of viable bacteria were calculated as follows:

$$\text{Bacteria inhibition rate (\%), } B_i = 100 \times (N_0 - N_i) / N_0 \quad (3)$$

$$\text{Normalized number of viable bacteria (\%) = } 100 - B_i \quad (4)$$

where N_0 is bacterial CFU of the PA membrane and N_i is bacterial CFU of other membranes.

5.2.6. Characterizations.

Raman spectroscopy (LabRam ARAMIS, Horiba Jobin-Yvon, France) was used to observe the damaged crystalline structure of GO and GOT surfaces. Since fluorescences from PSf layer can disturb the Raman scattering signals, thin active layer of membrane transferred to silicon wafer was used for the Raman spectroscopy. The excitation source was a diode laser with an excitation wavelength of 785 nm and a power of 5 mW. The laser excitation was focused using a 100× objective and the Stokes-shifted Raman scattering was recorded using a 1400/600 groove min^{-1} grating. The surface compositions of the GO and GOT were analyzed by X-ray photoelectron microscopy (XPS, PHI-1600) using Mg K α (1254.0 eV) as radiation source. Survey spectra were collected over a range of 0–1100 eV, followed by high resolution scan of the C 1s and O 1s regions. Fourier-transform

infrared (FT-IR) spectra of GO and GOT were measured in transmission mode in the frequency range of 4000–650 cm^{-1} on a Nicolet 6700 instrument (Thermo Scientific, USA). FT-IR spectra of dried membranes were recorded in attenuated total reflectance (ATR) mode in the frequency range of 4000–650 cm^{-1} . The spectrum as collected as the average of 32 scans with the resolution of 8 cm^{-1} . Surface morphologies of the membranes were inspected by scanning electron microscopy (SEM, JSM-6701F, JEOL) using a field emission scanning electron microscope (FESEM). To observe the bottom side of active layer, the active layer of the membrane was reversely-transferred to the silicon wafer after the PSf layer was removed by tetrahydrofuran. The cross-sectional images of the membranes were observed by transmission electron microscopy (TEM, LIBRA 120, Carl Zeiss, Germany). Small pieces of membranes were placed into viscous Spur resin and placed into 120 °C for 24 h. The harden resin was cut by an ultramicrotome (MTX, RMC) and placed on TEM grids. The mechanical properties of the membranes were measured by universal tensile testing machine (UTM). The dumbbell specimens were prepared using the ASTM standard D638 (Type V specimens dog-bone shaped membrane samples). Thermal gravimetric analysis

(TGA) was performed in a Q-5000 IR from TA Instruments, using a heating rate of $10\text{ }^{\circ}\text{C min}^{-1}$ under the nitrogen atmosphere. The investigation of radical scavenging effect of the CNT and GO was performed using electron spin resonance (ESR) spectrometer (JEOL, JES-TE200). The production of free radicals from sodium hypochlorite was monitored in the presence of the spin trap agent DMPO. The membrane active layer was soaked in the solution containing sodium hypochlorite (500 ppm) and DMPO (2 ppm), and then the ESR spectrum was obtained in every 30 min.

5.3. Results and Discussion

5.3.1. Preparation of graphene oxide (GO) and graphene oxide coated by tannic acid (GOT)

Since well-modified graphene derivatives can much improve the performance of polymer nanocomposite,[18, 19, 37, 38] tannic acid (TA), one of the natural polyphenol materials, was selected as a GO modification material.[7, 28, 32, 39] TA has been known to form a stable polymeric coating layer under basic conditions,[28, 32]

therefore, the surface of GO was modified by TA coating using the basic buffer solution (Figure 5.1). The formation of GO and GOT was confirmed by FT-IR, Raman spectroscopy, XPS, and TGA analysis. Figure 5.2a shows the FT-IR spectra of graphite, GO, and GOT. Since GO was prepared to have oxygen functional groups, such as epoxy, carbonyl, hydroxyl, and carboxylic acid groups, by the oxidation of graphite, the characteristic peaks from the oxygen functional groups were observed at 3400 cm^{-1} (O-H stretch) and 1720 cm^{-1} (ester O-C=O stretch) for GO. The characteristic peaks of the TA coating appeared at 2940 cm^{-1} (C-H sp^2), 1720 cm^{-1} (C=O stretch), 1370 and 1050 cm^{-1} (ester C-O stretch), and 1240 cm^{-1} (phenolic O-H stretch) in the spectrum of GOT, indicating that the surface of GO was well-coated by TA. Similar characteristic peaks were observed in the FT-IR spectrum of TA powder (Figure 5.3). Raman spectroscopic study provided the structural information of the carbon nanomaterials. A slight increase of the D3 and S3 band peak intensities ($\sim 1500\text{ cm}^{-1}$ and $\sim 2950\text{ cm}^{-1}$) for GOT is evidence of TA coating on GO, because D3 and S3 bands originate from the amorphous carbon fraction of soot (Figure 5.2b).[40, 41] The TA coating on GO was further confirmed by XPS and TGA analysis. Although oxygen content of GOT (32.60

wt%) is close to that of GO (30.78 wt%) (Table 5.3), the amount of C-O bonds in GOT is quite larger than that in GO. This is due to an increased amount of phenolic groups from TA coating layer on GOT (Figure 5.2c and d). The amount of TA coating on GOT could be estimated by TGA analysis (Figure 5.4). The large weight change below 300 °C in GO has been ascribed to the oxygen functional groups,[19, 20] and that over 300 °C is due to the degradation by both polymerized-TA and the graphitic part of GO. Therefore, the amount of TA coating on GO may roughly be calculated by the weight difference at around 300 °C, and it was found to be about 10.5 wt% (Figure 5.5).

5.3.2. Preparation of the polyamide membrane (PA membrane) and the polyamide membranes containing TA, GO, GOT, and the mixture of TA and GO (PA-T, PA-GO, PA-GOT, and PA-T-GO membranes)

PA, PA-T, PA-GO, and PA-GOT membranes were prepared by the typical interfacial polymerization,[3, 4, 9, 11, 15, 42-45] by changing the MPD aqueous solutions as shown in Table 1. Maximum water flux

value with reasonably large salt rejection value was obtained for the PA membrane prepared using 2wt% of MPD aqueous solution and PA-T, PA-GO, and PA-GOT membranes prepared using 3wt% of MPD aqueous solution with TA, GO and GOT, respectively, in the screening filtration test (Table 1). Therefore, those membranes having the largest water flux values were used to analyze the membrane and to investigate the effects of TA, GO, and GOT on the membrane performances. The formation of a polyamide active layer was confirmed by FT-IR analysis (Figure 5.6a). Characteristic peaks from the polyamide structures are shown at 3243-3392 cm^{-1} (N-H and O-H stretch), 1614 cm^{-1} (NH-CO vibration), and 1542 cm^{-1} (N-H bend) for the PA, PA-T, PA-GO, and PA-GOT membranes. While, the characteristic peaks from the GO and GOT were not clearly observed in PA-GO and PA-GOT membranes, respectively, because only very small amount of GO and GOT were included in the active layers. The GO and GOT contents in polyamide layers are less than 0.2 wt% when PA-GO and PA-GOT membranes were prepared using 3 wt% of MPD solutions containing 0.005 wt% of GO and GOT, respectively. Therefore, the presence of GO and GOT in the polyamide layer was observed by Raman spectroscopy (Figure 5.6b). Since graphitic

carbon structures show the inelastic scattering behavior from the laser light, a small amount of carbon materials in organic or inorganic matrix can be detected through the Raman spectroscopic studies. D (1308 cm^{-1}) and G (1600 cm^{-1}) band Raman shifts originated from GO and GOT structures were observed for PA-GO and PA-GOT membranes, demonstrating that the successful incorporation of GO and GOT in the membranes.

The morphologies of the membrane surfaces were observed by SEM. Figure 5.7a shows the SEM images of the top surface of the PA membrane. As expected, the typical ridge-and-valley structures well-covered on the PSf membrane was observed as reported before by others.[42, 47, 48] On the contrary, the PA-T membrane showed smaller ridge-and-valley structures with a large number of defects on the PSf membrane surface as directed by the arrows in Figure 5.7b (magnified image is shown in Figure 5.8). Since TA in the aqueous solution can also react with TMC during interfacial polymerization, the polyamide layer on the PSf membrane could not be effectively formed, and then such defects can be formed. This reaction has been reported by the others before.[49] Furthermore, since TA can be polymerized in basic conditions such as the MPD solution,[28, 32] the

polymerized TA structures can also produce defects on the membranes.[50, 51] PA-GO and PA-GOT membranes also have the ridge-and-valley structures well-covered on the PSf membrane without any defects. Their ridge-and-valley sizes are slightly smaller than those on the PA membrane, as shown in Figure 5.7c and d because GO and GOT having various oxygen functional groups can affect the interfacial polymerization forming the polyamide layers. In addition to the ridge-and-valley structures, PA-GO and PA-GOT membranes show protruding domains with planer shapes on the top and bottom of the active layers. As mentioned in the experimental section, the bottom images were observed from the active layer reversely-transferred on the silicon wafer. Those protruding domains should originate from the planer sheet structures of GO and GOT because they are not observed from PA and PA-T membranes. The populations of those domains are larger in the bottom part than top surface because the densities of GO and GOT are larger than water, then GO and GOT can sank into the bottom/inner part of the active layer during the membrane preparation procedure (Figure 5.7c, d, g, and h). When PA-GO and PA-GOT membranes were prepared using 0.005 wt% or smaller concentrations of GO and GOT, respectively, no

aggregated structures were observed. However, large aggregated clusters of over 3 μm in size were observed, when the concentration larger than 0.005 wt% was used (Figure 5.9). Therefore, 0.005 wt% should be the maximum concentration for the preparation of PA-GO and PA-GOT membranes with well-dispersed GO and GOT without aggregation, which could be further confirmed from the water flux and salt rejection behavior shown in the later part of this chapter.

5.3.3. Water flux and salt rejection

The water flux and salt rejection values of the membranes were measured by lab-scale cross-flow RO systems. When the PA membrane was prepared using 2 wt% MPD aqueous solution, the largest water flux (34.21 ± 1.74 LMH) and salt rejection values (96.80 ± 0.85 %) were obtained; those values are larger than those observed from the PA membranes prepared using 1 and 3 wt% of MPD aqueous solution (Table 1). Therefore, the change of the membrane performances by the addition of the carbon nanomaterials and/or TA was compared with the PA membrane prepared using 2 wt% MPD aqueous solution having the largest water flux and salt rejection values

among the PA membranes in this study.

As shown in Table 1, large water flux values (about 40 LMH) were observed for PA-T membranes, while effective salt rejection is not possible due to the defects on the membrane surface. Similarly, TFC membrane prepared by interfacial polymerization between the TA aqueous solution and TMC organic solution was reported to have a small NaCl salt rejection value about 20 %.[49] Although the salt rejection value of PA-T membrane is too small to be used in the BWRO process, the membrane performances of the PA-T membrane were measured to investigate the effects of TA, GO, and GOT on membrane performances. In contrast, PA-GO and PA-GOT membranes show quite large salt rejection values comparable to those of the PA membranes. As observed from the SEM images, those membranes do not have any defect structures, and this can maintain the high salt rejection. The salt rejection values of PA-T-GO membranes prepared using the mixture of TA and GO in the aqueous solutions were found to be quite small close to those of PA-T membranes because the TA existing as the mixture with GO can produce the defect structures as observed in PA-T membrane. Interestingly, 3 wt% MPD aqueous solution was found to be the

optimum concentration for the preparation of PA-GO and PA-GOT membranes having the maximum water flux and salt rejection values, although 2 wt% MPD aqueous solution was the optimum concentration for the PA membrane. It is very possible that a small amount of GO and GOT can change the surface morphology, although it is not clearly distinguished from the SEM studies, and the hydrophilicity as shown in water contact angle results (Figure 5.10), which can in turn change the membrane performances such as water flux and salt rejection behaviors.[43-45, 52] It can further change the optimum MPD concentration for the membrane preparation as reported before.[43-45] It is also possible that some of the oxygen functional groups including carboxylic acid and aldehyde on GO and GOT can be reacted with the amine groups of MPD. This may increase the MPD optimum concentration for the membrane preparation.[3, 11] The membranes showing the best performances such as the PA membrane prepared by 2 wt% MPD aqueous solution and PA-T, PA-GO, PA-GOT membranes prepared by 3 wt% MPD aqueous solutions were used for the systematic study to observe the effects of the carbon nanomaterials on membrane performances.

Figure 5.11 shows the water flux and salt rejection values of the PA-

GO and PA-GOT membranes prepared using various amount of GO and GOT in 3 wt% MPD aqueous solution, respectively. The water flux and salt rejection values are very close to those of the PA membrane when the PA-GO and PA-GOT membranes were prepared using 0.0002 wt% of GO and GOT in the aqueous solutions, respectively; since the very small amounts of GO and GOT are used, the effects of carbon nanomaterials are negligible. The water flux values of the PA-GO and PA-GOT membranes prepared using 0.001 to 0.005 wt% of GO and GOT in aqueous solution, respectively, are larger than that of the PA membrane although the salt rejection values are very close. The slightly larger water flux values of the PA-GOT membranes compared to the PA-GO membranes are attributed to the hydrophilic surface properties of GOT that can affect the water sorption and membrane morphologies. When the PA-GO and PA-GOT membrane were prepared using larger than 0.005 wt% of GO and GOT in the aqueous solution, respectively, the salt rejection values became smaller accompanied by a large increase in water flux values. The formation of large void structures formed by aggregation of GO and GOT as observed by SEM (Figure 5.9) should cause these results. Large voids could work as defects, providing large channels for water

and ion molecules.[11, 15, 23] Although the water flux values of the PA-GO and PA-GOT membranes prepared using 0.005 wt% of GO and GOT, respectively, are larger than that of the PA membrane by 6.43 LMH (18.8 % increase) and 9.00 LMH (26.3 % increase), respectively, while their salt rejection values are very close; their difference is less than 0.5 %. The quite large increase in water flux by the incorporation of GO and GOT could be explained by the water transport properties of carbon nanomaterials, as described in the previous studies.[3, 11, 23-25, 53] Carbon nanomaterials including carbon nanotubes and graphene derivatives have been known to increase water flux because hydrated ions can flow quickly on the carbon surfaces.[11, 21, 22, 53] Although PA-GO and PA-GOT membranes show quite large increase of water flux by the carbon nanomaterials, the decrease in salt rejection was not observed, if any, because the carbon nanomaterials are well-dispersed in continuous polyamide matrix without any aggregated defect structures as observed by SEM (Figure 5.7).[3, 11, 23] Furthermore, since GO and GOT can affect the polyamide formation during the interfacial polymerization, the changes in polyamide morphologies (SEM images in Figure 5.7) and thickness (TEM images in Figure 5.12) should

affect the membrane performances.

5.3.4. Chlorine resistant properties

Biofilms formed on the membrane surface decrease the membrane performances significantly, then additional disinfection processes should be included in the membrane-based filtration.[10, 12, 54, 55] Sodium hypochlorite, one of the most commonly used oxidizing agent for the disinfection process, was used as the active chlorine agent in this study.[4, 5, 11-13] Since PA membranes have been known to be degraded by chlorine agent,[4, 5, 11] the salt rejection of the PA membrane decreases by 7.8 % after only 7,500 ppm h of chlorine exposure, and then drops down rapidly with increase of chlorine exposures until 20,000 ppm h of chlorine exposure, and then the salt rejection value of 25.5 % maintains afterward as shown in Figure 5.13a. Such large decrease of salt rejection should be caused by the cleavage of the amide groups by oxidative agents such as chlorine radical, hydroxyl radical, and hypochlorite that can easily diffuse into the polyamide active layer.[11, 14] Therefore, the chlorine resistance can be improved by incorporating the cross-linked structures[44, 45]

and/or the radical capturing moieties such as phenol groups that can be found in TA.[56, 57] Additional cross-linked structures can be incorporated by TA due to the reactions of the multi-phenol groups with the acylchloride groups in TMC during the interfacial polymerization, therefore, PA-T membrane showed improved the chlorine resistant properties, compared with the PA membrane as shown in Figure 5.13a and 7b; the PA and PA-T membranes show the salt rejection values of 50.6 % and 64.5 %, respectively, after 20,000 ppm h of chlorine exposure. The chlorine resistance of the PA-GO membrane was found to be larger than that of the PA-T membrane upon the chlorine exposure; the salt rejection value of the PA-GO membrane is 52.6 % after 35,000 ppm h of chlorine exposure, which is larger than that of the PA-T membrane, 31.7 %. The large chlorine resistant properties of the PA-GO membrane could be ascribed to the combined effect of GO sheets having the barrier properties and the radical scavenging phenol groups. GO sheets have been known to disturb the diffusion of organic molecules, then they can also block the active radicals.[11, 14] The PA-GOT membrane showed the best chlorine resistant properties among the membranes used in this study as shown in Figure 5.13d; the salt rejection value of the PA-GOT

membrane after 35,000 ppm h of chlorine exposure was 90.0 %. The best chlorine resistant properties of the PA-GOT membrane could be ascribed to synergistic combination of TA and GO in the active layer; the diffusion of active radicals can be also prevented by the GOT sheets as the GO sheets and the radical scavenging ability of GO can be further improved by the TA coating layer. This synergistic effect of GOT could be clearly explained by the relatively low chlorine resistant properties of the PA-T-GO membrane prepared using 3 wt% MPD aqueous solution containing the mixture of TA and GO (Figure 5.14); the salt rejection value was 55.2 % after 35,000 ppm h of chlorine exposure. The antioxidant properties of the PA-GOT membrane could be estimated by ESR analysis, as previously reported.[11] The ESR intensity of the PA-GOT membrane decrease much more than those of other membranes due to the synergistic effect of GOT sheets in the PA-GOT membrane having improved radical scavenging and barrier properties (Figure 5.15 and 5.16). The reference ESR analysis of GO and GOT without polyamide also indicates that GOT has larger radical scavenging ability than GO; the ESR in GOT decreases more than that in GO (Figure 5.17).

5.3.5. Antimicrobial properties

It is very desirable to develop filtration membranes having antimicrobial properties because it can reduce the biofouling, and then lower operating cost.[8, 10] Figure 5.18 shows the normalized number of viable bacteria (CFU % of the PA membrane) after 24 h of incubation with the membranes. The PA-T membrane was found to have better antimicrobial property than the PA membrane; 85.94 ± 13.62 % of viable bacteria was observed for the PA-T membrane as compared to the PA membrane. Enhanced antimicrobial properties of the PA-T membrane could be attributed to the phenol groups in the TA unit. The phenol groups of TA can react with enzymes and/or essential elements of microorganisms or directly act as biocidal agent through the inhibition of oxidative phosphorylation.[30, 36, 39] GO, known to inactivate bacteria by physical disruption, oxidative stress, and direct damaging mechanisms, was found to be even more effective to deactivate the microorganism than TA;[17, 58] the number of viable bacteria incubated with the PA-GO membrane (75.52 ± 6.31 %) is smaller than that with the PA-T membrane (85.94 ± 13.62 %). The least number of viable bacteria was found in the incubation with the

PA-GOT membrane (52.08 ± 14.18 %), indicating that GOT is the most effective additive to impart the antimicrobial properties to the membrane. The oxidative stress should be increased by the TA coating layer on GO because it is known that oxygen functional groups on carbon nanostructures can improve the antimicrobial property due to the increased oxidative stress.[59] The synergistic increase of the antimicrobial properties of the TA coating layers on GO could be again confirmed by less effective antimicrobial properties of the PA-T-GO membrane prepared using the mixture of TA and GO; the number viable bacteria with the PA-T-GO membrane was found to be 81.04 ± 12.41 %. Similar synergistic antimicrobial effects of phosphonium functionalized GO have been reported before.[60]

5.4. Conclusions

In this study, graphene oxide coated by tannic acid (GOT) was prepared via simple self-polymerization of tannic acid and used as filler materials of polyamide reverse osmosis membranes to improve membrane performances. Chlorine resistance properties significantly increased by incorporating GOT; the polyamide membrane containing

GOT (PA-GOT membrane) showed 0.94 normalized salt rejection value even at 35,000 ppm h of chlorine exposure. Furthermore, the PA-GOT membrane showed improved antimicrobial properties compared to polyamide membrane without fillers and the polyamide membranes containing tannic acid (TA) and/or graphene oxide (GO). These results should be ascribed to the synergistic effects of TA and GO in GOT; the barrier property and oxidative stress capability of GO are combined with radical scavenging and antimicrobial properties of TA coating on GO surfaces. The advantageous properties of polymer nanocomposites containing GOT including antimicrobial and antioxidant properties might be also useful for other applications such as tissue engineering, battery membranes, sensing, and gas separation processes.

5.5. References

- [1] B.D. Freeman, I. Pinnau, *ACS Symposium Series; American Chemical Society: Washington* **2004**, 876, 1-23.
- [2] M.A. Shannon, P.W. Bohn, M. Elimelech, J.G. Georgiadis, B.J. Marinas, A.M. Mayes, *Nature* **2008**, 452, 301-310.

- [3] H.J. Kim, K. Choi, Y. Baek, D.-G. Kim, J. Shim, J. Yoon, J.-C. Lee, *ACS Appl. Mater. Interfaces* **2014**, 6, 2819-2829.
- [4] S.C. Yu, M.H. Liu, Z.H. Lu, Y. Zhou, C.J. Gao, *J. Membr. Sci.* **2009**, 344, 155-164.
- [5] H.B. Park, B.D. Freeman, Z.B. Zhang, M. Sankir, J.E. McGrath, *Angew. Chem. Int. Edit.* **2008**, 47, 6019-6024.
- [6] D. Li, H.T. Wang, *J. Mater. Chem.* **2010**, 20, 4551-4566.
- [7] H.J. Kim, D.-G. Kim, H. Yoon, Y.-S. Choi, J. Yoon, J.-C. Lee, *Adv. Mater. Interfaces* **2015**, 2, 1500298.
- [8] M. Ben-Sasson, X.L. Lu, E. Bar-Zeev, K.R. Zodrow, S. Nejati, G.G. Qi, E.P. Giannelis, M. Elimelech, *Water Res.* **2014**, 62, 260-270.
- [9] H.J. Kim, Y. Baek, K. Choi, D.-G. Kim, H. Kang, Y.S. Choi, J. Yoon, J.-C. Lee, *RSC Adv.* **2014**, 4, 32802-32810.
- [10] J. Yu, Y. Baek, H. Yoon, J. Yoon, *J. Membr. Sci.* **2013**, 427, 30-36.
- [11] H.J. Kim, M.Y. Lim, K.H. Jung, D.-G. Kim, J.-C. Lee, *J. Mater. Chem. A* **2015**, 3, 6798-6809.
- [12] S. Hong, I.C. Kim, T. Tak, Y.N. Kwon, *Desalination* **2013**, 309, 18-26.
- [13] J. Park, W. Choi, S.H. Kim, B.H. Chun, J. Bang, K.B. Lee, *Desalin. Water Treat.* **2010**, 15, 198-204.

- [14] W. Choi, J. Choi, J. Bang, J.H. Lee, *ACS Appl. Mater. Interfacs* **2013**, 5, 12510-12519.
- [15] H.Y. Zhao, S. Qiu, L.G. Wu, L. Zhang, H.L. Chen, C.J. Gao, *J. Membr. Sci.* **2014**, 450, 249-256.
- [16] M. Ben-Sasson, K.R. Zodrow, G.G. Qi, Y. Kang, E.P. Giannelis, M. Elimelech, *Environ. Sci. Technol.* **2014**, 48, 384-393.
- [17] F. Perreault, M.E. Tousley, M. Elimelech, *Environ. Sci. Technol. Lett.* **2014**, 1, 71-76.
- [18] J. Shim, D.-G. Kim, H.J. Kim, J.H. Lee, J.H. Baik, J.-C. Lee, *J. Mater. Chem. A* **2014**, 2, 13873-13883.
- [19] M.Y. Lim, H.J. Kim, S.J. Baek, K.Y. Kim, S.S. Lee, J.-C. Lee, *Carbon* **2014**, 77, 366-378.
- [20] M.-Y. Lim, J. Oh, H.J. Kim, K.Y. Kim, S.-S. Lee, J.-C. Lee, *Eur. Polym. J.* **2015**, 69, 156-167.
- [21] L. Huang, Y.R. Li, Q.Q. Zhou, W.J. Yuan, G.Q. Shi, *Adv. Mater.* **2015**, 27, 3797-3802.
- [22] M. Hu, B.X. Mi, *Environ. Sci. Technol.* **2013**, 47, 3715-3723.
- [23] L. H. D, K. H. W, C. Y .H, P. H. B, *Small* **2014**, 10, 2653-2660.
- [24] D.R. Paul, *Science* **2012**, 335, 413-414.

- [25] S. Karan, S. Samitsu, X.S. Peng, K. Kurashima, I. Ichinose, *Science* **2012**, 335, 444-447.
- [26] K. Huang, G. Liu, J. Shen, Z. Chu, H. Zhou, X. Gu, W. Jin, N. Xu, *Adv. Func. Mater.* **2015**, 25, 5809-5815.
- [27] H. Akiyama, K. Fujii, O. Yamasaki, T. Oono, K. Iwatsuki, *J. Antimicrob. Chemoth.* **2001**, 48, 487-491.
- [28] D.G. Barrett, T.S. Sileika, P.B. Messersmith, *Chem. Commun.* **2014**, 50, 7265-7268.
- [29] H. Ejima, J.J. Richardson, K. Liang, J.P. Best, M.P. van Koevorden, G.K. Such, J.W. Cui, F. Caruso, *Science* **2013**, 341,154-157.
- [30] A. Mori, C. Nishino, N. Enoki, S. Tawata, *Phytochemistry* **1987**, 26, 2231-2234.
- [31] S. Quideau, D. Deffieux, C. Douat-Casassus, L. Pouysegu, *Angew. Chem. Int. Edit.* **2011**, 50, 586-621.
- [32] T.S. Sileika, D.G. Barrett, R. Zhang, K.H.A. Lau, P.B. Messersmith, *Angew. Chem. Int. Edit.* **2013**, 52, 10766-10770.
- [33] B.H. Jeong, E.M.V. Hoek, Y.S. Yan, A. Subramani, X.F. Huang, G. Hurwitz, A.K. Ghosh, A. Jawor, *J. Membr. Sci.* **2007**, 294, 1-7.
- [34] K.P. Lee, T.C. Arnot, D. Mattia, *J. Membr. Sci.* **2011**, 370, 1-22.

- [35] Y.S. Choi, H. Kang, D.G. Kim, S.H. Cha, J.-C. Lee, *ACS Appl. Mater. Interfaces* **2014**, 6, 21297-21307.
- [36] D.J. Kim, S.G. Chung, S.H. Lee, J.W. Choi, *Afr. J. Microbiol. Res.* **2012**, 6, 4620-4622.
- [37] B.P. Li, W.P. Hou, J.H. Sun, S.D. Jiang, L.L. Xu, G.X. Li, M.A. Memon, J.H. Cao, Y. Huang, C.W. Bielawski, J.X. Geng, *Macromolecules* **2015**, 48, 994-1001.
- [38] N. Prabhakar, T. Nareoja, E. von Haartman, D. Sen Karaman, S.A. Burikov, T.A. Dolenko, T. Deguchi, V. Mamaeva, P.E. Hanninen, I.I. Vlasov, O.A. Shenderova, J.M. Rosenholm, *Nanoscale* **2015**, 7, 10410-10420.
- [39] R. Liu, J.C. Zheng, R.X. Guo, J. Luo, Y. Yuan, X.Y. Liu, *Ind. Eng. Chem. Res.* **2014**, 53, 10835-10840.
- [40] A. Sadezky, H. Muckenhuber, H. Grothe, R. Niessner, U. Poschl, *Carbon* **2005**, 43, 1731-1742.
- [41] B.W. Zhang, L.F. Li, Z.Q. Wang, S.Y. Xie, Y.J. Zhang, Y. Shen, M. Yu, B. Deng, Q. Huang, C.H. Fan, J.Y. Li, *J. Mater. Chem.* **2012**, 22, 7775-7781.
- [42] J.T. Duan, Y.C. Pan, F. Pacheco, E. Litwiller, Z.P. Lai, I. Pinnau, *J. Membr. Sci.* **2015**, 476, 303-310.

- [43] A.K. Ghosh, B.H. Jeong, X.F. Huang, E.M.V. Hoek, *J. Membr. Sci.* **2008**, 311, 34-45.
- [44] M.H. Liu, D.H. Wu, S.C. Yu, C.J. Gao, *J. Membr. Sci.* **2009**, 326, 205-214.
- [45] T.Y. Wang, L. Dai, Q.F. Zhang, A. Li, S.B. Zhang, *J. Membr. Sci.* **2013**, 440, 48-57.
- [46] A.K. Ghosh, R.C. Bindal, S. Prabhakar, P.K. Tewari, *J. Polym. Mater.* **2011**, 28, 505-515.
- [47] M. Elimelech, X.H. Zhu, A.E. Childress, S.K. Hong, *J. Membr. Sci.* **1997**, 127, 101-109.
- [48] D. Emadzadeh, W.J. Lau, M. Rahbari-Sisakht, A. Daneshfar, M. Ghanbari, A. Mayahi, T. Matsuura, A.F. Ismail, *Desalination* **2015**, 368, 106-113.
- [49] Y. Zhang, Y.L. Su, J.M. Peng, X.T. Zhao, J.Z. Liu, J.J. Zhao, Z.Y. Jiang, *J. Membr. Sci.* **2013**, 429, 235-242.
- [50] S.G. Hovakeemian, R.H. Liu, S.H. Gellman, H. Heerklotz, *Soft Matter* **2015**, 11, 6840-6851.
- [51] C.H. Ma, C. Zhang, Y. Labreche, S.L. Fu, L. Liu, W.J. Koros, *J. Membr. Sci.* **2015**, 493, 252-262.

- [52] S. Qiu, L.G. Wu, L. Zhang, H.L. Chen, C.J. Gao, *J. Appl. Polym. Sci.* **2009**, 112, 2066-2072.
- [53] R.R. Nair, H.A. Wu, P.N. Jayaram, I.V. Grigorieva, A.K. Geim, *Science* **2012**, 335, 442-444.
- [54] J.S. Baker, L.Y. Dudley, *Desalination* **1998**, 118, 81-89.
- [55] M.A. Saad, *Desalination* **1992**, 88, 85-105.
- [56] I. Gulcin, Z. Huyut, M. Elmastas, H.Y. Aboul-Enein, *Arab. J. Chem.* **2010**, 3, 43-53.
- [57] G.K.B. Lopes, H.M. Schulman, M. Hermes-Lima, *Bba-Gen Subjects* **1999**, 1472, 142-152.
- [58] F. Perreault, A.F. de Faria, S. Nejati, M. Elimelech, *ACS Nano* **2015**, 9, 7226-7236.
- [59] S.B. Liu, T.H. Zeng, M. Hofmann, E. Burcombe, J. Wei, R.R. Jiang, J. Kong, Y. Chen, *ACS Nano* **2011**, 5, 6971-6980.
- [60] X. Cai, S.Z. Tan, M.S. Lin, A. Xie, W.J. Mai, X.J. Zhang, Z.D. Lin, T. Wu, Y.L. Liu, *Langmuir* **2011**, 27, 7828-7835.

Table 5.1. Water flux and salt rejection values of the membranes.

Membrane type ^a	MPD ^b	TA ^c	GO ^c	GOT ^c	Water flux [LMH]	Salt rejection [%]
LFC-1 (Commercial)	-	-	-	-	36.58 ± 1.17	96.98 ± 0.69
PA	1	- ^d	- ^d	- ^d	32.11 ± 2.85	95.75 ± 1.24
PA	2	- ^d	- ^d	- ^d	34.21 ± 1.74	96.80 ± 0.85
PA	3	- ^d	- ^d	- ^d	32.67 ± 2.42	96.22 ± 1.68
PA-T	2	1	- ^d	- ^d	40.00 ± 2.91	88.82 ± 4.46
PA-T	3	1	- ^d	- ^d	39.41 ± 2.49	89.18 ± 5.06
PA-GO	2	- ^d	1	- ^d	36.41 ± 1.79	95.44 ± 1.07
PA-GO	3	- ^d	1	- ^d	38.66 ± 0.69	96.96 ± 0.60
PA-GOT	2	- ^d	- ^d	1	37.33 ± 0.99	95.97 ± 0.65
PA-GOT	3	- ^d	- ^d	1	38.18 ± 1.16	96.32 ± 0.67
PA-T-GO	2	0.5	0.5	- ^d	38.89 ± 3.25	90.58 ± 4.58
PA-T-GO	3	0.5	0.5	- ^d	37.15 ± 4.54	90.92 ± 3.46

Table 5.1. (continued) Water flux and salt rejection values of the membranes.

a) The concentration of TMC organic solution for interfacial polymerization is 0.1 wt%. b) The concentration in aqueous solution for interfacial polymerization. (wt%) c) The concentration in aqueous solution for interfacial polymerization. (wt%, $\times 10^3$) d) Not used.

Table 5.2. Water flux and salt rejection values of PA membrane prepared 2 wt% MPD aqueous solution with additives; 0.5 wt% of DMSO, 2 wt% of TEA, 1 wt% of CSA, and 0.5 wt% of SDS.

Water flux [LMH]	Salt rejection [%]
38.84 ± 4.21	98.08 ± 0.54

Table 5.3. XPS elemental composition and O/C ratio of Graphite, GO, and GOT.

	C contents (%)	O contents (%)	O/C ratio
Graphite	94.05	5.95	0.06
GO	69.22	30.78	0.44
GOT	67.40	32.60	0.48

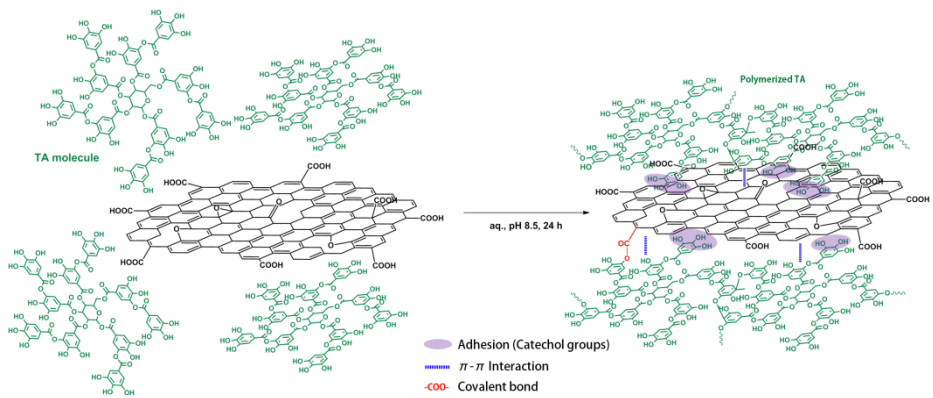


Figure 5.1. Preparation of graphene oxide coated by tannic acid (GOT).

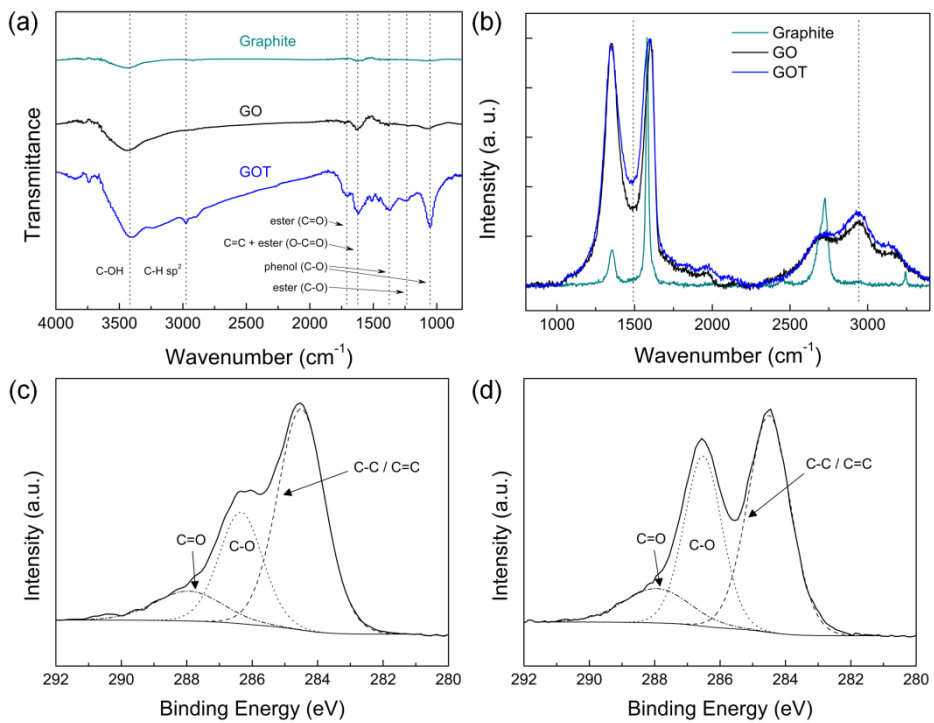


Figure 5.2. (a) FT-IR spectra, (b) Raman spectra of carbon materials, and XPS spectra of (c) GO and (d) GOT from XPS spectra.

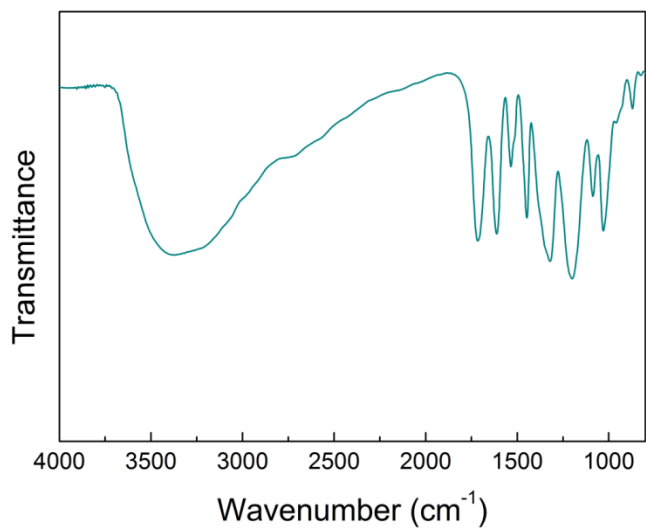


Figure 5.3. FT-IR spectrum of TA.

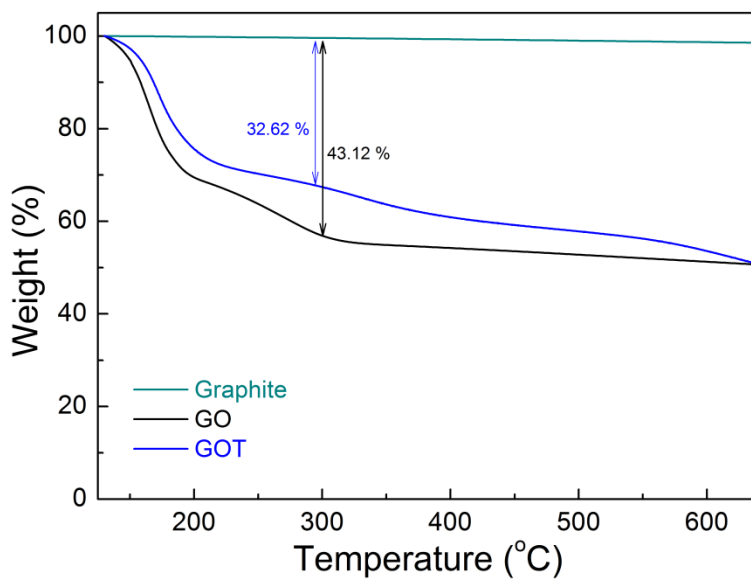


Figure 5.4. TGA results of graphite, GO, and GOT (10 min °C min⁻¹, under N₂ atmosphere).

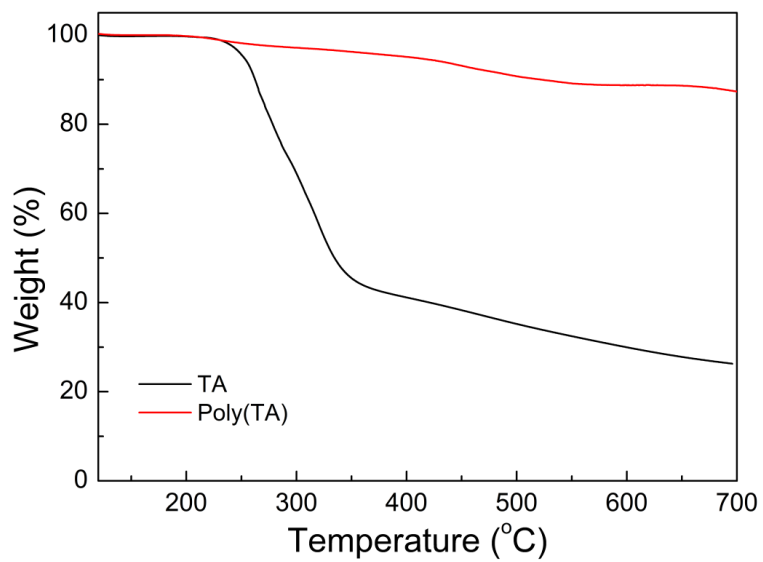


Figure 5.5. TGA results of TA and polymerized-TA (10 min °C min⁻¹, under N₂ atmosphere).

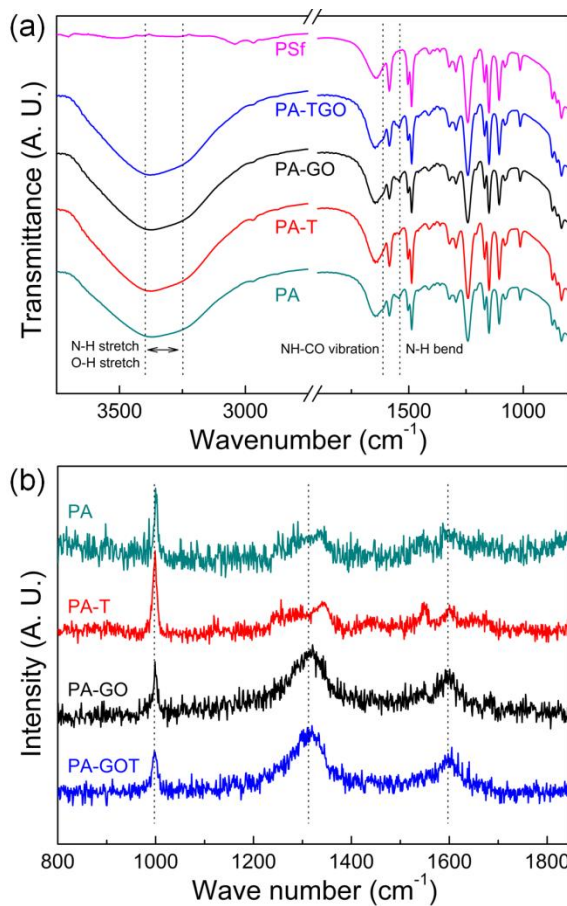


Figure 5.6. (a) FT-IR spectra and (b) Raman spectra of PA (prepared using 2 wt% MPD aqueous solution), PA-T (prepared using 3 wt% MPD aqueous solution containing 0.005 wt% of TA), PA-GO (prepared using 3 wt% MPD aqueous solution containing 0.005 wt% of GO), and PA-GOT (prepared using 3 wt% MPD aqueous solution containing 0.005 wt% of GOT) membranes.

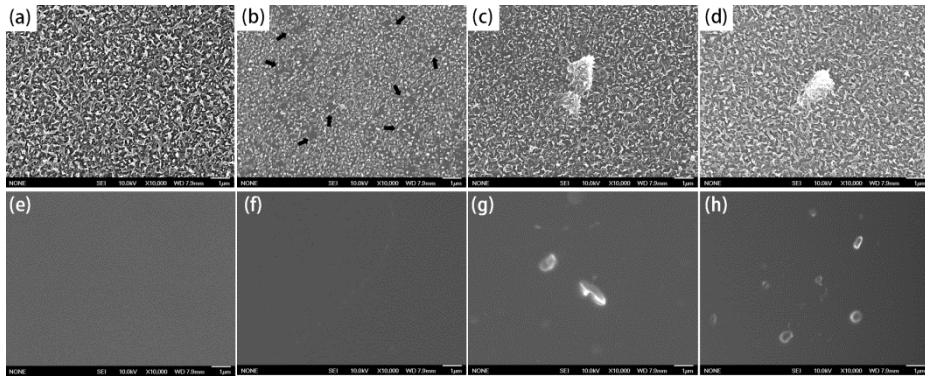


Figure 5.7. SEM images of top/bottom surface of active layer of the membranes; (a), (e) PA, (b), (f) PA-T (prepared using 0.005 wt% TA in aqueous solution), (c), (g) PA-GO (prepared using MPD aqueous solution containing 0.005 wt% of GO), and (d), (h) PA-GOT (prepared using MPD aqueous solution containing 0.005 wt% of GOT) membranes (size of the images is $12\ \mu\text{m}$ (width) \times $9.5\ \mu\text{m}$ (height)).

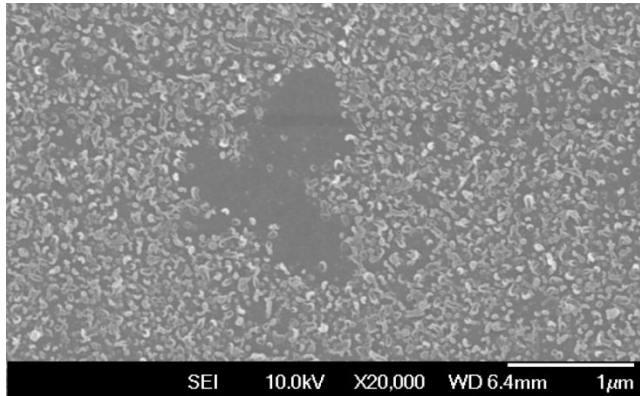


Figure 5.8. Magnified SEM images at the top surfaces of PA-T membrane (prepared using 3 wt% MPD aqueous solution containing 0.005 wt% of TA).

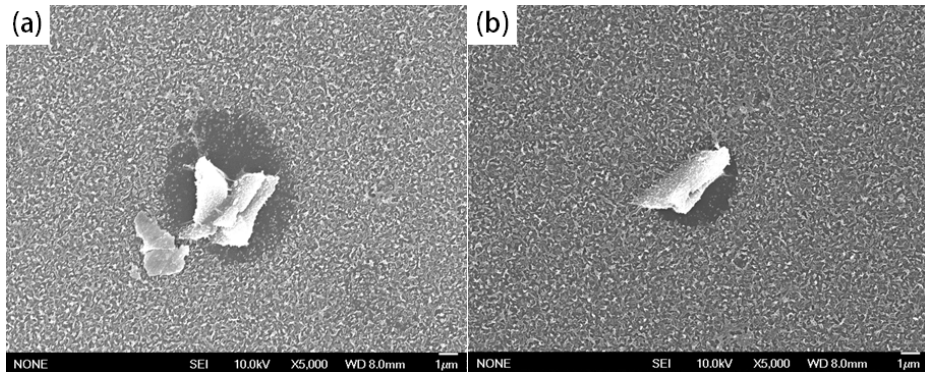


Figure 5.9. SEM images at the top surfaces of (a) PA-GO and (b) PA-GOT membranes prepared using 3 wt% MPD aqueous solution containing 0.01 wt% of GO and GOT, respectively.

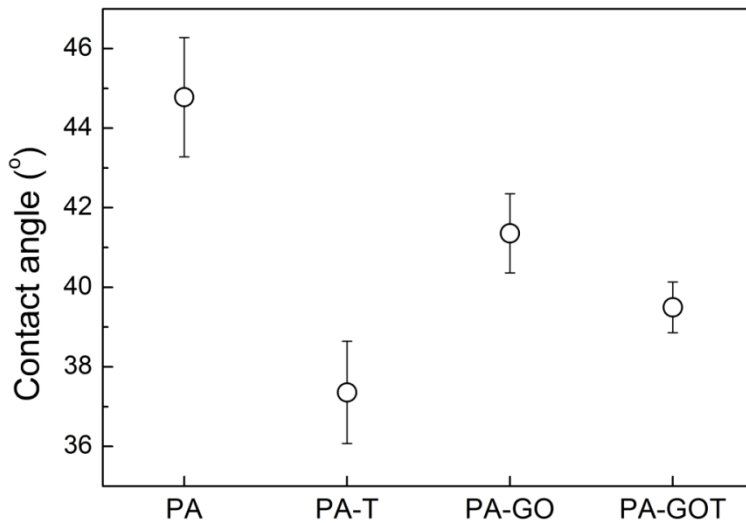


Figure 5.10. Contact angle values of PA (prepared using 2 wt% MPD aqueous solution), PA-T (prepared using 3 wt% MPD aqueous solution containing 0.005 wt% of TA), PA-GO (prepared using 3 wt% MPD aqueous solution containing 0.005 wt% of GO), and PA-GOT (prepared using 3 wt% MPD aqueous solution containing 0.005 wt% of GOT) membranes.

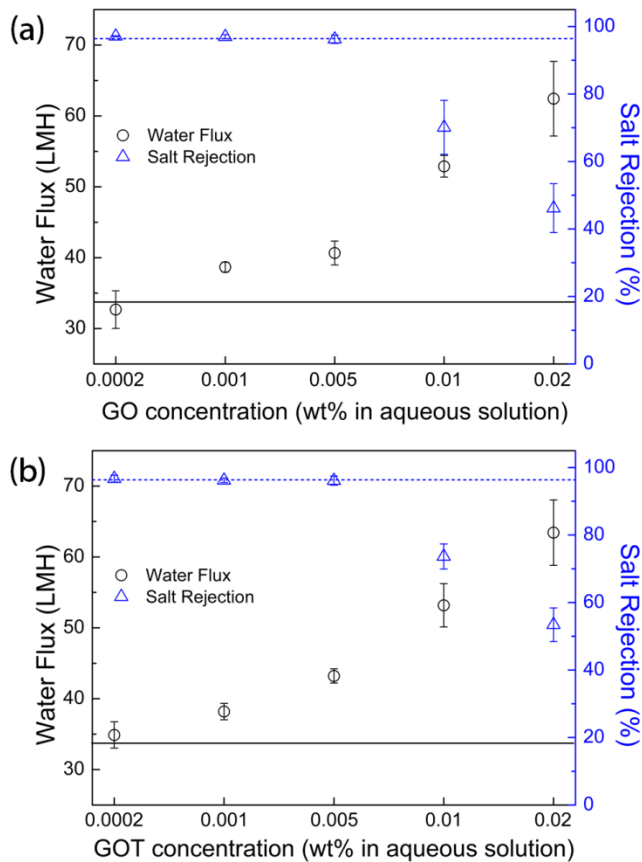


Figure 5.11. Water flux and salt rejection of (a) PA-GO, and (b) PA-GOT membranes prepared using various GO and GOT concentrations in 3 wt% MPD aqueous solution. The water flux and salt rejection values of PA membrane prepared using 2 wt% MPD aqueous solution were marked with black and blue dot lines, respectively. The feed pressure was controlled to 15.5 bar.

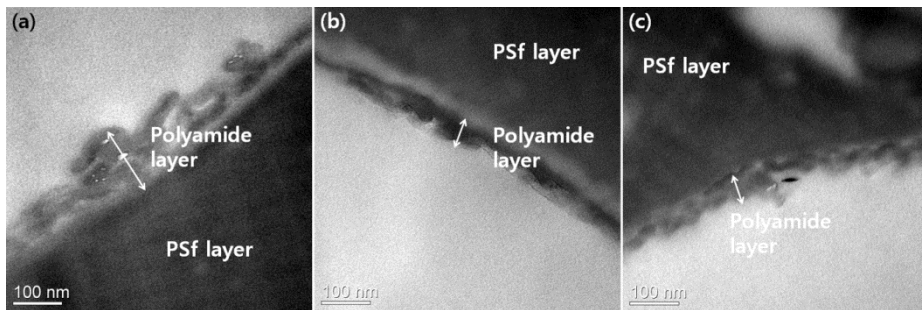


Figure 5.12. Cross-sectional TEM images of (a) PA, (b) PA-GO (prepared using MPD aqueous solution containing 0.005 wt% of GO), (c) PA-GOT (prepared using MPD aqueous solution containing 0.005 wt% of GOT) membranes.

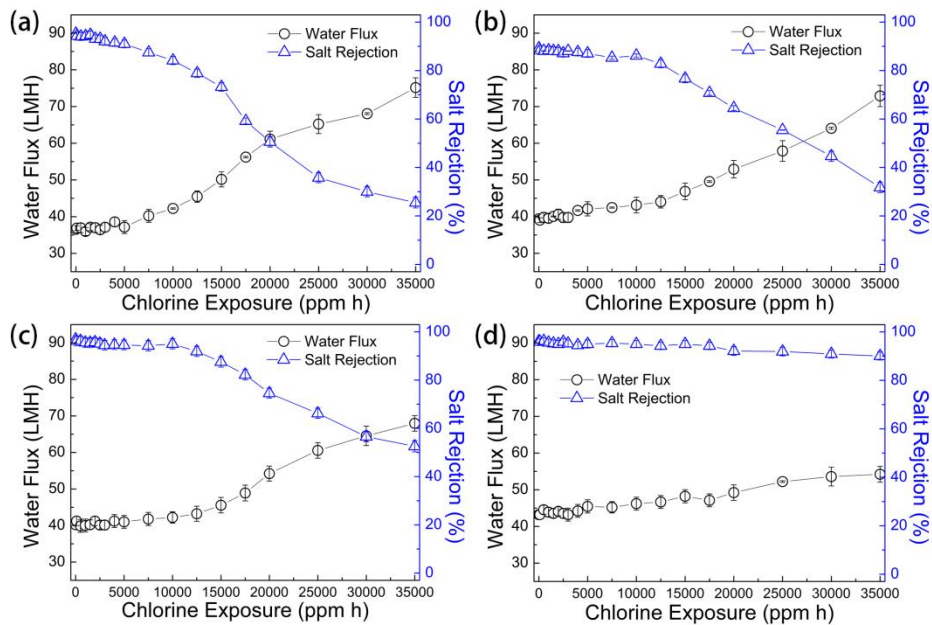


Figure 5.13. Water flux and salt rejection behaviors of the membranes under chlorine exposure; (a) PA (prepared using 2 wt% MPD aqueous solution), (b) PA-T (prepared using 3 wt% MPD aqueous solution containing 0.005 wt% of TA), (c) PA-GO (prepared using 3 wt% MPD aqueous solution containing 0.005 wt% of GO), and (d) PA-GOT (prepared using 3 wt% MPD aqueous solution containing 0.005 wt% of GOT) membranes. The feed solution containing 2000 ppm of NaCl and 500 ppm sodium hypochlorite was used and the feed pressure was controlled to 15.5 bar.

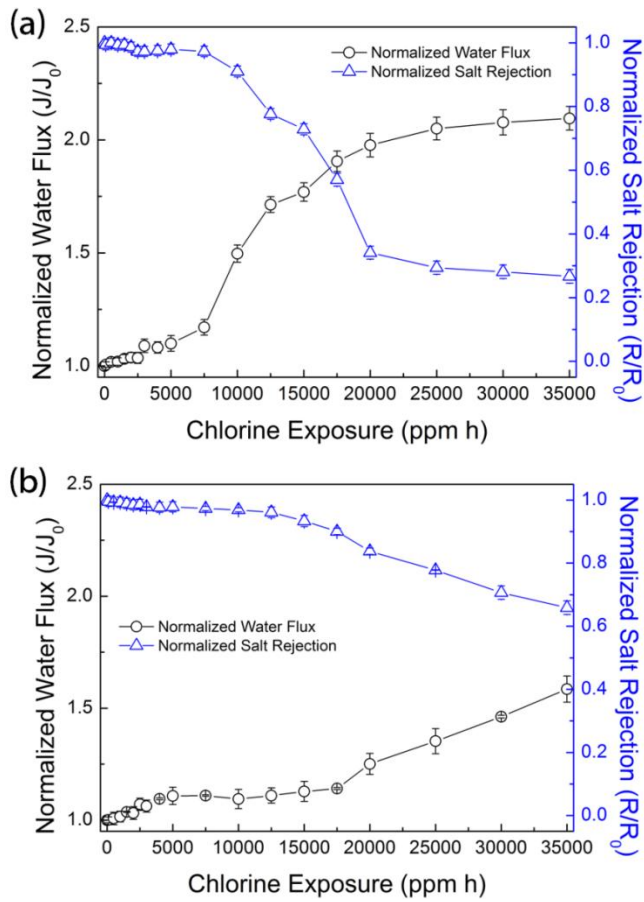


Figure 5.14. Water flux and salt rejection behaviors of the membranes under chlorine exposure; (a) commercial LFC-1 membrane for brackish water purification, and (b) PA-T-GO membrane (prepared using 3wt% MPD aqueous solution containing 0.0025 wt% of TA and 0.0025 wt% of GO).

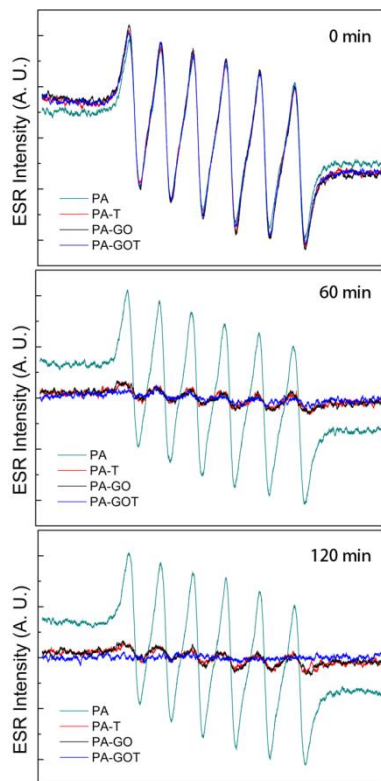


Figure 5.15. ESR spectra obtained during the active chlorine exposure to membrane active layers; PA (prepared using 2 wt% MPD aqueous solution), PA-T (prepared using 3 wt% MPD aqueous solution containing 0.005 wt% of TA), PA-GO (prepared using 3 wt% MPD aqueous solution containing 0.005 wt% of GO), and PA-GOT (prepared using 3 wt% MPD aqueous solution containing 0.005 wt% of GOT) membranes.

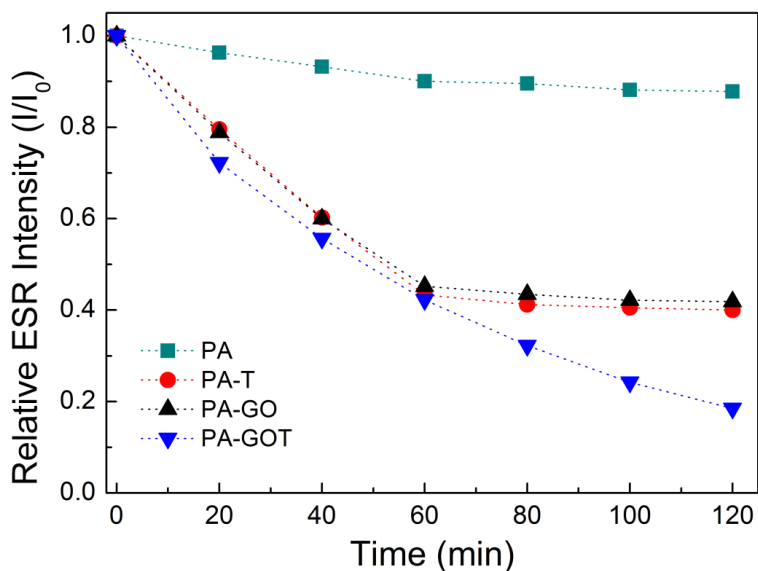


Figure 5.16. Time-dependant relative ESR intensity changes during the active chlorine exposure to membrane active layers; PA (prepared using 2 wt% MPD aqueous solution), PA-T (prepared using 3 wt% MPD aqueous solution containing 0.005 wt% of TA), PA-GO (prepared using 3 wt% MPD aqueous solution containing 0.005 wt% of GO), and PA-GOT (prepared using 3 wt% MPD aqueous solution containing 0.005 wt% of GOT) membranes.

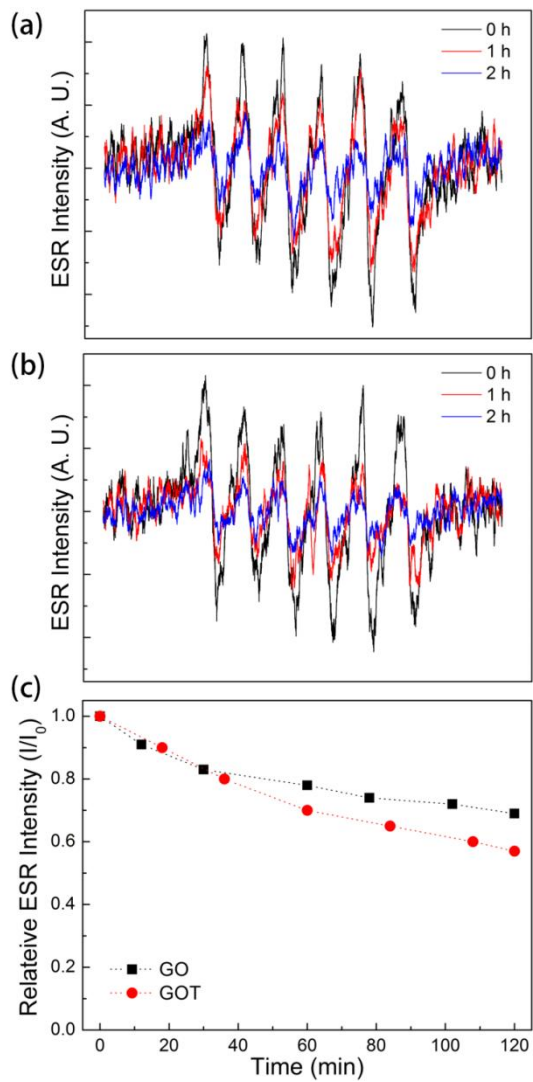


Figure 5.17. ESR spectra obtained during the active chlorine exposure to (a) GO and (b) GOT for 2 h and (c) time-dependant relative ESR intensity changes.

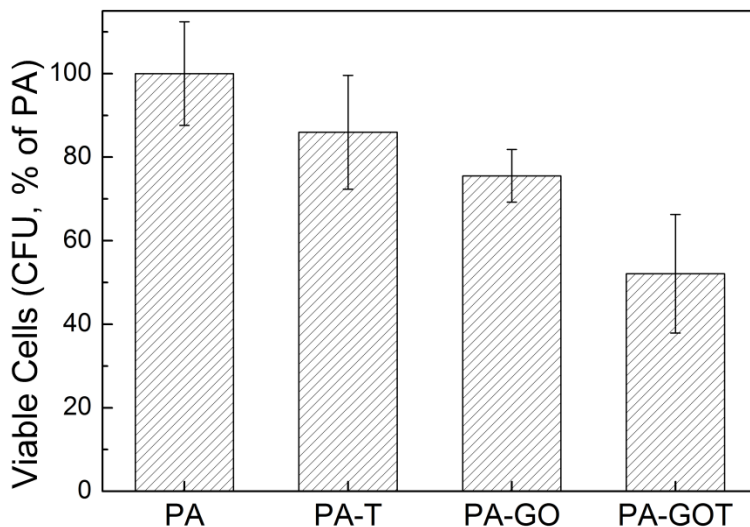


Figure 5.18. Cell viability of *E. coli* after contacting with the membranes for 24 h at room temperature; PA (prepared using 2 wt% MPD aqueous solution), PA-T (prepared using 3 wt% MPD aqueous solution containing 0.005 wt% of TA), PA-GO (prepared using 3 wt% MPD aqueous solution containing 0.005 wt% of GO), and PA-GOT (prepared using 3 wt% MPD aqueous solution containing 0.005 wt% of GOT) membranes.

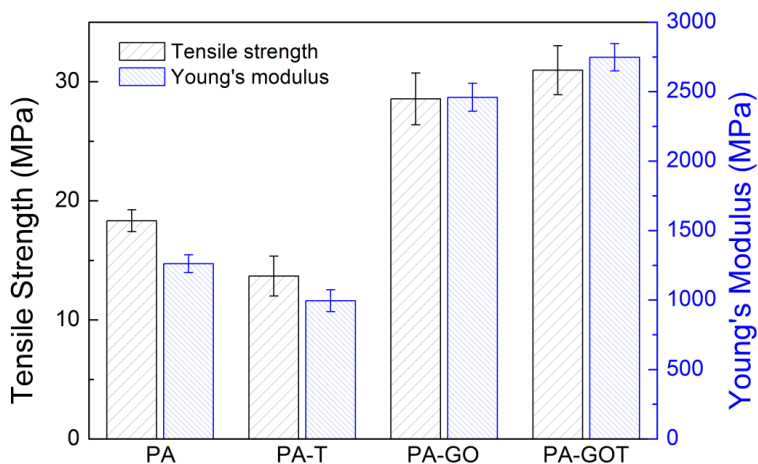


Figure 5.19. Mechanical properties of PA (prepared using 2 wt% MPD aqueous solution), PA-T (prepared using 3 wt% MPD aqueous solution containing 0.005 wt% of TA), PA-GO (prepared using 3 wt% MPD aqueous solution containing 0.005 wt% of GO), and PA-GOT (prepared using 3 wt% MPD aqueous solution containing 0.005 wt% of GOT) membranes.

Chapter 6

A Carbonaceous Membrane based on a Polymer of Intrinsic Microporosity (PIM-1) for Water Treatment

6.1. Introduction

Carbon-based membranes have been extensively studied because of their unique characteristics, such as high physicochemical stability, fast mass transport behavior, large surface area, biocidal property, and narrow pore size distribution.[1-11] Based on these properties, they have been utilized in diverse applications including gas or liquid separation,[1-4] catalytic reactions,[5] chemical sensing,[6-8] energy storage,[9] and tissue engineering.[10] In particular, water treatment membranes consisting of carbon nanomaterials, such as carbon nanotube (CNT) and graphene derivatives, have a unique advantage of fast water permeation by the low frictional water flow through their carbonaceous pores.[12-19] For example, CNT array membranes with aligned 1D carbonaceous nanochannels exhibit ultrahigh water flux values, which are several orders of magnitude higher than those exhibited by conventional ultrafiltration (UF) membranes.[13-16] Graphene oxides (GO) membranes with 2D carbonaceous nanochannels have been reported to exhibit fast water flux with controlled separation performance for sub-10 nm particles and molecules.[17, 18, 20] However, practical applications of these

membranes are still limited by several issues, such as high cost and complicated fabrication for CNT-based membranes,[13-17] as well as poor stability under hydrated conditions and difficult pore size control for graphene-based membranes.[4, 20] In addition, both membranes often suffer from relatively low salt rejection rates, attributed to the large pore size of CNT-based membranes[13] and the deterioration of integrity of graphene-based membranes by the hydration,[4, 20] which in turn hampers the application of the membranes for nanofiltration (NF) or reverse osmosis (RO). Hence, a more convenient and efficient method for preparing carbonaceous membranes with a high flux and salt rejection rate is required for the water treatment applications.

Microporous polymers are of great interest as promising next-generation molecular sieving and storage materials for the applications of gas sorption, separation and storage, pervaporation, and catalytic supports.[21-25] Recently, polymers of intrinsic microporosity (PIMs), a novel class of microporous polymers, have attracted considerable attention because of good solubility and processability, different available functional groups, high glass transition temperature, good thermal stability, and excellent mechanical and film-forming properties.[26-34] As PIMs contain fused-ring and ladder-like

structures integrated with contortion sites, they have uniform interconnected micropores (<2 nm) and a high surface area (300–1000 m² g⁻¹).[30-32] Several studies have reported the use of PIM membranes for gas separation by exploiting their high gas permeability and selectivity;[26-28,30,31,33,34] however, only a few studies have reported the use of PIM membranes for the filtration of organic solutions.[32] Moreover, thus far, a PIM membrane for water treatment applications has not been reported because it is difficult to utilize the hydrophobic micropores of PIMs for transporting water molecules. Considering the low frictional water flow through the pores of carbonaceous membrane, it might be possible to prepare microporous, carbonized PIM membranes with high water flux and selectivity by carbonization of the PIM membranes.

Previously, we have reported the preparation of 2–15 nm thick, graphene-like carbonaceous thin films on a quartz substrate by the carbonization of thin films of a polymer of intrinsic microporosity (PIM-1).[35] Herein, we report the fabrication of a new type of free-standing carbonaceous membrane based on PIM-1 via controlled carbonization; this membrane exhibits interconnected, sub-1 nm pores with a narrow size distribution. These characteristics result in high flux

and a good salt rejection rate for the filtration of an MgSO_4 aqueous solution, thus making the membrane attractive for NF applications. In addition, the water flux and antifouling property of the membrane can be further enhanced without sacrificing the salt rejection rate by subjecting the membrane to O_2 plasma treatment.

6.2. Experimental

6.2.1. Materials

5,5',6,6'-Tetrahydroxy-3,3',3',3'-tetramethyl-1,1'-spirobisindane (TTSBI, >97%, TCI Chemicals) was purified by recrystallization from a mixture of dichloromethane and methanol. Tetrafluoroterephthalonitrile (TFTPN, >98%, Matrix Scientific) was purified by vacuum sublimation at 150 °C under inert atmosphere. Potassium carbonate (K_2CO_3 , 99.99%, anhydrous), bovine serum albumin (BSA, >96%), magnesium sulfate (MgSO_4 , >99.5%, anhydrous), sodium chloride (NaCl , >99%, anhydrous), magnesium chloride (MgCl_2 , >98%, anhydrous), sodium sulfate (Na_2SO_4 , >99%, anhydrous), all from Sigma-Aldrich, were used as received. Deionized

(DI) water with a resistivity of 18.3 m Ω cm]was obtained from a water purification system (Synergy, Millipore, USA). A commercial nanofiltration (NF) membrane, NF2A, was purchased from Sepro Membranes (Oceanside, CA, USA). All other reagents and solvents, such as methanol (MeOH), dimethylformamide (DMF), tetrahydrofuran (THF), and chloroform (CHCl₃), were used as received from standard suppliers.

6.2.2. Synthesis of PIM-1

PIM-1 was synthesized according to a previously reported procedure with slight modifications. Under nitrogen (N₂) flow, TTSBI (3.4 g, 10 mmol), K₂CO₃ (4.1 g, 30 mmol), TFTP (2.0 g, 10 mmol), and DMF (70 mL) were added to a 250 mL two-necked round-bottomed flask equipped with a condenser. The reaction mixture was stirred at 55 °C for 72 h. After polymerization, THF (~140 mL) was added into the flask for removing low-molecular-weight oligomers. The resulting solution was precipitated into an excess of water. The polymer so obtained was dissolved in THF, and the solution was precipitated into MeOH. After drying under vacuum for several days, a yellow solid

product was obtained in 75% yield. The chemical structure of PIM-1 was confirmed by $^1\text{H-NMR}$ (Bruker Advance 700 MHz spectrometer) using tetramethylsilane (TMS) as the reference; $^1\text{H-NMR}$ (700 MHz, CDCl_3 , δ): 1.307 and 1.365 ($-\text{CH}_3$), 2.159 and 2.328 ($-\text{CH}_2-$), and 6.415 and 6.806 (CH , aromatic). Anal. calcd for $\text{C}_{29}\text{H}_{20}\text{N}_2\text{O}_4$: C 75.64, H 4.38, N 6.08, O 13.90. Found: C 76.38, H 4.61, N 5.82, O 13.19. The molecular weight (M_n) and molecular weight distribution (D) of PIM-1 were determined by gel-permeation chromatography (GPC); $M_n = 50,100 \text{ g mol}^{-1}$, $D = 1.87$.

6.2.3. Preparation of PIM-1, carbonized PIM-1 (C-PIM-1), and oxygen (O_2) plasma-treated C-PIM-1 (PC-PIM-1) membranes

PIM-1 membrane was prepared by a simple solution casting method. First, the PIM-1 was dissolved in CHCl_3 (0.5–2.0 wt%), and the solution was poured into a glass dish (diameter = 10 cm). After drying this solution at ambient temperature for 2 days, followed by drying under vacuum at 60 °C overnight, a free-standing, transparent, and light yellow PIM-1 membrane was obtained. The thickness of the

PIM-1 membrane was controlled by changing the concentration and amount of polymer solution, e.g., for preparing a 30 μm thick PIM-1 membrane, a 1.0 wt%, 16.5 mL PIM-1 solution was utilized. The thickness was measured using a micrometer (Kett LZ-370, Agelec Enterprises Pty Ltd).

The C-PIM-1 membrane was prepared by the controlled thermal treatment of the PIM-1 membrane. The PIM-1 membrane was placed on a silicon wafer (5 cm \times 5 cm) in a furnace (Nabertherm P330) under N_2/H_2 atmosphere (100 cc min^{-1} , 95/5 vol%). The membrane was carefully pressed using another silicon wafer (5 cm \times 5 cm) for preventing the deformation of membrane during thermal treatment. The following procedure was used for the preparation of C-PIM-1 membranes: First, the PIM-1 membrane was placed in a furnace (Nabertherm P330) and vacuum was applied. After the furnace was refilled with N_2/H_2 gas (95/5 vol%), flow rate of the mixed gas was controlled to be 100 mL min^{-1} . Then, the furnace was heated to a specific temperature (1100-1300 $^\circ\text{C}$) at 5 $^\circ\text{C min}^{-1}$. The membrane was kept at the final temperature for a specific time range (1-6 h). The degree of carbonization was controlled by changing the final temperature and dwell time; for example, PIM-1 membranes were

carbonized at 1100 °C for 2 h, at 1200 °C for 3 h, and 1300 °C for 6 h to obtain the C-PIM-1 membranes with a degree of carbonization of 40%, 50%, and 60%, respectively. The degree of carbonization is defined as membrane weight loss (%) during thermal treatment.

Both surfaces of the C-PIM-1 membrane were subjected to O₂ plasma treatment for preparing the PC-PIM-1 membrane. The plasma treatment instrument consisting of parallel electrodes operated at a radio-frequency of 13.56 MHz. The C-PIM-1 membrane was placed on a powered electrode under an Ar/O₂ flow (71/29 vol% and 30 sccm). Time and power of O₂ plasma treatment for preparing the PC-PIM-1 membrane were 30 s and 185 W, respectively. Distinct performance changes were not observed when the time and power of O₂ plasma treatment were changed in the range from 10 to 300 s and from 50 to 185 W, respectively.

6.2.4. Membrane filtration experiments

Membrane filtration for pure water and an aqueous MgSO₄ solution (2,000 ppm) was conducted using a stirred dead-end filtration cell (CF042, Sterlitech Corp., Kent, WA). The feed side of the system was

subjected to 10 bar pressure by N₂, and all experiments were conducted at an agitation speed of 200 rpm and room temperature. The water flux (J) measured by weighing the permeate solution at a given time was calculated as follows:

$$J = \Delta V / (A \times \Delta t) \quad (1)$$

where ΔV is the volume of permeate collected between two weight measurements, A is the membrane surface area, and Δt is the time between two weight measurements. The salt rejection rate (R) was calculated as follows:

$$R = (1 - C_p / C_f) \times 100 \% \quad (2)$$

where C_p and C_f represent the salt concentrations in the permeate and feed, respectively. Salt concentrations were measured using a conductivity meter (InoLab Cond 730P, WTW 82362, Weilheim). To investigate the Donnan exclusion ability of the membrane, solutions of various salts with different ion valences (Na₂SO₄, MgSO₄, NaCl, and MgCl₂) were used. As the salt rejection mechanism of NF membranes is normally explained in terms of charge, size effect (sieving), and/or diffusion of salts, filtration experiments were conducted with a relatively low feed pressure (5 bar) and low salt concentration (10 mM) for minimizing the transport of ions by convection and diffusion,

respectively. The water flux and salt rejection values shown in this study are the average values obtained by three re-test measurements from more than two membrane samples.

For the fouling resistance test, a BSA aqueous solution (1 g L^{-1}) was forced to permeate through the membranes, and the water flux was recorded at each time. The initial water flux values of the membranes were controlled to reach 55 LMH by controlling the feed pressure. The flux decline ratio (DR) was calculated as follows:

$$\text{DR} = (1 - J_{250} / J_0) \times 100 \% \quad (3)$$

where J_0 and J_{250} represent the initial water flux and the water flux recorded at 250 min after the filtration of the initial feed, respectively.

6.2.5. Instrumentation and characterization techniques

The chemical structure and molecular weight of PIM-1 were confirmed by $^1\text{H-NMR}$ (Bruker Advance 700 MHz spectrometer) and gel-permeation chromatography (GPC, Wyatt Technology), respectively. Thermogravimetric analysis (TGA) was performed using a Pyris 1 TGA apparatus from PerkinElmer at a heating rate of $10 \text{ }^\circ\text{C min}^{-1}$ under N_2 . The membrane surface composition was investigated

by X-ray photoelectron spectroscopy (XPS, PHI-1600) using Mg K α (1254.0 eV) as the radiation source. Survey spectra were collected in the range of 0–1100 eV, followed by the high-resolution scan of the C 1s, O 1s, and N 1s regions. The membrane atomic composition was analyzed using an elemental analyzer (EA, Flash2000, Thermo Scientific). Raman spectra were recorded on a LabRam Aramis Raman spectrometer (Horiba Jobin-Yvon). The excitation source was a diode laser with an excitation wavelength of 785 nm and a power of 5 mW. The Raman scattered light signal was collected in a back-scattering geometry using a 100 \times microscope objective lens. The diameter of the Raman excitation beam spot was approximately 1 μ m. Nitrogen adsorption isotherms were measured by surface characterization analyzer (3flex 3500, Micromeritics) at 77 K. The membranes were degassed at 200 $^{\circ}$ C for 24 h before the measurements. The specific surface area and median pore size of the membranes were calculated by using the Brunauer-Emmett-Teller (BET) method and Horvath-Kawazoe model, respectively. The membrane surface morphology was investigated by scanning electron microscopy (SEM, SigmaHD, Carl Zeiss) and atomic force microscopy (AFM, Asylum Research MFP-3D). The wetting

behaviors of water droplets on the membranes were evaluated using a contact angle analyzer (KRÜ SS DSA100) by the sessile drop method. Three replicate measurements were conducted for each membrane. The PC-PIM-1 membrane was prepared by the O₂ plasma treatment of the C-PIM-1 membrane using a plasma reactor (Korea Vacuum Co.). Zeta potential values of the membrane surfaces were recorded on an electrophoretic light scattering spectrophotometer (ELS-8000, Otsuka Electronics Co.). The membrane water uptake was determined by measuring the weight before and after membranes (1 cm × 1 cm) were soaked in deionized water for 24 h. After the membrane was removed and wiped, the weight of the wet membrane was obtained; it was calculated as follows:

$$\text{Water uptake (\%)} = [(W_{\text{wet}} - W_{\text{dry}}) / W_{\text{dry}}] \times 100 \quad (4)$$

where W_{wet} and W_{dry} represent the weights of the wet and dry membranes, respectively. The equilibrium water concentration in the membrane ($C_{\text{w,F}}^{\text{m}}$) was obtained from the water uptake experiments, which was calculated as follows:

$$C_{\text{w,F}}^{\text{m}} = (W_{\text{wet}} - W_{\text{dry}}) / V_{\text{dry}} \quad (5)$$

where V_{dry} is the volume of the dry membrane.

6.3. Results and Discussion

PIM-1 was synthesized by polycondensation of 5,5',6,6'-tetrahydroxy-3,3,3',3'-tetramethyl-1,1'-spirobisindane (TTsBI) and 2,3,5,6-tetrafluoroterephthalonitrile (TFTPN), as previously reported.[29, 35-37] ^1H NMR and elemental analysis (EA) revealed that the polymer was successfully synthesized. The number-average molecular weight (M_n) and molecular weight distribution (\mathcal{D}) of PIM-1, obtained by gel-permeation chromatography (GPC), are 50,100 g mol $^{-1}$ and 1.87, respectively. A PIM-1 membrane was prepared by a simple solution casting method (Figure 6.1a); a solution of PIM-1 in CHCl_3 was poured into a glass dish (diameter = 10 cm), followed by the slow evaporation of the solvent at room temperature. The thickness of the PIM-1 membrane was controlled by changing the concentration (0.5–2.0 wt%) and amount of the PIM-1 casting solution. After the PIM-1 membrane was completely dried under vacuum at 60 °C, controlled thermal treatment under N_2/H_2 atmosphere (95/5 vol%) was conducted to fabricate a carbonaceous PIM-1 membrane (C-PIM-1). The yellow transparent PIM-1 membrane changed into a glittering-grey opaque C-PIM-1 membrane

after carbonization (Figure 6.1b). The degree of carbonization, defined as the membrane weight loss (%) during thermal treatment, was controlled by changing the temperature (1,100–1,300 °C) and time (1–6 h). As shown in Table 6.1, the degree of carbonization for the C-PIM-1 membranes was controlled from 37.5% to 60%. Unfortunately, it was difficult to prepare C-PIM-1 membranes with a degree of carbonization below $\approx 35\%$ due to the abrupt weight loss of PIM-1 from 0% to $\approx 35\%$. The abrupt weight loss of PIM-1 could be also observed by TGA under N₂ flow (Figure 6.2), although the actual decomposition temperature under N₂/H₂ flow (95/5 vol%) might be different from the TGA result. In addition, the C-PIM-1 membranes with a degree of carbonization higher than 60% were prepared, however, they were too fragile to be used as the pressure-driven filtration membranes. Thus, C-PIM-1 membranes with a degree of carbonization from 37.5% to 60% were used because they are sufficiently robust, maintaining their free-standing film state from the filtration even under an applied pressure of 10 bar.

The carbonization the PIM-1 membrane to the C-PIM-1 membrane via the thermal treatment could be monitored by X-ray photoelectron spectroscopy (XPS) analysis; the carbon content of the membrane

increases from 82.60 at% to 96.82 at% upon the carbonization process, while the content of oxygen and nitrogen decreases (Table 6.2). In addition, the content of carbon in the C–C bond (284.4 eV) of the C-PIM-1 membrane was found to be much larger than that of the PIM-1 membrane (Figure 6.1c). The atomic composition results, obtained from EA and XPS experiments, indicate the uniform carbonization from surface to inside part of the membrane (Table 6.2). Raman spectroscopy clearly shows the D (1310 cm^{-1}) and G (1595 cm^{-1}) band peaks, corresponding to the graphitic carbon structures of the C-PIM-1 membrane (Figure 6.1d),[38-40] while such graphitic carbon structural peaks were not observed for the PIM-1 membrane. In addition, the relative intensity of D3 peak at 1500 cm^{-1} , compared to that of G peak at 1595 cm^{-1} , decreases with increasing the degree of carbonization; D3 and G peaks correspond to amorphous carbon and graphitic carbon lattice, respectively (Figure 6.3). Therefore, C-PIM-1 membrane with a high degree of carbonization has low amorphous carbon content.[38, 39] The degree of crystallinity, calculated from the integrated intensity ratio of the D and G bands (I_D/I_G), is 1.84 for the C-PIM-1 membrane with 40% carbonization; this is typical value for the carbonaceous materials prepared by the thermal treatment of

polymer precursors.[41, 42] The change of surface morphology of the membranes could be observed from scanning electron microscopy (SEM) and atomic force microscopy (AFM) analyses; a quite flat surface (root-mean-square roughness, $R_q=0.85\pm0.26$) of the PIM-1 membrane was found to be changed to a relatively rough surface ($R_q=15.51\pm2.10$) for the C-PIM-1 membrane, attributed to the nanoscale thermal shrinkage by the carbonization (Figure 6.4 and 6.5).[43, 44] Still the interconnected micropore characteristics of the PIM-1 membrane having median pore size of 0.824 nm and surface area of $819\text{ m}^2\text{ g}^{-1}$ are preserved for some degree after the carbonization for the C-PIM-1 membrane having median pore size of 0.778 nm and surface area of $643\text{ m}^2\text{ g}^{-1}$ (Figure 6.1e and 6.6).

Dead-end filtration test was performed to evaluate the pure water permeability behavior of the C-PIM-1 membrane with a thickness of 30 μm . Figure 6.7a clearly shows the very large increase of the pure water flux after the carbonization; pure water flux increases from 0.23 LMH bar^{-1} for the PIM-1 membrane to 6.43 LMH bar^{-1} for the C-PIM-1 membrane with 60% carbonization, which is a 28-fold increase in the water flux as a result of carbonization. The increase in water flux by carbonization is attributed to the low frictional water flow

inside the carbonaceous pores rather than the pore size and surface area of the membranes.[12-19] A solution-diffusion model, which is widely used to explain mass transport through dense membranes with sub-1 nm pores, was employed in order to elucidate the increase of water permeability by the carbonization.[12, 45, 46] Water flux (J_w , g $\text{cm}^{-2} \text{s}^{-1}$) in the solution-diffusion model is expressed as follows:

$$J_w = C_m^{\text{W,F}} \cdot D_w \cdot V_w \cdot (\Delta P - \Delta\pi) / (L \cdot R \cdot T) \quad (1)$$

where $C_m^{\text{W,F}}$ is the equilibrium water concentration in the membrane (g H_2O in a 1 cm^{-3} swollen membrane), D_w is the average water diffusion coefficient in the membrane ($\text{cm}^2 \text{s}^{-1}$), V_w is the partial molar volume of water (18.0 $\text{cm}^3 \text{mol}^{-1}$), which is typically approximated by the molar volume of pure water,[45, 46] ΔP is the difference in pressure between feed and permeate (bar), $\Delta\pi$ is the osmotic pressure difference across the membrane (bar), L is the membrane thickness (cm), R is the gas constant (83.1 $\text{cm}^3 \text{bar mol}^{-1} \text{K}^{-1}$), and T is the absolute temperature (298 K). Two parameters, $C_m^{\text{W,F}}$ and D_w , should be the key factors in determining the water flux behavior for the PIM-1 and C-PIM-1 membranes because all the other parameters are identical. The $C_m^{\text{W,F}}$ of the membranes was evaluated by the measurement of the equilibrium water uptake of the membranes in

pure water (Figure 6.8). The $C_m^{W,F}$ of the C-PIM-1 membrane with 40% carbonization (5.52×10^{-2} g H₂O in a 1 cm³ swollen membrane) is approximately 4.7 times larger than that of the PIM-1 membrane (1.18×10^{-2} g H₂O in a 1 cm³ swollen membrane). $C_m^{W,F}$ was also found to increase with the degree of carbonization. A membrane with a large $C_m^{W,F}$ is known to exhibit high water permeability because the larger amount of water in the membrane pores can provide the pathways for water molecules (i.e., convective frame of reference effect).[45, 46] The calculated D_w values of the C-PIM-1 membranes (7.08×10^{-3} – 8.90×10^{-3} cm² s⁻¹) are approximately 4.8–6.1 times larger than that of the PIM-1 membrane (1.47×10^{-3} cm² s⁻¹), which are close to those of other carbon-based membranes (5×10^{-3} – 8×10^{-3} cm² s⁻¹).[47, 48] Those of conventional polymeric membranes are in the range of 1×10^{-4} to 1×10^{-7} cm² s⁻¹.[45, 46] Therefore, the water diffusion behavior of the C-PIM-1 membrane is similar to that in the carbon-based membranes. The carbon-based membranes containing CNT and graphene derivatives have well-defined micropores and exhibit low frictional water flow inside the carbonaceous pores via the formation of agglomerated hydrogen bonds between water molecules, thus resulting in the high water permeability.[47, 48] The much larger

$C_m^{W,F}$ and D_w values of the C-PIM-1 membrane than those of the PIM-1 membrane can be explained for some degree by water contact angle study (Figure 6.9). It is well known that membranes with high water wettability exhibit large water sorption and diffusion coefficients.[45, 46] The C-PIM-1 membrane shows smaller water contact angle and higher water wettability than PIM-1 membrane possibly due to its graphitic carbon structure[49] and rough surface morphology,[50, 51] as presented in the Raman spectroscopy and AFM results, respectively (Figure 6.1d and 6.5). It has been reported that clean graphene surface exhibited quite low water contact angle value (37°), originated from the strong interaction between graphene surface and water molecules.[49] Higher water wettability of membrane could also be obtained by introducing the rough surface morphologies.[50,51]

Subsequently, the NF performance of the C-PIM-1 membrane was investigated using an aqueous $MgSO_4$ solution. The pure water flux behavior of the C-PIM-1 membrane is mirrored in Figure 6.2b for the $MgSO_4$ solution filtration, where the C-PIM-1 membrane also shows an increase of water flux with increasing degree of carbonization, and exhibits much larger water flux ($3.51\text{--}4.45\text{ LMH bar}^{-1}$) than the PIM-

1 membrane ($0.12 \text{ LMH bar}^{-1}$). Although the salt rejection rates of the C-PIM-1 membranes (78.76–82.94%) are somewhat smaller than that of PIM-1 membrane (91.41 %) due to the typical trade-off behavior between water diffusion coefficient and water/salt selectivity,[45,46] those are still comparable to or slightly larger than that of a commercial polyamide (PA) NF membrane (NF2A) (76.86%) measured in this study. The NF performance of NF2A is worse than that in the technical specification provided by the company, however, such discrepancy has been also reported by others, which is attributed to the effect of the membrane filtration condition.[52] The high salt rejection rate of the high-flux C-PIM-1 membrane is consistent with the BET results, which demonstrate the sub-1 nm sized, interconnected carbonaceous pores present in the membrane (Figure 6.1e and 6.6). Figure 6.7c shows that the C-PIM-1 membranes as thin as $20 \mu\text{m}$ can be easily prepared, yielding water flux as high as $4.91 \text{ LMH bar}^{-1}$ for the MgSO_4 solution filtration, when the degree of carbonization of the membrane is 37.5%. The increase in the water flux of the C-PIM-1 membrane with decreasing membrane thickness is attributed to the reduction of thickness resistance (Equation (1)).[17, 46] The salt rejection rate is almost independent of the membrane

thickness, indicating that membranes are substantially free from micro- or several nanometer-scale defects. 20 μm was found to be the minimum thickness for the free-standing C-PIM-1 membrane to have the physical and mechanical stability under the high pressure of NF. The water flux behavior of PIM-1 membranes with different thicknesses is similar to that of C-PIM-1 membrane (Table 6.1). However, because of their small values, the changes in water flux of the PIM-1 membrane were not clearly seen in Figure 6.7c.

Carbon-based membranes, such as CNT array membranes, are known to exhibit a large entrance/exit resistance for water molecules to pass through the inner pores of the membranes.[13, 53] For example, the entrance and exit resistances are larger than 120 bar and 1,000 bar, respectively, for the CNT array membrane, calculated by the molecular dynamic simulations.[13, 53] As compared to the CNT array membranes, the C-PIM-1 membrane possibly exhibits a relatively smaller entrance/exit resistance,[13, 53] as expected from its better water wettability (Figure 6.9). Still, the water permeability of the C-PIM-1 membrane can be further improved by hydrophilic surface modification for decreasing the entrance/exit resistance. Both surfaces of the C-PIM-1 membrane were subjected to O_2 plasma for

preparing the O₂ plasma-treated C-PIM-1 membrane (PC-PIM-1), as illustrated in Figure 6.10a. The oxygen content on the membrane surface, analyzed by XPS, significantly increases by the O₂ plasma treatment (Table 6.2), thereby increasing the water wettability on the membrane surface (Figure 6.9), while the bulk atomic composition of the membrane does not change much as observed from EA measurement. This clearly demonstrates that hydrophilic oxygen functional groups are formed on the membrane surface by the O₂ plasma treatment without changing the inner carbonaceous structure of the membrane. Furthermore, I_D/I_G ratios of C-PIM-1 and PC-PIM-1 membranes were found to be close from the Raman spectroscopy, indicating that the graphitic carbon structures on the C-PIM membrane are not damaged during O₂ plasma treatment (Figure 6.11). The effect of O₂ plasma treatment on membrane surface morphologies was also investigated by SEM and AFM (Figure 6.12 and 6.13); any distinct change was not observed after the O₂ plasma treatment, indicating that the O₂ plasma treatment does not change the surface morphologies much. The hydrophilic functional groups imparted by the O₂ plasma treatment were found to stably remain even after exposed to air for a week. The overall water permeability behavior of

the PC-PIM-1 membranes with different degrees of carbonization and thicknesses is close to that of the C-PIM-1 membranes, while the water permeability of the PC-PIM-1 membranes is about 1.5 times higher than that of the C-PIM membranes due to the decreased entrance/exit resistance (Table 6.1). We could obtain the highest water flux from a PC-PIM-1 membrane with a thickness of 20 μm and 60% carbonization; 15.43 LMH bar^{-1} and 13.30 LMH bar^{-1} for the filtration of pure water and MgSO_4 solution, respectively, as shown in Figure 6.10b.

The salt rejection rate is generally assumed to decrease with increasing water flux of filtration membranes.^{45, 46} However, both C-PIM-1 and PC-PIM-1 membranes exhibit similar salt rejection performance, despite the significant increase in water flux for the membranes after O_2 plasma treatment (Figure 6.10b and Table 6.1). This result could be attributed to the presence of negatively charged oxygen functional groups on the PC-PIM-1 membrane (Figure 6.14), which can improve the salt rejection rate by electrostatic repulsion (i.e., Donnan exclusion ability).[54, 55] To investigate the Donnan exclusion ability of the PC-PIM-1 membrane, filtration experiments were conducted with various salt solutions having different ion

valences under a relatively low feed pressure (5 bar) and low salt concentration (10 mM) for minimizing the transport of ions by convection and diffusion, respectively (Figure 6.15).[54, 55] Considering the hydrated salt size and charge effects, the rejection (R) of salt solutions should follow the orders of $R(\text{MgSO}_4) > R(\text{MgCl}_2) > R(\text{Na}_2\text{SO}_4) > R(\text{NaCl})$ and $R(\text{Na}_2\text{SO}_4) > R(\text{MgSO}_4) \approx R(\text{NaCl}) > R(\text{MgCl}_2)$, respectively (Table 6.3).[17, 54] The rejection of salt solutions of the C-PIM-1 membrane follows the order of $R(\text{MgSO}_4) > R(\text{MgCl}_2) > R(\text{Na}_2\text{SO}_4) > R(\text{NaCl})$, indicating that the salt rejection of the C-PIM-1 membrane is mainly determined by the size effect. However, the rejection of the PC-PIM-1 membrane follows the order of $R(\text{MgSO}_4) > R(\text{Na}_2\text{SO}_4) > R(\text{MgCl}_2) > R(\text{NaCl})$; the change of the rejection order and the significant increase for $R(\text{Na}_2\text{SO}_4)$ and $R(\text{NaCl})$ are observed for the PC-PIM-1 membrane, demonstrating that the salt rejection of the PC-PIM-1 membrane is determined by both of charge and size. Therefore, the PC-PIM-1 membrane shows increased water flux without decreasing the salt rejection compared to the C-PIM-1 membrane due to the Donnan exclusion from the negatively charged surface functional groups.

Antifouling properties of the membranes were also evaluated using

bovine serum albumin (BSA) as a model foulant, which is the most commonly used protein foulant for the antifouling tests.[56-63] Figure 6.10c presents the time-dependent normalized water flux variations of the NF2A, C-PIM-1, and PC-PIM-1 membranes during the filtration of a BSA solution. The NF2A and C-PIM-1 membranes show larger flux decreases as compared to the PC-PIM-1 membrane, especially in the initial filtration stage. Upon reaching a steady state after 250 min of filtration, the flux decline ratio (DR) of the PC-PIM-1 membrane (40.8%) is much smaller than those of NF2A (62.3%) and C-PIM-1 (70.1%) membranes; interestingly, the C-PIM-1 membrane shows the largest DR possibly due to its non-polar and uncharged surface (Figure 6.14).[62,63] Thus, the treatment of the C-PIM-1 membrane by O₂ plasma further imparts antifouling properties to the membrane against BSA, which would be another advantage of the O₂ plasma treatment. A hydrophilic and charged membrane surface can provide an energetic barrier for the adhesion of foulants on the membrane surface via favorable water-surface interaction and electrostatic repulsion between foulants and the surface.[60, 62, 63]

Figure 6.10d displays the salt rejection and water fluxes of various NF membranes for the filtration of MgSO₄ aqueous solutions (Table

6.4). Most of the membranes reported previously have been found to exhibit a typical trade-off phenomenon. For example, a PA membrane exhibits a high salt rejection rate (94.5%) but low water flux (6.20 LMH bar⁻¹) for the filtration of a 3,000 ppm MgSO₄ solution.[64] In contrast, a graphene/CNT composite membrane shows the highest water flux (12.13 LMH bar⁻¹) but a poor salt rejection rate (25.1%) for the filtration of a 1,200 ppm MgSO₄ solution.[19] As compared with representative results across recently published studies, the C-PIM-1 membrane exhibits a comparable water flux and salt rejection rate. Furthermore, the high flux and good salt rejection rate of the PC-PIM-1 membrane clearly exceed the upper limit of state-of-the-art NF membrane performance. Although the reported MgSO₄ rejection rate and water flux data were obtained under different conditions (Table 6.4), at least, such a comparison has demonstrated that the carbonaceous PIM-1 membrane with an O₂ plasma-treated surface (PC-PIM-1) could act as a high-performance NF membrane.

6.4. Conclusions

We have demonstrated that a carbonaceous NF membrane (C-PIM-1)

can be prepared by the controlled carbonization of a PIM-1 membrane. Sub-1 nm-sized, interconnected, low frictional carbonaceous pores of the C-PIM-1 membrane facilitate the permeation of water molecules through the membrane, leading to a high water flux and good salt rejection rate. Moreover, the O₂ plasma treatment of the C-PIM-1 membrane results in water flux enhancement without decreasing the salt rejection rate, as well as high fouling resistance against proteins. These properties are attributed to the negatively charged hydrophilic membrane surface that decreases the entrance/exit resistance of the carbonaceous pores while facilitating the Donnan exclusion and reduces the interaction of proteins with the membrane surface. This study provides insight into the design and preparation of carbonaceous PIM membranes for versatile applications including the filtration. In particular, the modification of the chemical structure of PIMs can possibly control the pore characteristics of the corresponding carbonaceous PIM membranes. Currently, studies for the further improvement of these membranes, such as fabrication of a thin, selective layer of carbonized PIMs on a supporting membrane for increasing water flux, are underway in our laboratory.

6.5. References

- [1] Karan, S., Samitsu, S., Peng, X. S., Kurashima, K. and Ichinose, I, *Science* **2012**, 335, 444-447.
- [2] Jiang, D. –E., Cooper, V. R. and Dai, S, *Nano Lett.* **2009**, 9, 4019-4024.
- [3] Huang, L., Li, Y. R., Zhou, Q. Q., Yuan, W. J. and Shi, G. Q, *Adv. Mater.* **2015**, 27, 3797-3802.
- [4] Hung, W. –S. *et al*, *Chem. Mater.* **2014**, 26, 2983-2990.
- [5] Lv, R. T. *et al*, *Adv. Funct. Mater.* **2011**, 21, 999-1006.
- [6] Salehi-Khojin, A. *et al*, *ACS Nano* **2011**, 5, 153-158.
- [7] Liu, Y. X., Dong, X. C. and Chen, P, *Chem. Soc. Rev.* **2012**, 41, 2283-2307.
- [8] Sippel-Oakley, J. *et al*, *Nanotechnology* **2005**, 16, 2218-2221.
- [9] Che, G. L., Lakshmi, B. B., Fisher, E. R. and Martin, C. R, *Nature* **1998**, 393, 346-349.
- [10] Harrison, B. S. and Atala A, *Biomaterials* **2007**, 28, 344-353.
- [11] Liu, S. B. *et al*, *ACS Nano* **2011**, 5, 6971-6980.
- [12] Paul, D. R, *Science* **2012**, 335, 413-414.
- [13] Lee, B. *et al*, *Nat. Commun.* **2015**, 6, 7109.

- [14] Hinds, B. J. *et al*, *Science* **2004**, 303, 62-65.
- [15] Holt, J. K. *et al*, *Science* **2006**, 312, 1034-1037.
- [16] Sholl, D. S. and Johnson, J. K., *Science* **2006**, 312, 1003-1004.
- [17] Han, Y., Xu, Z. and Gao C, *Adv. Funct. Mater.* **2013**, 23, 3693-3700.
- [18] Huang, H. B *et al*, *Nat. Commun.* **2013**, 4, 2979.
- [19] Han, Y., Jiang, Y. Q. and Gao, C, *ACS Appl. Mater. Interfaces* **2015**, 7, 8147-8155.
- [20] Yeh, C. -N., Raidongia, K., Shao, J. J., Yang, Q. -H. and Huang, J. X, *Nat. Chem.* **2015**, 7, 166-170.
- [21] Ghanem, B. S., Swaidan, R., Ma, X. H., Litwiller, E. and Pinnau, I, *Adv. Mater.* **2014**, 26, 6696-6700.
- [22] Zhang, P. F., Li, H. Y., Veith, G. M. and Dai, S., *Adv. Mater.* **2015**, 27, 234-239.
- [23] Pandey, P. *et al.*, *Chem. Mater.* **2010**, 22, 4974-4979.
- [24] Carta, M. *et al.*, *Science* **2013**, 339, 303-307.
- [25] Guiver, M. D. and Lee, Y. M., *Science* **2013**, 339, 284-285.
- [26] Bezzu, C. G. *et al.*, *Adv. Mater.* **2012**, 24, 5930-5933.
- [27] Lau, C. H. *et al.*, *Angew. Chem. Int. Edit.* **2015**, 54, 2669-2673.
- [28] Song, Q. L. *et al.*, *Nat. Commun.* **2014**, 5, 4813.

- [29] Budd, P. M. *et al.*, *Adv. Mater.* **2004**, 16, 456-459.
- [30] McKeown, N. B. and Budd, P. M., *Chem. Soc. Rev.* **2006**, 35, 675-683.
- [31] Du, N. Y., *Nat. Mater.* **2011**, 10, 372-375.
- [32] Gorgojo, P. *et al.*, *Adv. Funct. Mater.* **2014**, 24, 4729-4737.
- [33] Yong, W. F. *et al.*, *J. Membr. Sci.* **2012**, 407-408, 47-57.
- [34] Yong, W. F., Kwek, K. H. A., Liao, K. -S. and Chung, T. -S., *Polymer* **2015**, 77, 377-386.
- [35] Son, S. -Y. *et al.*, *Nanoscale* **2014**, 6, 678-682.
- [36] Kim, B. G. *et al.*, *Macromol. Res.*, **2014**, 22, 92-98.
- [37] Song, J. *et al.*, *Macromolecules* **2008**, 41, 7411-7417.
- [38] Li, P. *et al.*, *Carbon* **2005**, 43, 2701-2710.
- [39] Sadezky, A., Muckenhuber, H., Grothe, H., Niessner, R. and Poschl, U., *Carbon* **2005**, 43, 1731-1742.
- [40] Moon, I. K., Lee, J., Ruoff, R. S. and Lee, H., *Nat. Commun.* **2010**, 1, 73.
- [41] Li, Z. *et al.*, *Adv. Energy Mater.*, **2012**, 2, 431-437.
- [42] Xu, H. X., Guo, J. R. and Suslick, K. S., *Adv. Mater.* **2012**, 24, 6028-6033.
- [43] Amato, L. *et al.*, *Adv. Funct. Mater.* **2014**, 24, 7042-7052.

- [44] Zhi, L. *et al.*, *Adv. Mater.* **2007**, 19, 1849-1853.
- [45] Geise, G. M., Park, H. B., Sagle, A. C., Freeman, B. D. and McGrath, J. E., *J. Membr. Sci.* **2011**, 369, 130-138.
- [46] Geise, G. M., Paul, D. R. and Freeman, B. D., *Prog Polym Sci* **2014**, 39, 1-42.
- [47] Striolo, A., *Nano Lett.* **2006**, 6, 633-639.
- [48] Ma, M., Tocci, G., Michaelides, A. and Aeppli G., *Nat. Mater.* **2016**, 15, 66-72.
- [49] Li, Z. T. *et al.*, *Nat. Mater.* **2013**, 12, 925-931.
- [50] Sheng, Y. -J., Jiang, S. Y. and Tsao, H. -K., *J. Chem. Phys.* **2007**, 127, 234704.
- [51] Huh, C. and Mason, S. G., *J. Colloid Interf. Sci.* **1977**, 60, 11-38.
- [52] Van Wagner, E. M., Sagle, A. C., Sharma, M. M. and Freeman, B. D. *J. Membr. Sci.* **2009**, 345, 97-109.
- [53] Walther, J. H., Ritos, K., Cruz-Chu, E. R., Megaridis, C. M. and Koumoutsakos, P., *Nano Lett.* **2013**, 13, 1910-1914.
- [54] Schaep, J., Van der Bruggen, B., Vandecasteele, C. and Wilms, D., *Sep. Purif. Technol.* **1998**, 14, 155-162.
- [55] Fornasiero, F. *et al.*, *P. Natl. Acad. Sci. USA* **2008**, 105, 17250-17255.

- [56] Kim, D. -G, Kang, H., Han, S. and Lee, J. -C., *ACS Appl. Mater. Interfaces* **2012**, 4, 5898-5906.
- [57] Kim, H. J. *et al.*, *Adv. Mater. Interfaces* **2015**, 2, 1500298.
- [58] Kim, D. -G., Kang, H., Choi, Y. -S., Han, S. and Lee, J. -C., *Polym. Chem.* **2013**, 4, 5065-5073.
- [59] Sun, X. H., Wu, J., Chen, Z. Q., Su, X. and Hinds, B. J., *Adv. Funct. Mater.* **2013**, 23, 1500-1506.
- [60] Kim, D. -G., Kang, H., Han, S and Lee, J. -C., *J. Mater. Chem.* **2012**, 22, 8654-8661.
- [61] Kim, D. -G., Kang, H., Han, S., Kim, H. J. and Lee, J. -C., *RSC Adv.* **2013**, 3, 18071-18081.
- [62] Banerjee, I., Pangule, R. C. and Kane, R. S., *Adv. Mater.* **2011**, 23, 690-718.
- [63] Yang, R., Jang, H., Stocker, R. and Gleason, K. K., *Adv. Mater.* **2014**, 26, 1711-1718.
- [64] Mo, Y. H. *et al.*, *Environ. Sci. Technol.* **2012**, 46, 13253-13261.

Table 6.1. Pure water flux (PWP), water flux (WF), and salt rejection (R) values of the membranes in this study. The water flux and salt rejection values were obtained by filtration of MgSO₄ solution (2,000 ppm).

Membrane	Thickness (μm)	Carbonization (%)	PWP ^a	WF ^a	R ^b
NF2A	-	-	4.66	3.32	76.86
PIM-1	20	-	0.31	0.13	91.18
	30		0.23	0.12	91.41
	37.5		0.18	0.09	91.78
	40		0.13	0.09	91.42
	50		0.12	0.09	92.16
	60		0.11	0.09	93.39
	70		0.10	0.09	93.69

^a LMH bar⁻¹. ^b %

Table 6.1. Continued.

Membrane	Thickness (μm)	Carbonization (%)	PWP ^a	WF ^a	R ^b
C-PIM-1	30	40	4.85	3.51	82.69
		47.5	5.32	3.73	82.94
		50	5.65	3.90	81.54
		60	6.43	4.45	78.76
	20	37.5	7.08	4.91	79.29
	30		4.80	3.30	83.40
	35		4.09	2.76	83.64
	40		3.47	2.38	83.64
	45		3.12	2.20	79.29
	50		2.88	1.96	84.70
	70		2.06	1.47	85.76
	20	60	10.57	7.74	78.58

Table 6.1. Continued.

Membrane	Thickness (μm)	Carbonization (%)	PWP ^a	WF ^a	R ^b
PC-PIM-1	30	40	7.04	5.74	79.60
		47.5	8.38	6.33	78.94
		50	8.82	6.54	77.38
		60	10.79	7.95	76.51
	20	37.5	10.40	7.36	75.91
	30		6.98	4.91	78.50
	35		5.92	4.22	80.94
	40		5.08	3.71	83.03
	45		4.55	3.35	83.55
	50		4.19	3.07	83.85
	70		2.95	2.21	85.20
	20	60	15.43	13.3	77.37

Table 6.2. Bulk and surface elemental compositions (at%) of PIM-1, C-PIM-1, and PC-PIM-1 (40% carbonization) membranes obtained by EA and XPS, respectively.

Membrane	Bulk Composition (EA)			Surface Composition (XPS)		
	C	O	N	C	O	N
PIM-1	83.69	10.85	5.46	82.60	13.60	3.70
C-PIM-1	98.22	1.09	0.69	96.82	1.37	1.81
PC-PIM-1	98.14	1.16	0.70	87.51	11.60	0.89

Table 6.3. Diffusion coefficient values (D_i) of salts (at 25 °C) and hydrated ionic radius (R_i) of the corresponding ions.

Salt	$D_i (\times 10^9, \text{m}^2 \text{s}^{-1})$	Ion	R_i (nm)
NaCl	1.61	Cl^-	0.33
Na_2SO_4	1.23	Na^+	0.36
MgCl_2	1.25	SO_4^{2-}	0.38
MgSO_4	0.85	Mg^{2+}	0.44

Table 6.4. MgSO₄ rejection (R, %) and water flux (WF, LMH bar⁻¹) values of optimized C-PIM-1 and PC-PIM-1 membranes in this study and other NF membranes in the literature.

Name	Membrane Type	Selective Layer	WF	R	MgSO ₄ Concentration	Ref
NF2A	TFC ^a	Polyamide	3.32	76.9	2,000 ppm	This Work
C-PIM-1 ^c	Single ^b		7.7	78.6		
PC-PIM-1 ^c			13.3	77.3		
GNm	Single	Graphene	4.76	82.8	1,200 ppm	7
G-CNTm (8:1)		Graphene -CNT	8.02	44.2		
G-CNTm (4:1)			8.05	42.3		
G-CNTm (8:3)			9.51	40.6		
G-CNTm (2:1)			11.33	30.9		
G-CNTm (8:5)			12.13	25.1		

Table 6.4. Continued.

Name	Membrane Type	Selective Layer	WF	R	MgSO ₄ Concentration	Ref
uGNM	Single	Graphene	3.3	30.0	2,400 ppm	8
Cub _{bi}	Single	Cubic liquid crystal	3.73	26.0	1,500 ppm	9
Amorphous	Single	liquid crystal	8.40	20.0		
TFC-NFM	TFC	Zirconia	8.33	69.0	2,000 ppm	10
TMC	TFC	Polyamide	6.20	94.5	3,000 ppm	11
IPC			2.90	77.7		

^a Thin-film composite membrane. ^b Single layer membrane. ^c 20 μ m thickness, 60% carbonization.

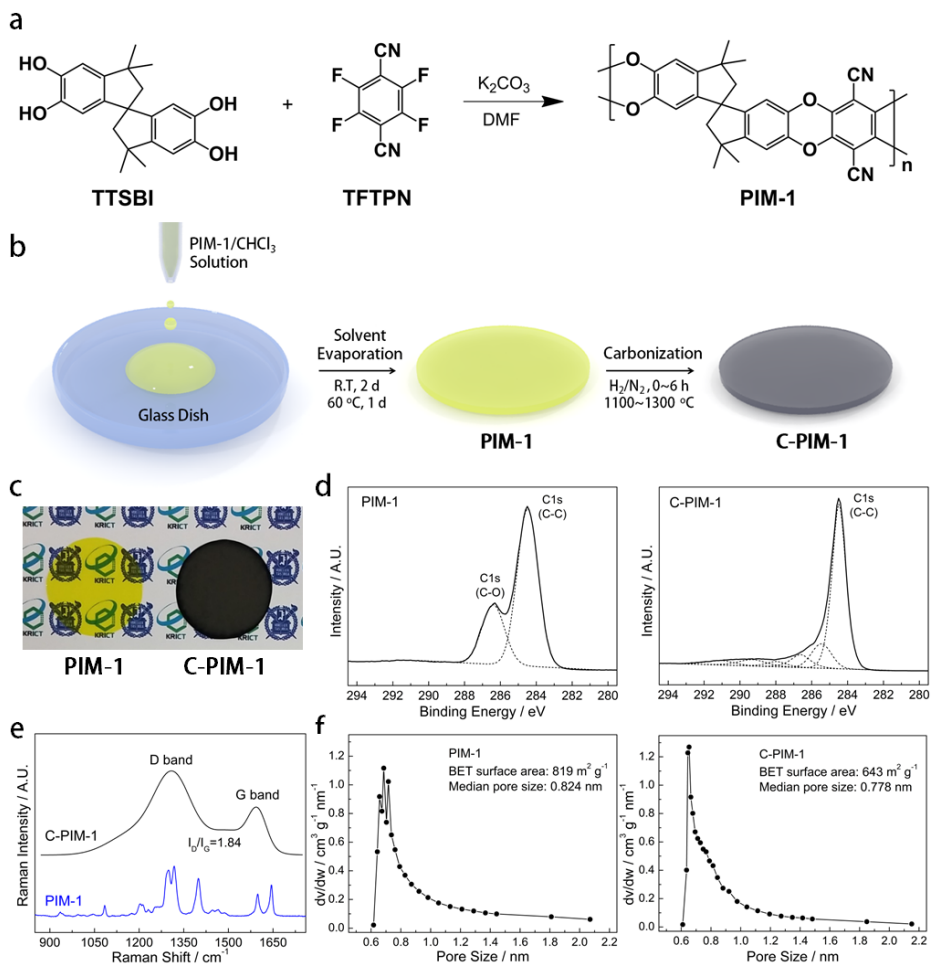


Figure 6.1. Preparation and characteristics of PIM-1 and C-PIM-1 membranes. (a) Preparation procedure of PIM-1 and C-PIM-1 membranes. (b) Photographs of the PIM-1 and C-PIM-1 membranes. (c) XPS C 1s spectra, (d) Raman spectra, and (e) pore size distributions of the PIM-1 and C-PIM-1 (40% carbonization) membranes.

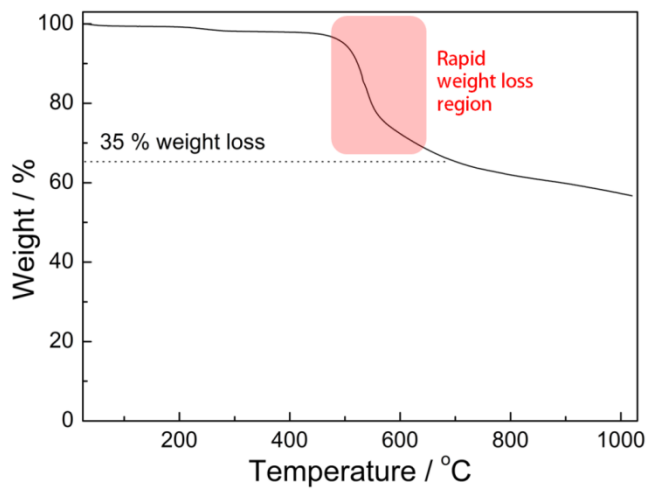


Figure 6.2. TGA curve of PIM-1.

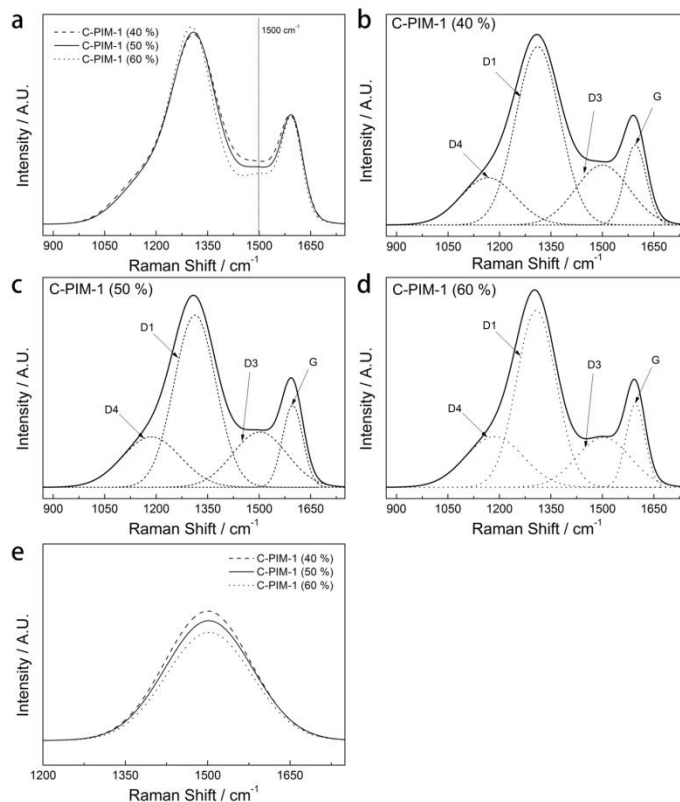


Figure 6.3. Raman spectra of C-PIM-1 membranes. G band peak intensities in all the Raman spectra were normalized for clear comparison. a) Raman spectra of C-PIM-1 membranes with different degrees of carbonization. Deconvoluted Raman spectra of C-PIM-1 membranes with b) 40%, c) 50%, and d) 60% carbonization using Gaussian curve fitting for the D1, D3, D4, and G band peaks. e) D3 band peaks of C-PIM-1 membranes with different degrees of carbonization.

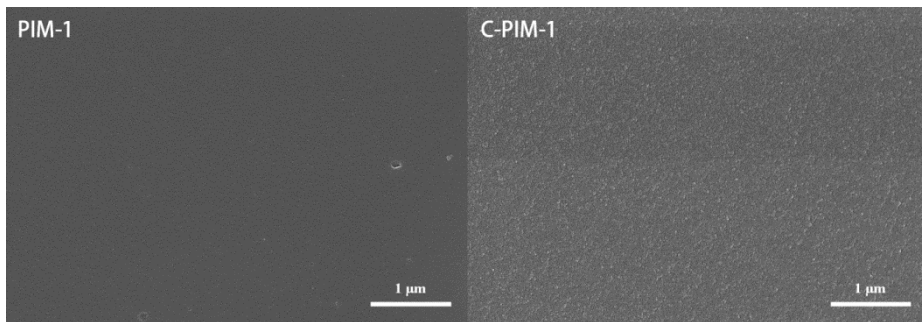


Figure 6.4. SEM images of PIM-1 and C-PIM-1 (40% carbonization) membrane surfaces.

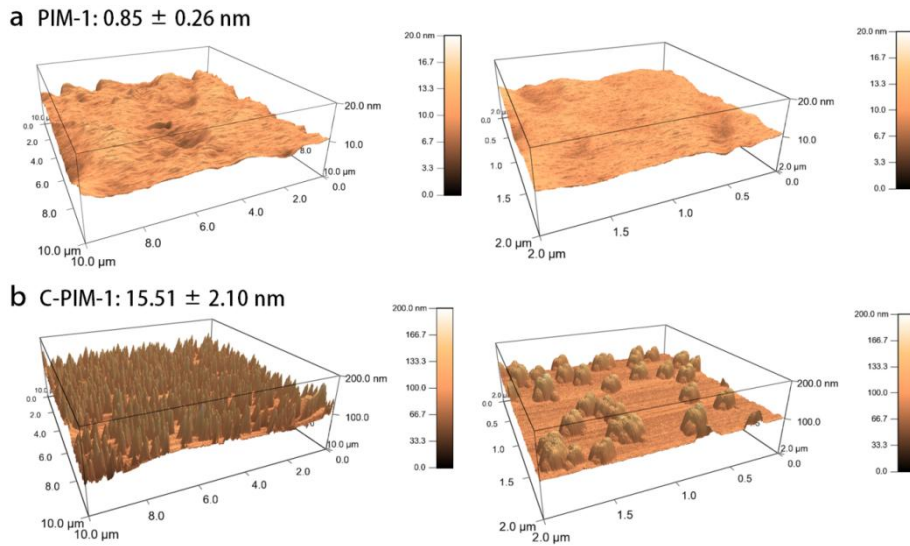


Figure 6.5. AFM surface morphologies and root mean square (RMS) roughness values of a) PIM-1 and b) C-PIM-1 (40% carbonization) membranes (left, $10\ \mu\text{m} \times 10\ \mu\text{m}$; right, $2\ \mu\text{m} \times 2\ \mu\text{m}$ images).

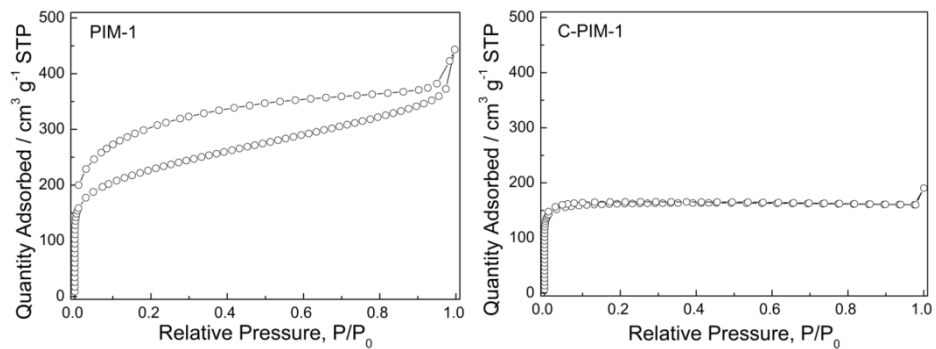


Figure 6.6. N₂ adsorption and desorption isotherms of PIM-1 and C-PIM-1 (40% carbonization) at 77 K.

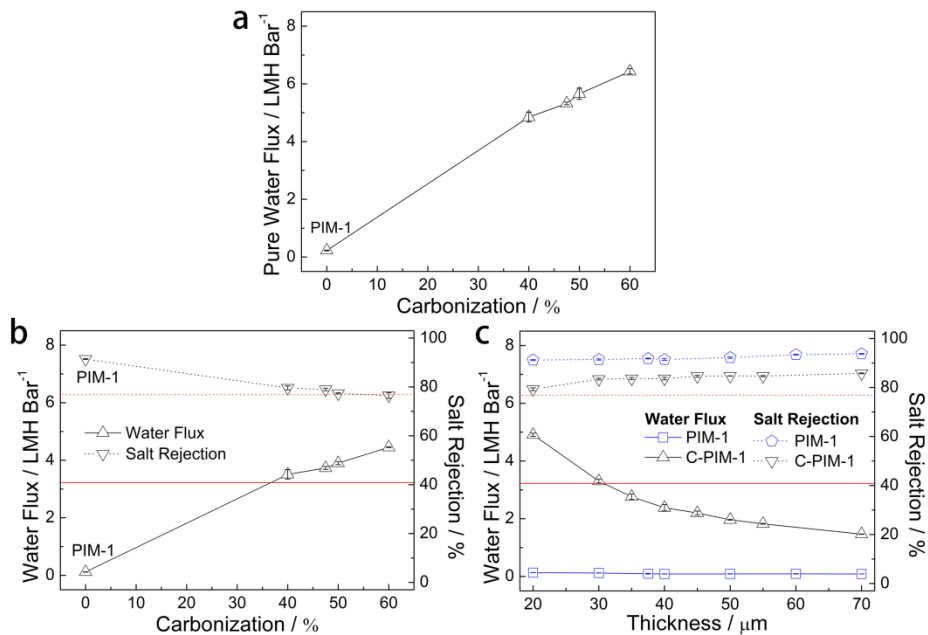


Figure 6.7. Water flux and salt rejection performance of the PIM-1 and C-PIM-1 membranes. The effect of degree of carbonization on water flux and salt rejection of the membranes with a thickness of 30 μm upon (a) pure water and (b) MgSO_4 solution (2,000 ppm) filtrations. (c) The effect of membrane thickness on water flux and salt rejection of the membranes with the degree of carbonization of 37.5% upon MgSO_4 solution (2,000 ppm) filtration. The red solid and dotted lines indicate the water flux and salt rejection of a commercial polyamide NF membrane (NF2A), respectively.

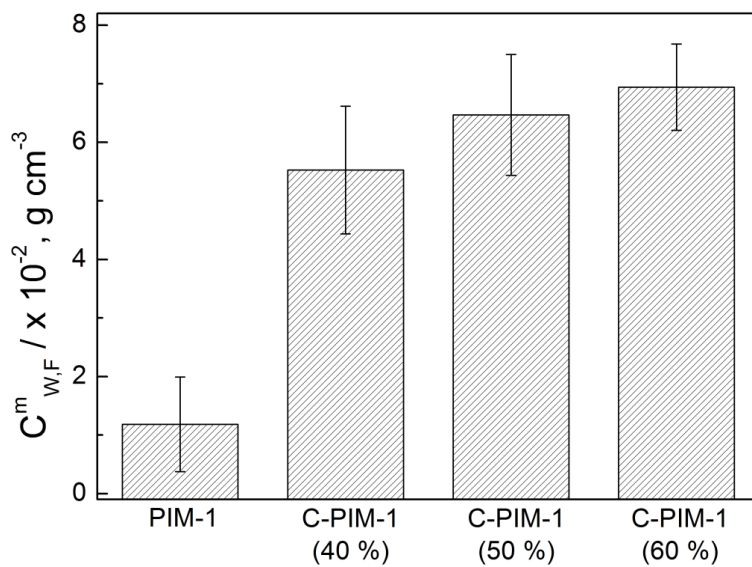


Figure 6.8. $C_{w,F}^m$ values of PIM-1 and C-PIM-1 membranes (carbonization = 40–60%) obtained from water uptake measurements.

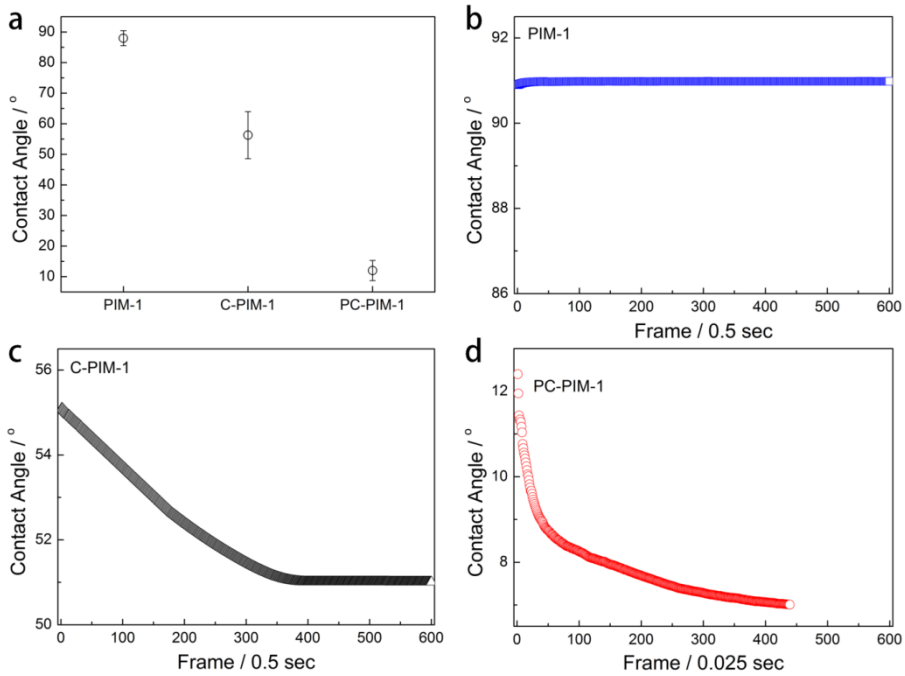


Figure 6.9. a) Sessile drop water contact angle values of PIM-1, C-PIM-1, and PC-PIM-1 membranes. Wetting behaviors of water droplets on b) PIM-1, c) C-PIM-1 (40% carbonization), and d) PC-PIM-1 (40% carbonization) membranes. The relative humidity was maintained over 65% to minimize the evaporation of water droplets during the wetting experiment. Much shorter frame time (1 frame = 0.025 sec), compared to that for PIM-1 and C-PIM-1 membranes (1 frame = 0.5 sec), was used for the PC-PIM-1 membrane due to the rapid decrease of water contact angle on the membrane surface.

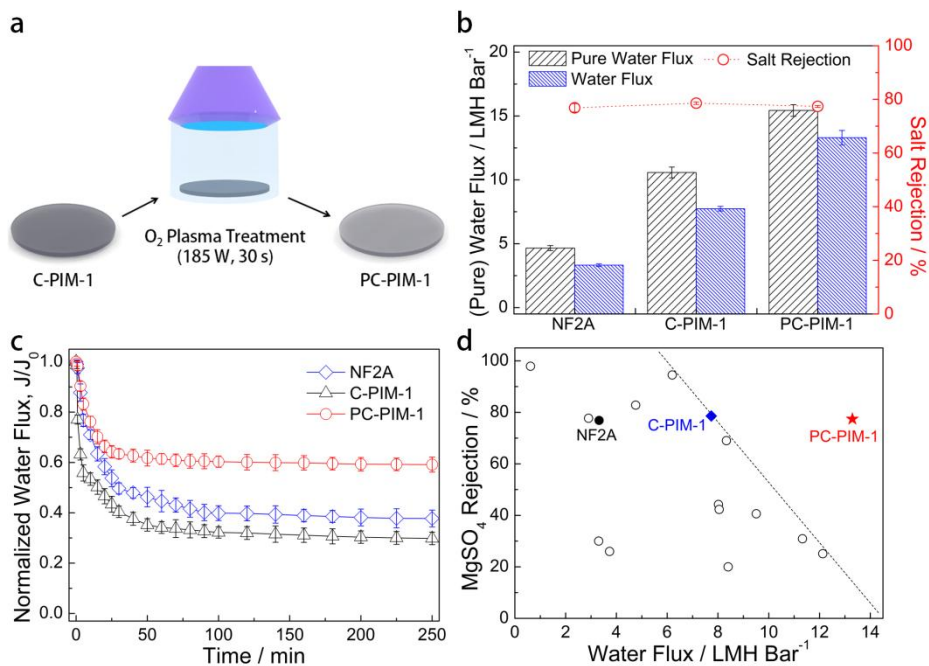


Figure 6.10. Preparation and performance of O₂ plasma-treated C-PIM-1 membrane (PC-PIM-1). (a) Preparation procedure of PC-PIM-1 membrane. (b) Pure water flux, water flux, and salt rejection performance of NF2A, and C-PIM-1 and PC-PIM-1 membranes with a thickness of 20 μm and a degree of carbonization of 60%. (c) Time-dependent normalized water flux variations of the NF2A, C-PIM-1, and PC-PIM-1 (20 μm, 60% carbonization) membranes during BSA solution (1 g L⁻¹) filtration. (d) MgSO₄ rejection rate and water flux performance of optimized C-PIM-1 and PC-PIM-1 membranes in this study and other NF membranes in the literature.

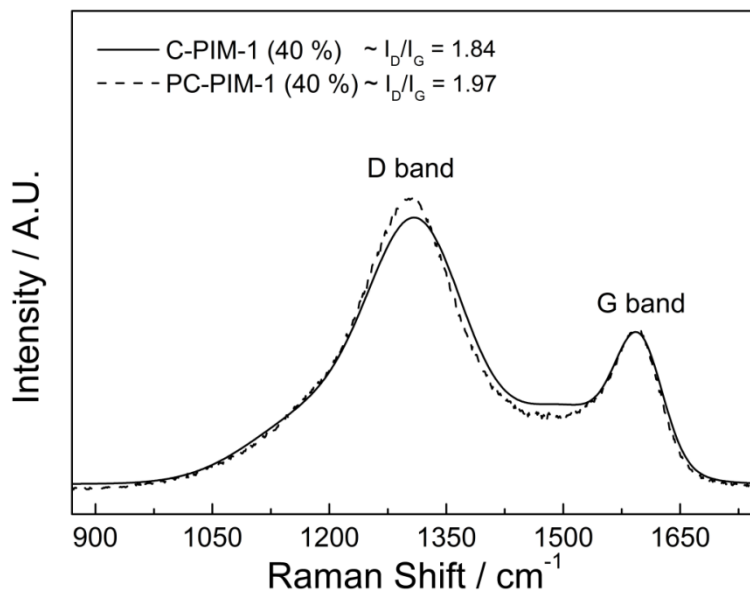


Figure 6.11. Raman spectra of C-PIM-1 and PC-PIM-1 membranes with 40% carbonization. The G band peak intensities were normalized for clear comparison.

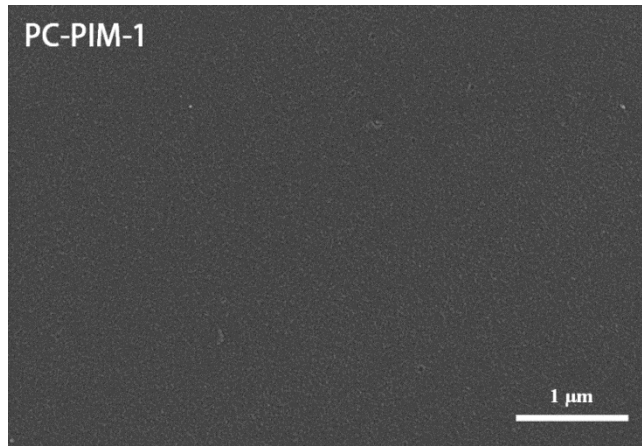


Figure 6.12. SEM images of the PC-PIM-1 (40% carbonization) membrane surface.

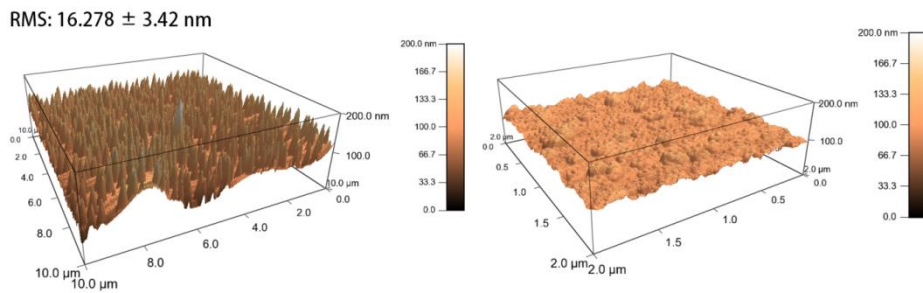


Figure 6.13. AFM surface morphologies and root mean square (RMS) roughness value of the PC-PIM-1 membrane (40% carbonization) (left, $10 \mu\text{m} \times 10 \mu\text{m}$; right, $2 \mu\text{m} \times 2 \mu\text{m}$ images).

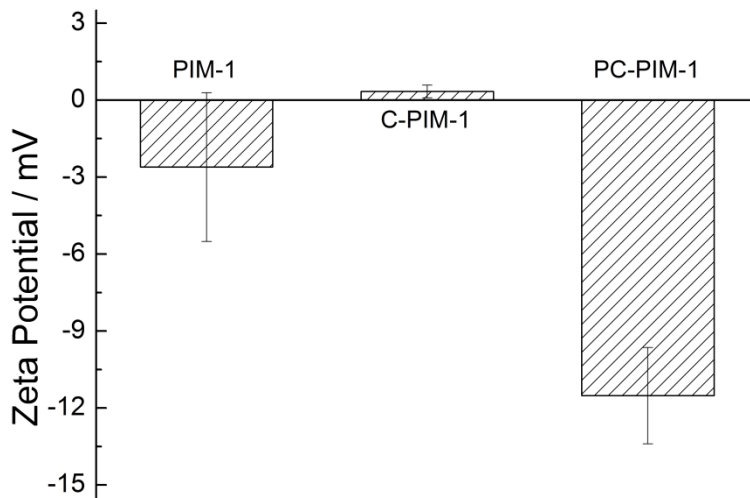


Figure 6.14. Zeta potential values of PIM-1, C-PIM-1 (40% carbonization), and PC-PIM-1 (40% carbonization) membranes.

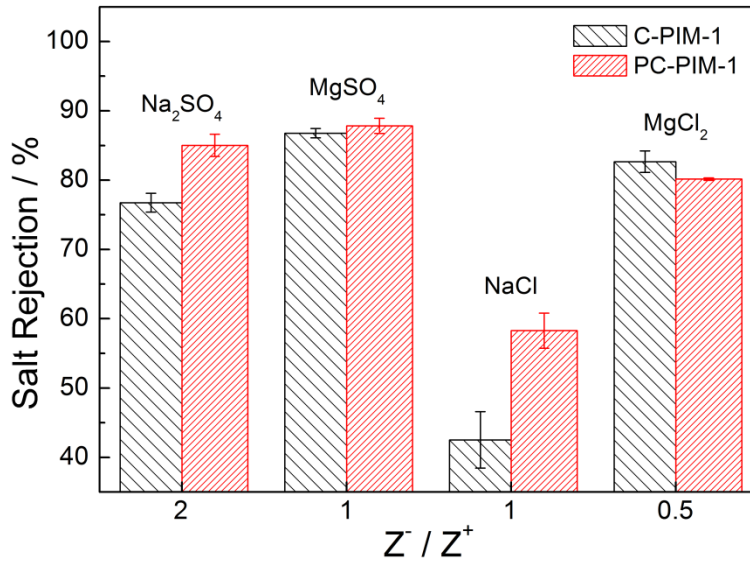


Figure 6.15. Salt rejection rates of C-PIM-1 and PC-PIM-1 membranes (40% carbonization) for various salt solutions (10 mM). Filtrations were conducted under 5 bar of feed pressure with a stirring speed of 200 rpm.

초 록

본 논문은 탄소 구조를 포함하는 고분자 막의 합성 및 분석, 그리고 나노여과와 역삼투 여과를 포함하는 수처리로의 응용에 대하여 기술하였다. 첫째, 카본나노튜브 (Carbon nanotube, CNT) 를 포함하는 역삼투막을 메타 페닐렌 다이아민 (m-phenylene diamine, MPD) 수용액과 트리메조일 클로라이드 (trimesoyl chloride, TMC) 유기용액 간 계면중합을 통해 제조하였다. 표면개질이 최적화된 CNT는 폴리아마이드 (Polyamide, PA) 매질 내에 고르게 분산되어 있으며, 이러한 것은 원자 힘 현미경, 전자 현미경, 라만 분광법 등을 통하여 확인되었다. CNT가 함유된 혼합 역삼투막은 탄소나노튜브가 포함되지 않은 PA막보다 우수한 수투과도를 보였으며, 이 때 염제거율은 유사하였다. 또한, 혼합 역삼투막이 PA막보다 우수한 기계적, 화학적 안정성을 나타내었다. 이러한 우수한 수투과도 및 막 안정성은 CNT의 나노기공 및 매질 내 잘 분산되어 있는 상태에 의한 것이다.

둘째, PA 역삼투막 표면에 CNT를 도포한 후 폴리비닐알코올 (Polyvinylalcohol, PVA)를 코팅하여 복합 역삼투막을 제조하였다. 이 때, CNT는 산 처리 과정을 거쳐

표면이 개질된 후 그 분산액을 진공여과하여 도포되었다. 복합 역삼투막은 우수한 기계적 안정성을 보였다. 또한, 미생물에 대한 방오특성이 PA 막, 상용화된 기수용 역삼투막 (LFC-1) 보다 우수하였다. 이러한 복합 역삼투막의 우수한 특성은 CNT의 항균성 및 우수한 기계적 물성, 그리고 PVA의 코팅 및 가교에 기인한 것이다.

셋째, CNT와 그래핀 옥사이드 (GO)를 동시에 함유하는 혼합 역삼투막을 제조하였다. CNT와 GO가 함께 혼합될 때, 증대된 분산도로 인해 많은 양의 탄소나노물질이 역삼투막에 도입될 수 있었다. 따라서, 좋은 분산도로 많은 양의 탄소나노물질이 함유된 CNT, GO를 모두 함유하는 혼합 역삼투막이 가장 우수한 막 성능을 나타내었다.

넷째, GO의 표면이 자가중합이 가능한 탄닌산으로 코팅되었다. 탄닌산의 자가중합은 약염기 완충용액 하에 진행되었다. 표면이 탄닌산으로 코팅된 GO (GO coated by tannic acid, GOT)를 함유하는 혼합 역삼투막은 계면중합법으로 제조되었다. GOT를 함유하는 혼합 역삼투막은 수투과도, 내염소성, 항균성 측면에서 우수한 성능을 나타내었다. 이러한 우수한 막 성능은 GOT의 친수성, 산화성 힘, 장벽 물성, 고분자 매질간 상용성에 기인한 것이다.

마지막으로, 미세기공을 가지는 고분자 막의 탄화를 제어하여 나노여과막을 제조하였다. 기공이 1 나노미터 이하의, 연결된, 마찰력이 적은 탄소기공을 가지는 탄화막은 물 분자를 선택적으로 빠르게 투과시킬 수 있었으며, 좋은 염 제거율을 나타내었다. 더하여, 산소 플라즈마 처리를 통해 염 제거율 감소 없이 수투과도를 더욱 증대시킬 수 있었다. 또한, 표면 처리로 인해 단백질에 대한 방오성능도 함께 증가하였다.

주요어: 고분자막, 탄소 구조, 폴리마아이드, 미세기공 고분자, 탄소나노튜브, 그래핀 옥사이드, 수처리, 여과막

학 번: 2011-21033